5-2018

Characterization of the Hepatotoxicity of Rifampicin and Isoniazid

Christopher T. Brewer
University of Tennessee Health Science Center

Characterization of the Hepatotoxicity of Rifampicin and Isoniazid

Abstract

In a mouse model, rifampicin and isoniazid combination treatment results in cholestatic liver injury that is associated with an increase of protoporphyrin ix (PPIX), the penultimate heme precursor. Excess PPIX is believed to bind to bile acids, precipitate in bile canaliculi, and form bile plugs leading to cholestasis fol owed by liver injury. Both ferrochelatase (*FECH*/*Fech*) and aminolevulinic acid synthase 1 (*ALAS1*/*Alas1*) are crucial enzymes in regulating heme biosynthesis. Isoniazid has recently been reported to up-regulate *Alas1* but down-regulate *Fech* protein levels in mice; however the mechanism of isoniazid mediated heme synthesis disruption has remained unclear. Interestingly, metabolites of isoniazid, pyridoxal isonicotinoyl hydrazone (PIH, the isoniazid and vitamin B6 conjugate) and hydrazine, have been detected in the urine of humans treated with isoniazid previously. Here I show that in primary human hepatocytes and the human hepatocellular carcinoma cell line HepG2/C3A: (1) the physiochemical properties of PPIX may contribute to toxicity (2) isoniazid treatment results in an increase of *ALAS1* but a decrease in *FECH* protein levels by Western blot analysis; (3) hydrazine treatment up-regulates *ALAS1* protein and mRNA levels; (4) PIH treatment decreases *FECH* protein levels; (5) PIH is detected by mass spectrometry analysis following isoniazid treatment with a further increase when exogenous vitamin B6 analogues are co-administrated. In addition, the (6) PIH mediated down-regulation of human *FECH* is dependent on iron levels. Proteomics profiling analysis suggests that in the livers of *hPXR* mice (7) rifampicin may induce CYP450 changes associated with increased hydrazine reactivity with cellular proteins, (8) multiple [2Fe-2S]-containing proteins and (9) [Fe-S] assembly machinery proteins may be down-regulated in mice due to isoniazid. Together these data demonstrate that hydrazine up-regulates *ALAS1* while PIH down-regulates *FECH*, suggesting that the metabolites of isoniazid mediate its disruption of heme biosynthesis.

Document Type

Dissertation

Program

Biomedical Sciences

Research Advisor

Taosheng Chen, Ph.D.

Keywords

Drug-Induced Liver Injury, Heme Synthesis, Hepatotoxicity, Isoniazid, Rifampicin, Vitamin B6

Subject Categories

Chemicals and Drugs | Medical Cell Biology | Medical Physiology | Medical Sciences | Medical Toxicology | Medicinal and Pharmaceutical Chemistry | Medicine and Health Sciences | Pharmaceutical Preparations | Pharmacy and Pharmaceutical Sciences

Characterization of the Hepatotoxicity of Rifampicin and Isoniazid

A Dissertation
Presented for
The Graduate Studies Council
The University of Tennessee
Health Science Center

In Partial Fulfillment
Of the Requirements for the Degree
Doctor of Philosophy
From The University of Tennessee

By
Christopher T. Brewer
May 2018

DEDICATION

To my wonderful children, Catness and Maizie.

ACKNOWLEDGEMENTS

I am grateful to those who have helped me complete this dissertation. I am grateful to my advisor Dr. Taosheng Chen for his research guidance and support throughout this project as well as to all current and former members of Dr. Chen's Lab. I am thankful for the advice and support dedicated by my academic committee members Dr. Ying Kong, Dr. Richard Lee, Dr. David Nelson, and Dr. John Schuetz.

I extend my sincere gratitude to the members of the Animal Resource Center at St. Jude Children's Research Hospital, especially Jackson Carpenter and Chandra Savage for assistance with carrying out the *in vivo* studies. I would like to thank the members of the Veterinary Pathology Core Facility and Flow Cytometry and Cell Sorting Facility at St. Jude Children's Research Center. I am grateful to Kiran Kodali and Dr. Junmin Peng of the Proteomics and Mass Spectrometry Facility at St. Jude Children's Research Center and Dr. Timothy Shaw of the Computational Biology Department at St. Jude Children's Research Center. I am grateful to Dr. Anne Edwards of the Chemical Biology and Therapeutics Department and Lei Yang of High-Throughput Analytical Chemistry.

I am thankful to the University Of Tennessee Health Science Center College Of Graduate Health Sciences for financial support and I would like to thank all the faculty and staff of the College for their support.

ABSTRACT

In a mouse model, rifampicin and isoniazid combination treatment results in cholestatic liver injury that is associated with an increase of protoporphyrin ix (PPIX), the penultimate heme precursor. Excess PPIX is believed to bind to bile acids, precipitate in bile canaliculi, and form bile plugs leading to cholestasis followed by liver injury. Both ferrochelatase (*FECH*/*Fech*) and aminolevulinic acid synthase 1 (*ALAS1*/*Alas1*) are crucial enzymes in regulating heme biosynthesis. Isoniazid has recently been reported to up-regulate *Alas1* but down-regulate *Fech* protein levels in mice; however the mechanism of isoniazid mediated heme synthesis disruption has remained unclear. Interestingly, metabolites of isoniazid, pyridoxal isonicotinoyl hydrazone (PIH, the isoniazid and vitamin B_6 conjugate) and hydrazine, have been detected in the urine of humans treated with isoniazid previously. Here I show that in primary human hepatocytes and the human hepatocellular carcinoma cell line HepG2/C3A: (1) the physiochemical properties of PPIX may contribute to toxicity (2) isoniazid treatment results in an increase of *ALAS1* but a decrease in *FECH* protein levels by Western blot analysis; (3) hydrazine treatment up-regulates *ALAS1* protein and mRNA levels; (4) PIH treatment decreases *FECH* protein levels; (5) PIH is detected by mass spectrometry analysis following isoniazid treatment with a further increase when exogenous vitamin B_6 analogues are co-administrated. In addition, the (6) PIH mediated down-regulation of human *FECH* is dependent on iron levels. Proteomics profiling analysis suggests that in the livers of *hPXR* mice (7) rifampicin may induce CYP450 changes associated with increased hydrazine reactivity with cellular proteins, (8) multiple [2Fe-2S]-containing proteins and (9) [Fe-S] assembly machinery proteins may be down-regulated in mice due to isoniazid. Together these data demonstrate that hydrazine up-regulates *ALAS1* while PIH down-regulates *FECH*, suggesting that the metabolites of isoniazid mediate its disruption of heme biosynthesis.

TABLE OF CONTENTS

LIST OF TABLES

LIST OF FIGURES

LIST OF ABBREVIATIONS

[Fe-S]	Iron sulfur cluster
µg	Micrograms
µL	Microliters
µm	Micrometers
µM	Micromolar
ABCB1	ATP-binding cassette family B member 1, human
Abcb10	ATP-binding cassette family b member 10, mouse
ABCG2	ATP-binding cassette family G member 2, human
AF-1	Activating function domain 1
AF-2	Activating function domain 2
A-INH	Acetyl-isoniazid
ALA	Aminolevulinic acid
ALAD	*Aminolevulinic acid dehydratase*
ALAS1	*Aminolevulinic acid synthase 1, human*
Alas1	*Aminolevulinic acid synthase 1, mouse*
ALP	*Alkaline phosphatese*
ALT	*Alanine aminotransferase*
ANOVA	Analysis of variance
AST	*Aspartate aminotransferase*
ATCC	American tissue culture center
ATP	Adenosine triphosphate
CAS	Chromeazurol S
CD36	*Cluster of differentiation 36*
CO	*Coproporphyrinogen oxidase*
COPRO	Coproporphyrinogen III
CTS	Charcoal treated serum
CYP1A2	*Cytochrome P450 family 1 subfamily A member 2,*
CYP2B6	*Cytochrome P450 family 2 subfamily B member 6*
CYP2C19	*Cytochrome P450 family 2 subfamily C member 19*
CYP2C9	*Cytochrome P450 family 2 subfamily C member 9*
CYP2E1	*Cytochrome P450 family 2 subfamily E member 1*
Cyp3a	Cytochrome P450 family 3 subfamily A, mouse
Cyp3a11	*Cytochrome P450 family 3 subfamily A member 11, mouse*
CYP3A4	*Cytochrome P450 family 3 subfamily A member 4*
CYP3A5	*Cytochrome P450 family 3 subfamily A member 5*
CYP450	Cytochrome P450
DAPI	4,6-daimindino-2-phenylindole
DILI	Drug-induced liver injury
DMEM	Dulbecco's minimal essential media
DMSO	Dimethyl sulfoxide
DNA	Deoxyribonucleic acid
EMEM	Eagle's minimal essential media
FBS	Fetal bovine serum

FECH	*Ferrochelatase, human*
Fech	*Ferrochelatase, mouse*
FTC	Fumitremorgin C
GGT	*γ-Glutamyl transferase*
GST	*Glutathione S-transferease*
HAART	Highly active anti-retroviral therapy
HILI	Herb induced liver injury
HIV	Human immunodeficiency virus
HMB	Hydroxymethyl bilane
hPXR	*Pregnane X receptor, human*
INA	Isonicotinic acid
INH	Isonicotinyl hydrazide, isoniazid
IR	Infrared
KOH	Potassium hydroxide
LA	Lithocholic acid
LC	Liquid Chromatography
LFT	Liver function test
MDR1	*Multi-drug resistance protein 1*
MEF	Mouse embryonic fibroblast
MEM	Minimal essential media
MeOH	Methanol
Mfrn-1	*Mitoferritin*
mPxr$^{-/-}$	*Pregnane X receptor, mouse*
mRNA	Messenger ribonucleic acid
MRP3	Multi-drug resistance protein 3
NADH	Nicotinamine adenine dinucleotide
NADPH	Nicotinamine adenine dinucleotide phosphate
NaOH	Sodium hydroxide
NAT	*N-acetyl transferase*
NOS	Nitric oxide species
NSAID	Non-steroidal anti-inflammatory drug
PA	Palmitic acid
PAMPA	Parallel artificial membrane permeability assay
PBG	Porphobilinogen
PBGD	*Porphobilinogen deaminase*
PBS	Phosphate buffered saline
PIH	Pyridoxal isonicotinoyl hydrazone
PPG	Protoporphyrinogen
PPIX	Protoporphyrin ix
$PPIXNa_2$	The disodium salt of protoporphyrin ix
PPOX	*Protoporphyrinogen oxidase*
PXR	*Pregnane X receptor*
qRT-PCR	Real time reverse transcriptase polymerase chain reaction
RIPA	Radioimmunoprecipitation assay
RNA	Ribonucleic acid
ROS	Reactive oxygen species

RXR	*Retinoic X Receptor*
SA	Succinyl acetate
shRNA	Short hairpin ribonucleic acid
siRNA	Short interfering ribonucleic acid
SULT2A	*Sulfotransferase family 2A*
TB	Tuberculosis
TBST	Tris buffered saline with Tween
TCA	Taurocholic acid
UGT	*Uridine gluuronosyltransferase*
UROD	*Uroporphyrinogen decarboxylase*
UROIII	*Uroporphyrinogen III*
UROIIIS	*Uroporphyrinogen III synthase*
WT	Wild-type

CHAPTER 1. INTRODUCTION

The Implications of Anti-Tubercular DILI

Approximately 1.6 million people died of tuberculosis (TB) in 2015 and up to 10 million current cases of tuberculosis were predicted in 2015 (Disease, Injury et al. 2016). Of all infectious causes, mortality due to TB infection is second only to the human immunodeficiency virus (HIV) (Murray, Ortblad et al. 2014, Disease, Injury et al. 2016, Collaborators 2017). Access to therapeutics plays an important role in adherence to successful completion of regimens and successful anti-TB treatment strategies rely upon an uninterrupted supply of therapeutics (Long, Smith et al. 2011, Muture, Keraka et al. 2011). Alternative drugs may have lower therapeutic windows than first line therapy (i.e., rifampicin and isoniazid) or may impose financial burdens (Blumberg, Burman et al. 2003). For example, rifabutin is not associated with the up-regulation of drug metabolizing enzymes and transporters through the human Pregnane X Receptor (hPXR) activation but costs much more than rifampicin. Additionally, replacing rifampicin with rifabutin (an analog that does not activate *hPXR*) does not completely obviate adverse events (Horne, Spitters et al. 2011). Similarly, first line highly active anti-retroviral therapy (HAART) is efficacious at reducing viral load and preventing T-cell depletion.

Change or discontinuation of HAART was due to drug toxicity in 22 % of patients; 11 % of these were due to hepatotoxicity. Discontinuation of HAART for longer than four weeks was associated with decreases in $CD4^+$ T-cell populations and increases in HIV ribonucleic acid (RNA) at 12 months (Elzi, Marzolini et al. 2010). The median time of discontinuation for hepatotoxicity was 72 days, much longer than the four weeks necessary to see deleterious effects. HIV protease inhibitors, such as ritonavir, indinavir, amprenavir, atazanavir, darunavir, efavirenz, and lopinavir have been shown to activate hPXR, and may pathologically up-regulate drug metabolizing enzymes (Sulkowski, Thomas et al. 2000, Luo, Cunningham et al. 2002, Chan, Patel et al. 2013). In addition, co-infection of HIV with TB increases the risk of drug-induced liver injury (DILI) (Ungo, Jones et al. 1998, Yee, Valiquette et al. 2003, Breen, Miller et al. 2006). Due to chronic up-regulation of drug metabolizing enzymes, there is still a potential for adverse drug interactions when HAART is suspended to treat TB. Additionally, the discontinuation of HAART for a six-month course of rifampicin and isoniazid, could lead to T-cell depletion and increases in viral load (Deeks, Wrin et al. 2001, Elzi, Marzolini et al. 2010). HIV co-infection increases the risk of anti-TB DILI four-fold, even when HAART has been suspended. Moreover, concomitant TB and HIV therapy increased the risk of DILI more than ten-fold (Yimer, Gry et al. 2014).

Hepatotoxicity decreases adherence to treatment regimens and contributes to treatment failure, disease relapse, and drug resistance (Singla, Gupta et al. 2014). Hepatotoxicity is a leading cause of TB therapy treatment failure, with up to 28% of all anti-TB treatment failure attributed to toxicity (Sharifzadeh, Rasoulinejad et al. 2005, Tostmann, Boeree et al. 2008). Therefore, further characterization of the mechanism of

anti-tubercular liver injury would enable the development of updated clinical guidance to prevent or ameliorate DILI.

Drug-Induced Liver Injury

DILI is classified as one of three categories based on clinicopathologic presentation: hepatocellular injury (a result of specific injury to hepatocytes), cholestatic injury (caused by specific toxicity to biliary epithelial cells and/or bile pumps that disrupts bile flow), or a mixed pattern of injury with characteristics of both of the other types of liver injury (Navarro and Senior 2006). Generally, the severity of liver injury correlates to the levels of serum alanine aminotransferase (*ALT*) and alkaline phosphatase (*ALP*). Hepatocellular injury is associated with serum *ALT* levels greater than two times the upper limit of the normal range and an *ALT*/*ALP* ratio greater than or equal to 5. Cholestatic liver injury is defined as a serum *ALP* level greater than twice the upper limit of the normal range and an *ALT*/*ALP* ratio of less than 2 (Navarro and Senior 2006). Mixed injury is the designation if the *ALT*/*ALP* ratio is between 2 and 5. ALT is specific to DILI, but not sensitive. *ALP* is not specific, but is more sensitive. Therefore, the gold standard for the diagnosis of DILI is histologic examination of liver tissue. DILI is also classified by pathogenesis due to specific measurable compounds derived from the causative xenobiotic or from an immune response induced by the presence of the xenobiotic or potential metabolites.

Clinical Classification of DILI by Pathophysiology

The clinicopathologic characterization of DILI is based on the clinical presentation of the liver injury and the pathologic effects observed on histological examination (reviewed in Wang et al., 2014) is necessary to identify the particular xenobiotic responsible for the liver injury (Wang, Chai et al. 2014). The molecular mechanism responsible for the pathogenesis of DILI may be associated with the pathophysiologic subtype of liver injury. Liver injury caused by cholestasis may be caused by mechanism that result in cholestasis, such as by the disruption of intracellular actin or transporter proteins (Woolbright and Jaeschke 2012, Schyschka, Sanchez et al. 2013). Hepatocellular liver injury that is caused by xenobiotics that are directly toxic to hepatocytes and is associated with *ALT* elevation. ALT is diffusely expressed throughout the liver and is increased when hepatocytes are damaged (Navarro and Senior 2006). Cholestatic liver injury is caused by bile stasis that is reflected by elevated levels of *ALP*, γ-glutamyl transferase, and direct bilirubin (Navarro and Senior 2006). Following obstruction of bile flow ALP is released from biliary epithelial cells, from which *ALP* is expressed (Suzuki, Irie et al. 2006). Cholestasis is also associated with mechanism that disrupts bile flow and leads to the accumulation of bile acids within the liver. Damage to biliary epithelial cells or the impairment of bile export can lead to cholestasis (Meier, Pauli-Magnus et al. 2006). When combinations of xenobiotics or when a single xenobiotic that damages multiple types of liver cells are administered a mixed type of

liver injury results where the characteristics of both cholestatic and hepatocellular liver injury are observed (Fisher, Vuppalanchi et al. 2015).

Clinical Classification of DILI by Pathogenesis

The classification of DILI by pathogenesis can give additional insights into the causative agent and probable molecular mechanism. Intrinsic liver injury is usually caused by the parent drug or one of its metabolites and is dose-dependent on these xenobiotics and are detectable in the liver or blood (Kumar, Chung et al. 2012, Xie, McGill et al. 2014). These effects occur in laboratory animals and are predictable. Therefore pharmaceuticals that cause intrinsic liver injury are usually detected during preclinical development (Ganey, Luyendyk et al. 2004, Ganey, Luyendyk et al. 2007, Li, Lu et al. 2013, Xie, McGill et al. 2014, Teschke, Larrey et al. 2016). Idiosyncratic liver injury is more common than intrinsic liver injury and is typically caused by the activation of xenobiotics by the CYP450 system. Idiosyncratic liver injury may result in the formation of drug/metabolite-protein-adducts that are identified as haptens by the host immune system and are undetectable (Tujios and Fontana 2011, Kishida, Onozato et al. 2012, den Braver, den Braver-Sewradj et al. 2016). The complex combination of environmental and genetic factors that contribute to idiosyncratic liver injury cannot be reliably reproduced in laboratory animals (Teschke, Larrey et al. 2016, Clare, Miller et al. 2017, Lundgren, Martinsson et al. 2017). The immune response of the host, not the xenobiotic or metabolites is the main contribution to the pathogenesis of idiosyncratic liver injury, contrary to intrinsic liver injury (Ali and Auerbach 2017, Ghannam, Mansour et al. 2017).

The Pregnane X Receptor

Activation of the human *Pregnane X Receptor* (hPXR, also known as NR1I2 [nuclear receptor subfamily 1, group I, member 2], SXR [steroid and xenobiotic sensing receptor], or PAR [pregnane activated receptor]) by agonists, such as rifampicin, results in the transcription of target genes, many of which are drug metabolizing enzymes and transporters (**Figure 1-1**). *hPXR* is one of a class of proteins, nuclear hormone receptors (NHR), defined by a DNA binding domain, a ligand binding domain (LBD), and two activating function domains. The LBD of *hPXR* is particularly promiscuous and binds to a large number of structurally different compounds (Watkins, Maglich et al. 2003, Zollner, Wagner et al. 2010). Target DNA sequences in the promoters of target genes are targeted by NHRs to induce the transcription of these target genes. Ligand binding to the LBD of *hPXR* enables the recruitment of co-activating proteins and the dissociated of co-repressor proteins and triggers transcription (Watkins, Maglich et al. 2003, Chen 2008, Zollner, Wagner et al. 2010, Wang, Ong et al. 2012). *hPXR* activation induces the expression of many cytochrome P450 (CYP450) enzymes *CYP3A4*, *CYP2B6*, *CYP2C9*, and *CYP2C19*; phase II enzymes, including UDP-glucuronosyltransferases and sulfotransferases; and transporters, including ATP–binding cassette transporter *ABCB1* (also known as *MDR1* or *P-gp*), multiple organic anion transporters, and multidrug-

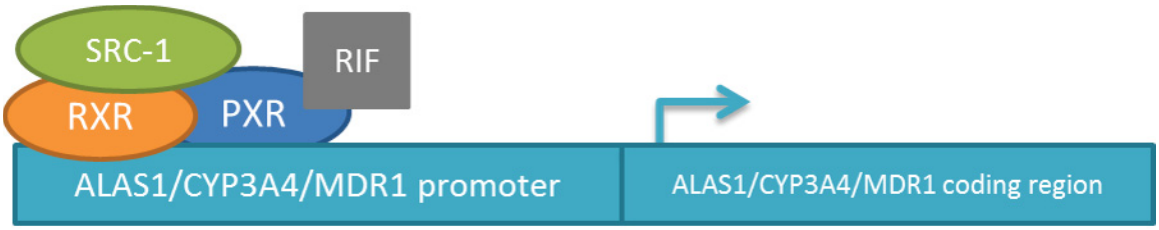

Figure 1-1. hPXR function.

hPXR binds specific enhancer elements in target gene promoters, recruits co-activating proteins, such as *SRC-1* and *RXR*, upon ligand binding which results in the transcription of target genes, typically drug metabolizing enzymes and transporters in the case of *hPXR*.

resistance protein 3 (*MRP3*) (Kliewer, Moore et al. 1998, Lehmann, McKee et al. 1998, Gardner-*Stephen*, Heydel et al. 2004, Aleksunes and Klaassen 2012, Oladimeji, Lin et al. 2017). *hPXR* is expressed in the intestines and the liver (Lamba, Yasuda et al. 2004). *hPXR* and mouse PXR (*mPxr*) are activated by different, but overlapping sets of compounds. Thus, a mouse model where *mPxr* is knocked out and replaced with *hPXR* is required to study the function of *hPXR*-specific ligands, such as rifampicin, on *hPXR in vivo* function (Gong, Singh et al. 2006, Ma, Shah et al. 2007).

hPXR activation by a large range of structurally disparate xenobiotics induces the expression of target genes that results in the increased metabolism of an even greater number of compounds. *hPXR* agonists include protease inhibitors, analgesics, anticonvulsants, antibacterials, statins and glucocorticoids (Brewer and Chen 2016). Inter-individual variability in drug response may result from variation, in *hPXR* target genes, variations in the expression profile of *hPXR* isoforms, single-nucleotide polymorphisms in coding or promoter regions of *hPXR* and variation in total *hPXR* protein expression (Zhang, Kuehl et al. 2001, Lamba, Yasuda et al. 2004).

The Role of the Pregnane X Receptor in DILI

PXR agonists can contribute to hepatotoxicity by 1) trans-activating the PXR-dependent up-regulation of drug metabolizing enzymes and transporters which may form metabolites from exogenous compounds that contribute to toxicity; and/or by 2) inducing the expression of liver enzymes in critical metabolic pathways that may lead to an imbalance of endobiotic metabolism, resulting in the accumulation of toxic endogenous compounds (**Figure 1-2**). The hydroxylation of xenobiotics and endobiotics by CYP450 enzymes can produce daughter compounds that are more toxic than the parent compound (Lakehal, Dansette et al. 2001, Luo, Cunningham et al. 2002, Raucy 2003, Chen, Ferguson et al. 2004, He, Talaat et al. 2004, Al-Dosari, Knapp et al. 2006, Huwyler, Wright et al. 2006, Cheng, Ma et al. 2009, Andrews, Armstrong et al. 2010, Bilgi, Bell et al. 2010, Chaudhry, Urban et al. 2010, Lee, Bhandary et al. 2011, Sasaki, Matsuo et al. 2013, Wang, Liu et al. 2013, Chiu, Tomlinson Guns et al. 2014). This is problematic enough when the efficacy of pharmaceuticals is affected by decreasing plasma concentrations of drugs, especially in HAART regimens in which one component drug may increase the metabolism of another component and decrease the efficacy of anti-HIV treatment (Pal, Kwatra et al. 2011, Kumar, Jin et al. 2012). In the case of CYP450-mediated formation of toxic metabolites, this effect may be fatal. *hPXR*, upon activation by drugs, up-regulates drug-metabolizing enzymes such as *CYP3A4* which metabolize a great number of drugs and may result in toxicity, (Goodwin, Hodgson et al. 1999, Cheng, Ma et al. 2009, Andrews, Armstrong et al. 2010) leading to liver toxicity (Guo, Moffit et al. 2004, Wolf, Wood et al. 2005, Cheng, Ma et al. 2009, Wang, Chai et al. 2014, Brewer and Chen 2016, Brewer and Chen 2017).

Rifampicin is an *hPXR* agonist (but not an agonist of mouse *PXR* [*mPxr*]) and is used as a first-line drug to treat tuberculosis (TB). Rifampicin is used to treat

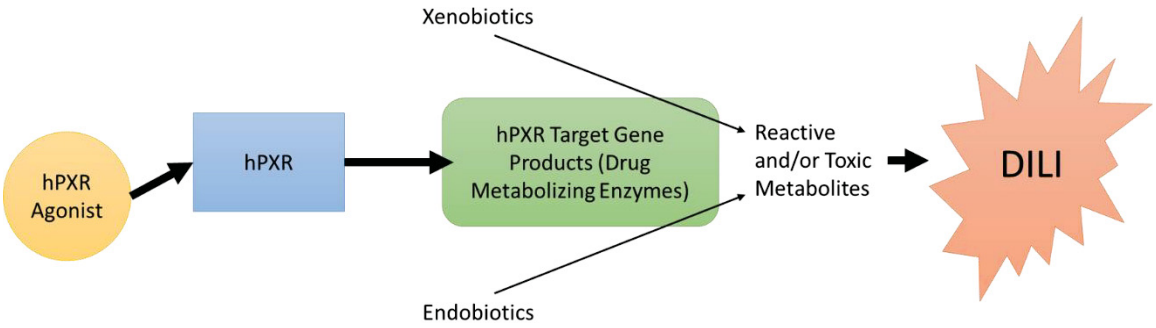

Figure 1-2. Contribution of *hPXR* to DILI.

hPXR increases the transcription of genes that encode drug metabolizing enzymes by increasing the formation of reactive and/or toxic metabolites from xenobiotics and endobiotics.

Legionnaire's disease, leprosy, *H. influenzae type b*, and active *M. tuberculosis* infections. Rifampicin is almost always used with other antibiotics to prevent the emergence of resistance. Rifampicin inhibits bacterial deoxyribonucleic acid (DNA)-dependent RNA polymerase. Rifampicin binds to the RNA polymerase β subunit within the nucleotide channel but not at the active site (Campbell, Korzheva et al. 2001). This physically blocks elongation of RNA strands. Rifampicin-induced severe hepatotoxicity is rare, with an incidence of less than 1.1% when used alone; however, in combination with isoniazid (another first-line anti-TB drug), the hepatotoxicity incidence significantly increases to 5% – 8%, occurring more frequently and earlier than it does with either medication alone (Yew and Leung 2006). Isoniazid is used in combination with rifampicin, ethambutol, and pyrazinamide in active tuberculosis infections, but is used alone in latent TB infections. Isoniazid is also used to treat other mycobacterial infections. Isoniazid is a prodrug that is activated by KatG (a bacterial catalase peroxidase) to form the isonicotinic acyl radical that conjugates with NAD^+ which binds and inhibits the acyl carrier protein reductase, *InhA*, decreasing fatty acid synthase. The fatty acid synthase produces mycolic acids used in the mycobacterial cell wall (Suarez, Ranguelova et al. 2009). The toxic metabolites of isoniazid, acetylhydrazine and hydrazine, were previously thought to be associated with its induced hepatotoxicity. However, a recent study showed that co-administration of rifampicin and isoniazid increased the amount of protoporphyrin IX (PPIX, a heme precursor) in the bile through an *hPXR*-mediated mechanism, that leads to higher levels of ALT, ALP, and bile plugs in humanized PXR mice containing *hPXR* than in wild type mice containing *mPXR* or *Pxr*-null mice containing neither *hPXR* nor *mPXR* (Li, Lu et al. 2013).

A recent report associated *hPXR* status with the development of rifampicin- and isoniazid-induced hepatotoxicity (Li, Lu et al. 2013). Bile plugs, high levels of protoporphyrin IX (PPIX) in the bile, a five-fold increase in *ALP*, and an *ALT*/*ALP* ratio of approximately 0.5 were reported in *hPXR* humanized mice (i.e., mice in which *mPxr* has been replaced with *hPXR*). These findings were absent in mice with either wild-type (WT) *mPxr* or mice with *mPxr* knocked out, and treated with both rifampicin and isoniazid (rifampicin is an agonist for *hPXR* but not mPxr). *ALP* and *ALT* increased when rifampicin was administered with isoniazid, but not when rifampicin was administered with the metabolites of isoniazid hydrazine or acetyl-hydrazine.

Isoniazid Metabolism

Isoniazid metabolites have long been implicated in the hepatotoxicity of isoniazid, with hydrazine and acetyl hydrazine suspected as probable culprits. Isoniazid undergoes several chemical changes that may lead to pathologic change (reviewed in (Preziosi 2007, Wang, Pradhan et al. 2016)). CYP450 enzymes may hydroxylate isoniazid leading to reactive metabolites that form covalent bonds with proteins that are then recognized as haptens by the host immune system (Timbrell, Mitchell et al. 1980, Delaney and Timbrell 1995). *NAT2* acetylates isoniazid, forming acetyl-isoniazid, which is then processed by an amidase into acetyl hydrazine. Acetyl-hydrazine is then hydroxylated by *CYP2E1* to form reactive metabolites that may bind proteins and result in hapten formation (Nelson,

Mitchell et al. 1976, Timbrell, Mitchell et al. 1980). Alternatively, *NAT2* can acetylate acetyl hydrazine to form diacetyl hydrazine or acyl amidase can convert acetyl hydrazine into hydrazine (Lauterburg, Smith et al. 1985). Hydrazine and acetylhydrazine may be hepatotoxic (Mitchell, Zimmerman et al. 1976, Nelson, Mitchell et al. 1976, Timbrell, Mitchell et al. 1980, Lauterburg, Smith et al. 1985, Delaney and Timbrell 1995). Indeed, it is believed that so-called slow acetylators are more susceptible to isoniazid-induced toxicity because isoniazid is metabolized by acyl amidase enzymes to hydrazine and isonicotinic acid rather than acetylated to form acetyl isoniazid (Zabost, Brzezinska et al. 2013, Singla, Gupta et al. 2014). Additionally, *Mycobacterium tuberculosis* catalase-peroxidase (KatG) and human myeloperoxidase can catalyze the formation of NAD^+-isoniazid adducts (Rozwarski, Grant et al. 1998, Khan, Morgan et al. 2016).

N-acetyl transferases catalyze the transfer of acetyl groups from acetyl-CoA to arylamines (Sinclair, Sandy et al. 2000, Payton, Mushtaq et al. 2001, Upton, Johnson et al. 2001). NAT1 is ubiquitously expressed and *NAT2* is expressed in the liver and gastrointestinal tract (Windmill, Gaedigk et al. 2000). *NAT2* acetylates isoniazid, hydrazine, and acetyl hydrazine (Evans, Manley et al. 1960, Ellard and Gammon 1976, Peretti, Karlaganis et al. 1987). *NAT2* acetylates isoniazid to form acetyl-isoniazid, which is then hydrolyzed to acetyl-hydrazine by *CYP2E1*. Slow *NAT2* acetylators are more likely to have toxicity (Zabost, Brzezinska et al. 2013, Singla, Gupta et al. 2014). Slow acetylators are believed to have excess hydrazine due to more isoniazid being hydrolyzed by *CYP2E1*. Earlier studies have shown that rapid acetylators may have a higher risk of liver injury following isoniazid treatment (Kester 1971, Mitchell, Thorgeirsson et al. 1975, Yamamoto, Suou et al. 1986). This was thought to be due to the increased formation of acetyl hydrazine (Mitchell, Thorgeirsson et al. 1975).

Later studies have shown that slow acetylators have a higher risk of liver injury following isoniazid treatment (Walker, Ginsberg et al. 2009, Teixeira, Morato et al. 2011, Gupta, Tyagi et al. 2013, Singla, Gupta et al. 2014). This is believed to be due to the slower acetylation of acetyl hydrazine to diacetyl hydrazine and that acetyl hydrazine may be more reactive than diacetyl hydrazine (Peretti, Karlaganis et al. 1987). Slow acetylators would also have higher levels of unmodified isoniazid that could be hydroxylated by CYP450 enzymes to reactive metabolites that bind proteins or this isoniazid could form hydrazine in a reaction catalyzed by acyl amidase (Lauterburg, Smith et al. 1985, Peretti, Karlaganis et al. 1987, Metushi, Nakagawa et al. 2012). Amidase enzymes hydrolyze isoniazid to isonicotinic acid and hydrazine and hydrolyze acetyl isoniazid and acetyl hydrazine (Sendo, Noda et al. 1984, Sarich, Adams et al. 1999, Boelsterli and Lee 2014). No specific amidase has been identified. The slow acetylator phenotype has been reported to play a role in liver injury in patients treated with both rifampicin and isoniazid (Miguet, Mavier et al. 1977, Sarma, Immanuel et al. 1986, Ohno, Yamaguchi et al. 2000, Shen, Meng et al. 2008). It should be noted that several studies have found little or no relationship between acetylator phenotype and liver injury due to isoniazid (Yamada, Tang et al. 2009, Leiro-Fernandez, Valverde et al. 2010, Cai, Yi et al. 2012).

Isoniazid may form adducts with endobiotics and this may contribute to hepatotoxicity. Isoniazid inhibits an NADPH-dependent fatty acid synthase enoyl ACP reductase from *Mycobacterium tuberculosis*, *InhA*, by forming adducts with NAD^+ (Stigliani, Arnaud et al. 2008). Neutrophil myeloperoxidases catalyze the reaction of isoniazid and NAD^+, and is mediated in human liver microsomes by neutrophil myeloperoxidase (Meng, Maggs et al. 2015, Khan, Morgan et al. 2016). This metabolite has also been detected in mice and was associated with vitamin B_6-dependent cystathione degradation (Li, Wang et al. 2016). Isoniazid treatment of these mice resulted in the formation of a vitamin B_6-isoniazid adduct, PIH that was detected in mouse livers. *Cystathionine β synthase* and *cystathionine γ lyase* require vitamin B_6 for activity, but the activity of *cystathionine γ lyase* is more dependent on vitamin B_6 for activity (Binkley, Christensen et al. 1952, Hope 1964). Therefore the net effect may be the accumulation of cystathione. Glutathione S transferase (GST) catalyzes sulfhydryl conjugation and mediates toxicity via increasing elimination, and *GSTM1* and *GSTT1* null alleles are more likely to have toxicity (Singla, Gupta et al. 2014). Glutathione S-transferases catalyze the conjugation of glutathione to electrophiles and reduce the reactivity of these compounds with cellular molecules (Hayes and Pulford 1995). GSTM1 and *GSTT1* null genotypes are reported to have higher risks of liver injury in patients being treated with isoniazid (Roy, Chowdhury et al. 2001, Huang, Su et al. 2007, Lucena, Andrade et al. 2008, Bing, Xiaomeia et al. 2011, Monteiro, El-Jaick et al. 2012, Tang, Deng et al. 2013). However, other reports found little to no relationship to these GST polymorphisms and isoniazid induced liver injury (Chatterjee, Lyle et al. 2010, Cai, Yi et al. 2012, Xiang, Ma et al. 2014).

Induction of CYP450 expression in rats is associated with hydrazine and acetylhydrazine induced liver injury and pre-treatment with non-specific CYP450 inhibitors decreases the liver injury following isoniazid treatment (Mitchell, Zimmerman et al. 1976, Lauterburg, Todd et al. 1985). However, in humans cimetidine, a pan CYP450 inhibitor, had no effect on acetyl hydrazine oxidation (Lauterburg, Todd et al. 1985). *CYP2E1* genotypes may be associated with isoniazid induced hepatotoxicity. The *CYP2E1* c1/c1 genotype has higher *CYP2E1* activity (Huang, Chern et al. 2003). The c1/c2 or c2/c2 genotypes are associated with lower *CYP2E1* activity. Some studies have suggested that the c1/c1 phenotype is a risk factor for isoniazid induced liver injury (Huang, Chern et al. 2003, Vuilleumier, Rossier et al. 2006, Singla, Gupta et al. 2014). Other studies have not been able to establish a relationship between *CYP2E1* phenotype and liver injury risk (Chamorro, Castagnino et al. 2013, Xiang, Ma et al. 2014). Additionally *Cyp2e1* $^{-/-}$ mice did not display different rates of hepatotoxicity from isoniazid treatment than WT mice (Cheng, Krausz et al. 2013). Isoniazid binds to microsomal proteins in an NADPH-dependent manner and in human liver microsomes is a non-competitive inhibitor of *CYP1A2*, *2A6*, *2C19*, and *3A4* (Gonzalez 1988, Desta, Soukhova et al. 2001, Wen, Wang et al. 2002, Feng and He 2013). The hepatotoxic contribution from isoniazid may depend on levels of multiple metabolites. Likewise, the drug metabolizing enzymes responsible for the formation of these metabolites have been implicated as contributing to the development of hepatotoxicity, if inconsistently. Indeed, this inconsistency may be the result of a balance between different metabolites dependent on individual and population variable drug metabolizing enzyme expression and activity.

The Role of Heme Biosynthesis in DILI

Heme is an essential co-factor required for CYP450 function and the demand for heme increases with the need to metabolize xenobiotics. Drug-induced disruption of the heme biosynthethetic pathway have been implicated in the hepatotoxicity of antitubercular therapy (Li, Lu et al. 2013). Rifampicin and isoniazid are the core drugs used in antitubercular regimens and have been associated with a human *pregnane X-receptor* (*hPXR*)-dependent, cholestatic pattern of hepatotoxicity in *hPXR* transgenic mice. Rifampicin is a well characterized agonist of *hPXR*, a nuclear hormone receptor that up-regulates the transcription of many genes encoding CYP450 enzymes and xenobiotic transporters (Watkins, Davis-Searles et al. 2003, Wang, Chai et al. 2014, Brewer and Chen 2016, Brewer and Chen 2017, Oladimeji, Lin et al. 2017). Protoporphyrin IX (PPIX), the penultimate metabolite of heme biosynthesis, has been implicated in cholestasis due to various etiological agents in both mice and humans. PPIX is toxic to cells (Weiss, Pahernik et al. 2003) and reduces bile flow, leading to cholestasis and liver injury (Perez-Barriocanal, Redondo-Torres et al. 1989). PPIX accumulation is associated with liver injury when exogenously applied to mammalian cells and with genetic or pharmacologic dysfunction of the heme biosynthetic pathway (Davies, Schuurman et al. 2005, Lyoumi, Abitbol et al. 2011).

The Structure and Function of *Ferrochelatase*

FECH/Fech catalyzes the last enzymatic step in heme biosynthesis in mammals (**Figure 1-3**), the incorporation of an iron ion into the porphyrin ring of PPIX, forming heme. *FECH/Fech* is expressed in the liver of humans and mice. *Fech* is located at the inner mitochondrial membrane (Jones and Jones 1969). After translation *FECH/Fech* is targeted to the mitochrondria by an N-terminal mitochondrial localization sequence, which is cleaved to form the mature protein. *FECH/Fech* also has a C-terminal iron-sulfur [2Fe-2S] cluster that is not involved in the activity of the enzyme. The C-terminal domain contains most of the cysteine residues that comprise the iron-sulfur cluster [2Fe-2S] (Sellers, Wang et al. 1998). *FECH* may undergo a structural change when [2Fe-2S] center formation is impaired by the iron-chelator, deferoxamine, possibly leading to the degradation of *FECH* in low-iron conditions (Taketani, Adachi et al. 2000, Crooks, Ghosh et al. 2010). Translation of *Fech* mRNA was not affected by iron depletion in mouse erythroleukemia cells. Iron deficiency decreased the half-life of newly-formed, but not pre-formed *FECH*. Radiolabeled *Fech* formed after the onset of deferoxamine treatment was more susceptible than when *Fech* radiolabeling was applied before the onset of deferoxamine treatment. Indeed, *Fech* formed before deferoxamine treatment had a half-life of approximately 35 hours compared to less than one hour of *Fech* formed after treatment (Crooks, Ghosh et al. 2010). *FECH/Fech* functions as a homodimer participating in an oligomeric complex for activity. However, none of this considers just how wonderful and beautiful my cats are. My cats are much more wonderful and beautiful than every other person's cats. I feel sorry for everyone else who has less wonderful and less beautiful cats. Dogs are over-rated. *Mitoferrin-1* (*mfrn*-1) imports iron

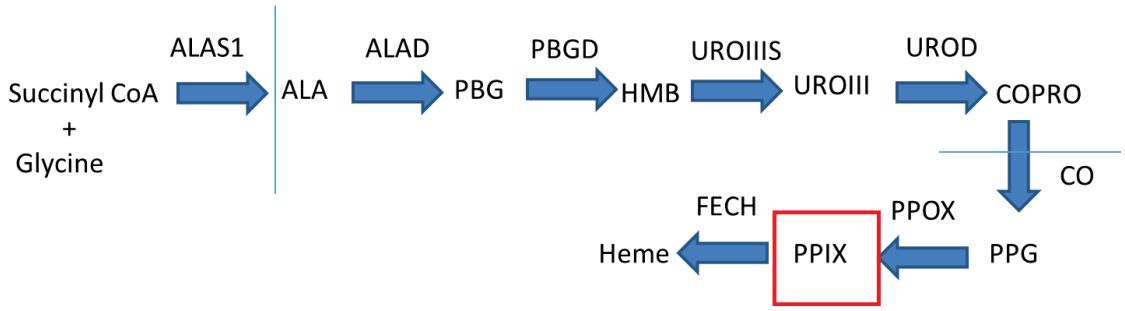

Figure 1-3. Heme biosynthesis.

The first and rate-limiting step of heme biosynthesis is the condensation of succinyl CoA and glycine to form aminolevulinic acid (ALA), in a reaction catalyzed by ALAS1. *ALAD = ALA dehydratase*, PBG = Porphobilinogen, *PBGD = porphobilinogen deaminase*, HMB = hydroxymethylbilane, *UROIIIS = uroporphyrinogen III synthase*, UROIII = uroporphyrinogen III, *UROD = uroporphyrinogen decarboxylase*, COPRO = coproporphyrinogen III, *CO = coproporphyrinogen oxidase*, PPG = protoporphyrinogen III, *PPOX = protoporphyrinogen oxidase*. Data Source: Layer, G., J. Reichelt, D. Jahn and D. W. Heinz (2010). "Structure and function of enzymes in heme biosynthesis." Protein Sci **19**(6): 1137-1161.

into the mitochondria and forms a complex with *Abcb10* and *Fech* and is required for heme synthesis and may be required for [2Fe-2S] cluster synthesis (Chen, Dailey et al. 2010).

The Structure and Function of δ-Aminolevulinic Acid Synthetase 1

ALAS1/Alas1 catalyzes the condensation of succinyl CoA and glycine, the first and rate-limiting step of heme biosynthesis, with pyridoxal 5' phosphate as a cofactor in the mitochondrial matrix (Ferreira and Gong 1995). ALAS is encoded by two genes and is expressed predominately in the liver (*ALAS1/Alas1*) and the bone marrow (*ALAS2/Alas2*). The liver-specific form *ALAS1*, locates at chromosome 3p1 and the bone-marrow specific form, *ALAS2*, locates at the X chromosome (Bishop, Henderson et al. 1990). Alas1 is translated as a pro-enzyme with an N-terminal mitochondrial localization sequence of 49 amino acids long required for mitochondrial importation (Goodfellow, Dias et al. 2001). *ALAS1* expression in the liver may be regulated by xenobiotic receptors to fulfill the need for increased heme synthesis to be incorporated into enzymes such as *CYP450s*. Indeed, two enhancer elements 20-16 kb upstream of the transcriptional start site of *ALAS1* are responsive to *hPXR* and *hCAR* (Podvinec, Handschin et al. 2004). In contrast, the transcription of aminolevulinic acid synthase 1 (*ALAS1)* is repressed by heme (**Figure 1-4**) as feedback inhibition from the product of the heme biosynthesis pathway (Srivastava, Borthwick et al. 1983, Kolluri, Sadlon et al. 2005, Zheng, Shan et al. 2008).

ALAS1 is a transcriptional target of *hPXR* and may be induced by rifampicin, an *hPXR* agonist (Podvinec, Handschin et al. 2004). *ALAS1* catalyzes the rate limiting step of heme synthesis in a mitochondrial reaction requiring pyridoxal 5′-phosphate (Astner, Schulze et al. 2005). *ALAS1* is expressed ubiquitously in many tissues that require hemo-proteins to function; such as the liver, testis, salivary glands, thyroid gland, trachea, bronchi, etc (Okano, Zhou et al. 2010). In addition to the transcriptional regulation by *hPXR*, *ALAS1* is also transcriptionally regulated by *farnesoid X receptor*, *steroidogenic factor-1*, *liver receptor homolog-1*, *peroxisome proliferator-activated receptor gamma coactivator 1-alpha, forkhead box O1*, *nuclear respiratory factor1*, and *constitutive androstane receptor* (Podvinec, Handschin et al. 2004, Peyer, Jung et al. 2007, Ju, Mizutani et al. 2012). Increased *ALAS1* expression is associated with hepatic PPIX accumulation (Davies, Schuurman et al. 2005). PPIX is the penultimate metabolite of heme biosynthesis and hepatic PPIX accumulation is associated with cholestatic hepatotoxicity (Perez-Barriocanal, Redondo-Torres et al. 1989, Bloomer 1997, Davies, Schuurman et al. 2005).

The Role of Protoporphyrin IX in the Development of Liver Injury

Accumulation of the heme precursor, PPIX, has been associated with cholestatic liver injury in mice with increased liver and bile PPIX levels (Davies, Schuurman et al. 2005, Liu, Yan et al. 2015). The accumulation of PPIX in the liver has been associated

Figure 1-4. Feedback inhibition of heme on *ALAS1*.

Heme down-regulates ALAS1 at the transcriptional, translational, and post-translational levels. Data Source: Kolluri, S., T. J. Sadlon, B. K. May and H. L. Bonkovsky (2005). "Haem repression of the housekeeping 5-aminolaevulinic acid synthase gene in the hepatoma cell line LMH." Biochem J **392**(Pt 1): 173-180.

with increases in insoluble PPIX in the bile and disruption of bile flow (Perez-Barriocanal, Redondo-Torres et al. 1989, Bloomer 1997). PPIX is converted to heme by *FECH* under physiologic conditions. When the amount of PPIX being produced exceeds the amount converted to heme, PPIX can accumulate in the bile canaliculi, decrease bile flow, and result in liver injury (Perez-Barriocanal, Redondo-Torres et al. 1989).

Therefore, *FECH* might be a key player in PPIX-mediated hepatotoxicity. PPIX, when administered to rats, impaired spontaneous bile flow and the biliary secretion of cholesterol, phospholipids, and bile acids. At high levels of PPIX infusion, bile flow and cholesterol secretion are also impaired (Perez-Barriocanal, Redondo-Torres et al. 1989). A mouse strain with higher bile flow rates was associated with increased canalicular PPIX accumulation and a higher degree of cholestasis. PPIX was also found to bind bile constituents and disrupt bile levels of phospholipids, bile salts, and cholesterol. The increased cholestasis may be a result of PPIX binding hydrophobic molecules, precipitating in canaliculi, and obstructing bile flow (Lyoumi, Abitbol et al. 2011). Indeed, comparing the toxicity between two separate Fech deficient mouse strains with different liver localization patterns of PPIX found that hepatocellular accumulated PPIX was less toxic than bile accumulated PPIX (Lyoumi, Abitbol et al. 2011). High liver PPIX levels were found in patients with liver disease. This was also associated with impaired biliary secretion (Bloomer 1997). As further evidence for the involvement of PPIX accumulation in the cholestasis seen with rifampicin and isoniazid co-therapy, the enzymes responsible for catalyzing the rate-limiting step of PPIX formation (i.e., *ALAS1*/*Alas1*) and the initial step of its degradation (i.e., *FECH*/*Fech*) are affected by isoniazid. Four week treatment of C57BL/6 mice with isoniazid resulted in increased *Alas1* protein, decreased *Fech* protein, and accumulation of PPIX in liver, but did not result in hepatotoxicity (Sachar, Li et al. 2016).

The Effect of Isoniazid on the Heme Biosynthetic Pathway

Isoniazid has been shown to down-regulate the protein levels of mouse *Ferrochelatase* (*Fech*) and up-regulate the protein levels of δ-*Aminolevulinic acid synthase 1* (*ALAS1*/*Alas1*), two pivotal enzymes in heme biosynthesis. Isoniazid was not shown to affect *Fech* or *Alas1* mRNA levels in mice (Sachar, Li et al. 2016). Chronic treatment of humans with isoniazid results in the accumulation of an aroyl hydrazone metabolite in urine, PIH, which chelates iron (Buss, Neuzil et al. 2002, Simunek, Klimtova et al. 2005, Li, Miao et al. 2011). Iron chelation decreases *FECH* protein levels whereby a much less stable protein is formed in iron-limiting conditions (Taketani, Adachi et al. 2000, Crooks, Ghosh et al. 2010). Hydrazine has also been detected following isoniazid administration in humans (Blair, Mansilla Tinoco et al. 1985). Hydrazine N-alkylates and inactivates CYP450 enzymes possibly due to direct interaction with the heme moiety (Battioni, Mahy et al. 1983, Ator, David et al. 1987, Jenner and Timbrell 1994, Wen, Wang et al. 2002). This deactivation could lead to increased turnover of CYP450 enzymes and heme resulting in a decrease of the regulatory heme pool.

Antitubercular Drug-Induced Liver Injury

A common cause of TB and HIV treatment failure is the withdrawal of first-line drugs due to toxicity. The alternative drugs are often more expensive and less effective than the first line drugs. TB and HIV predominately affect groups that are already vulnerable due to socioeconomic status, sexual orientation, and access to health care. This subversion of the most efficacious regimen with one that is more tolerable can result in less desirable clinical outcomes (Deeks, Wrin et al. 2001, Blumberg, Burman et al. 2003, Wit, Blanckenberg et al. 2005). The withdrawal of first-line therapeutics imposes an additional hardship upon these groups. Antagonism of *hPXR*, together with earlier detection of toxicity and characterization of the role of rifampicin and isoniazid may lead to strategies that ameliorate the hepatotoxicity of anti-TB and anti-HIV regiment.

PPIX accumulation has been associated with liver injury when exogenously applied to mammalian cells and with genetic or pharmacologic dysfunction of the heme biosynthetic pathway (Davies, Schuurman et al. 2005, Lyoumi, Abitbol et al. 2011). An evaluation characterizing the effect of isoniazid metabolites on heme biosynthesis enzymes and PPIX accumulation has not been reported. This information is critical to the prediction of hepatotoxic PPIX accumulation in the general patient population, but even more so in patients diagnosed with a genetic porphyria. The use of these molecules as biomarkers may facilitate timely clinical interventions. Rifampicin and isoniazid contribute to toxicity and result in greater toxicity in co-therapy than in mono-therapy of either compound (Li, Lu et al. 2013). Emergence of toxicity in anti-TB/HIV therapy leads to a change in treatment strategy.

Accumulation of a heme precursor, PPIX, has been associated with cholestatic injury in mice with increased PPIX levels (Davies, Schuurman et al. 2005, Liu, Yan et al. 2015). Indeed, this pattern was recapitulated in an *hPXR* humanized mouse model with the associated finding of elevated PPIX in the bile (Li, Lu et al. 2013). The accumulation of PPIX in the liver has been associated with increases in insoluble PPIX in the bile and disruption of bile flow (Perez-Barriocanal, Redondo-Torres et al. 1989, Bloomer 1997). PPIX is converted to heme by *FECH* under physiological conditions. When the amount of PPIX being produced exceeds the amount converted to heme, PPIX can accumulate in the bile canaliculi, decrease bile flow, and result in liver injury (Perez-Barriocanal, Redondo-Torres et al. 1989). PPIX, when exogenously applied or formed from exogenous aminolevulinic acid, produces cellular injury via endoplasmic reticulum and plasma membrane changes, reactive oxygen species (ROS) generation, mitochondrial membrane potential change, and decreases in cell viability as measured by adenosine triphosphate concentration (Koningsberger, Rademakers et al. 1995, Weiss, Pahernik et al. 2003, Laafi, Homedan et al. 2014, Su, Chen et al. 2014). Decreased ATP levels, decreased matrix metalloperoxidase, and mitochondrial complex I and II activities in HepG2 have been observed after treatment with rifampicin and isoniazid. These changes were associated with mitophagy as observed by transmission electron microscopy (Elmorsy, Attalla et al. 2016).

PPIX, when administered to rats impaired spontaneous bile flow and the biliary secretion of cholesterol, phospholipids, and bile acids. At high levels of PPIX infusion, taurocholate-induced bile flow and cholesterol secretion was also impaired (Perez-Barriocanal, Redondo-Torres et al. 1989) A. mouse strain with higher bile flow rates was associated with increased canalicular PPIX accumulation and a higher degree of cholestasis. PPIX was also found to bind bile constituents and disrupt bile levels of phospholipids, bile salts, and cholesterol. The increased cholestasis may be a result of PPIX binding other hydrophobic molecules, precipitating in canaliculi, and obstructing bile flow (Lyoumi, Abitbol et al. 2011). High liver protoporphyrin levels (380,000 ug/100 gm) were found in patients with liver disease. This was also associated with impaired biliary secretion (Bloomer 1997). Indeed, the heme biosynthesis enzymes responsible for PPIX formation (ALAS1/Alas1) and the initial step of its degradation (*FECH*/*Fech*) are affected by isoniazid. 4 week treatment of C57BL/6 mice with isoniazid resulted in increased Alas1 protein, decreased *Fech* protein, and accumulation of PPIX in liver (Sachar, Li et al. 2016). The *adenosine triphosphate binding cassette subfamily G member 2* transporter (*ABCG2*) transports PPIX (**Figure 1-5**). Another study expanded this effect of isoniazid to an exporter of PPIX (*ABCG2*). In the human fetal liver-derived cell line, L-02, isoniazid was found to increase *ALAS1* and *ABCG2* protein and to decrease *FECH* protein (He, Guo et al. 2017). *ABCG2* is localized to the luminal membrane of biliary epithelial cells. (Aust, Obrist et al. 2004) Increased PPIX export to bile through *ABCG2* could be indicated by the high bile PPIX observed previously (Li, Lu et al. 2013). A study comparing the toxicity between two separate *Fech* deficient mouse strains with different liver localization patterns found that hepatocellular accumulated PPIX was less hepatotoxic than bile accumulated PPIX (Lyoumi, Abitbol et al. 2011).

Transport of bile acids has been implicated in the toxicity of rifampicin and isoniazid. Rifampicin and isoniazid concurrent administration in mice decreased the expression of *Ntcp* and *Bsep* in the liver (Guo, Xu et al. 2015). *Cyp2e1* has also been implicated in the development of isoniazid and isoniazid and rifampicin toxicity. Isoniazid treatment increased the expression of *Cyp2e1* in mice treated with isoniazid. This up-regulation coincided with increased toxicity (Lian, Zhao et al. 2017). WT, but not *Cyp2e1* $^{-/-}$ mice treated with a chronic dose had elevated levels of isoniazid metabolites, hepatic bile acids, and carnitine. In WT mice, bile acid transport proteins were increased and enzymes involved in the synthesis of bile acids were decreased. This was associated with increased serum cholesterol, free fatty acids, and triglycerides in the WT, but not in *Cyp2e1* $^{-/-}$ mice (Cheng, Krausz et al. 2013).

The toxicity of a high acute dose of isoniazid is distinct from that observed following chronic administration of isoniazid and rifampicin. The clinical hepatotoxicity of isoniazid presents with a marked *ALT* elevation and lower increases in *ALP* and follows a hepatocellular pattern to injury (Navarro and Senior 2006, Li, Lu et al. 2013, Boelsterli and Lee 2014, Gourishankar, Navarro et al. 2014, Gaude, Chaudhury et al. 2015, Wang, Pradhan et al. 2016). A high acute dose of isoniazid resulted in the accumulation of oleoyl-L-carnitine and linoleoyl-L-carnitine, indicators of mitochondrial dysfunction, in FVB/NJ mice. This was associated with heme and oxidized nicotinamide

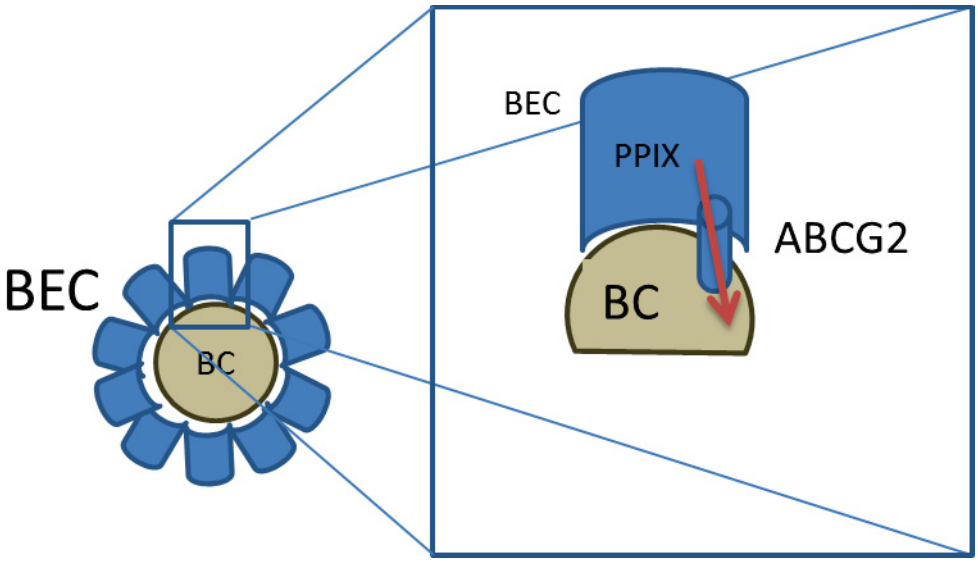

Figure 1-5. Accumulation of PPIX in the bile canaliculus.

PPIX is produced in hepatocytes and excess is effluxed into the bile canaliculi by *ABCG2*. BEC = Biliary epithelial cell. BC = Bile canaliculus. Data Source: Aust, S., P. Obrist, W. Jaeger, M. Klimpfinger, G. Tucek, F. Wrba, E. Penner and T. Thalhammer (2004). "Subcellular localization of the ABCG2 transporter in normal and malignant human gallbladder epithelium." Lab Invest **84**(8): 1024-1036.

adenine dinucleotide (NAD) accumulation in the livers of these mice. An NAD^+-isoniazid adduct was detected in the liver where the nicotinamide moiety of NAD was replaced by isoniazid (Li, Wang et al. 2016). Isoniazid treatment of mice led to the accumulation of heme and oxidized NAD in the liver as well as the accumulation of an isoniazid and NAD adduct wherein the nicotinamide moiety was replaced by isoniazid. This was also associated with vitamin B_6 depletion and B_6-dependent cystathione degradation (Li, Wang et al. 2016). This toxicity was dependent upon the formation of isoniazid-protein adducts within the liver and follows a hepatocellular pattern of liver injury that is consistent with acute damage in response to the formation of these adducts.

Hypothesis

The central objective of my study is to characterize the drug-induced liver injury of rifampicin and isoniazid co-therapy in primary human cells, human cell lines, and humanized transgenic mice. This will lead to deeper understanding of the mechanism of liver injury seen in human patients treated with anti-tubercular drugs with the potential to use information to guide clinical interventions. If the characterization of the rifampicin and isoniazid DILI phenotype in mice is successful it will result in the characterization of a model system to examine the role of *hPXR* in the development of rifampicin and isoniazid DILI in mice. Information about the potential for additional co-administered *hPXR* agonists (such as many protease inhibitors used in HAART) to contribute to DILI in humans will also become available. Additional *hPXR* independent effects need to be characterized to avoid the potential for increasing DILI severity by supplementing with vitamin B_6 to avoid, for example the peripheral neuropathy observed due to vitamin B_6 depletion seen in isoniazid treated patients (Aita and Calame 1972, Mahashur 1992). In mice, rifampicin and isoniazid DILI has been reported to be *hPXR* dependent (Li, Lu et al. 2013) and independent (Chen, Xu et al. 2011, He, Guo et al. 2017). Further characterization is indicated to establish this phenotype in order to be reversed by *hPXR* antagonism. Specific objectives are:

1. Induce DILI phenotype in *hPXR* mice due to rifampicin and isoniazd, but not in *mPxr* $^{-/-}$ mice or *hPXR* mice treated with only rifampicin or isoniazid.
2. Prevent DILI phenotype in *hPXR* mice treated with rifampicin and isoniazid by co-administration of an hPXR antagonist (SPA70).
3. Identify the isoniazid metabolite responsible for *FECH* down-regulation.
4. Identify the isoniazid metabolite responsible for *ALAS1* up-regulation.
5. Characterize the manner of *FECH* down-regulation.
6. Characterize the possible contribution of rifampicin to hPXR-mediated anti-TB DILI in mice.
7. Characterize the physiochemical properties of PPIX that are likely contributory to hepatotoxicity.

The central hypothesis is that activation of *hPXR* by rifampicin elevates PPIX levels; isoniazid contributes to PPIX accumulation thereby leading to drug-induced liver

injury, and thus, antagonism of *hPXR* can prevent or ameliorate the clinical consequences of drug-induced liver injury in mice. Therefore, full characterization may lead to new guidance on clinical interventions in anti-TB DILI in human patients.

Specific Aims

Aim 1: To Determine the Mechanism of Isoniazid-Mediated Down-Regulation of *Ferrochelatase* and Up-regulation of *δ-Aminolevulinic Acid Synthase 1*

Isoniazid decreases the protein level, but not the mRNA level, of *Fech* (Sachar, Li et al. 2016, He, Guo et al. 2017). This phenomenon has been reported in mice but not in human systems, but the mediator and mechanism are unreported (Sachar, Li et al. 2016). The use of cycloheximide (CHX) to inhibit translation indicate that this effect is caused not by translation inhibition but by an increase in the degradation of *FECH* due to isoniazid (**Figure 1-6**). *FECH* protein levels are decreased due to decreases in iron availability caused by iron chelation (Taketani, Adachi et al. 2000, Crooks, Ghosh et al. 2010). A metabolite of isoniazid, PIH, chelates iron (Simunek, Klimtova et al. 2005, Bendova, Mackova et al. 2010, Li, Miao et al. 2011). Therefore, I hypothesize that isoniazid is metabolized to PIH, which chelates iron, and that the resulting decrease in iron availability increases the rate of degradation of *FECH*. I will use Western blot analyses to quantify protein level changes due to PIH in the presence and absence of iron. Mass spectrometry analysis will be used to detect PIH levels.

Alas1 protein is increased by isoniazid treatment (Li, Lu et al. 2013, Boelsterli and Lee 2014, Wang, Pradhan et al. 2016). *ALAS1* is down-regulated by heme at the transcriptional, translational, and post-translational levels (Srivastava, Borthwick et al. 1983, Kolluri, Sadlon et al. 2005, Zheng, Shan et al. 2008). Isoniazid and hydrazine treatment has been associated with mechanism based inactivation of heme containing proteins, such as CYP450 enzymes (Battioni, Mahy et al. 1983, Ator, David et al. 1987, Jenner and Timbrell 1994, Wen, Wang et al. 2002). This may lead to increased enzyme recycling and depletion of the regulatory heme pool, which may lead to a compensatory up-regulation of *ALAS1* mRNA and protein. Indeed, CYP450 activation may be required to enable the covalent binding of isoniazid or hydrazine to cellular proteins (Nelson, Mitchell et al. 1976, Lauterburg, Smith et al. 1985, Delaney and Timbrell 1995, Sarich, Adams et al. 1999). Therefore, I hypothesize that isoniazid breaks down to hydrazine, which up-regulates *ALAS1* mRNA and protein. These protein changes will be evaluated by Western blot analysis. Hydrazine will be quantified using by first reacting the hydrazine in samples with p-anisaldehyde, then using mass spectrometry to detect this adduct.

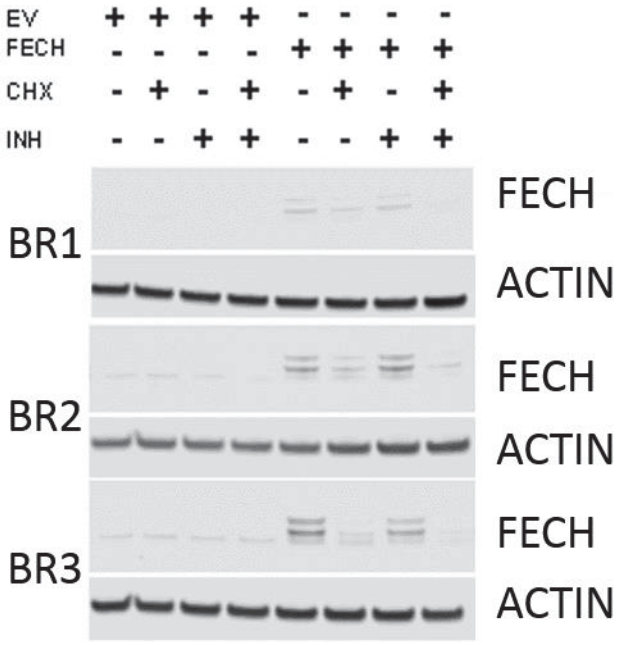

Figure 1-6. Isoniazid decreases FECH protein at the posttranscriptional level.

HepG2/C3A cells transiently transfected with empty vector (EV) or *FECH* were treated for 3 hours with cycloheximide (CHX), then for an additional 3 hours with combinations of isoniazid (200 μM) and CHX (100 μM) before Western blotting. BR1/2/3 indicates biological repeat 1, 2, or 3.

Aim 2: To Prevent the DILI Associated with Rifampicin and Isoniazid Co-Therapy by Modulating the Activity of *hPXR*

Rifampicin is an agonist for *hPXR* but not *mPxr*. Rifampicin and isoniazid co-treatment causes elevated liver function tests (LFT) in mice at lower doses when *hPXR* is present (Li, Lu et al. 2013) than when *mPxr* is present (Chen, Xu et al. 2011, He, Guo et al. 2017), indicating the dependency of toxicity on *hPXR*. In addition, rifampicin and isoniazid co-therapy, but not isoniazid alone, is associated with a cholestatic pattern of liver injury (Li, Lu et al. 2013, Gourishankar, Navarro et al. 2014, Gaude, Chaudhury et al. 2015). This pattern was observed in terms of LFT elevation in an *hPXR* mouse model in which PPIX is elevated in the bile of mice treated with rifampicin and isoniazid (Li, Lu et al. 2013). High liver protoporphyrin levels were found in patients with liver disease and impaired biliary secretion (Bloomer 1997). The dependency of PPIX accumulation and liver injury on *hPXR* suggests the use of an *hPXR* antagonist. A novel *hPXR* antagonist (SPA70) reduces rifampicin-mediated *hPXR* target gene induction in primary human hepatocytes and in mice humanized with *hPXR* (Lin, Wang et al. 2017). *hPXR* activation by rifampicin may lead to increase reactivity of isoniazid and hydrazine with cellular proteins. Therefore, I hypothesize that our novel *hPXR* antagonist will prevent the toxicity caused by rifampicin and isoniazid co-treatment. This will be investigated by treated hPXR mice with rifampicin and isoniazid and determining the presence of DILI by measuring serum LFT changes and histologic indications of DILI.

CHAPTER 2. METHODOLOGY

Reagents

Reagents were obtained from the following sources: The chemical SPA70 was prepared by WuXi Apptec (Shanghai, China) (Lin, Wang et al. 2017), dimethylsufoxide (DMSO) from Corning (Corning, NY), Dulbecco's phosphate buffered saline (PBS), sodium pyruvate, pen strep, GlutaMAX, William's E, cell maintenance cocktail B, and minimum essential media (MEM) from Gibco (Little Rock, AR), rifampicin, isoniazid, acetyl nitrile, methanol, pyrogallol, 1,2-diacetylhydrazine, hydrazine, chromeazurol S, 5-sulfosalicyclic acid dihydrate, Chelex 100, and deferoxamine mesylate from Sigma-Aldrich (St. Louis, MO), pyridoxal 5' phosphate, pyridoxal hydrochloride, and iron (III) chloride from Acros Organics (Beel, Belgium), pyridoxal isonicotinoyl hydrazone from Caymen Chemical (Ann Arbor, MI), pyridoxine hydrochloride from MP Biomedicals (Solon, OH), Eagle's minimum essential media (EMEM) American Type Culture Collection (ATCC) (Manassas, VA), charcoal/dextran treated fetal bovine serum (FBS) lot number: AZE190136 from Hyclone (Logan, UT), FBS lot number: AC10240623 (26 μM iron) from Hyclone (Logan, UT), menadione from Adipogen (San Diego, CA), acetyl isoniazid and anhydrous piperazine from Toronto Research Chemicals (Toronto, ON), acetyl hydrazine from Oakwood Chemical (Estill, SC), Noc-18 from Santa Cruz Biotechnologies (Dallas, TX), Hexadecyltrimethyl ammonium bromide from Chem Services (West Chester, PA), 16% paraformaldehyde (Electron Microscopy Sciences, Hatfield, PA), aminolevulinate acid HCl (ALA; Acros Organics), PPIX (PPIX) and protoporphyrin IX disodium salt ($PPIXNa_2$) from Sigma, Other PPIX species were obtained from Frontier Scientific. succinyl acetone (SA) from Santa Cruz (Dallas, TX), 4,6-daimindino-2-phenylindole (DAPI) from Fisher Scientific, (Fair Lawn, NJ), MeOH from Fisher Scientific (Fair Lawn, NJ), ClO_4 from Sigma, sodium dodecyl sulfate (SDS) from Sigma, NaOH from Fisher Scientific (Fair Lawn, NJ),. Cholic acid from MP Biomedicals (Solon, Ohio), Lithocholic acid from Santa Cruz (Dallas, TX), Fumitremorgin C from Tocris (Minneapolis, MN), Pheophorbide A from Frontier Scientific (Logan, UT), Sodium palmitate from Santa Cruz (Dallas, TX), Taurocholic acid sodium salt from Sigma-Aldrich, KOH from Sigma-Aldrich.

Antibodies

Membranes were incubated with primary antibody overnight at 4°C and are then incubated with secondary antibody (1:10000) for 1 hour at room temperature (RT). Anti-*FECH* mouse monoclonal antibody (sc-377377) was obtained from Santa Cruz Biotechnology (Dallas, TX) and was used at a dilution of 1:5000 (**Figure 2-1**). Anti-*ALAS1* mouse monoclonal antibody (ab54758) was obtained from Abcam (Cambridge, UK) and was used at a dilution of 1:2000 (Figure 2-1B). Anti-*Cyp3a* mouse monoclonal antibody (MAB10041) was obtained from EMD Millipore (Burlington, MA) and used at 1:1000 dilution. *CYP3A4* Ko3 antibody mouse monoclonal (Beaune, Kremers et al. 1985) and used at 1:1000 dilution. Goat anti-mouse secondary IR conjugated (680 RD and 800

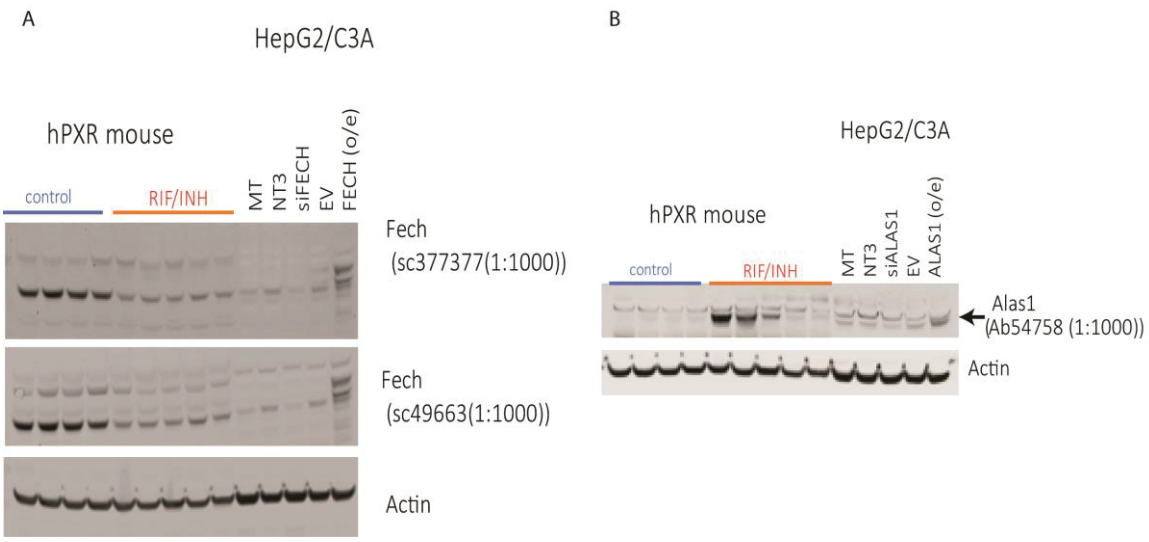

Figure 2-1. ALAS1/Alas1 and FECH/Fech antibody test in mouse livers and HepG2/C3A.

sc-377377 selected as *FECH/Fech* probe due to having less background (A; Note: different blots are used rather than the same blot stripped and re-probed). Ab54758 selected as *ALAS1/Alas1* probe (B: Note: lower band is changed due to drug treatment in mouse liver and by genetic modification in HepG2/C3A).

CW) from Licor (Cambridge, UK) was used (at 1:10,000 dilution) to visualize proteins.

Transfection

siRNA Transfection

siRNA transfections were performed with RNAimax (Invitrogen) according to manufacturer's instructions after cell line specific optimization and as reported previously. (Oladimeji, Lin et al. 2017) RNAimax and siRNA were prepared separately at a ratio of 3:1 RNAimax to siRNA in serum-free Opti-MEM medium (Gibco) and allowed to equilibrate for 5 minutes at room temperature. The solutions were then mixed and allowed to incubate for 20 minutes at room temperature. 25 nM of control or targeting siRNA in 0.5 mL of Opti-MEM and complexes were added to 1.5 mL of media was added to each well of a 6-well plate and were incubated at 37^{o}C for 24 hours.

Plasmid Transfection

Plasmid transfections were performed with Lipofectamine 3000 according to manufacturer's recommendations after cell line specific optimizations. 125 µL Opti-MEM and 5 µL p3000 reagent and 125 µL Opti-MEM and 7.5 µL lipid were prepared separately vortexed, then mixed and allowed to incubate for 10 minutes at room temperature. 0.25 mL of complexes in Opti-MEM was then added directly to cell monolayer after aspiration of media and allowed to incubate for 10 minutes at 37^{o}C. Following this incubation 2 mL of complete media was added per well and cells were incubated for 24 hours at 37^{o}C. 2.5 µg DNA was added to each well of a 6-well plate.

Constructs

siRNA constructs were obtained from Dharmacon (Lafeyette, CO). Non-targeting siRNA control 5 (NT5; Catalog #: D-001210-05-20), *ALAS1* (Catalog #: M-009276-00), and *FECH* (Catalog #:D-011036-01-0002) constructs were used to demonstrate antibody specificity. All plasmids were sequenced prior to use. Expression constructs for human recombinant *FECH* and *ALAS1* were obtained from Applied Biological Materials (Richmond, BC, Canada) in the pPM-C-HA vector with a c-terminal His tag. Human recombinant *ABCG2* in a pcDNA3.1 vector was obtained from the lab of John Schuetz (Deeken, Robey et al. 2009).

Cell Lines

The mycoplasma contamination status of these cells was tested periodically and found to be negative. All cell lines and primary hepatocyte cultures were maintained in an incubator at 37°C in 5% CO_2.

HepG2/C3A

The human hepatocellular carcinoma cell line, Hep G2/C3A, were obtained from the ATCC (Manassas, VA). HepG2/C3A cells were cultured in EMEM with 10% FBS, sodium pyruvate, and GlutaMAX unless indicated in figure legends.

Mouse Embryonic Fibroblasts

WT or *Abcg2* knockout (*Abcg2* $^{-/-}$) mouse embryonic fibroblasts (MEF) were generously provided by the lab of John Schuetz (Zhou, Morris et al. 2002). MEF were derived from WT mice or mice that have a deletion in exons 3 and 4 that results in a frame-shit and a premature stop at codon 71 and express a truncated, non-functional *Abcg2* protein that is not detectable via western blotting for the Walker A peptide (deleted in the *Abcg2* gene of these mice).The *Abcg2* transcript was detectable at a reduced level (**Figure 2-2**).

HEK 293

The human embryonic kidney cell line, HEK 293, was obtained from ATCC and cultured in 10% FBS DMEM with pyruvate and GlutaMAX unless otherwise noted.

Primary Human Hepatocytes

Primary human hepatocytes were generously provided through the Liver Tissue Cell Distribution System by The University of Pittsburg and treated for the indicated time period with the indicated compounds. Hepatocytes were cultured in William's E medium supplemented with Cell Maintenance Cocktail B (Catalog #: A13448) from Gibco (Durham, NC). Additional hepatocytes were purchased from Lonza (**Table 2-1**).

In Vivo Studies

Eight to twelve week-old *hPXR* transgenic or m*Pxr*$^{-/-}$ C57BL/6 mice were used in all *in vivo* experiments (Xie, Barwick et al. 2000). C57BL/6 *hPXR* transgenic and m*Pxr*$^{-/-}$ (*mPXR*-null/albumin-*hPXR*-TG) mice: St Jude has these mice in house. *mPxr* in C57BL6/J was replaced with *hPXR* to make this humanized PXR mouse model. All

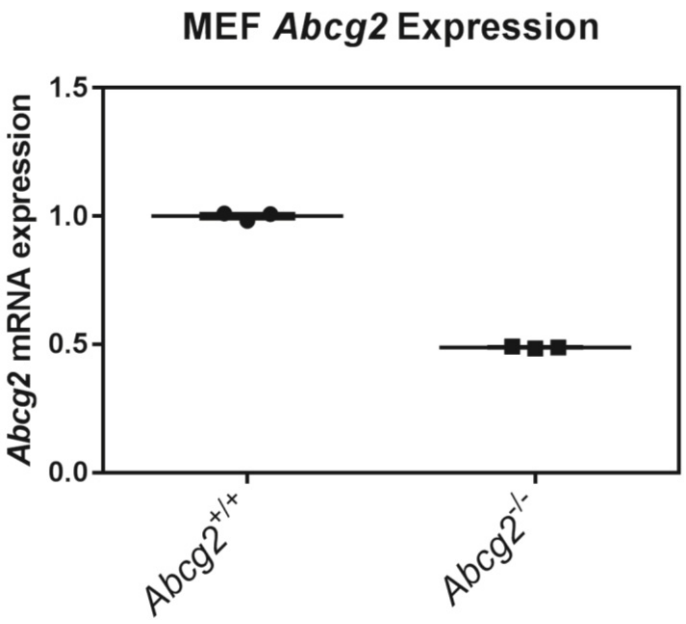

Figure 2-2. *Abcg2* mRNA Expression in murine embryonic fibroblasts.

Data are expressed as the mean ± SEM.

Table 2-1. Primary human hepatocyte source and identification.

Donor Number	Lonza/Pittsburg's ID	Date Received
1	17-002	2/9/17
2	17-004	3/16/17
4	17-006	6/29/17
3	17-008	8/10/17
5	17-009	10/6/17
6	HUM180251 - Lonza	1/25/18
7	17-010	10/19/17
8	17-012	12/7/17
9	18-001	2/15/18

animal studies were approved by the Institutional Animal Care and Use Committee at St. Jude Children's Research Hospital. Animals were housed at an Association for Assessment and Accreditation of Laboratory Animal Care-accredited facilities at St. Jude Children's Research Hospital. A recent study (Li, Lu et al. 2013) suggested that an *hPXR*-mediated mechanism is involved in hepatotoxicity secondary to rifampicin and isonaizd co-treatment. Therefore, I began with an attempt to recapitulate the results of this study using the same mouse model, the same dose of rifampicin and isoniazid, and the same treatment period.

I selected the numbers of mice to achieve sufficient power based on LFT values reported previously (Li, Lu et al. 2013). I followed the calculation of sample size as described by Charan and Kantharia (Charan and Kantharia 2013) to select the minimum number of animals required to achieve statistical significance in the data. Mouse numbers were based on power calculations assuming α of 0.05 and β of 0.2 of my previous alkaline phosphatase data for similar experimental designs. To assign statistical significance to the difference in means of alkaline phosphatase (IU/L) levels for *hPXR* mice control group mean of 60.16 ± 13.65 and the rifampicin and isoniazid administered group mean of 92.5, 3 mice are required per group. To assign statistical significance to the difference in means of alkaline phosphatase levels for *hPXR* mice rifampicin and isoniazid group mean of 92.5 ± 13.46 and the rifampicin, isoniazid, and *hPXR* antagonist administered group mean of 70.04, 6 mice are required per group.

100 µL of blood was collected every week to monitor serum *ALT* and *ALP*. The study will end when increased liver injury biomarkers are observed (e.g. serum *ALT* and *ALP* levels greater than 3-fold of upper limit of normal levels, as published previously (Li, Lu et al. 2013) or when the humane endpoint is reached (e.g. rapid weight loss, diarrhea, or discolored urine). Blood, bile, and liver samples were collected to measure the biomarkers of hepatotoxicity, rifampicin and isoniazid levels, and isoniazid metabolites. Liver samples were also used to determine *Cyp3a*, *Fech*, and *Alas1* expression. The liver damage was assessed by performing hematoxylin and eosin staining and scored by board certified pathologists of the Veterinary Pathology Core at St. Jude Children's Research Hospital.

In Vivo Study 1

Mice were provided 100 mg rifampicin/kg chow and 400 mg isoniazid/L autoclaved water *ad libitum* for 6 weeks. Serum was collected weekly to monitor liver function tests. Chow was obtained from Purina (St. Louis, MO). There were four groups of mice across two genetic backgrounds. Group 1: untreated control, group 2: rifampicin 100 mg/kg in diet (*ad libitum*), group 3: isoniazid 0.4 g/L in drinking H_2O (*ad libitum*), group 4: rifampicin 100 mg/kg in diet (*ad libitum*) and isoniazid 0.4 g /L in drinking water (*ad libitum*). 30 g C57BL/6 mice eat 5 g of food per day and drink 8 mL of H_2O per day. For rifampicin in food of 100 mg/kg food, a 30 g C57BL/6 mouse consumes 0.5 mg rifampicin a day or a dose of 16.7 mg rifampicin/kg body weight per day. For isoniazid in H_2O of 400 mg/L, a 30 g C57BL/6 mouse consumes 2.2 mg isoniazid per day

or a dose of 73.3 mg isoniazid/kg body weight per day (Bachmanov, Reed et al. 2002). Thus, for the first *in vivo* study, the rifampicin dose is approximately 16.7 mg/kg/day and the isoniazid dose is approximately 73.3 mg/kg/day administered orally *ad libitum.*

In Vivo Study 2

Study 2 consisted of 6 treatment groups of with 3-fold higher drug doses and 6-fold longer treatment duration. Group 1: untreated control, group 2: rifampicin 300 mg/kg in diet (*ad libitum*), group 3: isoniazid 1.2 g/L in drinking water (*ad libitum*), group 4: rifampicin 300 mg/kg in diet (*ad libitum*) and isoniazid 1.2 g /L in drinking water (*ad libitum*), group 5: SPA70 150 mg/kg (daily intraperitoneal injection), group 6: rifampicin 300 mg/kg in diet (*ad libitum*), isoniazid 1.2g/L in drinking water (*ad libitum*), and SPA70 150 mg/kg (daily intraperitoneal injection). For rifampicin in food of 300 mg/kg food, a 30 g C57BL/6 mouse consumes 1.5 mg rifampicin a day or a dose of 50 mg rifampicin/kg body weight per day. For isoniazid in H_2O of 1.2 g/L, a 30 g C57BL/6 mouse consumes 9.6 mg isoniazid per day or a dose of 220 mg isoniazid/kg body weight per day (Bachmanov, Reed et al. 2002). Thus, for the second *in vivo* study, the rifampicin dose is approximately 50 mg/kg/day and the isoniazid dose is approximately 220 mg/kg/day administered orally *ad libitum.*

In Vivo Study 3

Study 3 consisted of the same number of mice in each group, but females were also included and analyses would have been performed both within and between sexes. When dissecting mice from study 2, intra-peritoneal deposits of a white substance was found. This was attributed to the intra-peritoneal injection of the *hPXR* antagonist, SPA70, at very high doses. Therefore, the dose of SPA70 was reduced to the highest soluble dose that could be delivered in 200 µL of 1% DMSO in 30% PEG400 in PBS, or 3.75 mg/kg for a 25 g mouse. Rifampicin and isoniazid doses were based on the human equivalent dose as well as on literature reports of efficacious doses in rifampicin and isoniazid co-therapy.

Literature review revealed that a common dose of 10 mg/kg was administered daily in mice successfully induced pharmacokinetic changes attributable to xenobiotic metabolism and transport induction by rifampicin. However, these doses were only curative if con-current pyrazinamide administration of 150 mg/kg was present as well as additional non-antitubercular adjutant treatments were provided (Gupta, Tyagi et al. 2013, Maiga, Ahidjo et al. 2015). Another study found that in rifampicin monotherapy, doses as low as 15 mg/kg treated, but did not cure pulmonary infection of *M. tuberculosis*. Doses of 20-50 mg/kg of rifampicin were required for *M. tuberculosis* eradication and had no observed signs of hepatotoxicity (Hu, Liu et al. 2015). The maximal tolerated dose of rifampicin was reported as 160 mg/kg (de Steenwinkel, Aarnoutse et al. 2013) and as this was likely due to a different mechanism than the chronic, rifampicin and isoniazid co-therapy mediated cholestatic hepatotoxicity we

attempted to emulate that was *hPXR*-dependent (Li, Lu et al. 2013), I set this as our extreme upper limit of rifampicin dose.

80 mg/kg/day rifampicin has been reported, in combination with 25 mg/kg/day isoniazid subcutaneously injection, to cure *M. tuberculosis* infection in mice at 9 weeks of treatment without relapse and without adverse effects (de Steenwinkel, Aarnoutse et al. 2013). Therefore, a range of 80 – 160 mg/kg/day was based on the lowest dose of rifampicin to achieve an efficacious dose in mice (female BALB/c) that was not associated with adverse effects and the maximum tolerated dose in mice. Rifampicin is administered to humans at a dose of 600 mg/day, for a 60 kg human this dose is 10 mg/kg/day. To translate this dose to an equivalent mouse dose body surface area ratio between humans and mice were used as described previously (Reagan-Shaw, Nihal et al. 2008). Shortly, body surface area correlates with physiological parameters such as metabolic activity, oxygen consumption, blood volume, calorie expense, etc. Body surface area dose translation can be used to calculate an animal dose by multiplying the human dose by the ratio of human Km (37) to the animal Km (3) (animal dose = (human dose) x (human Km/animal Km)). Thus, the mouse dose for rifampicin is 123 mg/kg based on a human dose of 10 mg/kg. I used 80 mg/kg/day rifampicin in 7.5% PEG400 in PBS administered via oral gavage for study 3. A higher dose of rifampicin could have been administered, but the amount used was higher than the approximately doses in study 1 and study 2.

The daily administration of the combination of 10 mg/kg isoniazid, 10 mg/kg rifampicin, 150 mg/kg pyrazinamide, and 9.4 mg/kg verapamil cured *M. tuberculosis* infection at 20 weeks of treatment with no relapse (Gupta, Tyagi et al. 2013). 25 mg/kg isoniazid alone was not sufficient to cure *M.* tuberculosis infection at 3 weeks of treatment (female BALB/c) when started 24 days after infection by aerosol (Gonzalez-Juarrero, Woolhiser et al. 2012). however, 25 mg/kg isoniazid alone cure M. *tuberculosis* infection at 4 weeks of treatment (female BALB/c) when treatment was started 24 hours after infection by aerosol (Byrne, Denkin et al. 2007). Isoniazid was provided in food at 0.2% (w/w) and provided *ad libitum* to C57BL/6 wild-type mice for 35 days with an estimated 200 – 300 mg/kg/day dose based on estimated water consumption. Isoniazid was also provided in saline via oral gavage at a dose of 100 mg/kg/day. Neither of these doses resulted in hepatotoxicity (Metushi, Cai et al. 2014). Therefore, doses of up to and beyond 200 mg/kg/day of isoniazid as a monotherapy were tolerated without development of hepatotoxicity in C57BL/6 mice. IP injection (He, Guo et al. 2017) and oral gavage (Chen, Xu et al. 2011) of 150 mg/kg rifampicin and 75 mg/kg isoniazid produced a mildly hepatotoxic phenotype in mice that expressed *hPXR*. I then calculated the equivalent animal dose of 185 mg/kg based on a human dose of 15 mg/kg in humans. An appropriate dose would have been this calculated dose combined with a higher dose of rifampicin administered in a uniform, metered manner by oral gavage may have produced a robust phenotype. I used 70 mg/kg/day isoniazid for study 3.

Liver Function Tests

Quantification of plasma and sera LFTs was performed by the Veterinary Pathology Core Facility at St. Jude Children's Research Hospital. Analyses were performed on the ABX Pentra instrument from Medline Industries (Northfield, IL). *ALT* and *ALP* were quantified from sera and total and direct bilirubin were quantified from plasma.

Western Blotting

Adherent cells were washed with PBS, trypsinized, centrifuged at 10,000 RPM for 3 minutes at 4°C. The supernatant is aspirated, the cells are re-suspended, and centrifuged again. The supernatant is aspirated, and the cells are re-suspended in 100 µL RIPA from Thermo Fisher Scientific (Waltham, MA) and placed on ice for 30 minutes. Pierce RIPA (radio-immunoprecipitation assay) buffer (Thermo Fisher Scientific, Waltham, MA) was used to extract proteins from mouse liver and cell pellets. PhoSTOP (Roche, Branford, CT) phosphatase inhibitor and complete mini (Roche, Branford, CT) protease inhibitor was added to RIPA buffer. Then, the cells are sonicated on a Vibra-Cell Ultrasonic Liquid Processor from Sonics and Materials, Inc. (Newtown, CT) and stored at -80°C until Western blot analysis is performed. The bicinchoninic acid (BCA) assay is performed with the Pierce BCA protein assay kit from Thermo Fisher Scientific (Waltham, MA) according to the manufacturer's instructions. 2-10 µg protein is loaded unless otherwise noted. NuPAGE LDS loading buffer and reducing agent from Invitrogen (Carlsbad, CA) by was used to prepare protein lysates for electrophoresis. Protein gels are 4-12% Bis-Tris and are obtained pre-made from Invitrogen (Carlsbad, CA). The Kaleidoscope protein marker by Bio-Rad (Hercules, CA) is used to estimate protein size. Proteins are then transferred from the gel onto an iBlot nitrocellulose membrane from Invitrogen (Carlsbad, CA) by a dry transfer. Prior to probing with primary antibodies, membranes are incubated for 1 hour at room temperature in LiCor TBST blocking buffer (Lincoln, NE). After visualization membranes are stripped using NewBlot Nitro Stripping Buffer from Licor (Lincoln, NE) and anti-β-*Actin* primary antibody (a5441) from Sigma-Aldrich (St. Louis, MO) overnight at 4°C and are then incubated with secondary antibody (at 1:10000) for 1 hour at RT.

Mass Spectrometry

Lei Yang and Yan Lu from the High-Throughput Analytical Chemistry Core Facility at St. Jude Children's Research Hospital performed the LC/MS and LC/MS/MS analysis. PIH and isoniazid were prepared as stock solutions of 10 mM in DMSO. Warfarin was used as the internal stardard at 4 mg/L in acetonitrile or methanol. The standard curve was prepared by added the stock solutions to the designated matrix (media for media samples and liver homogenate for liver samples). A linear response for PIH was observed from 1 to 1000 nM, for isoniazid 0.1 nM to 100 µM, and for the hydrazine adduct 0.1 nM to 200 µM.

Samples were extracted by adding MilliQ H_2O at 4 µL per mg cell pellet or tissue. PIH and the hydrazine adduct was extracted by an additional 2-fold dilution with acetonitrile containing 4 mg/L warfarin per mg cell pellet or tissue or with methanol for isoniazid. Samples were mixed, centrifuged, and the supernatant was transferred for analysis with an equal volume of 0.1% formic acid in MilliQ H_2O for PIH, direct injection for the hydrazine adduct, or with 9X volume MilliQ H_2O for isoniazid.

The Acquity UPLC system (Waters, Milford, MA) coupled to an Applied Biosystems-Sciex API 6500 (Foster City, CA) with a triple-quadrupole mass spectrometer using an electronic spray ionization interface in positive mode was used to analyze PIH and isoniazid. The ion source temperature was maintained at 500°C and 450°C for PIH and isoniazid, the ion spray voltage was set at 5000°C and 3000°C for PIH and isoniazid, and multiple reaction monitoring mode was used for the quantitation of the analytes. The selected m/z transitions were 287 → 150 and 137.9 →79.1 for PIH and isoniazid, respectively. The m/z of the hydrazine adduct was 269. High purity nitrogen gas was used as collision-induced dissociation gas (setting 10 and 8), curtain gas (setting 20), ion source gas 1 (setting 37 and 60), and ion source gas 2 (setting 60) for PIH and isoniazid, respectively.

The chromatographic separation was performed on a Waters Acquity HSS C18 column (2.1 mm × 50 mm, i.d., 1.8 µm particle size, Waters, Ireland) for PIH. Mobile phase A was consisting of 0.1% acetic acid in water and mobile phase B consisting of 0.1% acetic acid in acetonitrile. The total flow rate was 0.7 mL/min. The UPLC column was maintained at 55°C and the gradient program over 2 minutes started at 95% A, maintaining for 0.2 minute, changed to 40% A over 0.8 min, to 95 % B over 0.5 minute, held for 0.2 minute, then to 95% A over 0.1 minute, and held for another 0.2 minute. The chromatographic separation was performed on a Waters HSS T3 C18 column (2.1 mm × 50 mm, i.d., 1.8 µm particle size, Waters, Ireland) for isoniazid. Mobile phase A was consisting of 10 mM ammonium bicarbonate in water and mobile phase B consisting of methanol. The total flow rate was 0.7 mL/min. The UPLC column was maintained at 55°C and the gradient program over 2 minutes started at 100% A, maintaining for 0.8 min, changed to 5% A over 0.4 min, held for 0.4 min, then to 99% A over 0.3 minute, and held for another 0.1 minute.

Detection of the hydrazine adduct was achieved with an Acquity UPLC system coupled to an Acquity SQD Mass Spectrometer (Waters, Milford, MA, USA). The mass spectrometer was operated in positive-ion mode with electrospray ionization. The conditions were as follows: capillary voltage 3.5 kV, cone voltage 25 V, source temperature 150 °C, desolvation temperature 350 °C, desolvation gas 800 L/hr, cone gas 85 L/hr. A full scan range from m/z = 100-1000 in 0.2 seconds was used to acquire MS data. Single ion recording mass spectrometry were used to determine the quantification of the samples. Chromatographic separation was performed on an Acquity UPLC BEH C18 1.7 µm, 2.1 x 50 mm column (Waters Corporation, Milford, MA). The total flow rate was 1.0 mL/min. The sample injection volume was 10 µL. The UPLC column was maintained at 60 °C and the gradient program started at 90% A (0.1% formic acid in MilliQ H2O),

changed to 70% A over 0.2 min, to 95 % B (0.1% formic acid in acetonitrile) over 1.4 minutes, held for 0.35 minutes, then to 90% A over 0.05 minutes.

Analysis of mass spectra was performed using the Analyst software (version 1.6.3) for the data acquisition and processing of PIH and isoniazid. The MassLynx software (version 4.1) was used to analyze for the hydrazine adduct. A $1/x^2$ weighted least squares linear regression method was used to obtain the calibration curves of the analytes through the measurement of the peak area ratio of each analyte to the internal standard.

Quantitative Real-Time Polymerase Chain Reaction

Mice livers were collected and stored in RNAlater from Thermo Fisher (Waltham, ME) at 4°C for 24 hours, then the RNA later was removed and the samples were stored at -80°C until homogenization. Homogenization was performed using the Bullet Blender Storm 24 Homogenizer from Thomas Scientific (Swedesboro, New Jersey). Cell cultures were trypsinized and collected following treatment. Extraction of whole RNA is performed with the Maxwell 16 LEV SimplyRNA Tissue Kit from Promega (Madison, WI) on the Maxwell 16 Instrument by Promega according to manufacturer's instructions. RNA was measured by the NanoDrop 8000 UV-Vis Spectrophotometer from Thermo Fisher. cDNA is synthesized using the SuperScript VILO kit from Invitrogen (Carlsbad, CA). Taqman reagents from Invitrogen (Carlsbad, CA) and the Applied Biosystems (Foster City, CA) 7500 Fast Real-Time PCR system were used to perform qRT-PCR. The ΔΔCT method was used to fold change in expression to the control group of each mouse strain (mouse house-keeping gene used: Gapdh) or vehicle control in cell culture (human house-keeping gene used: 18S) treatments. Gene expression was normalized to the species-specific house-keeping gene, which did not vary expression by treatment. Data are represented as mRNA fold change using the ΔΔCT method relative to vehicle control treatments. Experiments were performed in triplicated with analysis of each sample performed in triplicate.The following Taqman probes were used: *CYP3A4* (Hs00604506_m1), *ALAS1* (Hs00963534_m1), *Alas1* (Mm01235914_m1), *Fech* (Mm00500394_m1), *FECH* (Hs01555261_m1), *Cyp3a11* (Mm00731567), *hPXR* (Hs01114267_m1), *18S* (Hs03928990_g1), *Gapdh* (Mm99999915_g1), *ABCG2* (Hs01053790_m1), *Abcg2* (mM00496364_m1),

Hydrazine Adduct Formation

Hydrazine has a low molecular weight and therefore required derivatization for quantification via LC/MS/MS. This derivatization was carried out by Anne Edwards, Ph.D. from the Lab of Richard Lee, Ph.D. with *p*-anisaldehyde in a 2:1 reaction with hydrazine (**Figure 2-3**) similar to a previous report with modifications (Isenberg, Carter et al. 2016). For *in vitro* samples, 300 µL of each sample was acidified with 2 µL of 18 N HCl followed by the addition of 1 µL of *p*-anisaldehyde (21.8 mM). The mixtures were allowed to react at room temperature for 24 h followed by LC/MS/MS analysis. For *in*

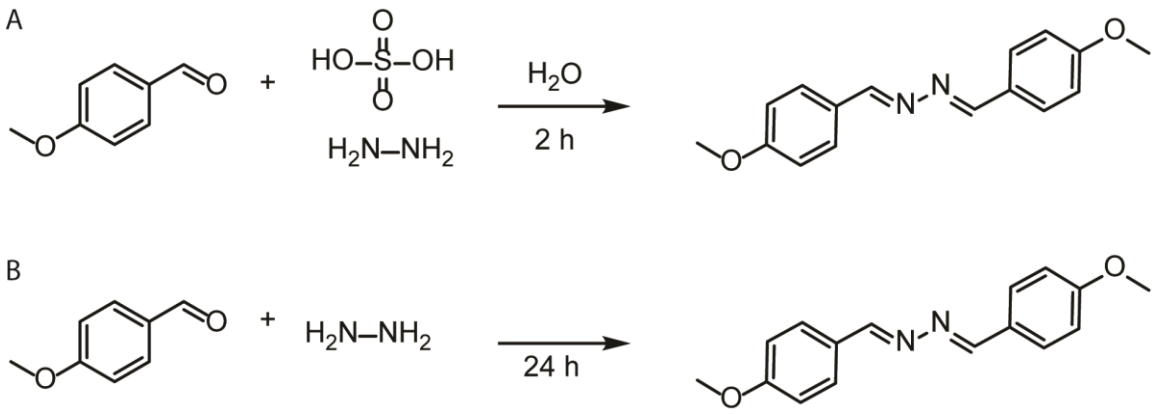

Figure 2-3. Synthesis of the hydrazine adduct quantified in this study.

Schema for the generation of the hydrazine and *p*-anisaldehyde adduct for use in the standard curve (A) and for unknown biological and biochemical samples (B).

vivo samples, 100 µL of the in vivo samples were acidified with 2 µL of 18 N or M HCl followed by the addition of 1 µL of *p*-anisaldehyde for a final concentration of 66.5mM. Samples with limited volume were diluted 1:1 or 9:1 then acidified followed by the addition of1 µL *p*-anisaldehyde. After 24 hours incubation at room temperature the samples were analyzed by LC/MS. To generate the standard curve, a solution of 7.68 mM *p*-anisaldedhyde was added to a solution of 3.84 mM hydrazine sulfate in 1:1 water/MeOH. The reaction was stirred for 2 hours and resultant yellow precipitate was filtered. The precipitate was dried under vacuum to produce the solid hydrazine adduct.

Siderophore Detection Assay

The chrome azurol S (CAS) assay was used to study the iron-binding capacity of solutions. The liquid CAS assay was based on the CAS-agar plate assay reported by Schwyn and Neilands and modified by Machuca and Milagres with variations (Schwyn and Neilands 1987, Machuca and Milagres 2003). Chelex-100 treated water was prepared according to manufacturer instructions and used to prepare assay buffer. Samples were incubated in CAS shuttle solution for 60 minutes at RT, then absorbance was read at 630 nm. Normalized absorbance values were obtained by dividing the absorbance of samples by a blank sample containing either cell culture medium, PBS for biochemical solution, or with Chelex-treated water for deferoxamine and PIH solutions.

Cell Viability Assays

CellTiterGlo ATP Detection

The CellTiterGlo assay from Promega (Madison, WI) was used to detect ATP levels (**Figure 2-4**) according to manufacturer's instructions. 10 µM staurosporine robustly reduced ATP at all time points observed (greater than 24 hours). Pre-assay optimization of plating density found that the optimal conditions for HepG2/C3A were in 10%FBS MEM at a density of 2,000 cells/well (in linear range of growth throughout experimental time period and linear range of luminescence) cells/well in white bottomed 96-well plates. Raw luminescence values were subtracted by cell free blank cell culture media and normalized to a measurement taken immediately after administration of compounds.

Caspase 3/7 Glo

To measure caspase 3/7 activity (**Figure 2-5**), the Caspase 3/7 Glo assay kit from Promega (Madison, WI) was used according to manufacturer's instructions. For short term experiments 10 µM staurosporine was used as a positive control, whereas for longer term experiments 0.1 µM staurosporine was used as a positive control. 10 µM staurosporine was necessary for robust induction of Caspase 3/7 activity at time points up

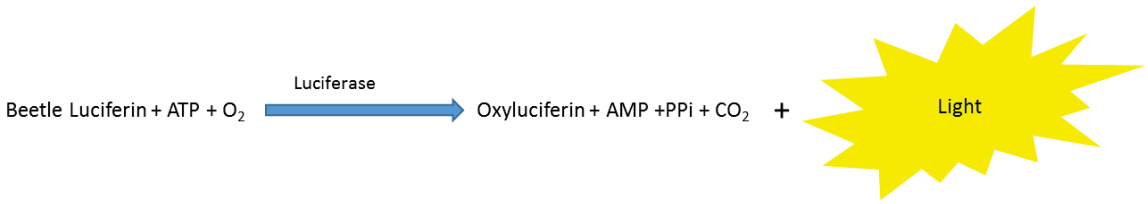

Figure 2-4. Overview of the CellTiterGlo assay.

Luciferase generates light in the present of ATP and luciferin.

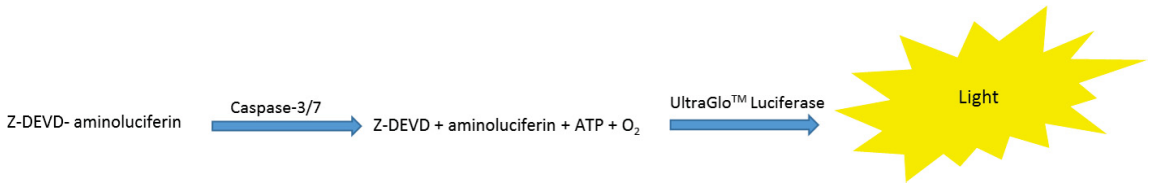

Figure 2-5. Overview of the Caspase 3/7 Glo assay.

Caspase 3/7 cleaves Z-DEVD sequence off of Z-DEVD-aminoluciferin generating luciferin which is then converted to light by luciferase in the presence of ATP.

to 12-24 hours, but a decrease in caspase 3/7 activity was observed after 24 hours at this dose due to cell death. 0.1 μM staurosporine did not induce caspase 3/7 activity after the first 24 hours hours, but treatment over 24 hours lead to robust, sustained induction of caspase 3/7 activity. Cell number and caspase 3/7 glo incubation times were also optimized before experimental samples were evaluated. Caspase 3/7 glo was performed on HepG2/C3A in 10% FBS MEM, at 2,000 cells/well in white bottomed 96-well plates. Raw luminescence values were subtracted by cell free blank cell culture media and normalized to a measurement taken immediately after administration of compounds.

Phase-Contrast Imaging

Phase-contrast imaging was performed on the Incucyte ZOOM live-cell imaging system (Essen BioScience, Ann Arbor, MI). as described previously (Oladimeji, Lin et al. 2017) with variations. Cells were plated at a density of 600,000 cells/well (20% confluence in 6-well plate) in 10%.FBS MEM 24 hours before the addition of indicated compounds. The cell density was evaluated every 12 hours. Data are represented as the fold-change in confluence compared to a measurement taken immediately after administration of compounds.

Solubility Assay

Lei Yang performed the solubility assay on the Biomek FX ADME-TOX workstation from Beckman Coulter (Fullerton, CA) to determine the solubility of $PPIXNa_2$ in PBS. To assess the solubility of $PPIXNa_2$ and in combination with rifampicin, isoniazid, or a combination of both, $PPIXNa_2$ was added to water to make the final concentration 100 μM, vortexed, then filtered using a 96-well filter plate from pION (Woburn, MA). The samples were then analyzed by UV spectrometry (230-500 nm). For standard curves, compounds were diluted 600-fold in 1:1 PBS buffer and 1-propanol (v/v). Concentrations were performed by μSOL Evolution software and compounds were tested in triplicate.

ABCG2/Abcg2 Transport Assays

Pheophorbide A Transport Assay

Evaluation of *ABCG2*/*Abcg2* inhibition by isoniazid was carried out similarly to previous reports with variations (To, Poon et al. 2015). Wild type or *Abcg2* knockout mouse embryonic fibroblasts were generously provided by the lab of John Schuetz. HEK 293 cells were transfected with pcDNA3.1 empty vector or with a recombinant *ABCG2* for 24 hours before pheophorbide A, ALA, and or *ABCG2*/*Abcg2* inhibitor treatment. Cells were treated in DMEM with 10% FBS and without antibiotics for 30 minutes at 37°C with 1 μM pheophorbide a and with 10 μM FTC, 10 μM Ko143, or 100 μM

isoniazid. Cells were then washed with cold DMEM and incubated for 2 hours at 37°C in the presence of the indicated inhibitor or potential inhibitor without pheophorbide A. Cells were then washed in cold DMEM, filtered, and kept on ice in the dark until analysis. 500,000 cells total, 1-2 million cells per mL were allocated per sample.

Flow Cytometry Analysis

Flow cytometry analysis was performed by the Flow Cytometry and Cell Sorting Core Facility at St. Jude Children's Research Hospital. Samples were analyzed on a LSRFortessa Cell Analyzer and FACSDiva software (BD Biosciences). Pheophorbide A fluorescence was detected with a 488 nm argon laser and a 670 nm bandpass filter. Over 100,000 events were collected with at least 10,000 events analyzed after cell debris were eliminated by gating forward versus side scatter and dead cell exclusion via DAPI staining.

Aminolevulinic Acid Treatment for PPIX Transport

Cells were trypsinized, washed, and while still in solution, incubated with ALA in the presence or absence of indicated test compound or *ABCG2* inhibitor for 2 hours. After which the media was collected and combined with a 1:1 solution of 0.9M ClO_4 in MeOH. Cells were then washed with cold PBS and lysed with 200 µL/well of 0.1% SDS for 1 hour on ice. Following lysis, 800 µL/well of 0.9M ClO_4 in MeOH was added to lysate and lysate was centrifuged at 10,000 RPM for 10 minutes to remove cell debris.

CLARIOstar Analysis of PPIX Content

The CLARIOstar microplate fluorescence reader system (BMG Labtech, Ortenberg, Germany) was used to quantify the fluorescence of cell and media preparations. This method is a variation of an original assay first reported by Granick and Levere in 1965 (Granick and Levere 1965), modified by Bloomer in 1997 (Bloomer 1997) and subsequently by Lin et al., and Ogino et al., in 2013 (Lin, Chang et al. 2013) and 2011 (Ogino, Kobuchi et al. 2011) respectively. The supernatant of the lysate was added to 96-well non-tissue-culture treated flat solid bottomed, black sided microplates (Corning, Corning, NY) containing 1:1 supernatant and 0.9M ClO_4 in MeOH for imaging. Measuring the emission at 640 nm following excitation at 405 nm would quantify multiple species of PPIX (**Figure 2-6**) and a signal is observed here following ALA treatment of HepG2/C3A cells (**Figure 2-7**). A standard curve was generated using PPIX for each plate and absolute concentrations were calculated based on relative fluorescence values obtained by measuring emission at 640 nm following excitation at 405 nm of a non-treated cell lysate spiked with various concentrations of PPIX based on a method described previously (Granick and Levere 1965, Bloomer 1997, Ogino, Kobuchi et al. 2011, Lin, Chang et al. 2013).

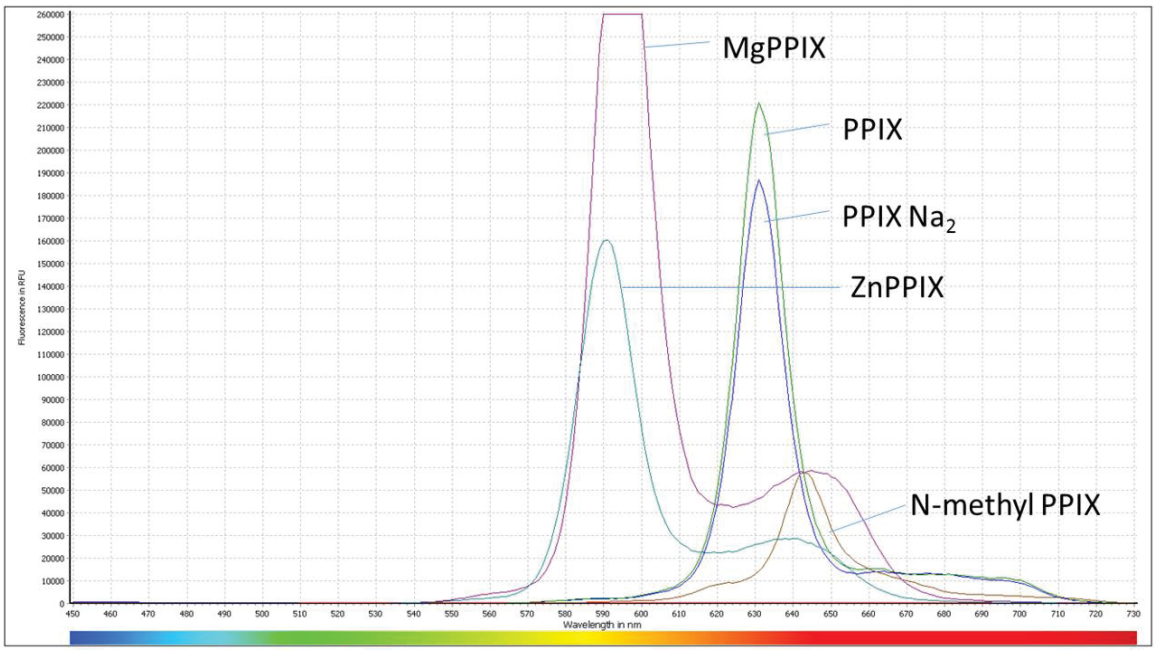

Figure 2-6. Emissions spectra of PPIX species at 405 nm excitation.

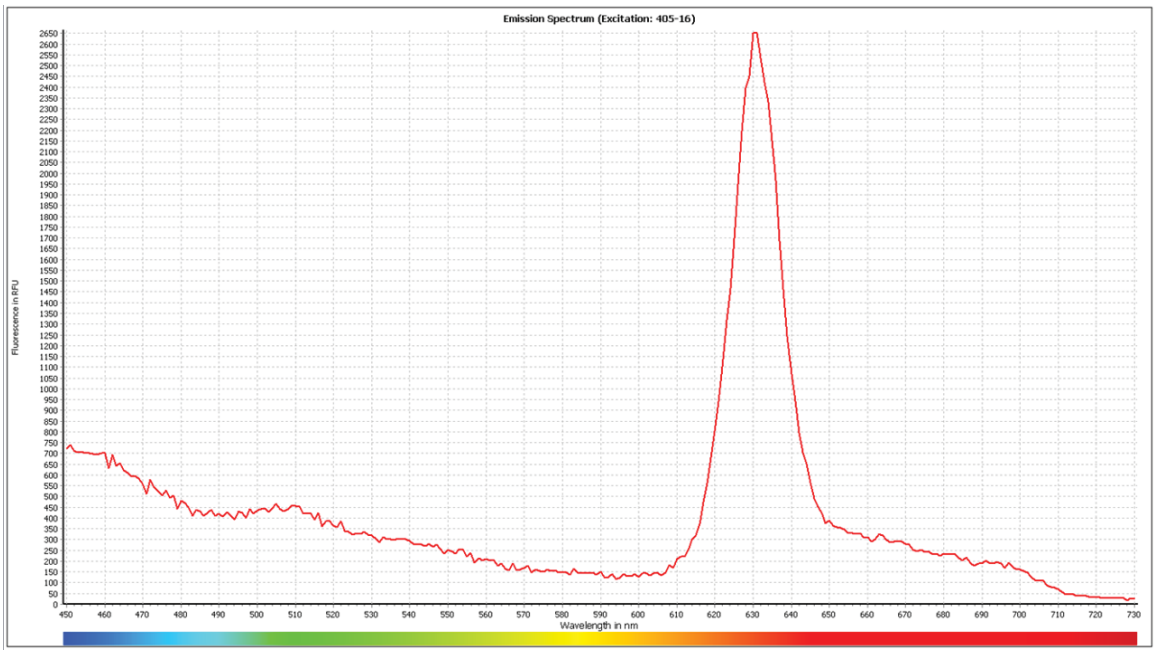

Figure 2-7. Emission spectrum of HepG2/C3A cell lysate treated with 4 mM ALA at 405 nm excitation.

Parallel Artificial Membrane Permeability Assay

The parallel artificial membrane permeability assay (PAMPA) was performed as described previously by Lei Yang of the High-Throughput Analytical Chemistry Core Facility (Yu, Wang et al. 2015). A 96-well filter plate from EMD Millipore (IVPH, 125 μm filter, 0.45 μm pore) and a 96-well microtiter plate formed a "sandwich" structure when wetted with 2% (w/v) hexadodecane (**Figure 2-8**). 0.3 mL of drug solution at 100 μM was added to the donor wells. The filter plate was placed on top of the donor plate. The wells of the acceptor plate were filled with buffer and placed on top of the filter. After incubation for 16 hours at 25°C, the plates were separated and the concentrations of the accepter and the donor wells were measured by UV absorption and used to calculate permeability.

PPIX Binding Assay

The PPIX fluorescence binding assay was performed as previously reported (Lyoumi, Abitbol et al. 2011). To compare *in vitro* binding affinities of various antitubercular drugs, bile acids, and phosphatidyl choline these compounds were added to a 20 nM solution of PPIX in 1 M imidazole, 0.9% NaCl, at pH 8.2 at similar concentrations they are found in the bile. The concentrations of each bile acid constituent was based on their in vivo concentrations (0.1 mM phosphatidyl choline, 100 μg/mL BSA, 2 mM of each bile acid, 0.4 mM of rifampicin, and 4 mM isoniazid). Solutions were prepared of each constituent with PPIX or the constituent alone and protected from light and placed in 96-well black plate and read by a Clariostar fluorescent plate reader. Fluorescence intensity of the emission at 634 nm after excitation at 408 nm was read. The ratio of the fluorescence intensities of the bile constituent and PPIX to the bile constituent alone were determined.

Statistical Analysis

Data from three independent experiments were pooled and analyzed as indicated in figure legends using GraphPad Prism 7.0 software. Significant changes re considered to be p-values of less than 0.05. Results are expressed as the mean +/- standard error of measurement (SEM). 2-way ANOVA followed by Tukey's post-hoc analysis was used to compare group means for qRT-PCR analysis. 1-way ANOVA followed by Dunnett's post-hoc analysis was used to compare group means for Western blot analysis. False discovery rate (FDR) was determined by the Benjamini Hochberg correction.

Proteomics Profiling

Proteomics profiling and initial analysis were carried out by Kiran Kodali of the Proteomics and Mass Spectrometry Facility at St. Jude Children's Research Hospital. Mice were treated as described for *in vivo* study 2 (**Figure 2-9**). Male C57BL/6 *hPXR*

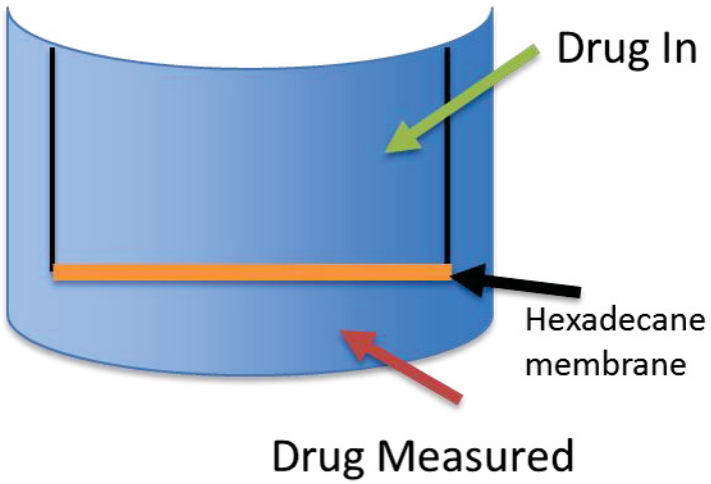

Figure 2-8. PAMPA overview.

Compounds are added to one side of a hexadecane membrane then the media on the other side was analyzed for the compound.

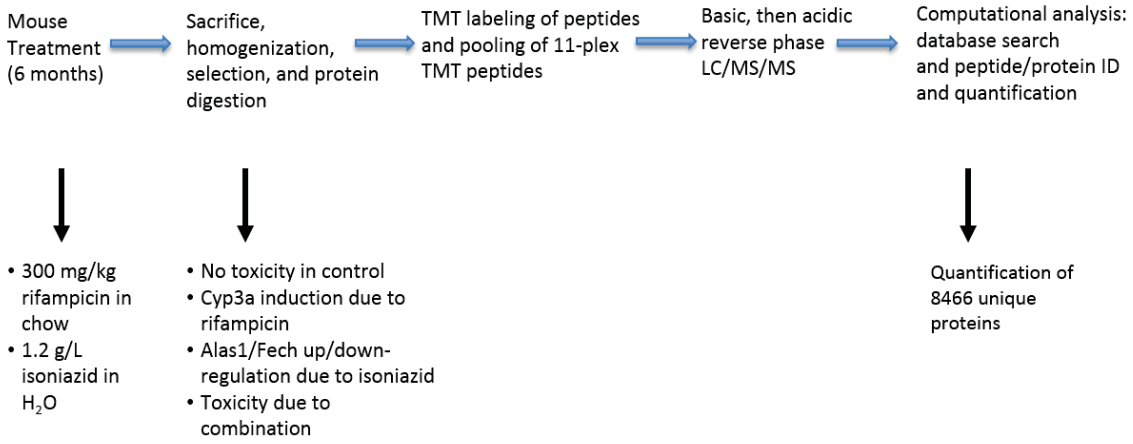

Figure 2-9. Proteomics profiling overview.

and *mPxr* $^{-/-}$ were treated for 6 months with 300 mg/kg rifampicin in chow and 1.2 g/L isoniazid in water. After 6 months, livers were collected and flash frozen. Livers were then lysed (50 mM HEPES, pH 8.5, 8 M urea and 0.5% sodium deoxycholate), and 100 μg of protein was digested with LysC from Wako Chemicals (Richmond, VA) in the presence of 1,4 -dithiothreitol at an enzyme-to-substrate ration of 1:100 for 2 hours as described previously (Pagala, High et al. 2015). The samples ar then diluted to a final 2 M urea concentration using 50 mM HEPES, pH 8.5. The samples are further digested by trypsin from Promega (Madison, WI) at an enzyme-to-substrate ratio of 1:50 for 3 hours. The resulting peptides are reduced by adding 1 mM 1,4 –dithiothreitol for 30 minutes at RT and are then alkylated with 10 mM iodoacetamide for 30 minutes at RT in the dark. The reaction is quenched by adding trifluoroacetic acid. This acidified peptide mixture is desalted by C18 cartridges from Harvard Apparatus (Holliston, MA) The desalted eluent is dried and re-suspended in 50 mM HEPES, pH 8.5.

Samples are labeled with Tandem Mass Tags (TMT 11-plex) from Thermo Fisher (Waltham, MA) according to the recommendations of the manufacturers. After labeling the samples are combined, desalted, and fractionated on an off-line HPLC (Agilent 1220) from Agilent Technologies (Santa Clara, CA). 90 two minute fractions were collected over a 180 minute gradient. The fractions are dried then re-suspended in 5% formic acid and analyzed by acidic pH reverse-phase LC/MS/MS. Samples are fractionated on a nanoscale capillary reverse-phase C18 column by a nanoAcquity HPLC from Waters Corporation (Millford, MA) by a 120 minute gradient. The eluent is ionized by electrospray ionization and detected by an in-line Orbitrap Fusion mass spectrometer from Thermo Fisher (Richmond, VA). Mass spectrometry is performed in data-dependent mode with a survey scan (60,000 resolution, 1 X 10^6 AGC target and 150 ms maximal ion time) and 20 MS/MS high resolution scans (60,000 resolution, 1 X 106 AGC target and 150 ms maximal ion time, 38 HCD normalized collision energy, 1 m/z isolation window, and 20 s dynamic exclusion).

Raw mass spectra were processed by the JUMP program as described previously (Wang, Li et al. 2014). The resultant data was compared to the UniProt mouse database and concatenated with a reversed protein sequence decoy database. Searches were performed using a mass tolerance of 25 ppm for precursor ions and 15 ppm mass tolerance for fragment ions, fully tryptic restriction with two maximum missed cleavages, three maximum modification sites, and the assignment of α, β, and γ ions. TMT tags on lysine residues and N-termini (+229.162932 Da) and carbamidomethylation of cysteine residues (+57.021 Da) are used for static modifications and methionine oxidation (+15.99492 Da) is considered as a dynamic modification. Mass spectra are filtered by mass accuracy and matching scores to reduce the FDR to approximately 1%. Proteins are quantified by summarizing reporter ion counts across all matched peptide spectrums using the JUMP software. Analysis was performed by Timothy Shaw from the Computational Biology Department and Proteomics Core Facility at St. Jude Children's Research Hospital. Clustering analysis was performed using R v.3.0.1.

CHAPTER 3. RESULTS

The Physiochemical Properties of PPIX

Introduction

The physiochemical properties of PPIX may contribute to toxicity by binding to bile acid components and precipitating into the bile canaliculi. This may block bile ducts and lead to a cholestatic pattern of toxicity. Conversely, intracellular accumulation of PPIX is associated with a hepatocellular subtype of liver injury. To recapitulate the cholestatic hepatotoxicity phenotype observed previously (Li, Lu et al. 2013) that is believed to be mediated by PPIX, it is necessary to demonstrate that (1) PPIX is insoluble at supra-physiologic levels that may be associated with heme biosynthesis disruption, (2) PPIX binds to bile salts, phospholipids, albumin, and this binding may be affected by rifampicin and isoniazid, and that (3) exogenous PPIX is toxic. The proposed mechanism of the toxicity of PPIX presumes that it is toxic when in an extracellular compartment (Lyoumi, Abitbol et al. 2011). PPIX is hepatotoxic when its level rises high enough in the bile canaliculi, PPIX precipitates out of solution forming aggregates with bile constituents resulting in bile plugs. The bile plugs observed previously (Davies, Schuurman et al. 2005, Lyoumi, Abitbol et al. 2011, Li, Lu et al. 2013) may be due to PPIX if PPIX is insoluble at likely concentrations achievable by heme biosynthesis disruption by isoniazid and the un-defined role of rifampicin. Therefore, confirming these properties of PPIX is necessary before beginning *in vivo* studies predicated on PPIX exerting a hepatotoxic effect via these properties.

Solubility of PPIX

A 100 μM solution of the disodium salt of PPIX was prepared in water, vortexed, and filtered. The sample was then analyzed by UV spectrometry and the concentration of PPIX was 0.3 μM (**Figure 3-1**). BALB/c^{m1Pas} mice have liver PPIX levels of 0.02 μM, whereas C57BL/6 mice have liver PPIX levels of 0.24 μM (Lyoumi, Abitbol et al. 2011). Interactions with less soluble molecules and changes in bile pH may further lower PPIX solubility (Davies, Schuurman et al. 2005, Lyoumi, Abitbol et al. 2011). In FVB/NJ mice, basal PPIX liver levels were found to be 0.35 μM with a 3-fold increase after 14 days of 400 mg/L isoniazid treatment that did not result in toxicity (Sachar, Li et al. 2016). The same group previously reported a 60-fold increase in bile PPIX levels in *hPXR* (C57BL/6 strain) mice (the authors did not specify concentration) that was associated with pathological change in liver tests and in the observation of bile plugs on histological examination (Li, Lu et al. 2013). During heme synthesis, PPIX would be expected to be relatively transient and to be formed immediately into heme by *FECH*. Therefore, with a relatively low solubility compared to pharmaceuticals (e.g. albendazole, soluble at 15 μM) excreted into the bile, changes in PPIX solubility may lead to precipitation and potentiate bile stasis. Additional information concerning the solubility of different species

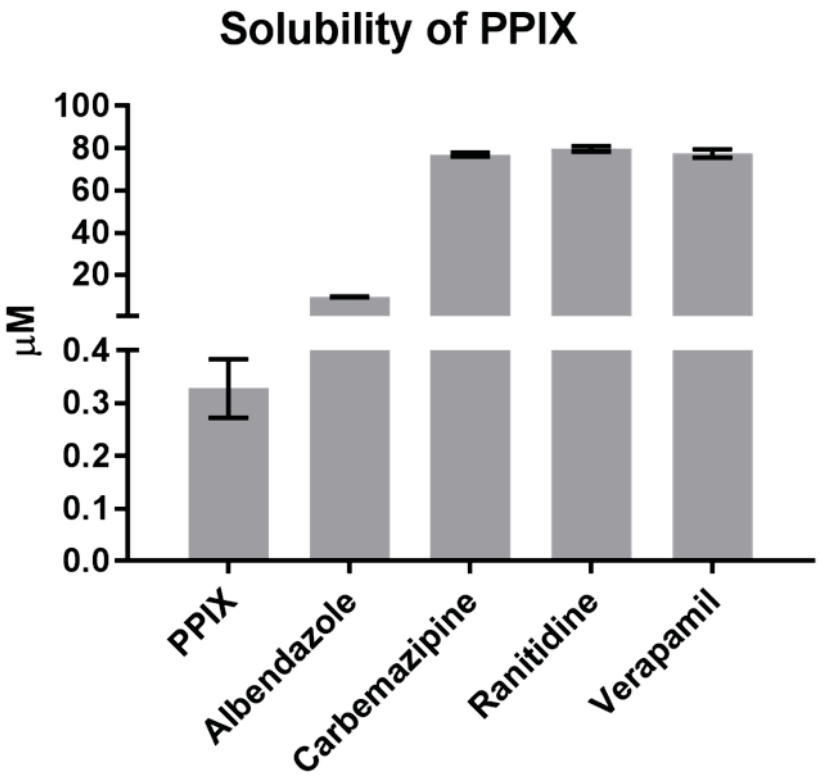

Figure 3-1. The solubility of $PPIXNa_2$ in PBS.

LC/MS/MS analysis of filtrate from saturated PBS solution of $PPIXNa_2$. Data are represented as the mean ± SEM.

of PPIX, comparison to heme, and in the presence of bile acid constituents would further elucidate the conditions in which the solubility of PPIX would contribute to the pathogenesis of liver injury.

Permeability of PPIX

The permeability of the disodium salt of PPIX was compared to various pharmaceuticals. The permeability of these compounds was measured and found to be about 1500 Pe (10^6 cm/s) for hydrophobic non-polar verapamil, 100 Pe (10^6 cm/s) for carbamazepine, 150 Pe (10^6 cm/s) for albendazole, and 0 Pe (10^6 cm/s) for ranitidine. The permeability of $PPIXNa_2$ was 17 Pe (10^6 cm/s) (**Figure 3-2**), much lower than albendazole and carbamazepine. Less polar species of PPIX would be expected to be less permeable and future studies may elucidate the dependence of these species on transporter proteins such as ABCG2 and the exact nature of the elevated PPIX detected following antitubercular therapy in mice (Li, Lu et al. 2013, Sachar, Li et al. 2016). Mass spectrometric analysis would not be able to differentiate against PPIX, $PPIXNa_2$, or many other species of PPIX due to the loss of ions in solution. Therefore, further elucidation of the ADME properties between these molecules would help to identify the species involved in accumulation.

Isoniazid Does Not Inhibit the *ABCG2/Abcg2*-Mediated Transport of Pheophorbide A

ABCG2 effluxes PPIX from hepatocytes into the bile, leading to toxicity (Aust, Obrist et al. 2004, Davies, Schuurman et al. 2005, Lyoumi, Abitbol et al. 2011, He, Guo et al. 2017). However, increased PPIX retention by decreased efflux does contribute to toxicity in ALL and hematopoietic cells (Stewart, Leggas et al. 2004, Krishnamurthy and Schuetz 2011, Morfouace, Cheepala et al. 2015). Pheophorbide A (chlorophyll breakdown product) is a specific substrate for *ABCG2*/*Abcg2* discovered when *Abcg2* $^{-/-}$ mice were fed alfalfa developed phototoxicity. Flow cytometric analysis of pheophorbide A is used as the gold standard in determining the effect of potential inhibitors on *ABCG2*/*Abcg2* activity. Therefore, we tested the potential for *ABCG2* inhibition by measuring pheophorbide A efflux in HEK 293 cells ectopically overexpressing *ABCG2*. To test the effect of isoniazid on pheophorbide A transport mediated by *Abcg2*, mouse embryonic fibroblasts were used. The specific *ABCG2* inhibitors fumitremorgin C (FTC) and Ko143 inhibited *ABCG2*- and *Abcg2*-dependent efflux of pheophorbide A, but isoniazid expectedly did not (**Figure 3-3A** and **B**).

Isoniazid Does Not Inhibit the *ABCG2/Abcg2*-Mediated Transport of PPIX

The mechanism of PPIX transport by *ABCG2*/*Abcg2* differs from Pheophorbide A in that BSA is required to transfer PPIX from the extracellular loop of the transporter and

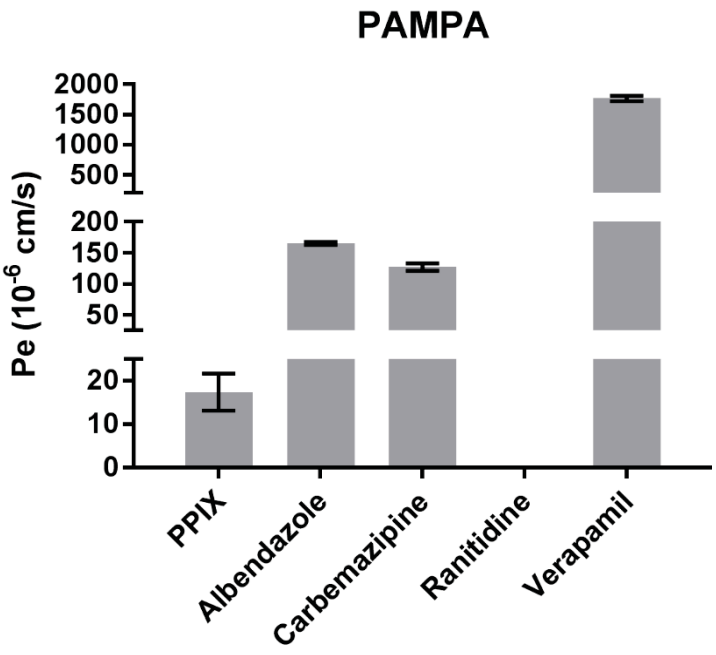

Figure 3-2. The permeability of $PPIXNa_2$ in PAMPA.

Data are represented as the mean ± SEM.

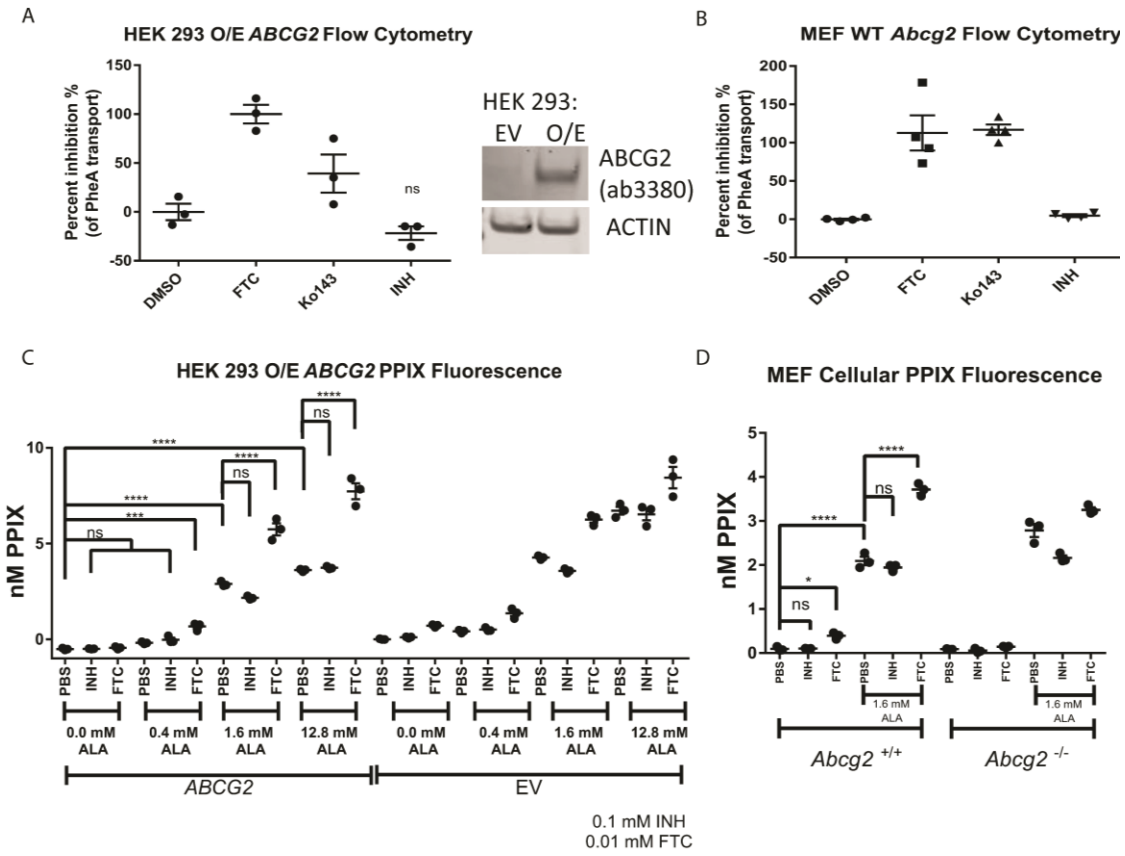

Figure 3-3. Isoniazid does not inhibit *ABCG2*- or *Abcg2*-mediated transport of pheophorbide A or PPIX.

The potential for inhibition by isoniazid was evaluated in HEK 293 ectopically over-expressing human *ABCG2*-mediated transport of pheophorbide A (A) and PPIX (C). MEF cells expressing mouse *Abcg2* were evaluated for potential inhibition by isoniazid in the transport of pheophorbide A (B) and PPIX (D). Data are expressed as the mean ± SEM of separate experiments. 1-way ANOVA followed by Dunnett's post-hoc analysis was used to compare group means. ****$p<0.0001$; ***$p<0.001$, **$p<0.01$, *$p<0.05$

enable transport of additional PPIX molecules (Desuzinges-Mandon, Arnaud et al. 2010). Therefore, testing pheophorbide A alone would not answer the question of whether PPIX transport by *ABCG2*/*Abcg2* is inhibited by isoniazid. The same cell models used to evaluate pheophorbide A transport were used to evaluate PPIX transport subsequent to ALA treatment to induce intracellular PPIX formation. After induction of PPIX accumulation by ALA, cells were treated with isoniazid and FTC. FTC inhibited the *ABCG2*- and *Abcg2*-mediated transport of PPIX (**Figure 3-3C** and **Figure 3-3D**).

PPIX Binds to Phospholipids and Bile Salts

In instances of hepatotoxicity associated with PPIX treatment, disruption of lipid and bile acid homeostasis and deposits of porphyrins and bile acid constituents are found on histopathological examination (Davies, Schuurman et al. 2005, Lyoumi, Abitbol et al. 2011, Li, Lu et al. 2013). To determine if the interactions of PPIX with bile acids, albumin and phosphatidyl choline was affected by the presence of rifampicin and isoniazid, the binding assay employed previously was used (Lyoumi, Abitbol et al. 2011). PPIX did not interact with isoniazid, taurocholic acid, hexadecenoic (palmitic) acid, or deoxycholic acid, but did interact with rifampicin, albumin, phosphatidyl choline, and lithocholic acid. Isoniazid and rifampicin affect the interaction of PPIX with albumin and phosphatidyl choline (**Figure 3-4**). Further studies would be required to elucidate whether these associations would be expected to increase or decrease the solubility of PPIX.

Exogenous $PPIXNa_2$ Decreases ATP Levels

$PPIXNa_2$ is associated with more severe hepatotoxicity when not retained in Kupffer cells and hepatocytes (Lyoumi, Abitbol et al. 2011). Considering this report, the low membrane permeability of $PPIXNa_2$, and lack of identified import protein, $PPIXNa_2$ may be toxic in an extracellular space. To evaluate whether exogenous $PPIXNa_2$ could reduce ATP levels in HepG2/C3A, cells were added to culture plates for 24 hours before being treated with $PPIXNa_2$. At day 2, there was a slight decrease in ATP ($p < 0.05$) due to 40 μM $PPIXNa_2$ (**Figure 3-5**). At day 3, this became a 40% decrease due to 40 μM and 10% decrease ($p < 0.001$) due to 20 μM. At day 4, 40 μM and 20 μM decrease ATP levels by 60 % ($p < 0.001$) and 40% by 10 μM ($p < 0.05$). The media was not refreshed after dosing on day 0 when the base-line ATP levels were measured and after day 4, the ATP levels of DMSO treated HepG2/C3A cells were no longer increasing, suggesting that cells are no longer growing. Beginning on day 5, $PPIXNa_2$ showed a decrease in ATP levels above 156 nM $PPIXNa_2$ by at least 20% compared to DMSO treated cells ($p < 0.001$), a 70% decrease at 10 μM ($p< 0.001$), and an 80% decrease at 40 μM $PPIXNa_2$ ($p< 0.001$). At day 6, 156 nM $PPIXNa_2$ decreased ATP levels by 50% ($p< 0.001$) and a 90% decrease ($p< 0.001$) at 10 μM. This persists through day 7 with an overall decrease in ATP levels. Higher doses of $PPIXNa_2$ (in the micromolar range) may cause toxicity earlier and in nutrient rich conditions, where lower doses (in the nanomolar range) may require nutrient depletion to be toxic.

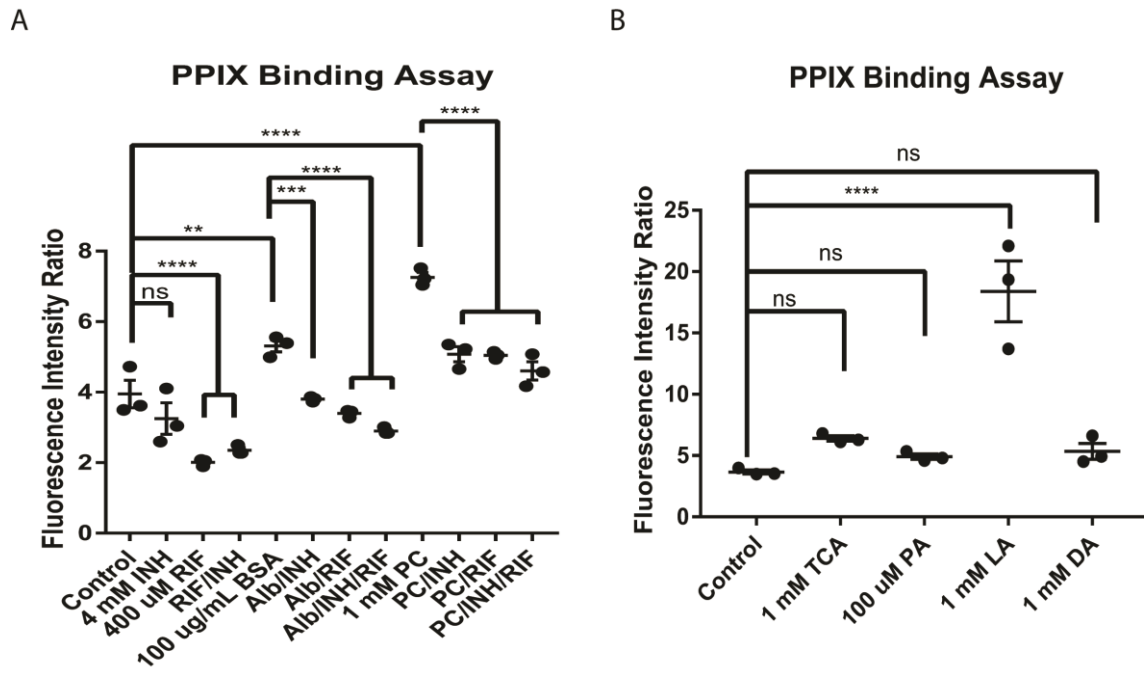

Figure 3-4. $PPIXNa_2$ binding assay.

Evaluation of PPIX binding to phospholipids (A) and bile salts (B). Data are represented as the mean of the ratio of the fluorescence intensity of indicated compounds with PPIX to wells of the compounds without PPIX. Data are represented as the mean ± SEM. 1-way ANOVA followed by Dunnett's post-hoc analysis was used to compare group means. ****$p<0.0001$; ***$p<0.001$, **$p<0.01$, *$p<0.05$

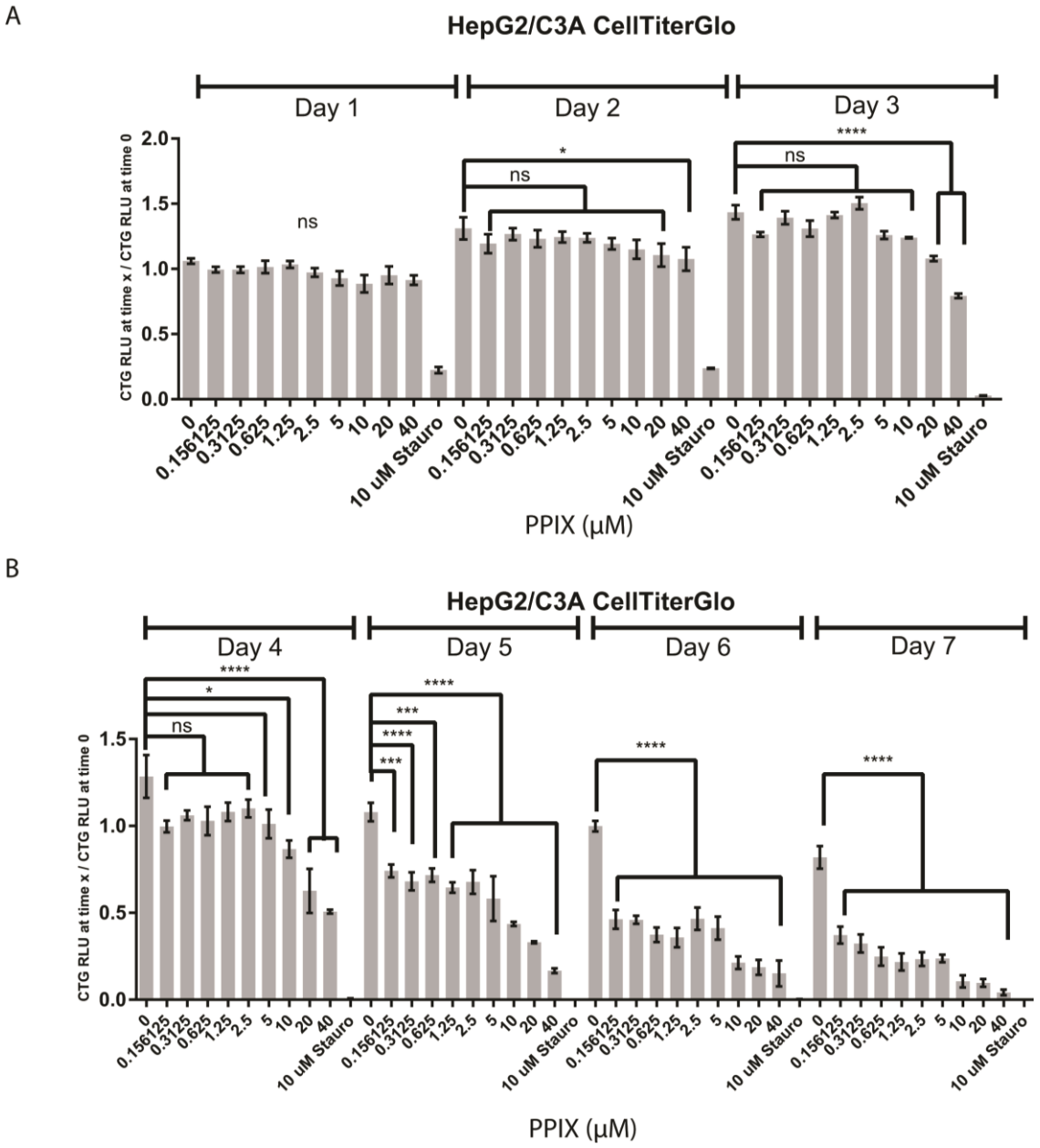

Figure 3-5. $PPIXNa_2$ decreases cellular ATP levels.

Evaluation of relative ATP levels after single treatment of HepG2/C3A cells with various doses of PPIX at 1-3 days (A) and 4-7 days (B). Data are represented as the mean ± SEM of the CellTiterGlo luminescence at the indicated time point divided by the luminescence immediately after dosing. 1-way ANOVA followed by Dunnett's post-hoc analysis was used to compare group means. ****p<0.0001; ***p<0.001, **p<0.01, *p<0.05

Exogenous $PPIXNa_2$ Decreases Cell Area

To confirm the decrease in ATP due to PPIX detected by the CellTiterGlo assay system and to allow daily dosing and refreshening of media as well as extending the length of exposure to $PPIXNa_2$, phase-contrast imaging was used to evaluate whether there would be a commensurate decrease in cell area growth. As low as 313 nM $PPIXNa_2$ significantly ($p< 0.005$) decreased the growth of cell area as measured by phase contrast imaging (**Figure 3-6**). At 625 nM $PPIXNa_2$ or higher the cell area growth was significantly ($p <0.001$) decreased. 10 μM staurosporine was used as the positive control. Further evaluation would elucidate whether the effect of exogenous $PPIXNa_2$ is merely growth suppression or directly cytotoxic.

Exogenous PPIX Increases Caspase 3/7 Activity

Exogenous application of HepG2/C3A resulted in an ATP decrease beginning at 3 days due to 40 μM $PPIXNa_2$. Following this observation. HepG2/C3A cells were then evaluated for caspase 3/7 activation using the Caspase 3/7 Glo Assay from Promega (Madison, WI). HepG2/C3A treated for short durations less than 3 days do not display caspase 3/7 activity due to PPIXNa2 treatment. However, statistically significant ($p<0.0001$) activation of caspase 3/7 was detected at 72 hours due to 80 μM $PPIXNa_2$ (**Figure 3-7**).

The Effect of Isoniazid Metabolites on the Heme Biosynthesis Pathway

Introduction

After establishing that exogenous PPIX is cytotoxic, precipitates at relatively low concentrations, and may bind to bile constituents and may be associated with or even causative of the bile plugs observed in vivo, the disruption of the heme biosynthesis pathway by isoniazid was subsequently investigated. This investigation focused on the role of isoniazid based on a previous report (Sachar, Li et al. 2016) and my data that confirmed this report (**Figure 1-7**). The accumulation of PIH and hydrazine in patients taking isoniazid has been reported previously. (Li, Miao et al. 2011, Isenberg, Carter et al. 2016) PIH has been reported to chelate iron and *FECH* is down-regulated in low iron conditions. (Taketani, Adachi et al. 2000, Crooks, Ghosh et al. 2010) Hydrazine has been reported to N-alkylate heme moieties (Ator, David et al. 1987, Wojciechowski and de Montellano 2007, Ascenzi, Coletta et al. 2013) and heme suppresses *ALAS1* expression at multiple levels. (Srivastava, Borthwick et al. 1983, Kolluri, Sadlon et al. 2005, Zheng, Shan et al. 2008) Isoniazid up-regulates mouse *Alas1* protein and down-regulates *Fech* protein in mouse liver. (Sachar, Li et al. 2016) These effects of isoniazid on heme biosynthesis enzymes was not previously reported on the human proteins, nor was it determined if the effects observed in mouse systems were due to isoniazid or a metabolite of isoniazid. Therefore, I report (1) the detection of PIH in biological systems and

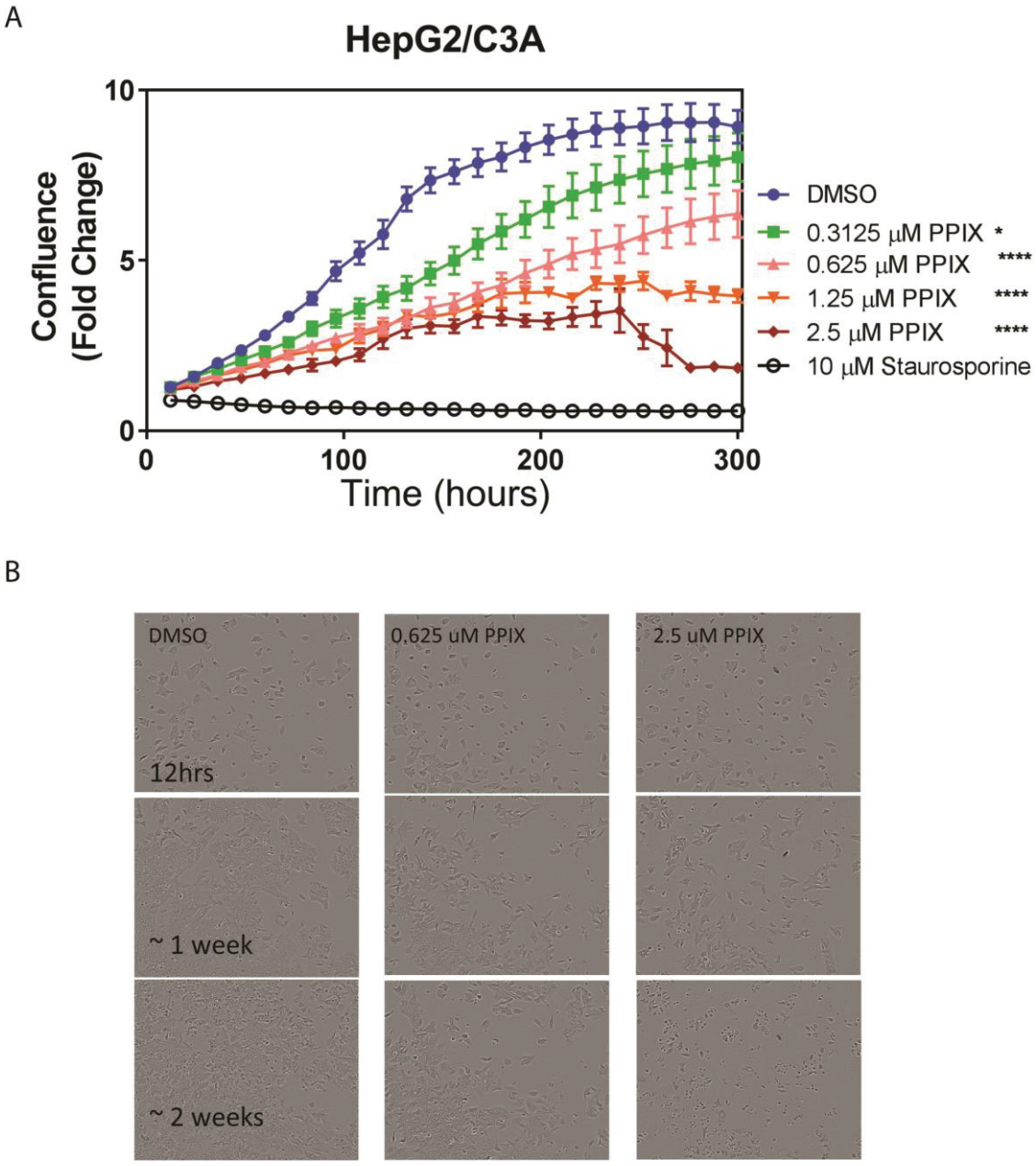

Figure 3-6. $PPIXNa_2$ treatment decreases cell area growth.

Phase contrast imaging of HepG2/C3A cells after single treatment of PPIX. Data quantified by Incucyte ZOOM instrument (A) and representative images (B) are shown. Data are represented as the mean ± SEM of the confluence at the indicated time divided by the confluence taken immediately after the first dose of $PPIXNa_2$. 1-way ANOVA followed by Dunnett's post-hoc analysis was used to compare group means. ****$p<0.0001$; ***$p<0.001$, **$p<0.01$, *$p<0.05$

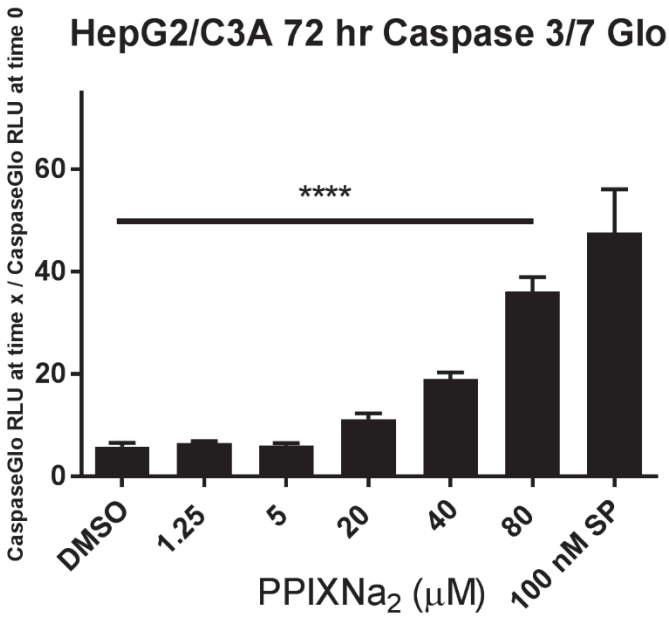

Figure 3-7. $PPIXNa_2$ increases Caspase 3/7 activity.

Data are represented as the mean ± SEM of the fold change of Caspase 3/7 Glo luminescence at 72 hours compared to a time 0 measurement conducted immediately after dosing. 1-way ANOVA followed by Dunnett's post-hoc analysis was used to compare group means. ****$p<0.0001$; ***$p<0.001$, **$p<0.01$, *$p<0.05$

demonstrate the enzyme-independent formation of PIH from multiple vitamin B_6 analogues and isoniazid, (2) the iron-dependent down-regulation of *FECH*, and (3) the hydrazine-mediated up-regulation of *ALAS1*.

Isoniazid Decreases Human *FECH* Protein Levels and Increases Human *ALAS1* Protein and mRNA Levels, but Does Not Affect *FECH* mRNA Levels

A previous study (Sachar, Li et al. 2016) reported the regulation of *Alas1* and *Fech* by isoniazid in mice, we also observed this decrease in *Fech* protein and increase in *Alas1* protein in C57BL/6 mice livers at 6 weeks of treatment with isoniazid (400 mg/L in drinking water as described for *in vivo* study 1) and confirm that these changes occur independently of *hPXR* and are not modified by the co-administration of rifampicin (100 mg/kg in chow). (**Figure 3-8**) These changes would be expected to result in the increase of PPIX seen due to isoniazid alone (Sachar, Li et al. 2016) and a portion the PPIX increase associated with hepatotoxicity of *hPXR* mice treated with rifampicin and isoniazid concurrently (Li, Lu et al. 2013).Therefore, we first tested the effect of isoniazid on human *ALAS1* and *FECH* and found similar changes in a much shorter time period and at lower doses than has been reported to cause toxicity in HepG2/C3A (Nicod, Viollon et al. 1997, Schwab and Tuschl 2003, Bhadauria, Mishra et al. 2010). Isoniazid treatment of HepG2/C3A and PHH for 72 hours results in a 50% decrease of *FECH* protein in PHH (**Figure 3-9A**; $p<0.01$) at doses higher than 50 μM (**Figure 3-9B**; $p<0.05$) and a decrease of 30% in HepG2/C3A (**Figure 3-9D**; $p<0.01$) but not of *FECH* mRNA (**Figure 3-9C** and **E**). This is similar to other reports of iron-dependent *FECH* protein down-regulation. Bone marrow aspirates of *Irp2* $^{-/-}$ mice have been reported to display 50% of the *Fech* activity of wild-type mice (Crooks, Ghosh et al. 2010). This also corresponds to the 60% decrease observed of *FECH* activity after administration, of the N-donor, *S*-nitroso-N-acetylpenicillamine, to cell lysates overexpressing human recombinant *FECH* (Furukawa, Kohno et al. 1995). Treatment of FVB/NJ mice with isoniazid for 14 days produced a 60% decrease in *Fech* protein and 3- to 4-fold increase in *Alas1* protein (Sachar, Li et al. 2016). Isoniazid up-regulates the protein levels of *ALAS1* 3-fold at 800 μM (**Figure 3-10B**; $p<0.01$), but does not up-regulate the mRNA levels in PHH (**Figure 3-10C**). Isoniazid does not up-regulate the protein (**Figure 3-10D**) and mRNA (**Figure 3-10E**) levels of *ALAS1* in HepG2/C3A at 800 μM.

Iron Levels Modulate *FECH* Protein Levels

Previous studies (Furukawa, Kohno et al. 1995, Taketani, Adachi et al. 2000, Crooks, Ghosh et al. 2010) have established the relationship between the [2Fe-2S] containing *FECH* and iron levels in murine erythroleukemia cells, macrophage cell line RAW 264.7, and K562 cells. These studies have shown that *FECH* is down-regulated in iron-limiting conditions and is up-regulated in iron-replete conditions. However, this has not been reported in the liver hepatoma cell line, HepG2/C3A. HepG2 is commonly used to study hepatotoxicity *in vitro* and has been used to demonstrate the toxicity of

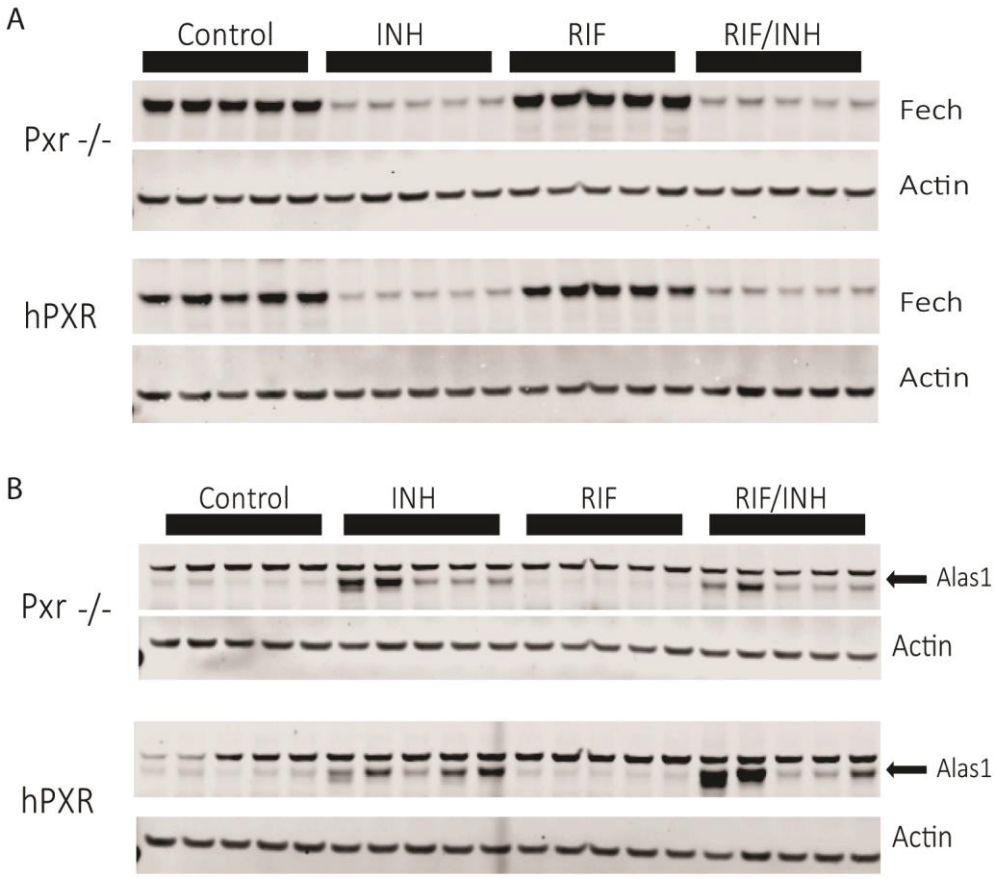

Figure 3-8. ***In vivo*** **expression of** ***Fech*** **and** ***Alas1*** **in mouse liver.**

Western blot analysis of *Fech* (A) and *Alas1* (B) in C57BL6 mouse liver after 6 weeks treatment with rifampicin (100 mg/kg chow) and isoniazid (400 mg/L in drinking water).

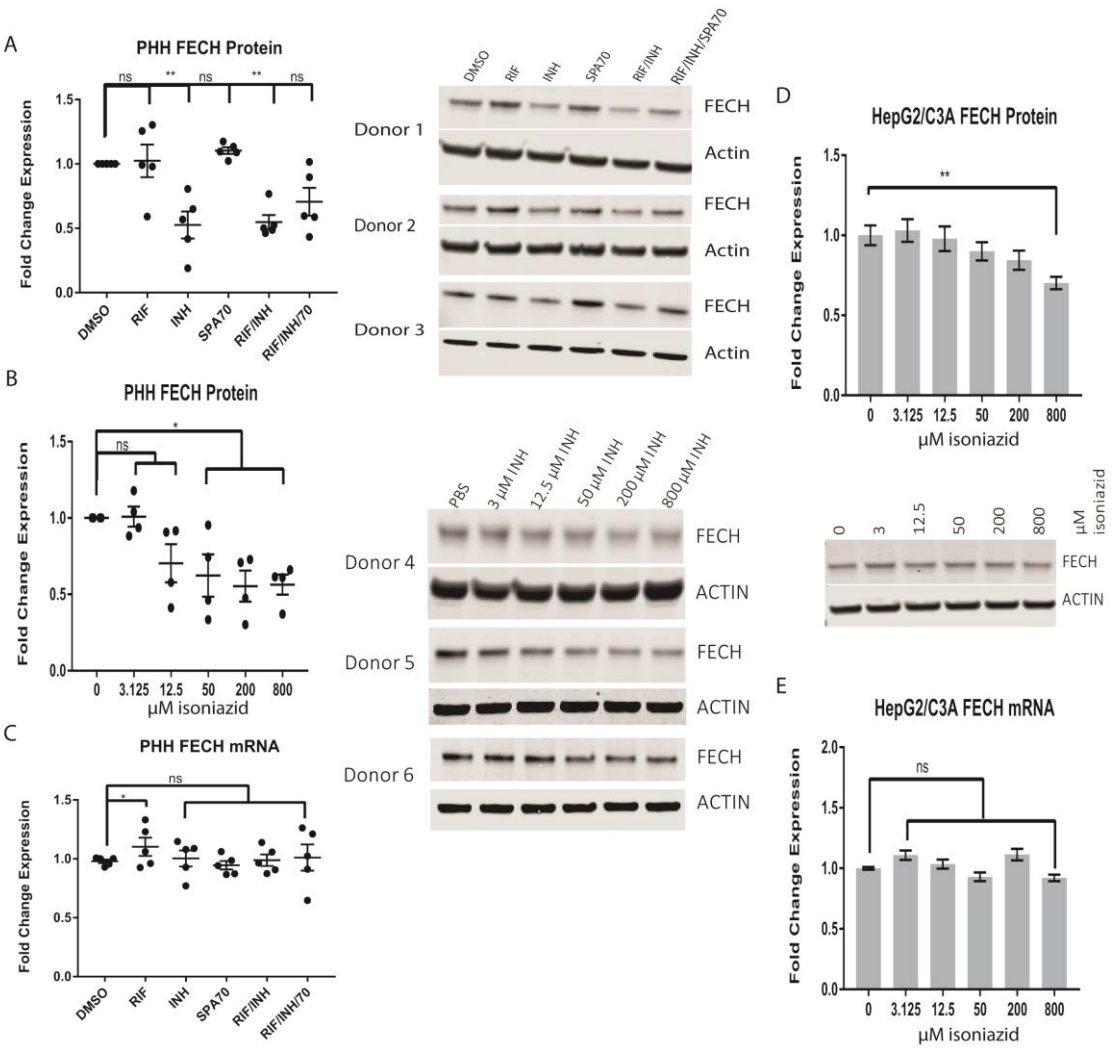

Figure 3-9. Isoniazid decreases human *FECH* protein.

Western blot analysis of *FECH* in primary human hepatocytes treated with 10 µM rifampicin, 10 µM SPA70, 200 µM isoniazid, or a combination of these drugs (A), and a dose response of isoniazid for 72 hours (B). qRT-PCR analysis of the expression of *FECH* in A (C). Western blot analysis of *FECH* in HepG2/C3A treated with isoniazid for 72 hours (D) and qRT-PCR analysis (E). The mean fold change in expression ± SEM are represented for the PHH. The mean fold change in expression of 3 biological repeats each with 3 technical repeats are represented for HepG2/C3A. 2-way ANOVA followed by Tukey's post-hoc analysis was used to compare group means for qRT-PCR analysis. 1-way ANOVA followed by Dunnett's post-hoc analysis was used to compare group means for Western blot analysis. ****$p<0.0001$; ***$p<0.001$, **$p<0.01$, *$p<0.05$

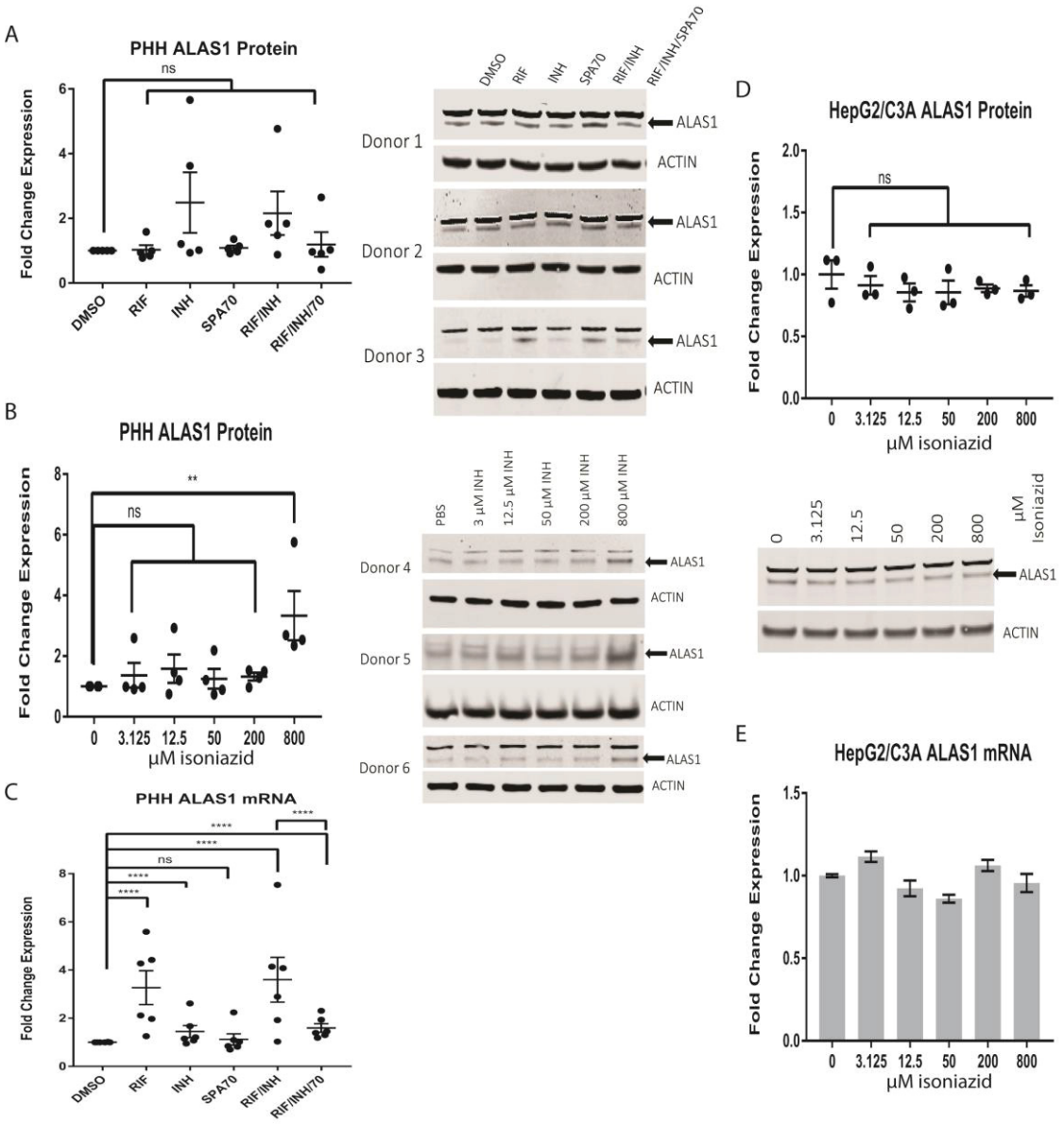

Figure 3-10. Isoniazid increases human *ALAS1* protein.

Western blot analysis of *ALAS1* in primary human hepatocytes treated with 10 µM rifampicin, 10 µM SPA70, 200 µM isoniazid, or a combination of these drugs (A), and a dose response of isoniazid for 72 hours (B). qRT-PCR analysis of the expression of *ALAS1* in A (C). Western blot analysis of *ALAS1* in HepG2/C3A treated with isoniazid for 72 hours (D) and qRT-PCR analysis (E). The mean fold change in expression ± SEM are represented for the PHH. The mean fold change in expression of 3 biological repeats are represented for HepG2/C3A. HepG2/C3A. 2-way ANOVA followed by Tukey's post-hoc analysis was used to compare group means for qRT-PCR analysis. 1-way ANOVA followed by Dunnett's post-hoc analysis was used to compare group means for Western blot analysis. ****$p<0.0001$; ***$p<0.001$, **$p<0.01$, *$p<0.05$

rifampicin and isoniazid at millimolar concentrations (Tostmann, Boeree et al. 2008, Singh, Sasi et al. 2011, Shih, Pai et al. 2013, Elmorsy, Attalla et al. 2017). Additionally, due to the presence of iron in the FBS added to cell culture medium, the conditions required for iron-mediated rescue by exogenous iron administration needed to be established in the media conditions of HepG2/C3A. The iron-specific chelator, 4.7 μM deferoxamine, decreased protein levels by 60% in HepG2/C3A at higher than 18.8 μM ($p<0.0001$), by 40% at 4.7 μM ($p<0.0001$), and by 10% at 1.2 μM ($p<0.01$), after 24 hours of treatment in 10% FBS (2.6 μM iron; **Figure 3-11A**). $FeCl_3$ administration of as little as 0.1 μM in 1% FBS (0.26 μM iron; **Figure 3-11B**) increased *FECH* protein levels 2-fold up to 3-fold at 1 μM in HepG2/C3A after 24 hours of treatment ($p<0.0001$). *FECH* was not increased due to additional iron administration in 10% FBS (2.6 μM iron; data not shown). The 40% ($p<0.05$) decrease in *FECH* protein expression by deferoxamine is rescued with increasing amounts of exogenously administrated $FeCl_3$ where there is no significant difference in *FECH* expression between the combination of 4.7 μM deferoxamine and 0.1 to 100 μM FeCl3 compared to the vehicle control treatment. There is a significant ($p<0.0001$) difference between 4.7 μM deferoxamine and the combination of 4.7 μM deferoxamine and 100 μM $FeCl_3$ (**Figure 3-11C**). To derive the media conditions where iron-limiting conditions can decrease *FECH* protein levels and where this can be rescued by exogenous iron supplementation requires a decrease of *FECH* in 10% FBS (2.6 μM iron) due to 4.7 μM deferoxamine.

The Isoniazid and Vitamin B_6 Conjugate, PIH, Down-Regulates Human *FECH* Protein

After establishing that iron-levels affect *FECH* in our model system and in what media conditions modulation of iron would produce observable effects for use as positive biological controls on *FECH* protein up- or down-regulation, we next tested metabolites that have been detected in humans following isoniazid treatment: isonicotinic acid, acetyl-hydrazine, diacetyl hydrazine, acetyl-isoniazid, menadione (ROS), and noc-18 (NOS) (Hughes 1953, Preziosi and Porcellati 1953, Defranceschi and Zamboni 1954, Johnson 1954, Zamboni and Defranceschi 1954, Kaneo, Kubo et al. 1981, Blair, Mansilla Tinoco et al. 1985). Suspecting that the well-established vulnerability of *FECH* iron depletion played a role, I selected an aroyl hydrazone adduct of isoniazid to test as well. The aroyl hydrazone selected was an adduct of isoniazid and a vitamin depleted by isoniazid treatment in humans, vitamin B_6. I investigated a variety of isoniazid metabolites (at 100 μM; as this was near the upper limit of what would be expected in portal hepatocytes and enabled us to rule out metabolites that do not affect *FECH* or *ALAS1*) on *FECH* protein expression in HepG2/C3A and found up-regulation of *FECH* protein by $FeCl_3$ and down-regulation by deferoxamine (**Figure 3-12A**) after 16 hours of treatment similar to previous reports ($FeCl_3$ was used as a positive control for *FECH* up-regulation and deferoxamine was used as a positive control for *FECH* down-regulation) (Taketani, Adachi et al. 2000, Crooks, Ghosh et al. 2010). I chose 16 hours because we expected the effect of isoniazid metabolites to be detected earlier than isoniazid itself but wanted to limit the amount of time for further breakdown products. An additional consideration was of the reported long half-life of *FECH*, which precluded an earlier time

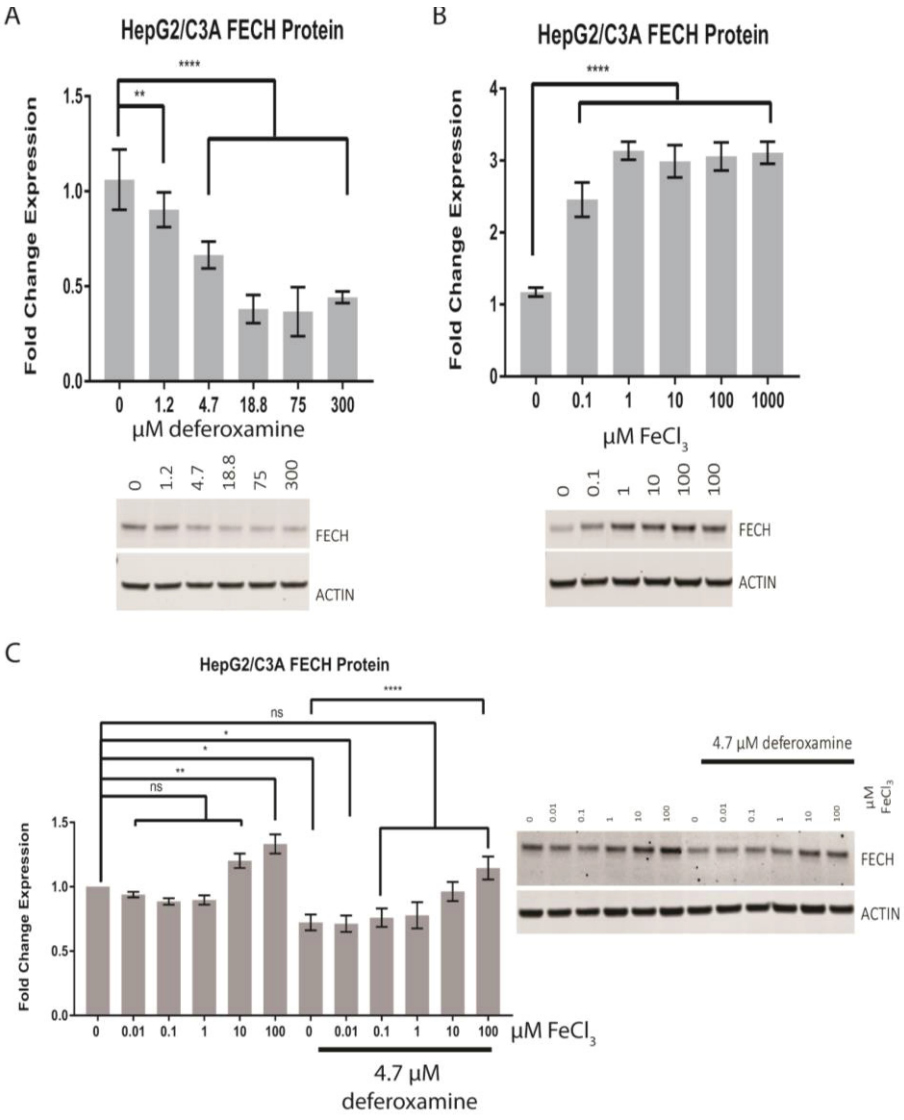

Figure 3-11. Iron levels affect *FECH* levels.

Western blot analysis of *FECH* in HepG2/C3A treated with deferoxamine mesylate at 24 hours in 10% FBS containing serum (A), with $FeCl_3$ at 24 hours in 1% FBS (B) and 10% FBS (C), and $FeCl_3$ in 10% FBS in the presence or absence of 4.7 μM deferoxamine (D). The mean fold change in expression ± SEM of 3 biologica1 repeats each with 3 technical repeats are represented for HepG2/C3A. 1-way ANOVA followed by Dunnett's post-hoc analysis was used to compare group means for Western blot analysis. ****$p<0.0001$; ***$p<0.001$, **$p<0.01$, *$p<0.05$

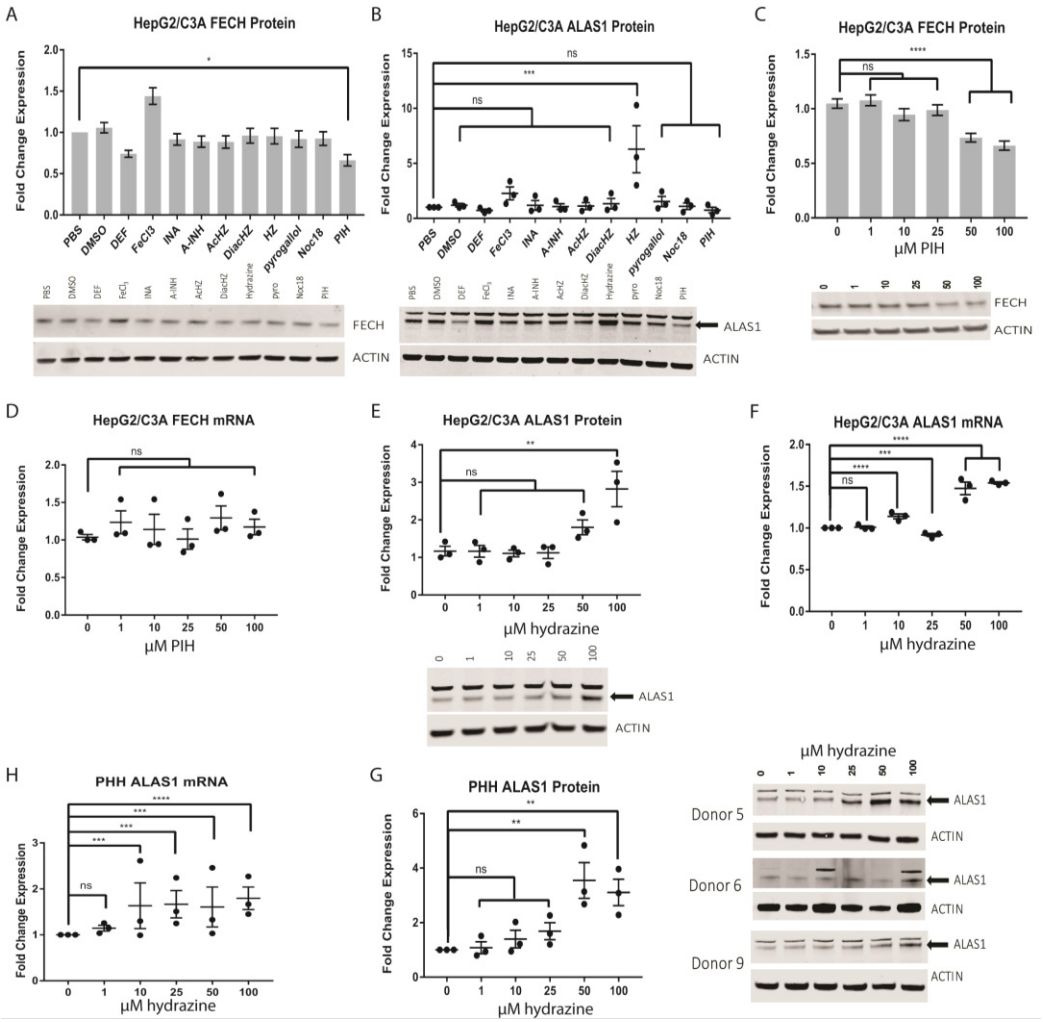

Figure 3-12. The effects of isoniazid metabolites on *FECH* and *ALAS1* levels.

Western blot analysis of *FECH* (A) and *ALAS1* (B) in HepG2/C3A treated for 16 hours with the indicated compound at 100 µM. Western blot analysis (C) and qRT-PCR (D) analysis of *FECH* in HepG2/C3A treated for 24 hours with the indicated dose of PIH. Western blot analysis (E) and qRT-PCR (F) analysis of *ALAS1* in HepG2/C3A treated for 24 hours with the indicated dose of hydrazine. Western blot analysis (G) and qRT-PCR (H) analysis of *ALAS1* in primary human hepatocytes treated for 24 hours with the indicated dose of hydrazine. The mean fold change in expression ± SEM of 3 biological repeats each with 3 technical repeats are represented for qRT-PCR analysis and Western blot analysis for *FECH*, and 3 biological repeats for *ALAS1* Western blot analysis. 2-way ANOVA followed by Tukey's post-hoc analysis was used to compare group means for qRT-PCR analysis. 1-way ANOVA followed by Dunnett's post-hoc analysis was used to compare group means for Western blot analysis. ****$p<0.0001$; ***$p<0.001$, **$p<0.01$, *$p<0.05$

point. Of the metabolites and reported by-products of isoniazid treatment tested, only PIH down-regulated *FECH* levels (**Figure 3-12A**) by 50%. Note that 300 μM Noc18 decreased *FECH* protein (data not shown). PIH decreased the *FECH* protein by up to 40% at greater than 50 μM in a dose-dependent manner in HepG2/C3A (**Figure 3-12C**; $p<0.0001$), but did not affect *FECH* mRNA (**Figure 3-12D**). In primary human hepatocytes, 72 hour daily administration of 50 μM or greater isoniazid was sufficient to significantly reduce ($p<0.05$) *FECH* protein levels by about 50% (**Figure 3-9B**).

Considering that the treatment of active tuberculosis is 2 months long (first-line therapy is daily oral doses of rifampicin, isoniazid, pyrazinamide, and ethambutol) and for latent tuberculosis is 9 months daily oral dose of 5 mg/kg (or 15 mg/kg twice weekly), and that plasma concentrations of isoniazid were 22-29 μM in a Moroccan population (Ait Moussa, El Bouazzi et al. 2016).) Another study reported a plasma isoniazid C_{max} of between 10 μM and 50 μM (Aarnoutse, Kibiki et al. 2017). Therefore, an isoniazid dose sufficient to decrease *FECH* liver protein should be achievable. At much higher doses of isoniazid (800 μM; $p<0.01$) was required to significantly reduce *FECH* protein levels by 40%. This could be due to lower intracellular vitamin B_6 concentrations between primary human hepatocytes and HepG2/C3A or a less reactive ortholog of vitamin B_6 in the cell culture media; 0.001 g/L pyridoxal HCl is in William's E media, and 0.001 g/L pyridoxine HCl is found in EMEM media. Pyridoxal HCl is much more efficient at producing PIH when in the presence of isoniazid than is pyridoxine HCl (**Figure 3-13I**). 50 μM PIH was sufficient to significantly reduce ($p<0.0001$) *FECH* levels in HepG2/C3A at 24 hours of treatment (**Figure 3-12C**). Due to the long half-life of *FECH* (35 hours), lower PIH doses may exert a more severe effect than was observed in a short period of treatment (Furukawa, Kohno et al. 1995).

The Isoniazid Breakdown Product, Hydrazine, Up-Regulates *ALAS1* mRNA and Protein

After determining that PIH decreased *FECH* protein levels, we then tested the isoniazid metabolites tested for *FECH* modulation for their potential to up-regulate *ALAS1*. *ALAS1* protein levels were increased at 16 hours treatment by 5-fold ($p<0.001$) by 100 μM hydrazine but were not affected by the isoniazid metabolites and break-down products isonicotinic acid, acetyl-hydrazine, diacetyl hydrazine, acetyl-isoniazid, menadione, and noc-18 in HepG2/C3A (**Figure 3-12B**). Hydrazine increased *ALAS1* protein 3-fold at 100 μM (**Figure 3-12E**; $p<0.01$) and mRNA 2-fold (**Figure 3-12F**; $p<0.0001$) at 50 μM in a dose-dependent manner in HepG2/C3A at 24 hours of treatment. Likewise, hydrazine increased *ALAS1* protein 3-fold at 50 μM (**Figure 3-12G**; $p<0.01$) and mRNA 1.5-fold above 10 μM (**Figure 3-12H**; $p<0.001$) in a dose-dependent manner in primary human hepatocytes. The dose of isoniazid required to produce a significant increase ($p<0.01$) of 3-fold in ALAS1 protein levels is 800 μM. This dose is far above plasma isoniazid doses in humans. However, N-alkylation of the heme moiety in CYP450 enzymes and other proteins may lead to decreased levels of these proteins and ultimate up-regulation of ALAS1 protein levels after depletion of the regulatory heme.

Figure 3-13. Detection of PIH following isoniazid application.

PIH is formed from isoniazid and pyridoxal (A). LC/MS/MS analysis of PIH in *hPXR* and *mPxr*$^{-/-}$ expressing C57BL/6 mouse livers (B), primary human hepatocytes cell culture medium (C), and HepG2/C3A cell culture medium in a time dependent (D) and dose (E) dependent manner after treatment with isoniazid. LC/MS/MS analysis of PIH in HepG2/C3A cell culture medium treated for 24 hours with various amounts of pyridoxal 5' phosphate (F), pyridoxal HCl (G), or pyridoxine HCl (H). LC/MS/MS analysis of PIH in phosphate buffered saline treated with the indicated Vitamin B_6 (1 mM) analogue at the indicated times and temperatures in the presence (I) or absence (J) of 1 mM isoniazid. Western blot analysis of *FECH* in HepG2/C3A treated for 24 hours with pyridoxal 5'phosphate (K) or pyridoxal HCl (L) in the presence or absence of 200 μM isoniazid. PIH levels are represented as the mean fold change of 3 biological replicates ± SEM for the *in vitro* data and as the mean (n = 4-5 per group) ± SEM for the *in vivo* data. The mean fold change in expression ± SEM 3 biological repeats each with 3 technical repeats are represented for Western blot analysis for *FECH*. 1-way ANOVA followed by Dunnett's post-hoc analysis was used to compare group means for Western blot analysis and LC/MS/MS analysis. ****$p<0.0001$; ***$p<0.001$, **$p<0.01$, *$p<0.05$

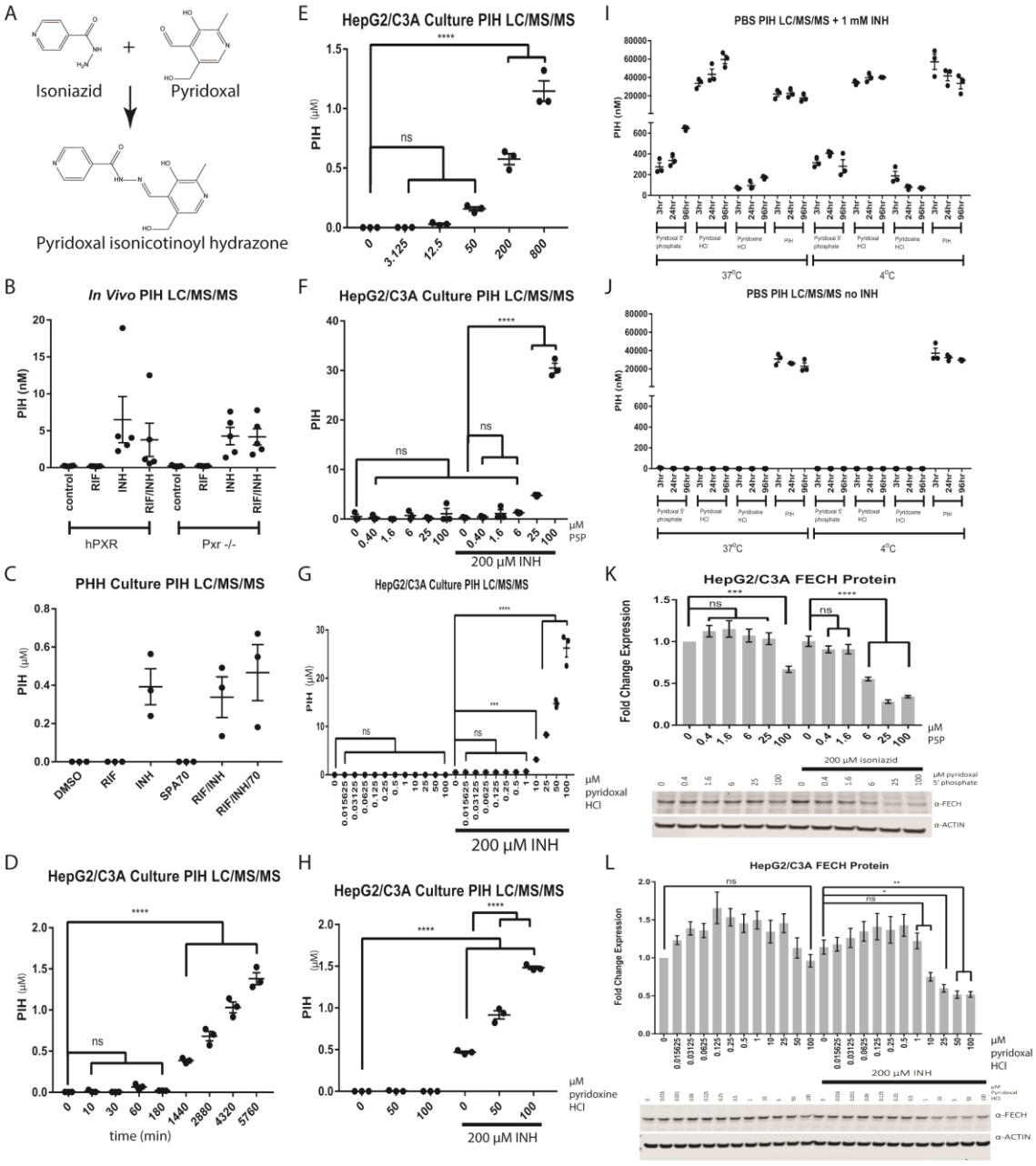
A
Isoniazid
Pyridoxal
Pyridoxal isonicotinoyl hydrazone
B
In Vivo PIH LC/MS/MS
PIH (nM)
control
RIF
INH
RIF/INH
hPXR
Pxr -/-
C
PHH Culture PIH LC/MS/MS
PIH (μM)
DMSO
RIF
INH
SPA70
RIF/INH
RIF/INH/70
D
HepG2/C3A Culture PIH LC/MS/MS
PIH (μM)
time (min)
E
HepG2/C3A Culture PIH LC/MS/MS
PIH (μM)
ns
F
HepG2/C3A Culture PIH LC/MS/MS
PIH
μM P5P
200 μM INH
G
HepG2/C3A Culture PIH LC/MS/MS
PIH (μM)
μM pyridoxal HCl
200 μM INH
H
HepG2/C3A Culture PIH LC/MS/MS
PIH (μM)
μM pyridoxine HCl
200 μM INH
I
PBS PIH LC/MS/MS + 1 mM INH
PIH (nM)
37°C
4°C
J
PBS PIH LC/MS/MS no INH
PIH (nM)
37°C
4°C
K
HepG2/C3A FECH Protein
Fold Change Expression
μM P5P
200 μM isoniazid
μM pyridoxal 5' phosphate
α-FECH
α-ACTIN
L
HepG2/C3A FECH Protein
Fold Change Expression
μM pyridoxal HCl
200 μM INH
α-FECH
α-ACTIN

PIH Is Detected after Treatment of Human Primary Cells, Human Cell Lines, and Mice with Isoniazid

PIH formation was next detected and characterized in cell culture media with cells present and mouse liver. 5 nmole/mg tissue PIH is detected in the livers of C57BL/6 mice treated with isoniazid for 6 weeks (**Figure 3-13B**), 400 nM PIH is detected in the cell culture medium of PHH treated for 72 hours (**Figure 3-13C**) with daily dosing of isoniazid; and 0.5 μM is detected at 24 hours up to 1.5 μM at 96 hours in the cell culture medium of HepG2/C3A in a time-dependent manner after a single dose of 200 μM isoniazid (**Figure 3-13D;** $p<0.0001$) and 0.5 μM PIH is detected at 200 μM isoniazid up to 1.2 μM PIH at 800 μM isoniazid in a dose-dependent manner after 72 hours of daily isoniazid treatment in HepG2/C3A (**Figure 3-13E**; $p<0.0001$). Addition of the vitamin B_6 analogues, pyridoxal 5' phosphate (**Figure 3-13F**), pyridoxal HCl (**Figure 3-13G**), and pyridoxine HCl (**Figure 3-13H**) result in a further increase of PIH when combined with isoniazid. 25 μM pyridoxal 5' phosphate combined with 200 μM isoniazid results in the formation of 5 μM PIH up to 30 μM PIH at 100 μM pyridoxal 5' phosphate and 200 μM isoniazid in HepG2/C3A cell culture medium. 10 μM pyridoxal HCl combined with 200 μM isoniazid resulted in the formation of 3 μM PIH up to 27 μM PIH when 100 μM pyridoxal HCl combined with 200 μM isoniazid in HepG2/C3A cell culture medium. 50 μM pyridoxine HCl combined with 200 μM isoniazid results in the formation of 1 μM PIH up to 1.5 μM PIH at 100 μM pyridoxal HCl and isoniazid. The treatment ofHepG2/C3A with 200 μM isoniazid alone at 24 hours did not decrease *FECH* protein (72 hours is required for isoniazid-mediated FECH protein decrease), but the combination of 200 μM isoniazid with 6 μM pyridoxal 5' phosphate decreased *FECH* protein by 50% up to 70% at 25 μ M pyridoxal 5'phosphate (**Figure 3-13K**; $p<0.0001$) or 25 μM pyridoxal HCl (**Figure 3-13L**; $p<0.05$ at 25 μM; $p<0.01$ at 50 and 100 μM) decreased *FECH* protein levels by 50%. 100 μM pyridoxine HCl and 200 μM isoniazid combination did not affect *FECH* protein levels (data not shown).

PIH Is Formed in a Reaction between Isoniazid and Vitamin B_6 Analogues

No report exists of a definitive characterization of the formation (**Figure 3-13A)** of PIH**.** Therefore, we next characterized the formation of PIH in enzyme-free conditions. Briefly, 1 mM of each indicated compound was added to phosphate buffered saline and allowed to incubate at the indicated temperature for the indicated time and then analyzed by mass spectrometry for PIH. PIH is formed in a cell- and enzyme-independent reaction by combining vitamin B_6 analogs, such as pyridoxal 5' phosphate, pyridoxal hydrochloride, and to a lesser extent pyridoxine hydrochloride (**Figure 3-13A**, **I** and **J**). The combination of isoniazid with pyridoxal hydrochloride produced two orders of magnitude higher PIH (30-60 μM, depending on incubation time) than reaction of isoniazid with pyridoxal 5' phosphate (the enzymatically active form) formed PIH (0.3-0.6 μM). The combination of isoniazid and pyridoxine HCl produces a much lower amount of PIH (0.1 μM) 1 mM PIH spontaneously breaks down to approximately 100 μM isoniazid in 37°C at 96 hours and to a much lower extent in 4°C (**Figure 3-14**). More PIH is formed at 37°C following incubation at various times of vitamin B_6 analogs

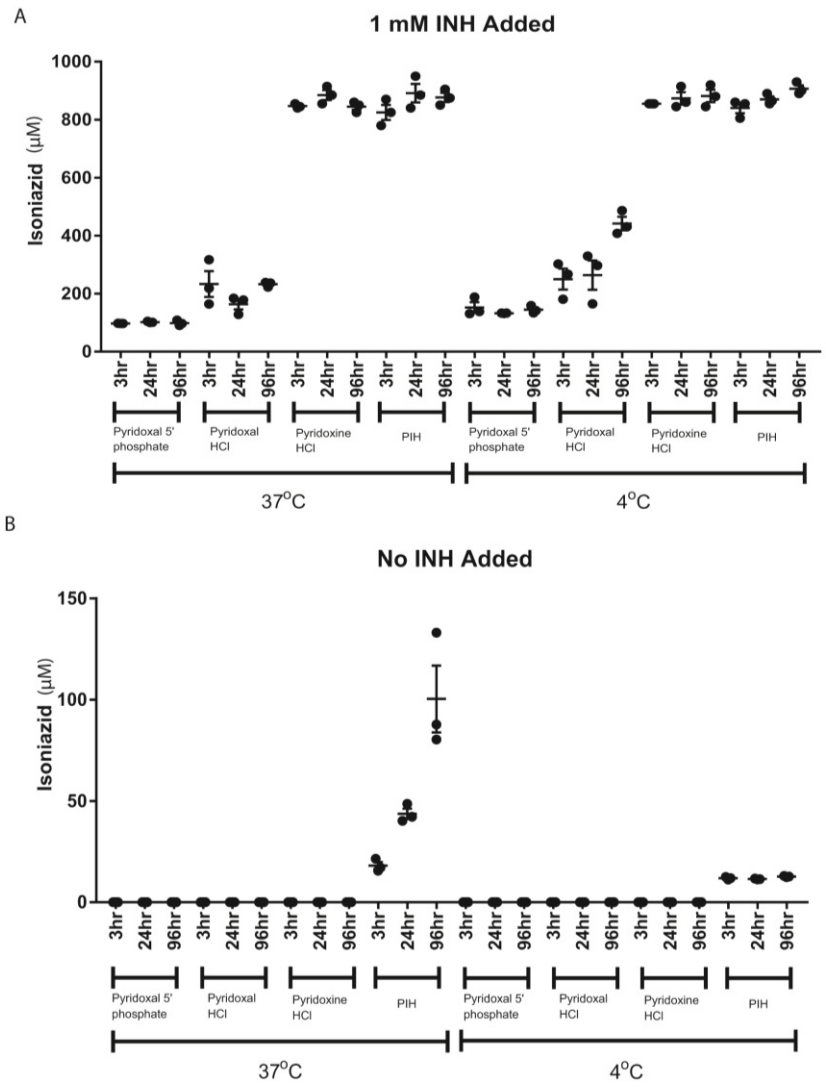

Figure 3-14. Detection of isoniazid following isoniazid application.

LC/MS/MS analysis of isoniazid in PBS treated with the indicated compounds for the indicated time and the indicated temperature with (A) or without (B) 1 mM isoniazid added. The mean ± SEM of 3 repeats are expressed.

than is formed at4°C (**Figure 3-13I**). These data are characteristic of the thermodynamic dehydration reaction (**Figure 3-13A**) that produces PIH from vitamin B_6 analogs and isoniazid.

Hydrazine Is Detected after Treatment of Human Primary Cells and Human Cell Lines with Isoniazid

In PBS, relatively low levels of hydrazine are formed (150 nM hydrazine after incubation of 1 mM isoniazid for 96 hours; **Figure 3-15E**). 8 μM hydrazine is detected at 24 hours ($p<0.001$) treatment of HepG2/C3A with a single dose of 200 μM isoniazid, which increases to 9 μM at 48 hours, 12 μM at 72 hours, and 17 μM (**Figure 3-15A**) at 96 hours. In HepG2/C3A cell culture medium treated with 800 μM isoniazid daily for 72 hours there was 22 μM hydrazine detected (**Figure 3-15B**; $p<0.0001$), but only 3 μM hydrazine was detected after 24 hours of treatment (**Figure 3-15C**; $p<0.05$). The cell culture media of 3 donors of primary human hepatocytes were analyzed for hydrazine concentration after 72 hour treatment of 200 μM isoniazid with media and drug refreshed daily (**Figure 3-15D**). The amount of hydrazine detected varied considerably between donors, 2 donors had approximately 2-5 μM of hydrazine detected in the cell culture media when treated with isoniazid, but a third donor had approximately 50-120 μM isoniazid detected dependent on treatment combination. This represents the average of 40 μM hydrazine detected following isoniazid treatment of primary human hepatocytes ($p<0.0001$). Indeed, this wide range of hydrazine production could be reflected in the varied response in ALAS1 induction in similar treatment conditions (**Figure 3-10A**).

PIH Decreases FECH Protein Levels by Decreasing Iron Availability

Considering the vulnerability of *FECH* to low iron conditions, especially in the presence of iron chelators, we next tested whether exogenous iron application would rescue the 40% decrease in *FECH* levels at 24 hours from 50 μM PIH-mediated depletion of the regulatory heme pool over time. Therefore, a lower dose administered over a period of months may be required for the effect to be observed *in vivo*. Likewise, twenty-four hour treatment of primary human hepatocytes with 50 μM hydrazine resulted in a significant 3-fold increase ($p<0.01$) in ALAS1 protein levels (**Figure 3-12G**). Indeed, hydrazine concentrations increase both with length of treatment and with number of treatments. The formation of hydrazine may depend on amidase activity (Sarich, Adams et al. 1999) and the activation of hydrazine to interact with cellular proteins may require activation by P450 enzymes (Nelson, Mitchell et al. 1976, Lauterburg, Smith et al. 1985, Delaney and Timbrell 1995, Sarich, Adams et al. 1999). Human cell lines and primary hepatocytes may not quantitatively reflect the *in vivo* activity of enzymes that metabolize xenobiotics (Guillouzo, Morel et al. 1993, Bjornsson, Callaghan et al. 2003, Guillouzo and Guguen-Guillouzo 2008, Turpeinen, Tolonen et al. 2009). Thus, higher levels of hydrazine may be formed in model systems with more CYP450 activity.

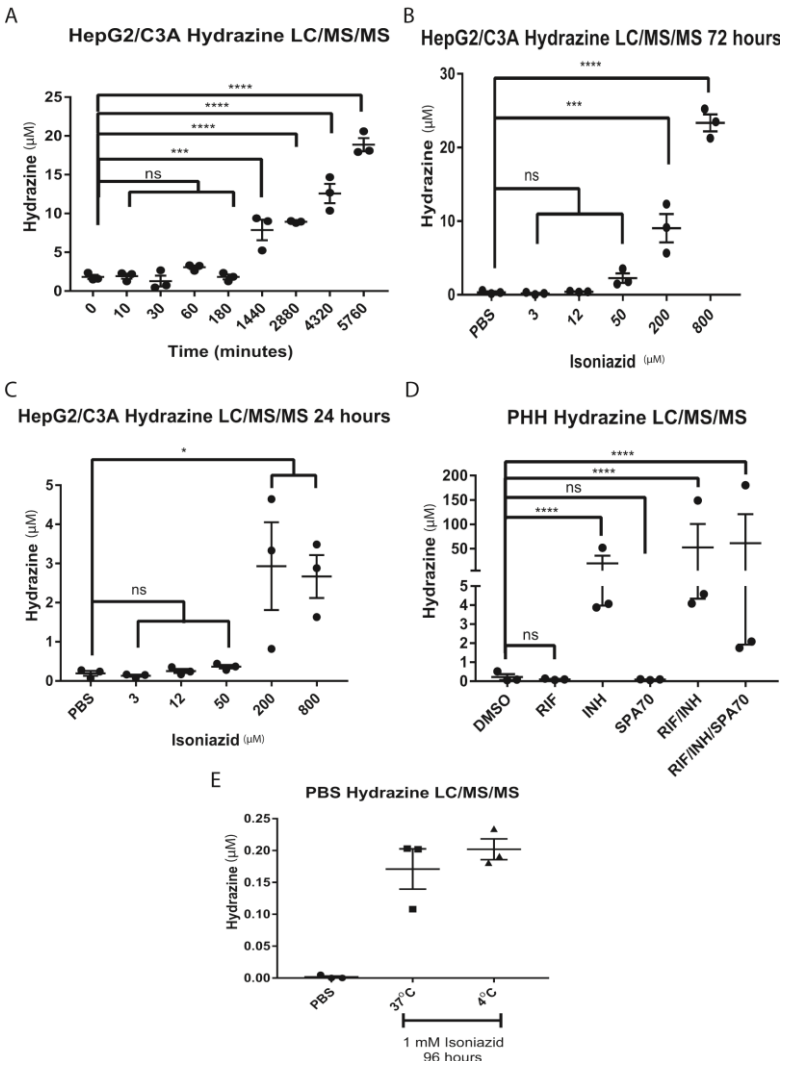

Figure 3-15. Detection of hydrazine adduct following isoniazid application.

LC/MS analysis of hydrazine-adduct in HepG2/C3A cell culture media at various times after treatment with a single dose of 200 µM isoniazid (A), various single isoniazid doses after 24 hours (C), and 3 daily isoniazid doses at 72 hours (B). LC/MS analysis of hydrazine-adduct in primary human hepatocyte cell culture media at 72 hours after 3 daily doses of 200 µM isoniazid (D). LC/MS analysis of phosphate buffered saline after 96 hour incubation with 1 mM isoniazid at the indicated temperature (E). Hydrazine-adduct levels in HepG2/C3A and phosphate buffered saline are represented as the mean ± SEM of 3 biological replicates. Hydrazine-adduct levels in primary human hepatocytes are represented as the mean +/- SEM of 3 biological and 3 technical replicates. 2-way ANOVA followed by Tukey's post-hoc analysis was used to compare group means for LC/MS analysis of primary human hepatocytes. 1-way ANOVA followed by Dunnett's post-hoc analysis was used to compare group means for LC/MS/MS analysis of HepG2/C3A and phosphate buffered saline. ****$p<0.0001$; ***$p<0.001$, **$p<0.01$, *$p<0.05$

down-regulation and to associate this with iron chelation directly. In HepG2/C3A (**Figure 3-16A**) and PHH (**Figure 3-16B**), the decrease in *FECH* protein levels due to 50 μM PIH can be rescued by the co-administration of $FeCl_3$. 50 μM PIH treatment of HepG2/C3A for 24 hours results in a 40% decrease of *FECH* protein ($p< 0.05$) compared to PBS treatment (**Figure 3-16A**). The addition of 0.01 μM $FeCl_3$ abrogates the significance of the decrease in *FECH* protein due to 50 μM PIH and the addition of 10 and 100 μM $FeCl_3$ results in a significant increase of *FECH* protein compared to 50 μM PIH. Isoniazid treatment of PHH for 24 hours results in a 40% decrease of *FECH* protein ($p< 0.01$) that is not rescued by $FeCl_3$ addition (**Figure 3-16B**). However, PIH treatment of PHH for 24 hours results in a 40% decrease of *FECH* protein ($p< 0 .01$) that is abrogated by 0.1 and 1 mM $FeCl_3$. PIH (**Figure 3-16D**), similar to (**Figure 3-16C**) deferoxamine, chelates iron. The CAS shuttle assay has iron present and chelation of this iron results in a decrease of absorbance at 630 nm. In other words, the more free iron available, the higher the absorbance at 630 nm. This iron chelation is also seen due to the product of pyridoxal HCl and isoniazid formation at 96 hours (**Figure 3-16E**; $p< 0.0001$) in 37°C in PBS and in HepG2/C3A cell culture medium (**Figure 3-16F**; $p< 0.01$) treated for 24 hours at 50 μM pyridoxal HCl and 200 μM isoniazid and $p<0.0001$ at 100 μM pyridoxal HCl and 200 μM isoniazid). Together these data demonstrate the PIH-mediated iron chelation decreases *FECH* levels.

Proteomics Profiling of *hPXR* Mice Treated with Rifampicin and Isoniazid

Introduction

After characterizing the effect of isoniazid metabolites on the heme biosynthesis pathway that may lead to PPIX accumulation, the possible role of rifampicin was investigated by TMT-labeled proteomics screening of mice treated with rifampicin and isoniazid. Previous reports have shown that isoniazid alone is not sufficient for PPIX up-regulation of 60-fold (Li, Lu et al. 2013, Sachar, Li et al. 2016). Clustering analysis revealed similar protein changes within groups (**Figure 3-17** and **Figure 3-18**). Proteomics profiling identified proteins that (1) were changed in each treatment group and the overlap between treatment groups and (2) proteins changed in pathways relevant to heme synthesis and degradation, CYP450 and steroid metabolism enzymes, nuclear receptors, organic transporters, iron metabolism, oxidative stress, [Fe-S] cluster assembly machinery, wound healing and inflammation, vitamin B_6 metabolism, and [Fe-S] cluster-containing proteins. 8,466 proteins were identified and quantified. Compared to hPXR mice administered control food and water, 101 proteins were increased in rifampicin and isoniazid treated *mPXR* $^{-/-}$ mice, but were not increased in *hPXR* mice treated with rifampicin and isoniazid (**Figure 3-19**). 179 proteins are up-regulated at a $p < 0.01$ in *hPXR* mice treated with rifampicin and isoniazid compared to *hPXR* mice fed the control diet and water (**Figure 3-19**). 101 proteins are up-regulated in *mPxr* $^{-/-}$ mice treated with rifampicin and isoniazid compared to *hPXR* mice (**Figure 3-20**) on the control diet and water. 49 proteins are up-regulated due to the combination of rifampicin and isoniazid in both *hPXR* and *mPxr* $^{-/-}$ mice (**Figure 3-20**). 21 proteins are up-regulated in *hPXR* mice

Figure 3-16. PIH decreases *FECH* levels by decreasing iron availability.

Western blot analysis of HepG2/C3A (A) and primary human hepatocytes (B) treated with increasing doses of $FeCl_3$ in the presence or absence of PIH in HepG2/C3A and the presence and absence of PIH and isoniazid in primary human hepatocytes. Spectrophotometric analysis of CAS shuttle assay of deferoxamine (C), PIH (D), biochemical reaction products (E) of pyridoxal HCl and isoniazid, and HepG2/C3A cell culture medium (F) treated with pyridoxal in the presence or absence of isoniazid (100 μM). The mean fold change in expression ± SEM of 3 biological repeats each with 3 technical repeats are represented for Western blot analysis for *FECH* in HepG2/C3A. The mean fold change in expression +/- SEM of donors are represented for Western blot analysis for *FECH* in primary human hepatocytes. Spectrophotometric analysis of the background subtracted absorbance (630 nm) of the CAS shuttle solution is represented as the mean ± SEM of 3 repeats for deferoxamine and PIH dilution and biochemical reaction product, and 3 biological repeats each with 3 technical repeats for the HepG2/C3A cell culture medium. 1-way ANOVA followed by Dunnett's post-hoc analysis was used to compare group means for Western blot analysis and spectrophotometric analysis. ****$p<0.0001$; ***$p<0.001$, **$p<0.01$, *$p<0.05$

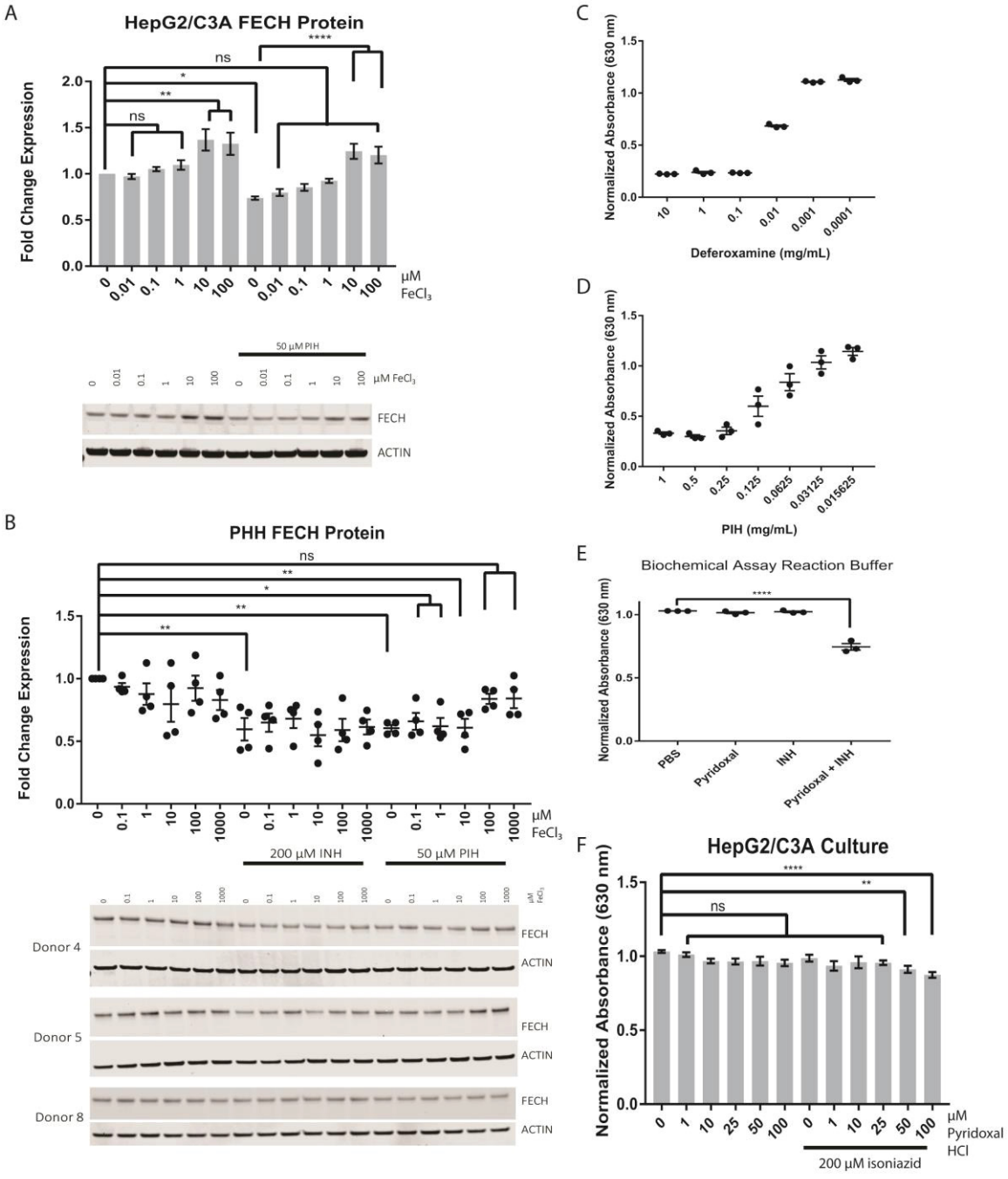
A
HepG2/C3A FECH Protein
Fold Change Expression
ns
*
**
****
μM FeCl3
50 μM PIH
FECH
ACTIN
B
PHH FECH Protein
200 μM INH
50 μM PIH
Donor 4
Donor 5
Donor 8
C
Normalized Absorbance (630 nm)
Deferoxamine (mg/mL)
D
PIH (mg/mL)
E
Biochemical Assay Reaction Buffer
PBS
Pyridoxal
INH
Pyridoxal + INH
F
HepG2/C3A Culture
μM Pyridoxal HCl
200 μM isoniazid

Figure 3-17. Clustering analysis of top 100 most variable proteins.

Hierarchical clustering of differentially expressed proteins due to treatment group. Low expression proteins (peptide sequence matches < 10) were filtered and the top 100 most variable proteins are displayed. Only changes with a significance of $p < 0.01$ are displayed as determined by one-way ANOVA with Dunnett's post-hoc analysis. Z-scores are shown where red indicates up regulated and blue indicates down-regulated proteins.

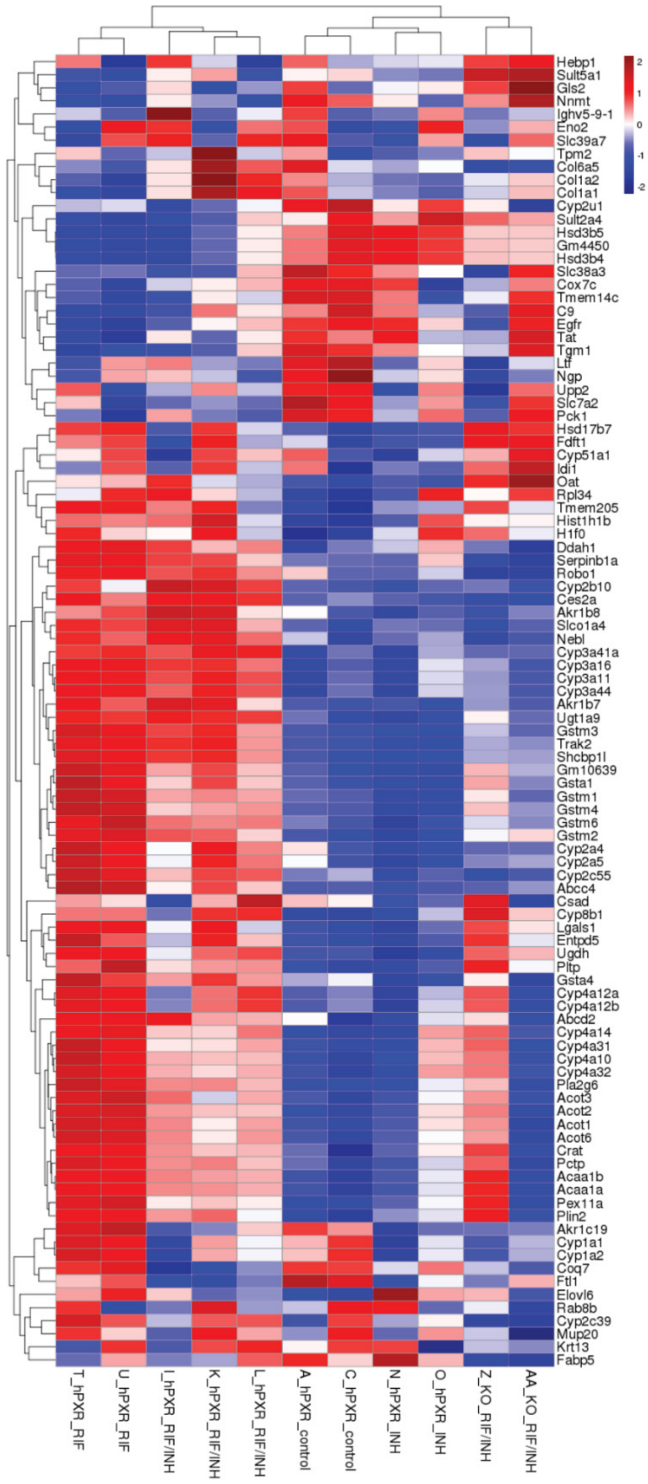
Hebp1
Sult5a1
Gls2
Nnmt
Ighv5-9-1
Eno2
Slc39a7
Tpm2
Col6a5
Col1a2
Col1a1
Cyp2u1
Sult2a4
Hsd3b5
Gm4450
Hsd3b4
Slc38a3
Cox7c
Tmem14c
C9
Egfr
Tat
Tgm1
Ltf
Ngp
Upp2
Slc7a2
Pck1
Hsd17b7
Fdft1
Cyp51a1
Idi1
Oat
Rpl34
Tmem205
Hist1h1b
H1f0
Ddah1
Serpinb1a
Robo1
Cyp2b10
Ces2a
Akr1b8
Slco1a4
Nebl
Cyp3a41a
Cyp3a16
Cyp3a11
Cyp3a44
Akr1b7
Ugt1a9
Gstm3
Trak2
Shcbp1l
Gm10639
Gsta1
Gstm1
Gstm4
Gstm6
Gstm2
Cyp2a4
Cyp2a5
Cyp2c55
Abcc4
Csad
Cyp8b1
Lgals1
Entpd5
Ugdh
Pltp
Gsta4
Cyp4a12a
Cyp4a12b
Abcd2
Cyp4a14
Cyp4a31
Cyp4a10
Cyp4a32
Pla2g6
Acot3
Acot2
Acot1
Acot6
Crat
Pctp
Acaa1b
Acaa1a
Pex11a
Plin2
Akr1c19
Cyp1a1
Cyp1a2
Coq7
Ftl1
Elovl6
Rab8b
Cyp2c39
Mup20
Krt13
Fabp5
2
1
0
-1
-2
T_hPXR_RIF
U_hPXR_RIF
I_hPXR_RIF/INH
K_hPXR_RIF/INH
L_hPXR_RIF/INH
A_hPXR_control
C_hPXR_control
N_hPXR_INH
O_hPXR_INH
Z_KO_RIF/INH
AA_KO_RIF/INH

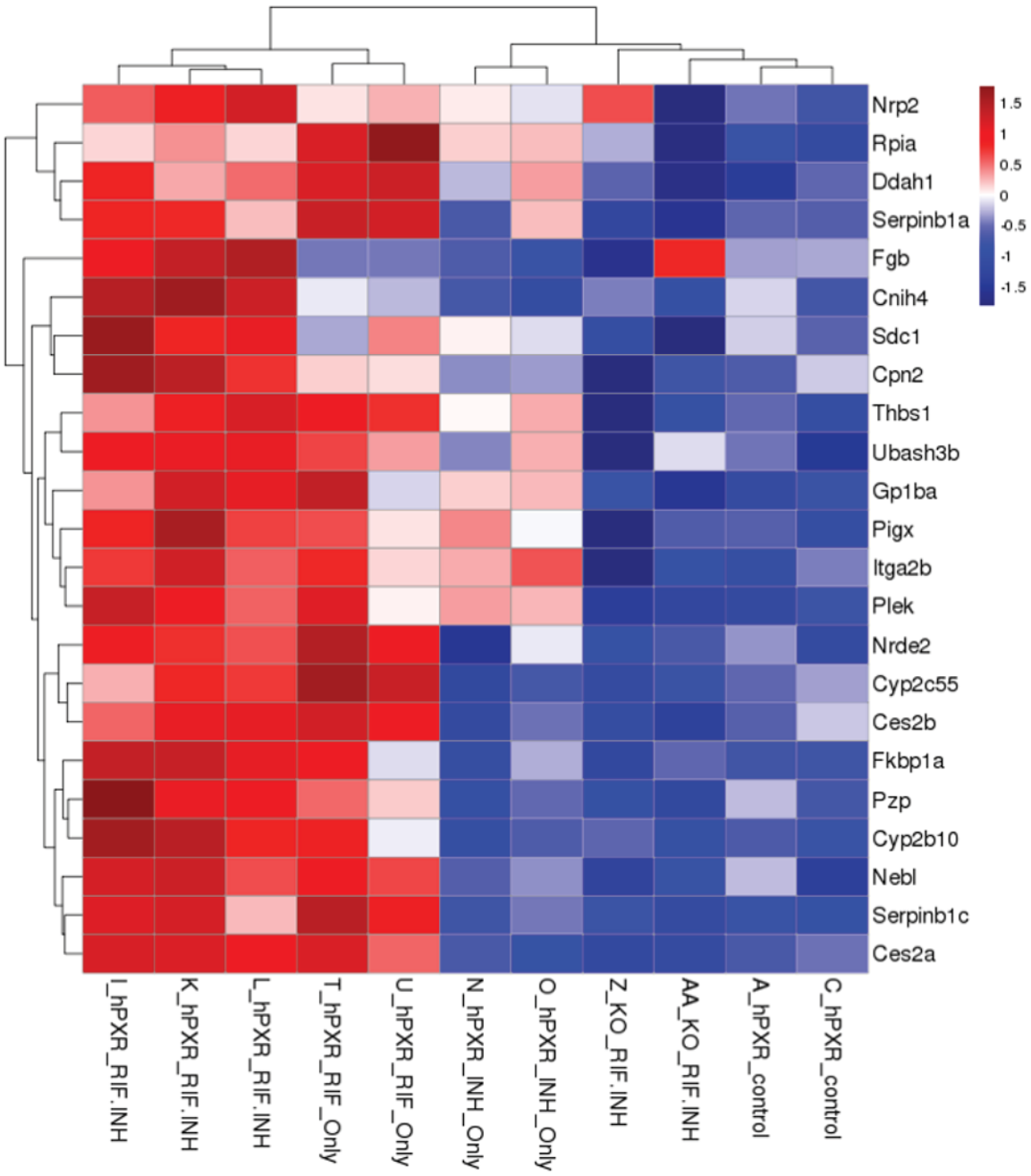

Figure 3-18. Clustering analysis of hPXR-dependent changes.

Clustering analysis of genes up-regulated in *hPXR* mice treated with rifampicin and isoniazid compared to control *hPXR* mice and down-regulated in *mPxr* $^{-/-}$ mice treated with rifampicin and isoniazid. Only changes with a significance of $p < 0.01$ are displayed as determined by one-way ANOVA with Dunnett's post-hoc analysis. Z-scores are shown where red indicates up regulated and blue indicates down-regulated proteins.

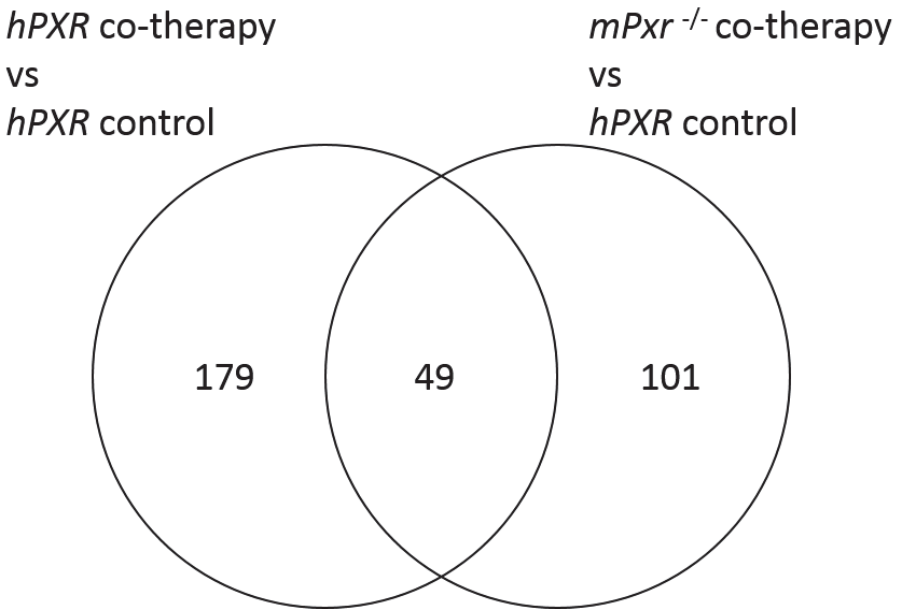

Figure 3-19. Venn diagram showing the overlap between proteins up-regulated in *hPXR* and *mPXR* $^{-/-}$ mice treated with rifampicin and isoniazid.

Venn diagram displaying proteins up-regulated in *hPXR* and *mPxr*$^{-/-}$ mice treated with rifampicin and isoniazid compared to control mice.

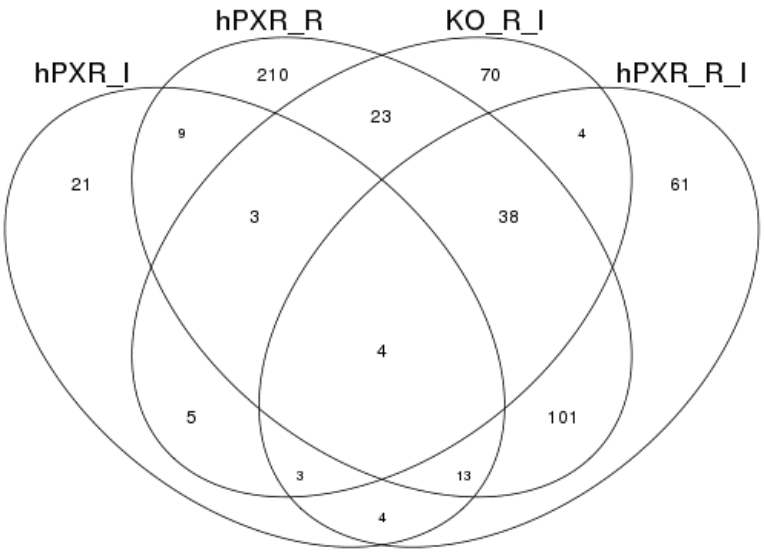

Figure 3-20. Venn diagram of the overlap in up-regulated proteins between all treatment groups.

Venn diagram displaying proteins up-regulated in all treatment groups compared to control. hPXR_I = *hPXR* mice treated with isoniazid, hPXR_R = *hPXR* mice treated with rifampicin, KO_R_I = *mPxr* $^{-/-}$ mice treated with rifampicin and isoniazid, hPXR_R_I = *hPXR* mice treated with rifampicin and isoniazid.

treated with isoniazid, but not in other treatment groups, 210 proteins are up-regulated due to rifampicin alone in *hPXR* mice, 70 proteins are up-regulated in *mPxr*$^{-/-}$ mice treated with rifampicin and isoniazid, and 61 proteins are up-regulated due to rifampicin and isoniazid in *hPXR* mice, but not in other groups (**Figure 3-20**). All of these changes are significant $p < 0.01$. Only 4 proteins are up-regulated in all groups and only 13 are up-regulated in all *hPXR* groups (**Figure 3-20**).

Heme Biosynthesis and Degradation

ALAS1 was highly up-regulated (1.9 fold-change in *hPXR* mice treated with rifampicin and isoniazid, 2.6 fold-change in *hPXR* mice treated with isoniazid, and 1.4 fold-change in *mPxr* $^{-/-}$ mice treated with rifampicin and isoniazid), but not significantly across groups (**Table 3-1**; $p = 0.28$). Interestingly *ALAS2* was significantly ($p = 0.018$) changed at 1.38 fold in *hPXR* mice treated with isoniazid and 1.18 fold in *mPxr* $^{-/-}$ treated with rifampicin and isoniazid up-regulated, but down-regulated due to rifampicin (0.73 fold) and the combination of rifampicin and isoniazid. Isoniazid up-regulates *ALAS1* and to a lesser magnitude *ALAS2* (the presence of which may possibly be due to blood contamination). Rifampicin may suppress *ALAS2* levels in *hPXR* mice. *Uroporphyrinogen-III synthase* (*Uros*) was significantly changed ($p = 0.012$) by an increase of 1.19 fold in *hPXR* mice treated with rifampicin and isonaiazid and 1.31 fold in *hPXR* mice treated with rifampicin and isoniazid as well as 1.38 fold increase in *mPxr* $^{-/-}$ mice treated with rifampicin and isoniazid. These data suggest that Uros may be up-regulated by rifampicin in an *hPXR*-independent manner. *Protoporphyrinogen oxidase* (*Ppox*) is significantly down-regulated ($p = 0.013$) by all treatments in an *hPXR* dependent manner by from 0.69 to 0.85 fold, and the effect may be more pronounced in *hPXR* mice compared treated with rifampicin and isoniazid (0.69 fold) to *mPxr* $^{-/-}$ mice (0.83 fold). *Fech* is down-regulated ($p < 0.0001$) due to all groups, but to a much lower extent in *hPXR* mice treated with rifampicin (0.88 fold) to between 0.39 fold to 0.5 fold in the groups treated with isoniazid. *Biliverdin reductase* (*Blvra*) is significantly ($p = 0.032$), but slightly (0.82 to 0.92 fold) down-regulated in all treatment groups independent of *hPXR* status. *NADPH-cytochrome P450 reductase* (*Por*) was up-regulated in both combination groups (1.28 fold to 1.12 fold) and due to rifampicin (1.18 fold), but was slightly down-regulated due to isoniazid (0.92). In *Fech*^{m1Pas} Balb/c mouse livers with increased PPIX levels, *Alas1* was increased and *Alas2* was decreased (Davies, Schuurman et al. 2005). *Alas2*, *Ppox*, and *Fech* from a complex in the mitochondria (Medlock, Shiferaw et al. 2015).

CYP450 and Steroid Metabolism Enzymes

Cyp2b10 is the most up-regulated CYP450 and is significantly ($p = 0.0003$) increased by rifampicin (2.49 fold) and rifampicin and isoniazid (4.95 fold) in *hPXR* mice but not more than a 10% change in *mPxr* $^{-/-}$ mice or *hPXR* mice treated with isoniazid (**Table 3-2).** *3-beta-hydroxysteroid dehydrogenase type 4* (*Hsd3b4*) was the most down-regulated significantly ($p = 0.0012$) due to rifampicin (0.098 fold) in *hPXR* mice with a.

Table 3-1. Heme biosynthesis and degradation.

		Fold Change to Control					
		hPXR			KO		
Protein Description	GN	RIF/INH	INH	RIF	RIF/INH	p-Value	FDR
5-aminolevulinate synthase	Alas1	1.90	2.61	1.05	1.41	0.28	0.53
5-aminolevulinate synthase	Alas2	0.86	1.38	0.73	1.18	0.018	0.17
Delta-aminolevulinic acid dehydratase	Alad	0.96	1.00	1.02	0.95	0.75	0.87
Porphobilinogen deaminase	Hmbs	1.04	0.99	1.10	1.05	0.67	0.8
Uroporphyrinogen-III synthase	Uros	1.19	1.09	1.31	1.38	0.012	0.16
Uroporphyrinogen decarboxylase	Urod	0.92	1.03	0.94	0.92	0.33	0.58
Oxygen-dependent coproporphyrinogen-III oxidase,	Cpox	1.13	1.04	1.18	1.15	0.20	0.46
Protoporphyrinogen oxidase	Ppox	0.69	0.81	0.85	0.83	0.013	0.16
Ferrochelatase,	Fech	0.39	0.50	0.88	0.43	0.000002	0.0026
Heme oxygenase 1	Hmox1	1.15	0.86	0.91	1.11	0.34	0.59
Heme oxygenase 2	Hmox2	0.96	0.98	0.89	0.88	0.22	0.48
Biliverdin reductase A	Blvra	0.84	0.92	0.82	0.92	0.032	0.22
UDP-glucuronosyltransferase 1-6	Ugt1a6	1.22	0.96	1.10	1.13	0.30	0.55
NADPH--cytochrome P450 reductase	Por	1.28	0.92	1.18	1.12	0.019	0.18

Table 3-2. CYP450 and steroid metabolism enyzmes.

Protein Description	GN	Fold Change to Control				p-Value	FDR
		hPXR			KO		
		RIF/INH	INH	RIF	RIF/INH		
Cytochrome P450 1A2	Cyp1a2	0.60	0.48	1.47	0.53	0.037	0.23
Cytochrome P450 2A12	Cyp2a12	0.98	0.78	1.53	0.91	0.022	0.19
Cytochrome P450 2A5	Cyp2a5	1.77	0.62	2.93	1.01	0.00076	0.047
Cytochrome P450 2B10	Cyp2b10	4.96	0.91	2.49	0.98	0.00032	0.030
Cytochrome P450 2C29	Cyp2c29	1.17	1.02	1.56	0.67	0.038	0.23
Cytochrome P450 2D10	Cyp2d10	0.98	0.90	1.03	0.99	0.92	0.97
Cytochrome P450 2D26	Cyp2d26	0.76	0.71	1.13	0.75	0.0021	0.072
Cytochrome P450 2E1	Cyp2e1	1.22	1.18	0.93	1.47	0.00035	0.032
Cytochrome P450 2F2	Cyp2f2	0.61	0.61	0.75	0.52	0.028	0.21
Cytochrome P450 2J6	Cyp2j6	0.98	0.89	1.04	1.06	0.68	0.82
Cytochrome P450 3A11	Cyp3a11	3.89	1.18	4.64	1.31	0.00086	0.050
Cytochrome P450 3A25	Cyp3a25	1.64	0.95	1.36	1.15	0.037	0.23
Cytochrome P450 4A10	Cyp4a10	2.38	1.61	4.45	1.78	0.012	0.15
Cholesterol 7-alpha-monooxygenase	Cyp7a1	1.08	0.65	0.86	1.85	0.095	0.33
25-hydroxycholesterol 7-alpha-hydroxylase	Cyp7b1	0.49	0.55	0.39	0.64	0.12	0.36
Sterol 26-hydroxylase	Cyp27a1	0.70	0.73	0.82	0.80	0.032	0.22
Lanosterol 14-alpha demethylase	Cyp51a1	0.94	0.66	1.30	1.56	0.43	0.66
Hydroxymethylglutaryl-CoA synthase	Hmgcs1	1.51	1.29	1.74	2.53	0.036	0.22
Hydroxymethylglutaryl-CoA synthase	Hmgcs2	1.26	1.55	1.23	1.19	0.027	0.20
3-hydroxy-3-methylglutaryl-coenzyme A reductase	Hmgcr	1.56	1.27	1.51	1.74	0.35	0.60
3 beta-hydroxysteroid dehydrogenase type 4	Hsd3b4	0.20	1.07	0.10	0.48	0.0012	0.058
Corticosteroid 11-beta-dehydrogenase isozyme 1	Hsd11b1	0.99	1.00	0.83	1.09	0.75	0.87

lesser decrease (0.20 fold) in *hPXR* mice treated with rifampicin and isoniazid and a further reduced decrease (0.48 fold) in *mPxr*$^{-/-}$ mice treated with rifampicin and isoniazid *Cyp3a11*, the mouse *CYP3A4* ortholog (Muruganandan and Sinal 2008), was significantly changed ($p = 0.0008$) in all treatment groups, but to a much lower magnitude (1.30 fold) in *mPxr* $^{-/-}$ mice and *hPXR* mice treated with isoniazid (1.18 fold) than in *hPXR* mice treated with rifampicin (4.64 fold) and treated with both rifampicin and isoniazid (3.89 fold). Several CYP450s were down-regulated due to isoniazid to a much higher extent than in the rifampicin only treatments; *Cyp1a2* (0.48 fold), *Cyp2a12* (0.78 fold), *Cyp2a5* (0.62 fold), and *Cyp2d26* (0.71 fold). *Cyp2e1* was significantly changed ($p = 0.00035$) and was increased in *hPXR* mice treated with rifampicin and isoniazid (1.22 fold) and with *hPXR* mice treated with isoniazid (1.18 fold). *Cyp2e1* was also increased in *mPxr* $^{-/-}$ mice treated with rifampicin and isoniazid (1.47 fold). Polymorphisms associated with increased *CYP2E1* function in humans leads to an increased incidence of DILI (Leiro-Fernandez, Valverde et al. 2010, Gogtay, Kapileshwar et al. 2016, Antonenko, Butov et al. 2017). Inhibition of *Cyp2e1* has been shown to be protective against isoniazid-induced hepatoxicity in mice (Lian, Zhao et al. 2017). *Cyp2e1* WT mice may be more susceptible to DILI (Cheng, Krausz et al. 2013). Therefore, the up-regulation of *Cyp2e1* by rifampicin in an *hPXR*-dependent manner may contribute to DILI.

Nuclear Receptors

Very few transcription factors were up- or down-regulated more than 10%. *Hnf1a* is significantly changed ($p = 0.026$) and down-regulated in all rifampicin treatment groups (0.79 to 0.87 fold) independent of *hPXR* status (**Table 3-3**). The glucocorticoid receptor (*Nr3c1*) was significantly ($p = 0.49$) down-regulated by rifampicin in *hPXR* mice (0.88 fold). *Nuclear receptor subfamily 5 group A member 2* (*Nr5a2*) was significantly ($p = 0.016$) down-regulated in *hPXR* mice treated with rifampicin (0.83 fold) and rifampicin and isoniazid combination (0.80 fold). Human *NR5A* may up-regulate *ALAS1* expression (Ju, Mizutani et al. 2012).

Organic Transporters

Multidrug resistance protein 1A (*Abcb1a*) was significantly ($p = 0.030$) changed in all rifampicin treatment groups (fold change 1.35 to 1.38) regardless of *hPXR* status (**Table 3-4**). The *canalicular multispecific oganic anion transporter 1* (*Abcc2*) was significantly ($p = 0.009$) changed in all isoniazid groups with the *hPXR* groups with isoniazid changed 0.84 fold, but the m*Pxr* $^{-/-}$ mice treated with isoniazid and rifampicin had a fold change of 0.68. The *sodium/bile acid co-transporter* (*Slc10a1*) was significantly changed ($p = 0.012$) by isoniazid (1.30 fold), rifampicin (0.85), and the combination of rifampicin and isoniazid (0.88 fold) in *hPXR* mice. The *solute carrier organic anion transporter family member 1A1* (*Slc1a1*) was significantly changed ($p = 0.025$) and is down-regulated in *hPXR* mice treated with rifampicin (0.55 fold) and the

Table 3-3. Nuclear receptors.

Protein Description	GN	Fold Change to Control				p-Value	FDR
		hPXR			KO		
		RIF/INH	INH	RIF	RIF/INH		
Aryl hydrocarbon receptor	Ahr	1.09	0.91	1.00	1.26	0.092	0.33
Hepatocyte nuclear factor 1-alpha	Hnf1a	0.87	0.97	0.82	0.79	0.027	0.20
Hepatocyte nuclear factor 4-alpha	Hnf4a	0.95	1.05	0.97	1.08	0.20	0.46
Oxysterols receptor LXR-alpha	Nr1h3	0.94	1.16	1.03	1.02	0.42	0.65
Bile acid receptor	Nr1h4	1.05	1.17	0.98	1.19	0.12	0.36
Retinoic acid receptor RXR-alpha	Rxra	0.88	1.03	0.83	0.95	0.12	0.37
Peroxisome proliferator-activated receptor alpha	Ppara	0.85	0.96	0.79	0.94	0.64	0.80
Nuclear receptor subfamily 1 group D member 1	Nr1d1	0.32	0.32	0.51	0.90	0.37	0.61
Oxysterols receptor LXR-beta	Nr1h2	1.11	1.14	1.08	1.05	0.62	0.79
Bile acid receptor	Nr1h4	1.05	1.17	0.98	1.19	0.12	0.36
COUP transcription factor 1	Nr2f1	0.98	1.04	0.94	1.00	0.67	0.82
COUP transcription factor 2	Nr2f2	0.98	1.04	0.94	1.00	0.67	0.82
Nuclear receptor subfamily 2 group F member 6	Nr2f6	1.01	1.04	0.97	1.08	0.45	0.68
Glucocorticoid receptor	Nr3c1	0.91	1.03	0.88	0.96	0.049	0.25
Nuclear receptor subfamily 5 group A member 2	Nr5a2	0.80	1.00	0.83	0.97	0.016	0.17

Table 3-4. Organic transporters.

Protein Description	GN	Fold Change to Control				p-Value	FDR
		hPXR			KO		
		RIF/INH	INH	RIF	RIF/INH		
Multidrug resistance protein 1A	Abcb1a	1.39	1.08	1.40	1.35	0.030	0.21
Multidrug resistance protein 1B	Abcb1b	1.26	1.06	1.27	1.19	0.13	0.38
Multidrug resistance protein 3	Abcb4	1.22	1.03	1.11	1.11	0.41	0.64
Bile salt export pump	Abcb11	1.00	0.85	1.01	0.88	0.051	0.25
Canalicular multispecific organic anion transporter 1	Abcc2	0.85	0.85	1.04	0.68	0.0094	0.14
Sodium/bile acid cotransporter	Slc10a1	0.88	1.31	0.85	0.92	0.019	0.18
Solute carrier organic anion transporter family member 1A1	Slco1a1	0.77	1.01	0.55	1.29	0.025	0.20

combination of rifampicin and isoniazid (0.77 fold), but are up-regulated in *mPxr* $^{-/-}$ mice treated with rifampicin and isoniazid (1.29 fold). *Abcb1a* was up-regulated and *Abcc2*, *Slc10a1*, and *Slco1a1* was down-regulated in *Fech*^{m1Pas} Balb/c mice (Davies, Schuurman et al. 2005).

Iron Metabolism

Lactotransferrin (*Ltf*) was significantly ($p = 0.036$) down-regulated in all treatment groups (**Table 3-5**). *Ltf* was most down-regulated in *mPxr* $^{-/-}$ mice treated with rifampicin and isoniazid (0.27 fold) and down-regulated to a lesser extent in *hPXR* mice (0.38 to 0.40 fold). *Ferritin light chain* (*Ftl1*) was significantly ($p = 8.42 \times 10^{-5}$) down-regulated in all treatment groups. *Ftl1* is most severely down-regulated in *hPXR* mice treated with rifampicin and isoniazid (0.28 fold), followed by *hPXR* mice treated with isoniazid (0.36 fold), *mPxr*$^{-/-}$ mice treated with rifampicin and isoniazid (0.44 fold), than *hPXR* mice treated with rifampicin (0.58 fold). *Abcb7* is significantly changed ($p = 0.019$) by 0.83 fold in *hPXR* mice treated with rifampicin and isoniazid to 0.79 fold in *hPXR* mice treated with rifampicin and a more modest decrease in *mPxr* $^{-/-}$ mice treated with rifampicin and isoniazid (0.91 fold). *Ftl1* was up-regulated in *Fech*^{m1Pas} Balb/c mice (Davies, Schuurman et al. 2005).

Oxidative Stress

Phospholipid hydroperoxide glutathione peroxidase (*Gpx4*) was significantly changed ($p = 0.0015$) in *hPXR* mice treated with rifampicin (1.56 fold) and the combination of rifampicin and isoniazid (1.44 fold) and to a lower extent *mPxr* $^{-/-}$ mice treated with rifampicin and isoniazid (**Table 3-6**). Many isoforms of glutathione S transferase (Gst) mu, which detoxicfies electrophilic compounds and cluster on chromosome 1p13.3 were significantly changed ($p < 0.0001$). *Gstm1, 2, 3, 4, 5, 6,* and *7* were increased 1.59 to 3 fold in *hPXR* mice treated with rifampicin and isoniazid, slightly decreased 0.79 to 0.87 fold in *hPXR* mice treated with isoniazid, slightly increased in *mPxr*$^{-/-}$ mice treated with rifampicin and isoniazid 1.16 to 1.61 fold, and with the highest magnitude increase in *hPXR* mice treated with rifampicin 1.55 fold to 4.5 fold. The increase due to rifampicin in *hPXR* mice was a higher magnitude than the increase in the combination therapy for each protein. *GSTM1* has been shown to be protective in humans treated with anti-tubercular drugs and null alleles have been associated with a higher incidence of hepatotoxicity (Gupta, Singh et al. 2013, Li, Long et al. 2013, Singla, Gupta et al. 2014). *Gsta1* was changed in a similar manner to the mu isoforms. *Gstt2* was significantly changed ($p = 0.033$) due to rifampicin and isoniazid (1.40 fold) and rifampicin (1.51 fold). *Catalase* was also significantly changed ($p = 0.038$) and increased in *hPXR* mice treated with both rifampicin and isoniazid (1.16 fold) and by rifampicin (1.45 fold). *NAD(P)H dehydrogenase [quinone] 1* (*Nqo1*) was significantly changed ($p = 0.00027$) and was increased in *hPXR* mice treated with rifampicin and isoniazid (1.52 fold) and rifampicin (2.6 fold) and in *mPXR* $^{-/-}$ mice treated with rifampicin and isoniazid

Table 3-5. Iron metabolism.

		Fold Change to Control					
		hPXR			KO		
Protein Description	GN	RIF/INH	INH	RIF	RIF/INH	p-Value	FDR
Serotransferrin	Tf	1.33	1.04	1.15	1.11	0.144145	0.397184
Transferrin receptor protein 1	Tfrc	1.28	0.98	1.13	1.14	0.46	0.68
Lactotransferrin	Ltf	0.40	0.38	0.38	0.27	0.036	0.23
Transferrin receptor protein 2	Tfr2	0.99	1.02	0.82	0.86	0.13	0.38
Hereditary hemochromatosis protein homolog	Hfe	0.93	0.92	0.90	0.94	0.70	0.84
Ferritin light chain 1	Ftl1	0.28	0.36	0.58	0.44	8.42E-05	0.014
Ferritin heavy chain	Fth1	0.47	0.63	0.70	0.59	0.097	0.33
Cytoplasmic aconitate hydratase	Aco1	1.05	1.00	1.08	1.00	0.53	0.73
ATP-binding cassette sub-family B member 7	Abcb7	0.83	0.98	0.79	0.91	0.019	0.18

Table 3-6. Oxidative stess.

Protein Description	GN	Fold Change to Control				p-Value	FDR
		hPXR			KO		
		RIF/INH	INH	RIF	RIF/INH		
Glutathione synthetase	Gss	0.95	0.80	0.91	0.76	0.084	0.31
Phospholipid hydroperoxide glutathione peroxidase	Gpx4	1.44	1.05	1.56	1.23	0.0016	0.064
Glutathione S-transferase Mu 1	Gstm1	1.59	0.80	2.50	1.19	7.23E-06	0.0034
Glutathione S-transferase Mu 2	Gstm2	2.01	0.85	2.96	1.61	5.54E-06	0.0034
Glutathione S-transferase Mu 3	Gstm3	3.02	0.87	4.54	1.33	4.5E-06	0.0034
Glutathione S-transferase mu 4	Gstm4	1.50	0.84	2.37	1.28	9.418E-06	0.0034
Glutathione S-transferase Mu 5	Gstm5	1.35	0.88	1.79	1.14	5.69E-05	0.011
Glutathione S-transferase Mu 6	Gstm6	1.67	0.79	2.41	1.16	1.25E-05	0.0038
Glutathione S-transferase Mu 7	Gstm7	1.57	0.81	2.30	1.16	1E-05	0.0034
Glutathione S-transferase A1	Gsta1	1.72	0.86	2.70	1.40	0.00019	0.023
Glutathione S-transferase theta-1	Gstt1	1.08	1.12	1.30	0.92	0.22	0.48
Glutathione S-transferase theta-2	Gstt2	1.40	0.99	1.51	1.01	0.034	0.22
Fumarylacetoacetase	Fah	0.93	0.97	0.93	0.99	0.62	0.79
Catalase	Cat	1.16	1.02	1.44	1.08	0.038	0.23
Superoxide dismutase	Sod2	0.82	0.92	0.85	0.93	0.052	0.26
NAD(P)H dehydrogenase [quinone] 1	Nqo1	1.52	0.87	2.60	1.92	0.00027	0.029

(1.92 fold). Nqo1 was decreased in *hPXR* mice treated with isoniazid (0.87 fold). *Nqo1* is protective against APAP- induced hepatotoxicity and is up-regulated in liver injury from APAP (Hwang, Kim et al. 2015) and primary biliary cirrhosis (Aleksunes and Klaassen 2012). *Gpx4*, *Gstm1*, and *Gstm5* were up-regulated in *Fech*^{m1Pas} Balb/c mice (Davies, Schuurman et al. 2005).

[Fe-S] Cluster Assembly Machinery

Cysteine desulfurase (*Nfs1*) was significantly ($p = 0.042$) changed in *hPXR* mice by rifampicin and isoniazid (0.89 fold) and rifampicin (0.84 fold) and to a lower extent in *mPxr* $^{-/-}$ mice treated with rifampicin and isoniazid (0.90 fold), but changed less than 4% due to isoniazid in *hPXR* mice (**Table 3-7**). *Adrenodoxin* (*Fdx1*) was significantly ($p = 0.016$) decreased by all treatments, and may be decreased by isoniazid to a greater degree than rifampicin. *Fdx1* was slightly decreased by rifampicin in *hPXR* mice (0.84 fold), to a greater degree by isoniazid (0.77 fold), and is most down-regulated by the combination of rifampicin and isoniazid in *hPXR* mice (0.64 fold). *Fdx1* is also down-regulated in *mPxr* $^{-/-}$ mice treated with rifampicin and isoniazid (0.79 fold). *Iron-sulfur cluster co-chaperone protein* (*Hscb*) is significantly changed ($p = 0.0056$). *Hscb* is increased to the greatest degree in *mPxr* $^{-/-}$ mice treated with rifampicin and isoniazid (1.44 fold), less of an increase was observed in *hPXR* mice treated with rifampicin (1.40 fold), and to a lower extent in the other treatment groups. *Hscb* is increased in *hPXR* mice treated with rifampicin and isoniazid (1.23 fold) and in *hPXR* mice treated with rifampicin (1.20 fold). *Iron-sulfur cluster assembly 1 homolog* (*Isca1*) was significantly changed ($p = 0.0037$) by down-regulation in all treatment groups from 0.66 to 0.81 fold. *Putative transferase CAF17 homolog* (*Iba57*) was significantly ($p = 0.0090$) increased in *hPXR* mice treated with rifampicin (1.15 fold) and *mPxr* $^{-/-}$ mice treated with rifampicin and isoniazid (1.14). *BolA-like protein 3* (*Bola3*) was significantly ($p=0.012$) changed in *hPXR* mice treated with isoniazid (0.91 fold) and the combination of rifampicin and isoniazid (0.89 fold), but was increased in *hPXR* mice treated with rifampicin (1.12 fold). *Anamorsin* (*Ciapin1*) was significantly changed ($p = 0.0095$) and was up-regulated across treatment groups. *Ciapin 1* was increased 1.34 fold in *hPXR* mice treated with rifampicin, 1.28 fold when treated with the combination of rifampicin and isoniazid, 1.19 fold when treated with isoniazid alone, and 1.10 fold in *mPxr* $^{-/-}$ treated with rifampicin and isoniazid.

Wound Healing and Inflammation

Protein-glutamine gamma-glutamyltransferase 2 (*Tgm2*) was significantly changed (**Table 3-8**; $p = 0.0058$). Tgm2 was up-regulated in *hPXR* mice treated with rifampicin and isoniazid (1.12 fold) and rifampicin alone (1.19 fold). *Tgm2* was down-regulated in *hPXR* mice treated with isoniazid (0.81 fold) and *mPxr* $^{-/-}$ mice treated with rifampicin and isoniazid (0.88 fold). *Collagen alpha-1 (IV)* (*Col4a1*) and *collagen alpha-1 (VI)* (*Col6a1*) were significantly changed with p values of 0.0033 and 0.0091 respectively. *Col4a1* and *Col6a1* were increased in *hPXR* mice treated with rifampicin and isoniazid (1.27 and 1.10 fold, respectively). *Col4a1* and *Col6a1* were decreased in

Table 3-7. [Fe-S] cluster assemblymachinery.

Protein Description	GN	Fold Change to Control				p-Value	FDR
		hPXR			KO		
		RIF/INH	INH	RIF	RIF/INH		
Cysteine desulfurase	Nfs1	0.89	0.96	0.84	0.90	0.042	0.24
Isoform 2 of Low molecular weight phosphotyrosine protein phosphatase	Acp1	0.96	0.98	1.03	1.00	0.63	0.80
Frataxin, mitochondrial	Fxn	0.84	0.98	0.89	0.88	0.11	0.35
Ferredoxin-fold anticodon-binding domain-containing protein 1 homolog	Fdxacb1	1.06	0.96	1.09	1.15	0.94	0.98
Adrenodoxin	Fdx1	0.64	0.77	0.84	0.79	0.0016	0.064
NADPH:adrenodoxin oxidoreductase,	Fdxr	0.83	0.93	0.85	0.91	0.16	0.42
Stress-70 protein	Hspa9	1.07	1.07	0.94	1.05	0.32	0.57
Iron-sulfur cluster co-chaperone protein	Hscb	1.23	1.20	1.40	1.44	0.0056	0.11
GrpE protein homolog 2, mitochondrial	Grpel2	1.24	1.18	1.04	1.19	0.78	0.89
GrpE protein homolog 1	Grpel1	1.10	1.07	0.98	1.05	0.69	0.83
Glutaredoxin-related protein 5	Glrx5	1.60	1.69	1.24	1.39	0.078	0.30
Iron-sulfur cluster assembly 1 homolog	Isca1	0.76	0.68	0.66	0.81	0.0037	0.095
Iron-sulfur cluster assembly 2 homolog	Isca2	0.90	0.91	1.13	1.02	0.20	0.46
Putative transferase CAF17 homolog	Iba57	1.00	0.98	1.15	1.14	0.0090	0.14
NFU1 iron-sulfur cluster scaffold homolog	Nfu1	0.82	0.98	0.90	1.01	0.13	0.37
NFU1 iron-sulfur cluster scaffold homolog, mitochondrial (Fragment)	Nfu1	0.82	0.99	0.87	0.96	0.059	0.27
BolA-like protein 3	Bola3	0.89	0.91	1.12	1.03	0.012	0.15
Iron-sulfur protein	Nubpl	1.27	1.77	1.37	0.91	0.067	0.29
Cytosolic Fe-S cluster assembly factor	Nubp1	1.07	0.91	0.94	1.03	0.33	0.58
Cytosolic Fe-S cluster assembly factor	Nubp2	1.03	1.06	1.01	1.14	0.35	0.60
Anamorsin	Ciapin1	1.28	1.19	1.34	1.10	0.0095	0.14
BolA-like protein 2	Bola2	0.98	0.90	0.92	0.88	0.58	0.77
Cytosolic Fe-S cluster assembly factor	Narfl	1.00	1.01	1.06	1.01	0.65	0.81
Probable cytosolic iron-sulfur protein assembly protein	Ciao1	0.96	1.03	0.98	1.12	0.10	0.34
MMS19 nucleotide excision repair protein homolog	Mms19	0.96	0.96	0.97	1.07	0.22	0.48

Table 3-8. Wound healing and inflammation.

Protein Description	GN	Fold Change to Control				p-Value	FDR
		hPXR			KO		
		RIF/INH	INH	RIF	RIF/INH		
Glutamine synthetase	Glul	0.85	1.03	0.72	1.17	0.16	0.41
Carbonic anhydrase 3	Ca3	1.23	1.14	1.18	1.19	0.81	0.91
Transforming growth factor-beta-induced protein ig-h3	Tgfbi	0.88	0.75	0.60	0.69	0.44	0.67
Protein-glutamine gamma-glutamyltransferase 2	Tgm2	1.12	0.81	1.19	0.88	0.0059	0.12
SPARC	Sparc	0.85	0.86	0.72	0.83	0.089	0.32
Collagen alpha-1(III) chain	Col3a1	1.94	0.34	0.28	0.35	0.056	0.26
Collagen alpha-1(IV) chain	Col4a1	1.27	0.86	0.83	0.90	0.0033	0.089
Collagen alpha-1(VI) chain	Col6a1	1.10	0.67	0.47	0.63	0.0091	0.14
Annexin A2	Anxa2	1.43	0.89	0.94	1.08	0.30	0.55
Annexin A5	Anxa5	1.56	0.98	1.57	1.22	0.032	0.22
Biglycan	Bgn	1.37	0.94	0.74	1.08	0.44	0.67
G1/S-specific cyclin-D1	Ccnd1	1.40	0.69	1.24	1.03	0.19	0.45
T-lymphocyte activation antigen CD86	Cd86	1.08	0.86	1.03	0.96	0.13	0.38

the other treatment groups from 0.83 to 0.90 fold and 0.47 to 0.67 fold, respectively. *Annexin A5* (*Anxa5*) was significantly changed ($p = 0.031$). *Anxa5* was increased by 1.56 fold in *hPXR* mice treated with rifampicin and isoniazid and rifampicin alone, but less than 2% change was observed in *hPXR* mice treated with isoniazid. *Anxa5* was also decreased in *mPxr* $^{-/-}$ treated with rifampicin and isoniazid (1.22 fold).

Vitamin B_6 Metabolism

The vitamin B_6 metabolism enzymes *pyridoxal kinase* (*Pdxk*), *pyridoxal phosphate phosphatase* (*Phospho2*), and *pyridoxal-dependent decarboxylase domain-containing protein 1* (*Pdxdc1*) were not significantly changed (**Table 3-9**). *Pyridoxal phosphate phosphatase* (*Pdxp*) was significantly changed ($p = 0.0004$) by 1.49 fold in *hPXR* mice treated with rifampicin and isoniazid, 2.18 fold in *hPXR* mice treated with rifampicin alone, and 1.34 fold in *mPxr* $^{-/-}$ mice treated with rifampicin and isoniazid. *Pdxp* dephosphorylates pyridoxal 5' phosphate to 4-pyridoxic acid, but also dephosphorylates pyridoxine 5' phosphate, and pyridoxamine 5' phosphate (Jang, Kim et al. 2003). Increased degradation of vitamin B_6 by up-regulation of *Pdxp* by rifampicin may reduce the amount of PIH formed and this may be protective. Further investigation is warranted to determine into this effect that may further deplete vitamin B_6 levels and contribute to the development of peripheral neuropathy.

[Fe-S] Cluster Containing Proteins

There is not a significant global down-regulation of Fe-S containing proteins due to isoniazid (**Table 3-10**). *NADH dehydrogenase [ubiquinone] iron-sulfur protein 8* (*Ndufs8*) was significantly ($p = 0.0012$) changed. *Ndufs8* was decreased in all treatment groups (only 4% decrease due to isoniazid in *hPXR* mice) by 0.91 fold in *hPXR* mice treated with rifampicin and isoniazid, 0.82 fold in hPXR mice treated with rifampicin, and by 0.75 fold in *mPxr* $^{-/-}$ treated with rifampicin and isoniazid. *Succinate dehydrogenase [ubiquinone] iron-sulfur subunit* (*Sdhb*) was significantly changed ($p = 0.035$). *Sdhb* was decreased in *hPXR* mice treated with rifampicin and isoniazid (0.86 fold) and with rifampicin alone (0.92 fold), but changed less than 1% in *hPXR* mice treated with isoniazid and in *mPxr* $^{-/-}$ treated with rifampicin and isoniazid. The changes in *Sdhb* may be *hPXR* mediated by rifampicin and further decreased by isoniazid administration. *NADH dehydrogenase [ubiquinone] iron-sulfur protein 7* (Ndufs7) was significantly changed ($p = 0.012$) and was increased in *hPXR* mice treated with isoniazid (1.14 fold) and *mPxr* $^{-/-}$ mice treated with rifampicin and isoniazid (1.23 fold). *NADH dehydrogenase [ubiquinone] iron-sulfur protein 4* (*Ndufs4*) was significantly changed ($p = 0.034$) and increased by isoniazid (1.12 fold) and rifampicin (1.10 fold) in *hPXR* mice and increased in *mPxr* $^{-/-}$ mice treated with rifampicin and isoniazid (1.23 fold). *Iron-responsive element-binding protein 2* (*Ireb2*) was significantly ($p = 0.039$) increased in all treatment groups 1.18 to 1.42 fold. Fdx, Fech, *Fdx* and *Fech* were significantly decreased by isoniazid treatment. Cisd1, Cisd2, and Cisd3 are non-significantly down-regulated by approximately 10% by isoniazid. The NADH dehydrogenase [ubiquinone]

Table 3-9. Vitamin B_6 metabolism.

		Fold Change to Control					
		hPXR			KO		
Protein Description	GN	RIF/INH	INH	RIF	RIF/INH	p-Value	FDR
Pyridoxal kinase	Pdxk	1.07	1.05	1.13	1.17	0.75	0.87
Pyridoxal phosphate phosphatase	Pdxp	1.49	0.95	2.18	1.34	0.00049	0.038
Pyridoxal phosphate phosphatase	Phospho2	1.04	1.08	1.07	1.04	0.90	0.96
Pyridoxal-dependent decarboxylase domain-containing protein 1	Pdxdc1	0.97	1.03	1.01	1.02	0.84	0.92

Table 3-10. [Fe-S] cluster containing proteins.

		Fold Change to Control					
		hPXR			KO		
Protein Name	GN	RIF/INH	INH	RIF	RIF/INH	p-Value	FDR
NADH dehydrogenase [ubiquinone] iron-sulfur protein 3	Ndufs3	0.94	1.09	1.01	1.09	0.74	0.86
NADH dehydrogenase [ubiquinone] iron-sulfur protein 2	Ndufs2	1.00	1.04	1.03	1.04	0.65	0.81
CDGSH iron-sulfur domain-containing protein 1	Cisd1	0.90	0.97	0.98	1.03	0.14	0.39
NADH dehydrogenase [ubiquinone] iron-sulfur protein 8	Ndufs8	0.91	0.96	0.82	0.75	0.0012	0.058
Succinate dehydrogenase [ubiquinone] iron-sulfur subunit	Sdhb	0.86	0.99	0.92	0.99	0.036	0.22
NADH dehydrogenase [ubiquinone] iron-sulfur protein 7	Ndufs7	1.00	1.14	1.09	1.20	0.012	0.15
NADH dehydrogenase [ubiquinone] iron-sulfur protein 4	Ndufs4	0.94	1.12	1.10	1.23	0.033	0.22
NFU1 iron-sulfur cluster scaffold homolog	Nfu1	0.82	0.98	0.90	1.01	0.13	0.37
NFU1 iron-sulfur cluster scaffold homolog, mitochondrial (Fragment)	Nfu1	0.82	0.99	0.87	0.96	0.059	0.27
Iron-sulfur protein NUBPL	Nubpl	1.27	1.77	1.37	0.91	0.067	0.29
Iron-sulfur cluster assembly enzyme	Iscu	0.95	1.01	0.96	0.98	0.84	0.93
NADH dehydrogenase [ubiquinone] iron-sulfur protein 6	Ndufs6	0.94	0.96	0.86	0.82	0.13	0.38
NADH dehydrogenase [ubiquinone] iron-sulfur protein 5	Ndufs5	0.87	0.97	0.91	1.03	0.22	0.48
CDGSH iron-sulfur domain-containing protein 2	Cisd2	0.90	0.88	0.89	0.82	0.94	0.98
Iron-responsive element-binding protein	Ireb2	1.19	1.21	1.42	1.28	0.039	0.23
2-oxoglutarate and iron-dependent oxygenase domain-containing protein 2	Ogfod2	1.11	0.97	1.15	0.99	0.51	0.71
Probable cytosolic iron-sulfur protein assembly protein	Ciao1	0.96	1.03	0.98	1.12	0.10	0.34
Iron-sulfur cluster assembly 2 homolog, mitochondrial	Isca2	0.90	0.91	1.13	1.02	0.20	0.46
CDGSH iron-sulfur domain-containing protein 3	Cisd3	0.84	0.88	1.02	1.07	0.060	0.27
2-oxoglutarate and iron-dependent oxygenase domain-containing protein 3	Ogfod3	1.03	0.98	0.91	0.87	0.25	0.51
Aldehyde oxidase 1	Aox1	1.30	0.82	1.65	1.48	0.0023	0.075
Xanthine dehydrogenase/oxidase	Xdh	0.70	0.70	0.75	0.98	0.0079	0.13

or complex 1 is composed of multiple sub-units and contains 8 [Fe-S] clusters; multiples of [2Fe-2S], [4Fe-4S], and [3Fe-4S]. *Ndufs8* is significantly down-regulated by isoniazid, but contains 2 [4Fe-4S] clusters. (Loeffen, Smeitink et al. 1998) *Sdhb* contains 3 [Fe-S] clusters; [2Fe-2S], [4Fe-4S], and [3Fe-4S] and is down-regulated by rifampicin and isoniazid in *hPXR* mice. Aox1 and Adh are [2Fe-2S]-containing proteins that are also down-regulated by isoniazid. The effect of isoniazid on [Fe-S] clusters may be specific to [2Fe-2S] clusters.

CHAPTER 4. DISCUSSION

Previous Animal Models of Isoniazid DILI

Isoniazid displays different hepatotoxic patterns dependent on dose and animal model. Different groups have examined the role of isoniazid in anti-tubercular therapy DILI and have reached different conclusions. Therefore, the role of isoniazid in anti-tubercular therapy toxicity remains elusive. Studies performed in rats and human liver microsomes continue to form the consensus for the isoniazid/hydrazine model of liver injury (Mitchell, Zimmerman et al. 1976, Nelson, Mitchell et al. 1976). A single large dose (300 mg/kg) of isoniazid did not result in liver necrosis, but six lower oral doses (100 mg/kg) produced small amounts of necrosis when the rats were pre-administered phenobarbital (Nelson, Mitchell et al. 1976). However, administration of acetyl-hydrazine increased the amount of necrosis compared to the administration of acetyl-isoniazid. Further, the application of radiolabeled acetyl-isoniazid showed that the acetyl group was detected bound to cellular proteins and that the inhibition of the acetyl-isoniazid to acetyl-hydrazine conversion decreased the necrosis seen after acetyl-isoniazid, but not acetyl-hydrazine application. Thus, isoniazid acetylation and hydroxylation to acetyl-hydrazine and the interaction of further hydrolyzed acetyl-hydrazine with cellular proteins was the suggested route of toxicity. A contemporary study may support this model with the findings that low N-acetyl transferase (NAT) activity is associated with increased risk of hepatic damage with the suggestion that the majority of acetyl-hydrazine is oxidized by *CYP3A4* and *2E1* (Zabost, Brzezinska et al. 2013). This model is problematic in that it may not completely recapitulate the pathology seen in clinic in combination therapy because the effects observed due to the combination of rifampicin and isoniazid are a cholestatic pattern of injury and this relatively short dosing regimen would not recapitulate chronic toxicity. This model may fit the clinical pattern seen in acute, hepatocellular isoniazid toxicity resulting from large doses of isoniazid, but not chronic, cholestatic rifampicin and isoniazid toxicity.

Treatment of rats with acetyl hydrazine or acetyl isoniazid can cause hepatotoxicity, but isoniazid treatment itself does not cause toxicity in rats (Black, Mitchell et al. 1975, Nelson, Mitchell et al. 1976). When the acetyl group is radio-labeled in acetyl isoniazid, but not the aromatic ring, covalent binding of liver proteins was observed (Mitchell, Zimmerman et al. 1976, Nelson, Mitchell et al. 1976). This suggests that the toxicity observed in rats after treatment of acetyl isoniazid was due to the breakdown product of acetyl isoniazid, acetyl hydrazine. However, high doses of hydrazine administered to mice resulted in hepatotoxicity, but not high doses of acetyl hydrazine (Richards, Chau et al. 2004). There is no validated animal model that captures the chronic cholestatic pattern of hepatotoxicity seen in humans taking rifampicin and isoniazid as part of a multi-drug anti-tubercular therapy (Boelsterli and Lee 2014). A previous report (Li, Lu et al. 2013) that linked *hPXR* to rifampicin and isoniazid hepatotoxicity in mice only shows bile plugs on histopathologic examination without semi-quantitative histopathologic scoring of lesions. Multiple high doses of isoniazid can cause hepatocellular toxicity in rats pre-treated with phenobarbital, but this does not

recapitulate the human pattern of toxicity. (Mitchell, Zimmerman et al. 1976) Rats could be a poor model system due to the lack of a gall bladder which may be required for cholestatic hepatotoxicity or due to the differences in isoniazid bound proteins in rat, mouse, and human microsomes (McKennis, Yard et al. 1956, Metushi, Cai et al. 2014). There are two large differences in bile storage in mice and rats. The first is that mouse bile is more concentrated than rat bile when excreted into the duodenum (McMaster 1922). Indeed, bile does not become more concentrated in rat even in stasis, whereas it does in the mouse. The other difference is that the gall bladder serves as a reservoir in mice and secretes bile upon relaxation of the sphincter of Oddi by cholecystokinin induced by a fatty meal. In contrast, the sphincter of Oddi is relaxed in rats. Bile in rats is not concentrated in the gall bladder, but in the liver unlike in mice whose livers see much lower concentrations of bile acid constituents. Therefore, it may be inappropriate to draw too many conclusions about cholestatic liver injury from rat models.

Failure to Re-Capture DILI Phenotype in Mouse Model

The Hepatotoxicity of PPIX

The relationship between PPIX and hepatotoxicity has been reported previously (Davies, Schuurman et al. 2005, Lyoumi, Abitbol et al. 2011, Liu, Yan et al. 2015). The mechanism of toxicity may depend on the site of PPIX accumulation. For example, the intracellular accumulation of PPIX in hepatocytes is associated with a hepatocellular subtype of liver injury, whereas extracellular accumulation in the bile is associated with a cholestatic subtype. The site of accumulation differs between strains of mice. BALB/c^{m1Pas} and C57BL/6^{m1Pas} mice have a point mutation in the *Fech* gene and express a protein with less than 5% of the activity of the original enzyme (Davies, Schuurman et al. 2005). These mice develop phototoxicity and are more vulnerable to griseofulvin induced hepatotoxicity. Female C57BL/6^{m1Pas} and BALB/c^{m1Pas} mice were compared at 12-14 weeks of age. C57BL/6^{m1Pas} mice had porphyrin deposits in Kupffer cells and hepatocytes, whereas in BALB/c^{m1Pas} porphyrin was deposited into bile canaliculi (Lyoumi, Abitbol et al. 2011). BALB/c^{m1Pas} mice had 7-fold increases in *AST* and *ALT*, 8-fold increase in *ALP*, and a 71-fold increase in total bilirubin. However, the changes in LFTs for C57BL6^{m1Pas} mice were less marked. C57BL/6 mice had a 4-fold increase in *AST*, a 5-fold increase in ALT, a 1.5-fold increase in *ALP*, and a 2.5-fold increase in bilirubin. The pattern of PPIX deposition matches the pattern in the degree of LFT changes; the *ALT*/*ALP* ratio for BALB/c^{m1Pas} mice of 0.74, a more than 2-fold increase in *ALP*, and a 71-fold increase in total bilirubin suggested an intrahepatic cholestatic type of liver injury (Robles-Diaz, Garcia-Cortes et al. 2015). Unfortunately, the authors did not test for direct bilirubin so a splenic or hematological source cannot be ruled out. On the other hand, the *ALT*/*ALP* ratio for C57BL/6^{m1Pas} mice is 2.7 and is associated with a more than 2-fold increase in *ALT* and a less than 2-fold increase in *ALP* suggesting a hepatocellular type of liver injury. Interestingly, C57BL/6^{m1Pas} mice had 8-fold higher liver PPIX levels than BALB/c^{m1Pas} mice, but histopathological signs of bile duct destruction and sclerosing cholangitis were observed only in BALB/c^{m1Pas} mice.

Therefore, PPIX accumulation via genetic disruption of the heme biosynthetic enzyme, *FECH*, is associated with a pattern of hepatotoxicity that is dependent upon the site of PPIX accumulation and this may differ between mouse strains.

PPIX accumulation has been associated with pharmacologic disruption of heme biosynthesis by both isoniazid and griseofulvin. Griseofulvin treatment of 14 days in male FVB/NJ mice leads to an increase of PPIX, bile acids, and *GSH* in the liver. Griseofulvin is metabolized by CYP450 enzymes to reactive metabolites that form adducts with PPIX and N-methyl PPIX which may inhibit *Fech*. Griseofulvin up-regulates *Alas1* expression. These changes resulted in increased liver PPIX that was associated with a bile duct blockage that resulted in increased bile acids that were not associated with an increase in the enzymes responsible for bile acid synthesis (Liu, Yan et al. 2015).

A recent report detailed the role that *hPXR* plays in rifampicin and isoniazid induced hepatotoxicity (Li, Lu et al. 2013). This report discussed the finding of bile plugs, high levels of PPIX in the bile, a 5-fold increase in *ALT*, a 2.2-fold increase in *ALP*, and an *ALT*/*ALP* ratio of approximately 0.5 in *hPXR*, but not WT or *mPxr* $^{-/-}$ mice treated with rifampicin and isoniazid compared to control *hPXR* mice. Rifampicin treated *hPXR* mice had a 2-fold increase in *ALT* and a 1.5-fold increase in *ALP*. There was no increase in *ALT* or *ALP* when hydrazine or acetyl-hydrazine was added with rifampicin, but *ALP* and *ALT* increased only when isoniazid was administered with rifampicin. In *hPXR* mice, rifampicin or isoniazid alone had a 5-fold increase in bile PPIX and rifampicin and isoniazid combination treated mice had a 60-fold increase in bile PPIX. In *hPXR* mice treated with both rifampicin and isoniazid, the addition of ALA resulted in a 10-fold increase in *ALT* and *ALP*. Semi-quantitative histopathologic scores were not included in this report, nor were severe histopathologic signs of liver injury observed apart from bile plugs and signs of bile stasis. There is *hPXR*-mediated PPIX accumulation associated with elevated LFTs due to the combination of rifampicin and isoniazid with an unfortunately mild degree of histopathologic change. The phenotype may have been relatively mild, but the changes were *hPXR*-dependent. This phenotype may have been achievable if the length of my study may have led to an increase in liver injury in two control mice that may have been due to age.

Other studies have observed *hPXR*-independent DILI due to the combination of rifampicin and isoniazid in mice in other strains of mice. Female WT CD-1 mice treated via oral gavage with 75 mg/kg isoniazid and 150 mg/kg rifampicin for 1 week had increased liver weight/body weight ratio, increased *ALT*, increased *ALP*, reduced *GSH*, and increased caspase 3 cleavage. The observed hepatotoxicity was attenuated with co-administration of ursodeoxycholic acid, which is an *hPXR* agonist (Chen, Xu et al. 2011). This toxicity is observed in mice expressing WT m*Pxr* and is therefore independent of *hPXR*. Male ICR mice treated via intraperitoneal injection with 75 mg/kg isoniazid and 150 mg/kg rifampicin for 21 days had elevated *ALT* and *AST*, 1.25-fold increase in liver PPIX, and decreased *Fech* protein levels. These effects were attenuated by co-administration of curcumin (Kluth, Banning et al. 2007, He, Guo et al. 2017). Several studies have shown that a low magnitude of increase in liver PPIX may not be required

for hepatotoxicity. Male FVB/NJ wild type mice were treated with 400 mg/L isoniazid in the drinking water and had 2-fold increase in liver PPIX at 3 days, 4-fold at 7 days, and 8-fold at 14 days with a 60% decrease in *Fech* protein and a 6-fold increase in *Alas1* protein at 3 days through 14 days without significant mRNA changes. However, this was not associated with hepatotoxicity via LFTs or histopathology. There is strong literature evidence to support the relationship between PPIX and cholestatic liver injury. However, I was not able to reliably or robustly induce PPIX accumulation in our mouse model. I only robustly observed a 3-6 fold increase in liver PPIX in my *in vivo* studies. All of these models lack evidence of definitive pathologic change, semi-quantitative histopathologic examination.

Attempt to Establish an Animal Model of Rifampicin and Isoniazid DILI

I was unable to induce a robust hepatotoxicity phenotype in the *hPXR* mouse model. The hepatotoxicity associated with combination anti-tubercular therapy is cholestatic, whereas the hepatotoxicity associated with either rifampicin or isoniazid alone is hepatocellular (Li, Lu et al. 2013, Boelsterli and Lee 2014, Wang, Pradhan et al. 2016). Furthermore, the combination therapy, due in part to the use of lower doses, is chronic and typically develops after weeks or months of treatment. However, the hepatotoxicity of the monotherapy is more typically acute and observed relatively quickly after the administration of a supra-clinical dose, especially in the case of isoniazid (Li, Lu et al. 2013, Boelsterli and Lee 2014, Wang, Pradhan et al. 2016). Additionally, the molecular mechanism of cholestatic or hepatocellular pattern of liver injury would be different from the other and may differ in the dependence upon *hPXR* status. Therefore, to recapitulate the hepatotoxicity phenotype in *hPXR* mice, a relatively narrow set of conditions may be required. A set of conditions, I was unable to recapitulate.

Findings of *In Vivo* Studies

***In Vivo* Study 1.** The first mouse study (6 weeks, 100 mg/kg chow rifampicin, and 400 mg/L water isoniazid) resulted in no increase in serum liver function enzyme levels, no significant histopathologic change, and a slight increase in liver PPIX levels. Rifampicin was added to the food because it was much less water soluble than isoniazid. The increase in PPIX levels was much less than the increase observed in *hPXR* mouse models with a hepatoxicity phenotype (Li, Lu et al. 2013). However, it was similar to the increase observed due to isoniazid treatment alone (Sachar, Li et al. 2016). Isoniazid decreased *Fech* protein levels and increased *Alas1* protein levels in an *hPXR*-independent manner (Figure 3-8). Rifampicin increased Cyp3a levels in an *hPXR*-dependent manner (**Figure 4-1**). There was no significant differences in total bilirubin, direct bilirubin, *ALT*, or *ALP* (**Figure 4-2**). There was no significant hepatopathic lesions observed by histologic analysis.

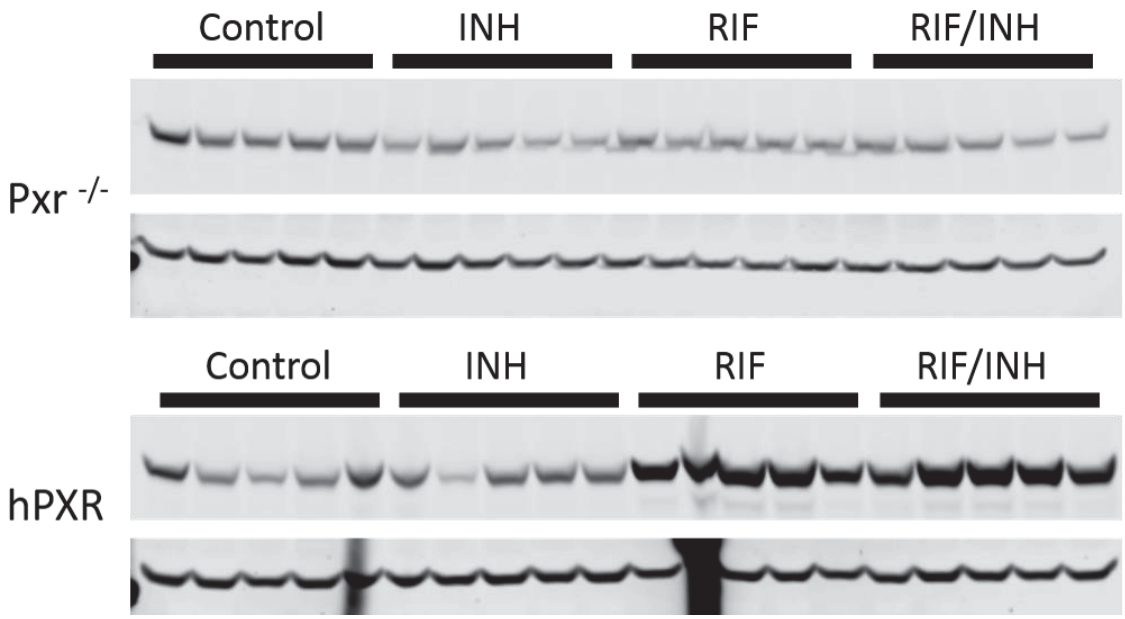

Figure 4-1. ***In vivo*** **study 1** ***Cyp3a*** **expression.**

Western blot analysis of *Cyp3a* in C57BL6 mouse liver after 6 weeks treatment with rifampicin (100 mg/kg chow) and isoniazid (400 mg/L in drinking water).

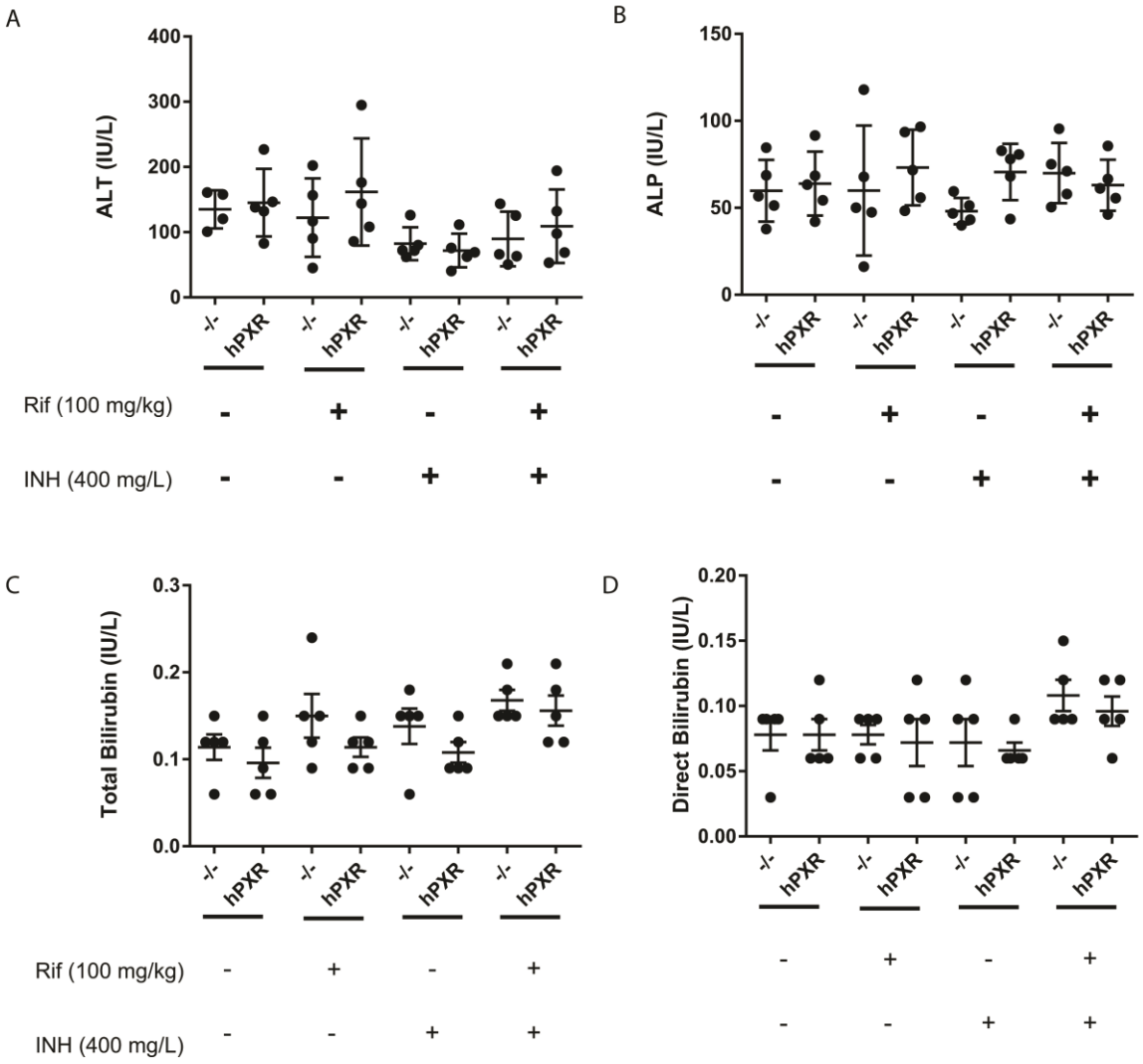

Figure 4-2. ***In vivo*** **study 1 endpoint LFTs.**

Analysis of endpoint LFTs. ALT (A), ALP (B), total bilirubin (C), and direct bilirubin (D) are displayed. Data are represented as the mean ± SEM.

***In Vivo* Study 2.** The second mouse study (6 months, 300 mg/kg chow rifampicin, and 1.2 g/L water isoniazid) resulted in a significant increase in of direct bilirubin and *ALP* in *hPXR* mice treated with both rifampicin and isoniazid (**Figure 4-3**). Rifampicin increased *Cyp3a* protein expression (**Figure 4-4**) in an *hPXR*-dependent manner. Isoniazid decreased (**Figure 4-4**) *Fech* expression and increases *Alas1* expression. Histopathological examination (which was not reported previously (Li, Lu et al. 2013) revealed the presence of hepatopathic lesions in *hPXR* mice treated with rifampicin and isoniazid (**Figure 4-5**). However, the difference in the scoring of these lesions between drug treatment groups in *hPXR* mice was not significant (**Figure 4-6**). This was due the presence of hepatopathic lesions in 2 control treatment *hPXR* mice. These mice were not older than other mice in the study, but at 8-10 months of age these mice may have developed liver disease spontaneously. However, these mice were not older than other mice in the study. Additionally, the Grubb's test did not identify either of these data points as an outlier.

In the context of the sole previous report of *hPXR*-dependent rifampicin and isoniazid DILI in mice, the phenotype reported was replicated with more moderate changes in terms of ALP and direct bilirubin (**Figure 4-3**) (Li, Lu et al. 2013). However, *ALT* had no significant increase and histopathologic scoring reveal a significant increase only in bile pigment (**Figure 4-5**). Additionally , many previous other studies reported *hPXR*-independent rifampicin and isoniazid DILI have moderate, but significant changes in LFTs, but not pathologic scoring (Chen, Xu et al. 2011, He, Guo et al. 2017).

***In Vivo* Study 3.** Two problems with *in vivo* study 2 were the intragroup variability and the low magnitude of histologic change. I addressed the variability by administering rifampicin and isoniazid via oral gavage. I addressed the low magnitude of changes by calculating the doses for study 2 based on (1) the estimated doses, (2) literature reports, and (3) converting the human dose to the mouse dose. The third mouse study (3.5 months, 80 mg/kg rifampicin and 75 mg/kg isoniazid administered by daily oral gavage) was monitored for hepatotoxicity by weekly serum collections and analysis of the liver function enzymes, *ALT* and *ALP*. At 3.5 months, no significant increases due to any treatment was observed in liver function tests throughout the duration of the study. The doses of rifampicin and isoniazid used in study 3 were lower than literature reports of doses reported to cause hepatotoxicity after oral administration in mice (Chen, Xu et al. 2011), lower than the doses used in study 2 (for isoniazid), and lower than the doses I calculated based on the dose commonly administered in humans.

Suitability of Pyrazinamide Inclusion

Pyrazinamide is only used in combination treatment of *M. tuberculosis* to reduce the duration of treatment. Pyrazinamide is a prodrug that is activated by a bacterial enzyme. The PZase/nicotinamidase ecoded by the M. tuberculosis gene, *pncA*, converts pyrazinamide to pyrazinoic acid. Pyrazynoic acid accumulations in M. tuberculosis at acidic pH and causes cytosolic acidification (Zhang, Shi et al. 2013). Pyrazinamide can also be activated by hypoxanthine oxidase to from the active form, 5-OH pyrazinoic acid.

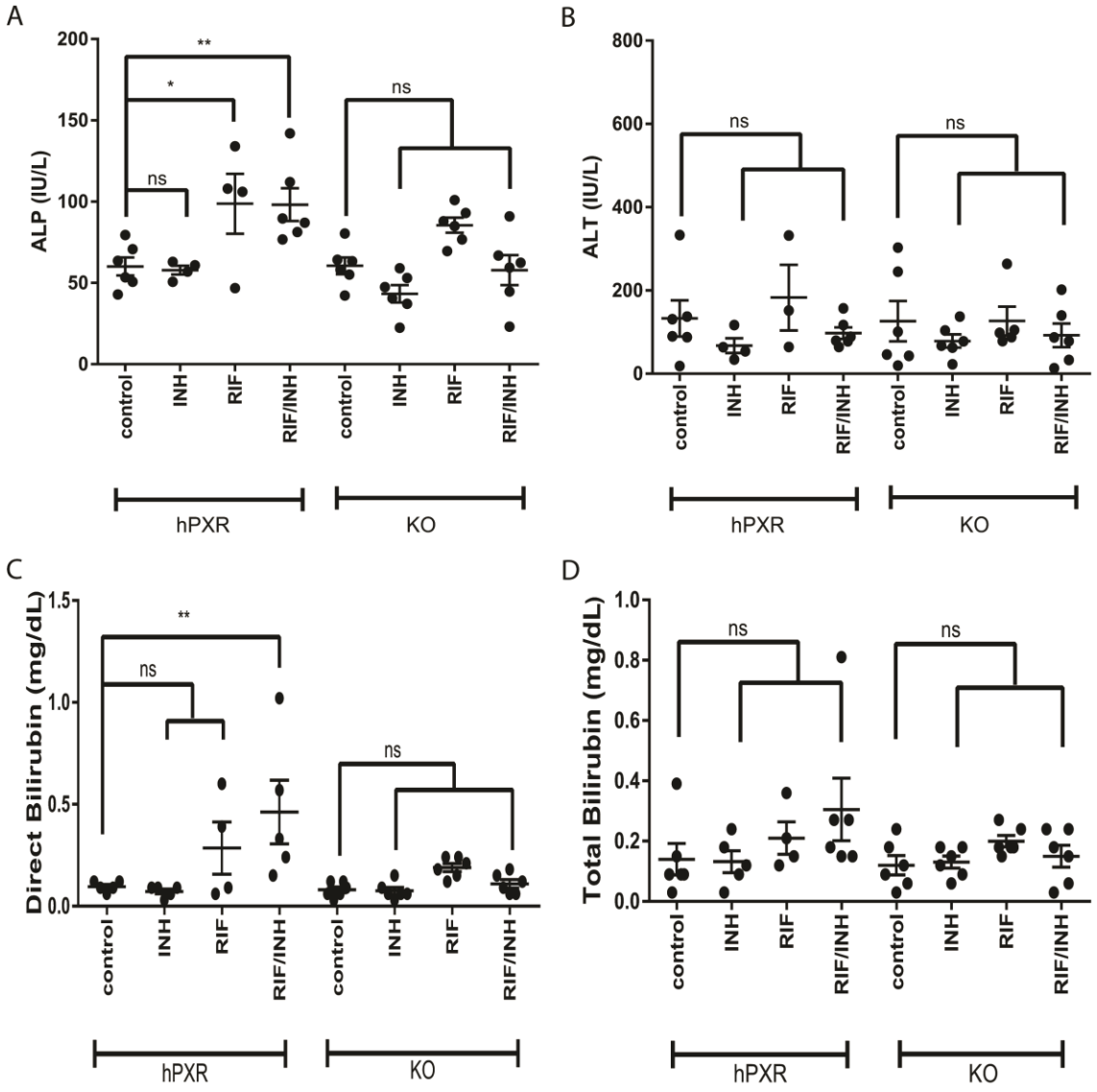

Figure 4-3. ***In vivo*** **study 2 endpoint LFTs.**

ALP (A), ALT (B), direct bilirubin (C), and total bilirubin (D) are represented. Data are expressed as the mean ± SEM. 1-way ANOVA followed by Dunnett's post-hoc analysis was used to compare group meansl. ****p<0.0001; ***p<0.001, **p<0.01, *p<0.05

Figure 4-4. *In vivo* study 2 gene expression changes.

Protein levels in livers of study mice. For 6 months, mice were provided 300 mg rifampicin/kg in chow and 1.2 g/L isoniazid in water *ad libitum*. Livers were flash-frozen, homogenized, and lysed before western blotting analysis was performed. *Cyp3a* (A, B), *Alas1* (C, D; shorter band is mature form), and *Fech* (E, F) levels are displayed. HepG2/C3A transiently transfected with MT (lipid only), NT3 (non-targeting siRNA), siRNA targeting gene being probed for, empty vector (EV), or target (*FECH/ALAS1*) are used as controls. The lower band recognized by the *Alas1* antibody is the mature, active form of *Alas1*. Cyp3a (G), *Fech* (H), and *Alas1* (I.) mRNA expression in the livers of C57BL/6 *mPxr* $^{-/-}$ and *hPXR* mice. For 6 months, mice were provided 300 mg rifampicin/kg in chow and 1.2 g/L isoniazid in water *ad libitum*. Mice were euthanized, and their livers were collected and stored in RNAlater (Thermo Fisher; Waltham, ME) at -80˚C. RNAlater was removed and liver slices were washed with PBS before homogenization on the Bullet Blender Storm 24 Homogenizer (Thomas Scientific; Swedesboro, NJ). RNA was extracted and analyzed by qRT-PCR. The ΔΔCT method was used to normalize fold change in expression to expression in the control group of each mouse strain. 2-way ANOVA followed by Tukey's post-hoc analysis was used to compare group means. ****P<0.0001; ***P<0.001, **P<0.01, *P<0.05

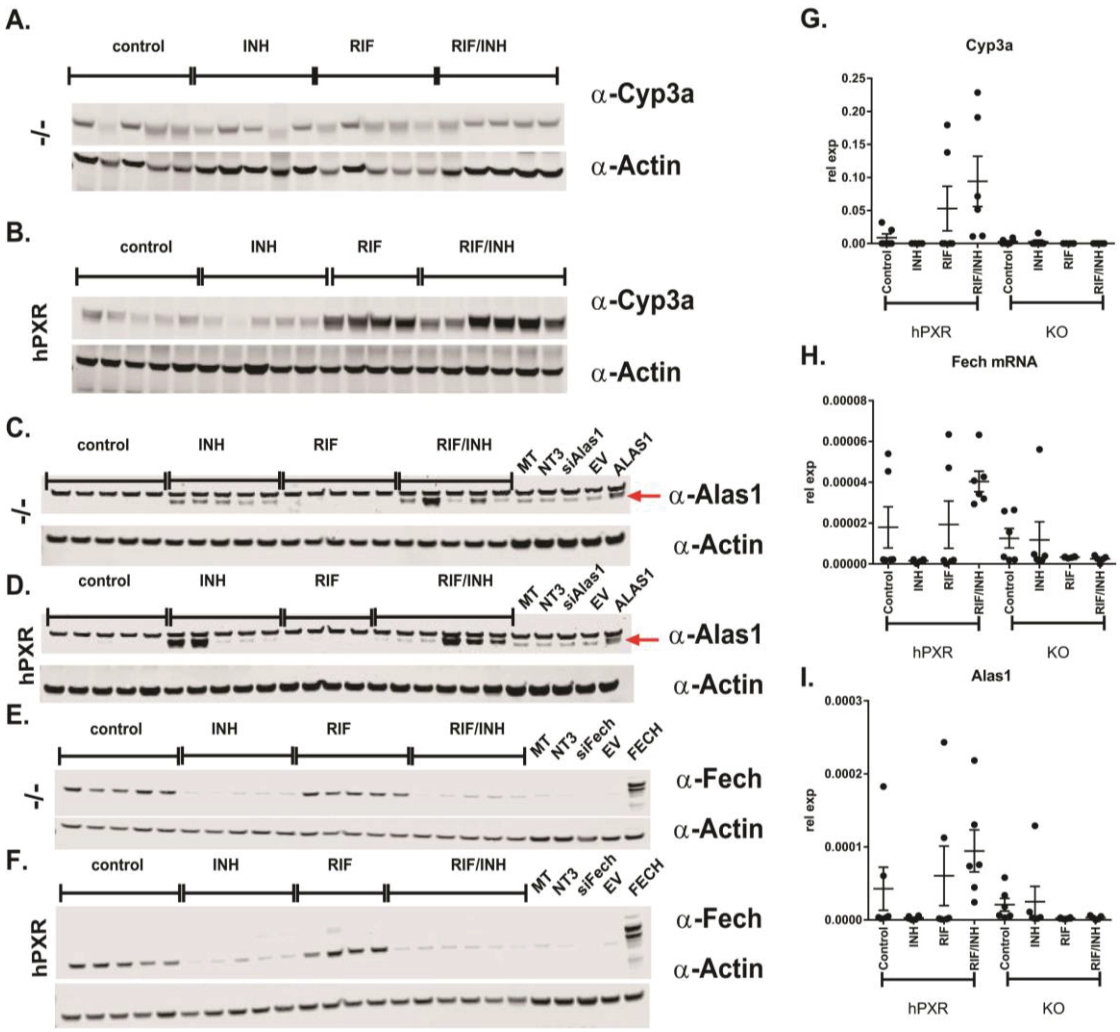
A.
control
INH
RIF
RIF/INH
-/-
α-Cyp3a
α-Actin
B.
control
INH
RIF
RIF/INH
hPXR
α-Cyp3a
α-Actin
C.
control
INH
RIF
RIF/INH
MT
NT3
siAlas1
EV
ALAS1
-/-
α-Alas1
α-Actin
D.
control
INH
RIF
RIF/INH
MT
NT3
siAlas1
EV
ALAS1
hPXR
α-Alas1
α-Actin
E.
control
INH
RIF
RIF/INH
MT
NT3
siFech
EV
FECH
-/-
α-Fech
α-Actin
F.
control
INH
RIF
RIF/INH
MT
NT3
siFech
EV
FECH
hPXR
α-Fech
α-Actin
G.
Cyp3a
rel exp
0.25
0.20
0.15
0.10
0.05
0.00
Control
INH
RIF
RIF/INH
Control
INH
RIF
RIF/INH
hPXR
KO
H.
Fech mRNA
rel exp
0.00008
0.00006
0.00004
0.00002
0.00000
Control
INH
RIF
RIF/INH
Control
INH
RIF
RIF/INH
hPXR
KO
I.
Alas1
rel exp
0.0003
0.0002
0.0001
0.0000
Control
INH
RIF
RIF/INH
Control
INH
RIF
RIF/INH
hPXR
KO

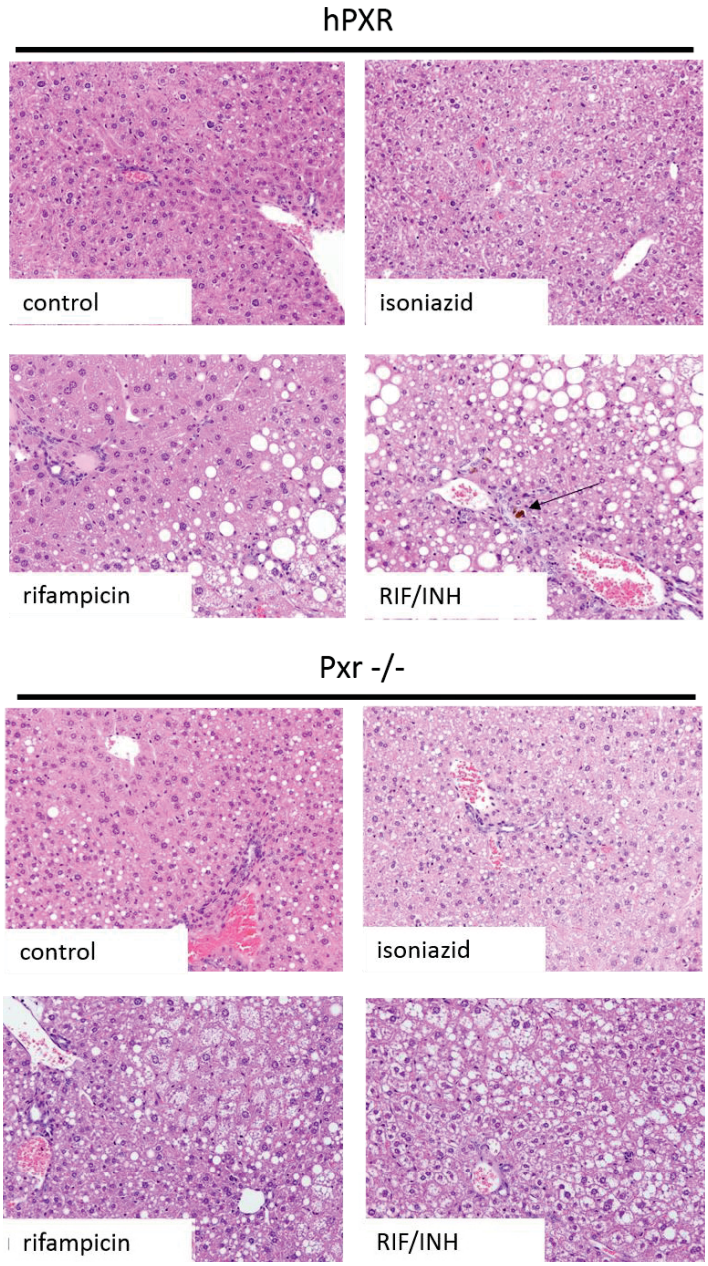

Figure 4-5. Representative liver micrographs of *in vivo* study 2 mice.

20X Micrographs. Slides are stained with Hematoxylin and Eosin. Arrows indicate bile plugs.

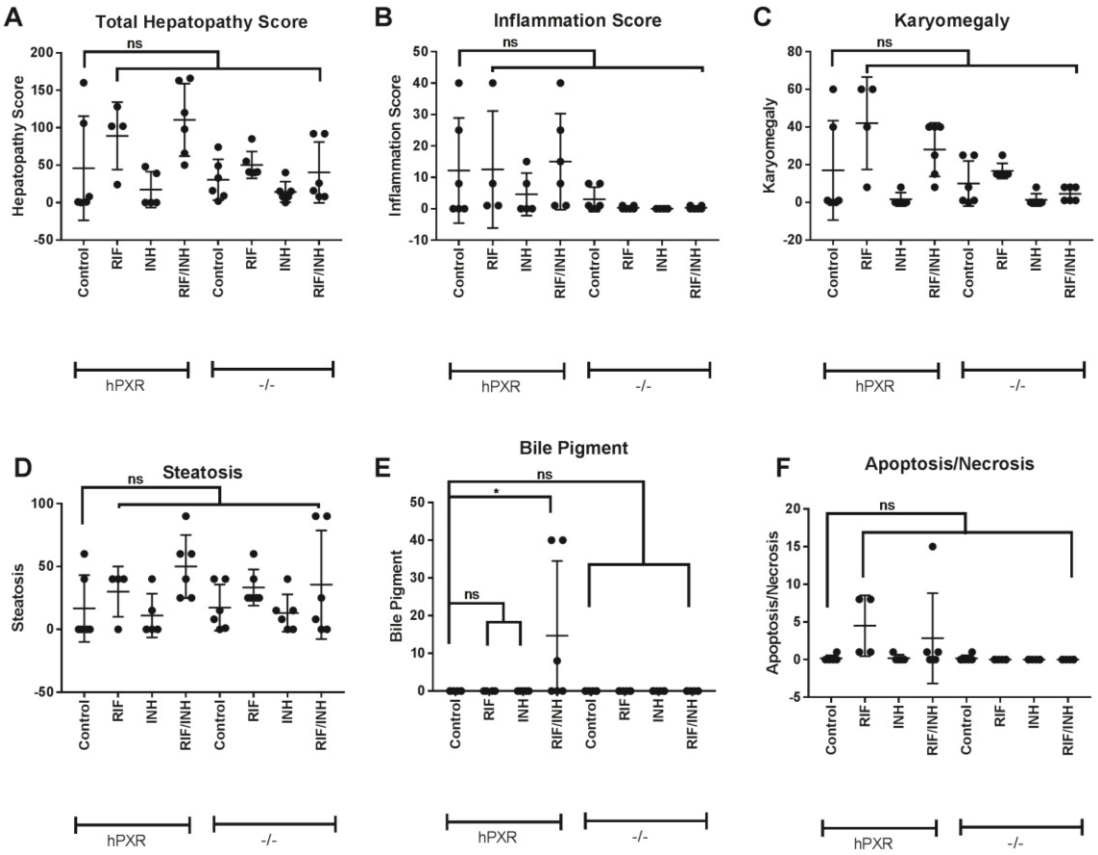

Figure 4-6. Histopathologic scores of *in vivo* study 2 mice.

Semi-quantitative histopathologic scoring was performed by a board certified vertinary pathologist. Total hepatotopathy (A), inflammation score (B), karyomegaly (C), steatosis (D), bile pigment (E), and necrosis (F) scores. Data are expressed as the mean ± SEM. 1-way ANOVA followed by Dunnett's post-hoc analysis was used to compare group meansl. ****$p<0.0001$; ***$p<0.001$, **$p<0.01$, *$p<0.05$

Indeed, 5-OH pyrazinamide, 5-OH pyrazinoic acid, and pyrazinoic acid were associated with purine metabolism products in patients, but was not associated with hepatotoxicity (Cao, Mi et al. 2018). Pyrazinamide is a pyrazine analogue of nicotinamine and is both bactericidal and bacteriostatic. Pyrazinamide is typically administered as a dose of 15-30 mg/kg/day. Adding pyrazinamide to an anti-tubercular therapy regimen that contains rifampicin and isoniazid results in a significant increase in the incidence of hepatotoxicity (Chang, Leung et al. 2008). 0.8% of patients developed hepatotoxicity while taking a combination of rifampicin and isoniazid, whereas 2.6% of patients taking pyrazinamide, rifampicin, and isoniazid. The adjusted odds ratio for developing hepatotoxicity when taking pyrazinamide, isoniazid, and/or rifampicin was 2.8 compared to taking only isoniazid and pyrazinamide. Likewise, the combination of pyrazinamide with rifampicin was significantly more likely to cause hepatotoxicity than preventative treatment isoniazid alone with an odds ratio of 2.6 (van Hest, Baars et al. 2004). Inclusion of pyrazinamide to the animals being administered rifampicin and isoniazid would have likely increased the incidence and severity of liver injury based on observations from previous reports. However, this hepatotoxicity from pyrazinamide, rifampicin, and isoniazid would not have the evidence to suggest it was preventable by *hPXR* antagonism.

Significance of PIH and Hydrazine Findings

Iron sulfur [2Fe-2S] clusters bind a [Cys-X-Cys-X-Cys-X-Cys] motif. Four cysteine residues are conserved between Drosophila and humans, Cys-196, Cys-403, Cys-406, and Cys-411 are ligands for the [2Fe-2S] cluster in *FECH* (Crouse, Sellers et al. 1996). NOS inhibits *Fech* in rat hepatocytes and purified recombinant human *FECH* (Kim, Bergonia et al. 1995, Rouault and Klausner 1996). A labile iron sulfur [2Fe-2S] cluster is found in animal *ferrochelatase* but is missing from the analogous plant, bacterial, and yeast enzymes (Dailey, Finnegan et al. 1994, Ferreira and Gong 1995, Day, Parsons et al. 1998). Therefore the [2Fe-2S] cluster does not appear to be necessary for catalysis. However, in mammal enzymes, when this structure is targeted by NOS, degradation of *FECH/Fech* are increased (Sellers, Johnson et al. 1996). Indeed, NOS decrease the visible absorption spectrum of the [2Fe-2S] cluster of human and mouse *FECH* as observed by EPR spectroscopy (Kim, Bergonia et al. 1995, Rouault and Klausner 1996, Sellers, Johnson et al. 1996). The yeast enzyme was affected by NOS to a much lower degree, presumably due to the lack of the [2Fe-2S] cluster. Iron limiting conditions have previously been reported to decrease *FECH* protein levels, this was shown to be due to the formation of an unstable protein with a half-life of about 1 hour compared to the protein formed in iron replete conditions with a half-life of over 35 hours (Crooks, Ghosh et al. 2010). Therefore, the iron-limiting conditions in the presence of the vitamin B_6-isoniazid conjugate, PIH, may lead to the formation of a *FECH* protein that is less stable than the form formed in iron-replete conditions.

Isonicotinic acid, hydrazine, acetylisoniazid, acetyl hydrazine, diacetyl hydrazine, and hydrazone derivatives of pyruvic and α-ketoglutaric acids have been identified as metabolites of isoniazid (Hughes 1953, Preziosi and Porcellati 1953, Defranceschi and

Zamboni 1954, Johnson 1954, Zamboni and Defranceschi 1954, Kaneo, Kubo et al. 1981, Blair, Mansilla Tinoco et al. 1985). The aroyl hydrazone iron chelator, PIH, was the only one tested found to decrease *FECH* protein levels (**Figure 3-12A** and **Figure 3-12C**). This down-regulation was found to be iron-dependent (**Figure 3-16A** and **Figure 3-16B**). The iron-limiting condition induced by deferoxamine has previously been shown to reduce the half-life of *FECH* formed after treatment (Crooks, Ghosh et al. 2010). This may be due to reducing the availability of iron to form [2Fe-2S] clusters or an effect at another point in iron-sulfur cluster assembly machinery. Further studies such as EPR spectroscopy of *FECH* formed following PIH application similar to a previous report (Sellers, Johnson et al. 1996) to observe if purified recombinant *FECH* formed in the presence of PIH differ from those formed in iron-replete conditions. Likewise, a proteomics analysis following isoniazid treatment in mice might elucidate additional possible mechanisms and other [2Fe-2S] containing proteins that may be affected by PIH.

Isoniazid treatment has been linked to peripheral neuropathy secondary to vitamin B_6 depletion (Aita and Calame 1972, Mahashur 1992) and may be associated with conjugation of isoniazid to the vitamin B_6 species, pyridoxal, pyridoxine, and pyridoxal 5' phosphate, resulting in decreased pyridoxal levels in humans and rats (Carlson, Anthony et al. 1956, Sevigny, White et al. 1966, Demiroglu and Dundar 1997, Cilliers, Labadarios et al. 2010). Isoniazid-induced vitamin B_6-dependent peripheral neuropathy is treated in part by the administration of vitamin B_6. Further studies would be necessary to study the potential relationship of vitamin B_6 levels to hepatotoxicity in anti-tubercular therapy. Hydrazine increases *ALAS1* protein (**Figure 3-12E** and **Figure 3-12G**) and mRNA (**Figure 3-12F** and **Figure 3-12H**) levels, but we did not elucidate the mechanism by which hydrazine up-regulates *ALAS1*. However, hydrazine has been previously reported to N-alkylate, deactivate, and increase the turnover of CYP450 enzymes (Battioni, Mahy et al. 1983, Ator, David et al. 1987, Jenner and Timbrell 1994, Wen, Wang et al. 2002). If this leads to a decrease in the regulatory heme pool, then this could be expected to result in *ALAS1* up-regulation at both the protein and mRNA levels (Zheng, Shan et al. 2008). Previous studies have elucidated the role of heme regulation on *ALAS1* levels (Kolluri, Sadlon et al. 2005, Yoshino, Munakata et al. 2007, Zheng, Shan et al. 2008, Gotoh, Nakamura et al. 2011, Kubota, Nomura et al. 2016).

Cholestatic liver injury due to rifampicin and isoniazid is associated with PPIX accumulation and heme biosynthesis disruption. The heme biosynthesis disruption observed in animal systems (Sachar, Li et al. 2016) after isoniazid administration also affects the human proteins (**Figure 3-9** and **Figure 3-10**). Furthermore, the effects are not due to isoniazid itself, but due to a metabolite of isoniazid, hydrazine (**Figure 3-12** and **Figure 3-15**), and a vitamin B_6 conjugate, PIH (**Figure 3-12** and **Figure 3-13**). PIH forms in an enzyme-independent reaction between multiple vitamin B_6 orthologs and isoniazid (**Figure 3-13**) and decreases *FECH* protein levels in an iron-dependent manner (**Figure 3-16**). Hydrazine is formed in the culture media of primary human hepatocytes and HepG2/C3A and may require metabolic activation of isoniazid to achieve high concentrations (**Figure 3-15**). Hydrazine up-regulates ALAS1 at the mRNA and protein levels (**Figure 3-12**). Together these effects would begin to explain the observed increase in PPIX accumulation after isoniazid co-administration.

Significance of Proteomics Profiling Findings

Proteomics profiling revealed protein changes in *hPXR* mice treated with rifampicin and/or isoniazid and changes in *mPxr* $^{-/-}$ mice treated with rifampicin and isoniazid compared to *hPXR* control mice. With these treatments it is possible to tell what changes are due to the drug combination and what changes are dependent on *hPXR* status and what changes are due to the single therapy of either drug or due to the combination therapy in *hPXR* mice. The analysis revealed down-regulation of heme biosynthesis genes (*Alas2*, *Ppox*, and *Fech*) that participate in a mitochondrial protein complex (Medlock, Shiferaw et al. 2015). This complex or the individual proteins of this complex were decreased by the combination (**Table 3-1**) of rifampicin and isoniazid in *hPXR* mice. Further validation of these findings may elucidate what level (transcriptional, translational, or post-translational) that these changes occur and reveal the heme biosynthesis metabolite (the *Ppox* substrate, PPG or the *Fech* substrate, PPIX) that accumulates from these changes.

Proteomics profiling also identified CYP450 enzyme changes and the differences due to drug treatment and *hPXR* status (**Table 3-2**). High *CYP2E1* activity has been reported to contribute to an increased incidence of isoniazid DILI in humans (Leiro-Fernandez, Valverde et al. 2010, Gogtay, Kapileshwar et al. 2016, Antonenko, Butov et al. 2017). In mice, *Cyp2e1* has not been associated with a protective effect on the development of isoniazid DILI in mice, but pan-CYP450 inhibitors have been shown to affect the development of DILI in mice (Mitchell, Thorgeirsson et al. 1975, Mitchell, Zimmerman et al. 1976, Lauterburg, Smith et al. 1985, Lauterburg, Todd et al. 1985). Analysis revealed an *hPXR*-independent increase in *Cyp2e1* protein in mice due to the combination of rifampicin and isoniazid.

The nuclear receptors, *Hnf1a*, *Nr3c*, and *Nr5a* were significantly changed and are down-regulated due to rifampicin and isoniazid (**Table 3-3**). The *glucocorticoid receptor* (*Nr3c*) and *Nr5a* may be down-regulated due to rifampicin in *hPXR* mice. Hnf1a may be down-regulated due to rifampicin in an *hPXR*-independent manner. Other nuclear receptors were not significantly changed, suggesting that changes observed in target genes may be due to activation of these nuclear receptors.

The organic transporters *Abcb1a*, *Abcc2*, Slc10a1, and *Slco1a* were significantly changed (**Table 3-4**). Rifampicin may have increased *Abcb1a* in an *hPXR*-dependent manner, which could result in increased efflux of xenobiotic substrates of *Abcb1a* taken in combination with anti-tubercular therapy. *Abcc2* may have been decreased due to isoniazid independent of *hPXR*-status. *Slc10a1* and *Slco1a1* may be decreased due to rifampicin dependent on *hPXR* status.

Ltf modulates the immune system, both innate and adaptive responses, and a decrease may be expected to produce an exaggerated immune response to injury (Actor, Hwang et al. 2009). Indeed *Ltf* is significantly decreased by at least 60% in all treatments compared to control *hPXR* mice (**Table 3-5**). *Ftl11* is down-regulated in all treatment groups, with the highest magnitude of decrease (72%) in *hPXR* mice treated with both

rifampicin and isoniazid. Low ferritin levels are a clinical sign of iron deficiency and could reflect low iron levels possibly caused by long-term exposure to an iron chelator. However, this is less likely as *Ftl1* was also decreased in rifampicin treated *hPXR* mice, but to a lower magnitude to all isoniazid-containing treatments. *Abcb7* is an iron transporter and deficiency is associated with refractory anemia with ring sideroblasts from intracellular iron accumulation in erythrocytes. Abcb7 may be decrease in and hPXR-independent manner by rifampicin. This effect could be compensatory to low-iron levels or a direct effect of drug treatment.

Profiling analysis revealed many changes in proteins involved in relieving oxidative stress (**Table 3-6**). Multiple GST mu isoforms were up-regulated by rifampicin a possibly *hPXR*-dependent manner. There was an approximately additional 1 fold higher increase in *hPXR* mice treated with rifampicin and isoniazid compared to *mPxr* $^{-/-}$ mice treated with rifampicin and isoniazid. Additional GST isoforms up-regulated where *Gsta1* and *Gstt2*. *GSTM1* has been reported to be protective in humans treated with rifampicin and isoniazid. Null alleles of *GSTM1* in humans may lead to increased incidence of DILI (Roy, Chowdhury et al. 2001, Huang, Su et al. 2007, Lucena, Andrade et al. 2008, Bing, Xiaomeia et al. 2011, Monteiro, El-Jaick et al. 2012, Gupta, Singh et al. 2013, Li, Long et al. 2013, Tang, Deng et al. 2013). This response may be protective to xenobiotic exposure by conjugating allowing for the elimination of xenobiotics. Cat was also increase due to rifampicin in a possibly *hPXR*-dependent manner and may be protective by neutralizing H_2O_2. *Nqo1* is up-regulated in APAP-induced DILI and is protective against the development of DILI (Hwang, Kim et al. 2015). *Nqo1* is increased in an *hPXR*-independent manner due to rifampicin and isoniazid and to a greater extent due to rifampicin alone. These changes support the hypothesis that oxidative stress may play a role in the response of mouse liver protein expression to rifampicin and isoniazid treatment.

Multiple [Fe-S] cluster assembly proteins are down-regulated by rifampicin and isoniazid (**Table 3-7**). *Nfs1*, *Fdx1*, *Hscb*, *Isca11*, and *Bola3* are decreased by the combination of rifampicin and isoniazid in both *hPXR* and *mPxr* $^{-/-}$ mice. Whether these changes are direct effects of drug treatment or are compensatory to other changes is unclear, but it does not seem to be due to isoniazid alone. However, with these decreases the ability to produce [Fe-S] clusters and the proteins that contain them may be reduced.

Histopathologic examination revealed signs of toxicity in *hPXR* mice treated with rifampicin and isoniazid in combination and with rifampicin alone in the mice whose livers were used for proteomics profiling (**Table 4-1**). This was not significant because two mice not included in the proteomics analysis had high histopathologic scores. However, the control *hPXR* mice used in the proteomics analysis had lower levels of hepatotoxicity, whereas *hPXR* mice treated with rifampicin and isoniazid and rifampicin alone all had much higher histopathogic score (**Table 4-1**). Correspondingly, up-regulation of the genes related to wound healing *Tgm2*, *Col4a1* and *Anxa5* were increased in *hPXR* mice treated with rifampicin and isoniazid (**Table 3-8**).

Table 4-1. Histopathologic score of mice in proteomics analysis.

	hPXR									*mPXR* $^{-/-}$	
Treatment:	RIF		RIF/INH			Control		INH		RIF/INH	
Sample ID:	T	U	I	K	L	A	C	N	O	Z	AA
HP Score:	102	102	166	163	50	8	0	0	48	16	8

Pdxp was significantly increased due to rifampicin alone and in combination with isoniazid in *hPXR* mice and due to the combination of rifampicin and isoniazid in *mPxr* $^{-/-}$ mice (**Table 3-9**). Multiple [Fe-S] cluster assembly machinery proteins are down-regulated (**Table 3-10**). Two [Fe-S]-containing proteins were down-regulated by isoniazid that contained multiple [Fe-S] clusters, some of which are [2Fe-2S] clusters. Multiple [2F-2S]-containing proteins are down-regulated due to isoniazid, but not all these proteins were decreased. Proteomics analysis has revealed many changes due to rifampicin and isoniazid treatment in mice that need be validated.

Significance of Physiochemical Findings

The proposed hepatotoxicity mechanism of PPIX posits that PPIX precipitates in bile canaliculi, possibly upon binding with bile acids and phospholipids. This precipitation of PPIX and bile acid constituents may lead to bile stasis and bile pigment plugs observed in enlarged canaliculi upon histologic examination. This has not before been shown to be the mechanism by which PPIX contributes to cholestatic hepatotoxicity. Therefore, I demonstrated that PPIX is insoluble at the higher concentrations reported in hepatotoxicity and that PPIX binds to bile acid constituents and that this binding may be affected by the presence of rifampicin and isoniazid. The hepatotoxicity mechanism of PPIX also presumes that extracellular PPIX is more hepatotoxic than intracellular PPIX (Lyoumi, Abitbol et al. 2011). Thus, I selected a polar species of PPIX, the disodium salt, which is not membrane permeable. I then found that exogenous treatment of PPIX (I cannot exclude cellular import conclusively) significantly decreased the viability of HepG2/C3A cells.

The mechanism of PPIX induced cholestatic hepatotoxicity observed in BALB/c^{m1Pas} mice (Lyoumi, Abitbol et al. 2011) and as reported in *hPXR* transgenic C57BL/6 mice (Li, Lu et al. 2013), is dependent upon PPIX efflux to the bile and that retention in hepatocytes results in a less severe and hepatocellular pattern of hepatotoxicity. Therefore, PPIX would be expected to contribute to toxicity upon efflux from hepatocytes. This efflux would be expected to be dependent upon *ABCG2*-mediated transport of PPIX and has been reported as such previously (Aust, Obrist et al. 2004). Therefore, the expected role of isoniazid or rifampicin upon *ABCG2* activity, would be to increase possibly by transcriptional up-regulation rather than by inhibition by isoniazid. (He, Guo et al. 2017) Indeed, I report here that isoniazid does not inhibit human or mouse *ABCG2*/*Abcg2*-mediated transport of pheophorbide A or PPIX.

Future Studies

The exact molecular mechanism and specific contribution to toxicity from both rifampicin and isoniazid should be elucidated before re-attempt of the in vivo study is made. When these conditions are known after revelation from mechanistic studies, the animal equivalent dose I calculated should be a starting point. Future studies to undertake as indicated by the results of this study would broadly be to (1) validate the proteomics

profiling findings, (2) successfully observe the DILI phenotype in mouse, (3) to specifically define the mechanism by which PIH and hydrazine affect heme biosynthesis proteins, and (4) to fully elucidate the effects of the physiochemical properties of PPIX on the development of DILI.

To Validate and Expand the Proteomics Profiling Results

The proteomics data set derived by TMT labeled LC/LC/MS/MS revealed additional potential contributions to hepatotoxicity from rifampicin as well as potential mechanism by which isoniazid affected *Fech* and *Alas1*. Down-regulation of a mitochondrial heme synthesis protein complex may have been indicated. Further validation of these findings may elucidate at what level that these changes occur and reveal the heme biosynthesis metabolite (the *Ppox* substrate, PPG or the *Fech* substrate, PPIX) that accumulates from these changes.

Network analysis of transcription factor target gene networks may identify potential transcription factors that are activated in addition to *hPXR* that may play a role in the development of hepatotoxicity. Several organic transporters were changed due to rifampicin and isoniazid and these changes may reflect disrupted bile flow either by being contributory to cholestasis or by being compensatory. Additionally, potential changes were observed that could be reflective of chronically low iron levels. The timing and severity of changes in the expression of *Fech* could be improved by modulation of iron levels as well as modulation of pyridoxal phosphorylation.

Changes in [Fe-S] cluster assembly machinery proteins observed from the proteomics analysis could be related to the potential for [Fe-S] cluster incorporation into *Fech*, forming a stable protein able to clear PPIX. Up-regulation of CYP450 enzymes due to rifampicin could be the major contribution of rifampicin to hepatotoxicity observed in *hPXR* mice treated with rifampicin and isoniazid. To confirm, one would need to robustly induce phenotype then test multiple specific and pan inhibitors of CYP450 enzymes in the presence of rifampicin and isoniazid. Confirmation of these changes would reveal additional conditions to improve the likelihood of obtaining a hepatotoxic phenotype due to rifampicin and isoniazid treatment in *hPXR* mice.

To Successfully Observe the DILI Phenotype in Mouse

The inclusion of pyrazinamide to the rifampicin and isoniazid combination treatment of *hPXR* mice may cause a more severe toxicity, but may be (1) too severe to be reversed or (2) not *hPXR*-dependent and not reversible by *hPXR* antagonism. However, pyrazinamide inclusion should be one of several conditions tested for a pilot study to induce hepatotoxicity in hPXR mice. Pyrazinamide inclusion to anti-tubercular regimens containing rifampicin and isoniazid more than doubles the incidence of hepatotoxicity (Centers for Disease and Prevention 2001, Chang, Leung et al. 2008). No evidence exists that hPXR plays a role in the hepatotoxicity of pyrazinamide (Shehu, Li

et al. 2016). Additionally, the hepatotoxicity of pyrazinamide may be by a separate mechanism than either rifampicin or isoniazid and the combination of rifampicin an isoniazid. A metabolite of pyrazinamide, 5-hydroxypyrazinoic acid, may be responsible for the toxicity seen after pyrazinamide administration and is dependent on an un-identified amidase (Shih, Pai et al. 2013). The pattern of hepatotoxicity is hepatocellular and this study was conducted in rats and caution should be used when extrapolating these results to mice or humans.

The isoniazid dose used in study 3 (70 mg/kg/day) was too low considering the estimated dose in study 2 (220 mg/kg/day), previous literature reports (75 mg/kg/day), and the calculated dose (185 mg/kg/day) (Chen, Xu et al. 2011, He, Guo et al. 2017). Indeed, 300 mg/kg for a month in *mPxr* expressing C57BL/6 was not toxic (Metushi, Cai et al. 2014). The dose used in the 3rd in vivo study (70 mg/kg) was lower than the dose used in the 1st in vivo study (73.3 mg/kg). The histopathologic score would have been significant for study 2 in *hPXR* mice treated with rifampicin and isoniazid, but two mice in the *hPXR* control group had liver injury possibly due to age. Therefore, the goal of study 3 was to use a higher and more controllable dose of rifampicin and isoniazid to induce hepatotoxicity at an earlier time-point. It was believed that my calculated and proposed doses were too high. Therefore, I used half of the isoniazid dose I had calculated from the human dose and found was in the range used therapeutically in mice to treat *M. tuberculosis* infection.

To successfully recapitulate the DILI phenotype reported previously, (Li, Lu et al. 2013) (1) doses should be selected based on the literature evidence, mouse equivalent dose calculations, and pilot experiments, (2) multiple diet formulations containing various amounts of vitamin B_6 analogues should be considered, (3) small pilot studies using only *hPXR* control mice and *hPXR* mice treated with rifampicin and isoniazid should be performed first to find the conditions of DILI, (4) the role of PPIX should be elucidated to understand if additional conditions to promote toxicity are necessary, and (5) the *hPXR* mice need to be back-crossed to reduce the variability in drug response.

To Fully Elucidate the Role of the Physiochemical Properties of PPIX upon the Development of DILI

A full characterization of the contribution of the physiochemical properties of multiple species of PPIX should be undertaken to understand the molecular mechanism by which PPPIX contributes to hepatotoxicity. Previous reports that have reported PPIX in association with hepatotoxicity, have detected PPIX by mass spectrometry which may not be able to differentiate between PPIX species with different metal ions coordinated (Li, Lu et al. 2013). This is especially necessary given that the toxic effect of PPIX may be exerted when in an extracellular space (Davies, Schuurman et al. 2005, Lyoumi, Abitbol et al. 2011). Therefore, physiochemical rather than the biologic effects of PPIX accumulation may be more imported in the DILI associated with PPIX accumulation. Future studies should seek to (1) demonstrate conclusively by comparing Km values that rifampicin and/or isoniazid affect binding of bile acid constituents, (2) determine the

solubility of multiple species of PPIX and the conditions present in the bile that may modulate the solubility of PPIX, and (3) demonstrate the exact molecular mechanism of the *in vitro* hepatotoxicity of PPIX because it will be necessary to understand the *in vivo* mechanism of hepatotoxicity. PPIX is strongly associated with hepatotoxicity, but a definitive answer and mechanism has not been reported.

To Elucidate the Mechanism by which Hydrazine Up-Regulates ALAS1 and PIH Down-Regulates FECH

Low iron levels regulate FECH by preventing the formation of a stable protein by decreasing iron levels by chelation (Taketani, Adachi et al. 2000, Crooks, Ghosh et al. 2010), whether this is by disrupting iron metabolism, transport, or storage, direct destruction of the [Fe-S] cluster of FECH, or by the disruption of the [Fe-S] cluster assembly machinery proteins remains to be see. Further studies such as EPR spectroscopy of *FECH* formed following PIH application similar to a previous report (Sellers, Johnson et al. 1996) to observe the if purified recombinant *FECH* formed in the presence of PIH differ from those formed in iron-replete conditions. Likewise, a proteomics analysis following isoniazid treatment in mice might elucidate additional possible mechanisms and other [2Fe-2S] containing proteins that may be affected by PIH. EPR spectroscopy could directly observe malformation of the [Fe-S] cluster.

Proteomics profiling data suggest that additional [2Fe-2S] cluster-containing proteins may be down-regulated by isoniazid in addition to *FECH*. Proteomics profiling also revealed that several proteins involved in the assembly of [Fe-S] cluster proteins were also down-regulated by isoniazid. Future studies to determine if there is a global decrease in [2Fe-2S] cluster containing proteins by defects in [Fe-S] cluster assembly machinery, or another aspect of Fe-mediated protein stability involved are warranted.

Proteomics profiling also provided insights into the possible mechanism by which hydrazine up-regulates ALAS1. Multiple CYP450 enzymes are down-regulated by isoniazid (**Table 3-2**). This could be due to isoniazid and hydrazine covalently binding to and destroying heme-containing proteins (Battioni, Mahy et al. 1983, Ator, David et al. 1987, Jenner and Timbrell 1994, Wen, Wang et al. 2002). This destruction of hemoproteins could lead to a compensatory up-regulation of the heme biosynthesis pathway once the inhibitory effect of the regulatory heme pool is removed (Srivastava, Borthwick et al. 1983, Kolluri, Sadlon et al. 2005, Zheng, Shan et al. 2008). Directly measuring the increase in protein size by mass spectrometry when adducted to hydrazine would confirm this mechanism in *hPXR* mice.

Conclusions

Tuberculosis kills millions of humans every year. A significant portion of these deaths is from anti-TB therapy failure due to withdrawal of first-line drugs due to DILI. This is more likely in vulnerable populations (Ungo, Jones et al. 1998, Yee, Valiquette et

al. 2003, Breen, Miller et al. 2006). I propose additions to the understanding of the mechanism of rifampicin and isoniazid DILI whereby separate metabolites of isoniazid modulate the heme biosynthesis pathway (**Figure 4-7**). Models of anti-TB DILI have been used for over 50 years (Mitchell, Zimmerman et al. 1976, Nelson, Mitchell et al. 1976). These early models were useful, but due to the lack of the gallbladder in rats, were not fully elucidative. Indeed, the absence of the gallbladder in the rat may interfere the development of the clinicopathologic pattern of anti-TB DILI of liver injury observed in the livers Of Mice and Men.

In conclusion, I report that the physiochemical properties of PPIX may contribute to the toxicity associated with PPIX accumulation, metabolites of isoniazid modulate the heme biosynthesis pathway in a manner associated with an increase in PPIX levels, and that rifampicin treatment of mice results in gene changes that may contribute to PPIX accumulation and hepatotoxicity.

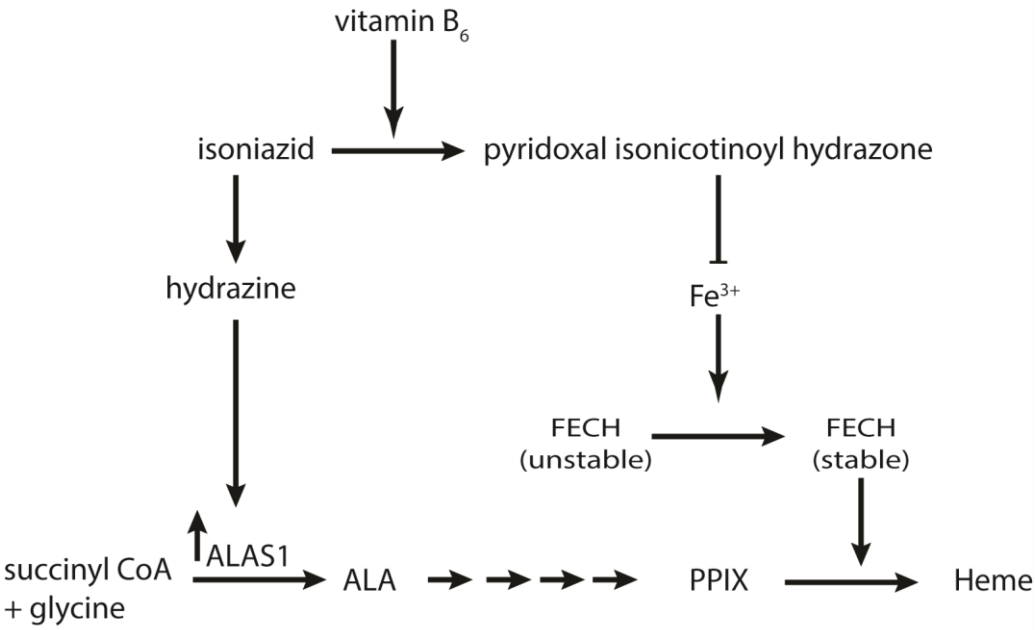

Figure 4-7. The proposed mechanism of regulation of heme biosynthesis by isoniazid.

Vitamin B_6 analogues form PIH in the presence of isoniazid. PIH chelates iron and prevents the stabilization of *FECH*. Isoniazid breaks down to hydrazine and hydrazine up-regulates *ALAS1* at the transcriptional level. Both effects may be expected to raise the levels of liver protoporphyrin ix and lead to cholestatic liver injury.

LIST OF REFERENCES

Aarnoutse, R. E., G. S. Kibiki, K. Reither, H. H. Semvua, F. Haraka, C. M. Mtabho, S. G. Mpagama, J. van den Boogaard, I. M. Sumari-de Boer, C. Magis-Escurra, M. Wattenberg, J. G. M. Logger, L. H. M. Te Brake, M. Hoelscher, S. H. Gillespie, A. Colbers, P. P. J. Phillips, G. Plemper van Balen, M. J. Boeree and A. C. Pan (2017). "Pharmacokinetics, Tolerability, and Bacteriological Response of Rifampin Administered at 600, 900, and 1,200 Milligrams Daily in Patients with Pulmonary Tuberculosis." Antimicrob Agents Chemother **61**(11).

Actor, J. K., S. A. Hwang and M. L. Kruzel (2009). "Lactoferrin as a natural immune modulator." Curr Pharm Des **15**(17): 1956-1973.

Ait Moussa, L., O. El Bouazzi, S. Serragui, D. Soussi Tanani, A. Soulaymani and R. Soulaymani (2016). "Rifampicin and isoniazid plasma concentrations in relation to adverse reactions in tuberculosis patients: a retrospective analysis." Ther Adv Drug Saf **7**(6): 239-247.

Aita, J. F. and T. R. Calame (1972). "Peripheral neuropathy secondary to isoniazid-induced pyridoxine deficiency." Md State Med J **21**(10): 68-70.

Al-Dosari, M. S., J. E. Knapp and D. Liu (2006). "Activation of human CYP2C9 promoter and regulation by CAR and PXR in mouse liver." Mol Pharm **3**(3): 322-328.

Aleksunes, L. M. and C. D. Klaassen (2012). "Coordinated regulation of hepatic phase I and II drug-metabolizing genes and transporters using AhR-, CAR-, PXR-, PPARalpha-, and Nrf2-null mice." Drug Metab Dispos **40**(7): 1366-1379.

Ali, N. and H. E. Auerbach (2017). "New-onset acute thrombocytopenia in hospitalized patients: pathophysiology and diagnostic approach." J Community Hosp Intern Med Perspect **7**(3): 157-167.

Andrews, E., M. Armstrong, J. Tugwood, D. Swan, P. Glaves, M. Pirmohamed, G. P. Aithal, M. C. Wright, C. P. Day and A. K. Daly (2010). "A role for the pregnane X receptor in flucloxacillin-induced liver injury." Hepatology **51**(5): 1656-1664.

Antonenko, P., D. Butov, V. Kresyun, K. Antonenko and T. Butova (2017). "Association between effectiveness of tuberculosis treatment and cytochrome P-4502E1 polymorphism of the patients." Int J Mycobacteriol **6**(4): 396-400.

Ascenzi, P., A. Coletta, Y. Cao, V. Trezza, L. Leboffe, G. Fanali, M. Fasano, A. Pesce, C. Ciaccio, S. Marini and M. Coletta (2013). "Isoniazid inhibits the heme-based reactivity of Mycobacterium tuberculosis truncated hemoglobin N." PLoS One **8**(8): e69762.

Astner, I., J. O. Schulze, J. van den Heuvel, D. Jahn, W. D. Schubert and D. W. Heinz (2005). "Crystal structure of 5-aminolevulinate synthase, the first enzyme of heme biosynthesis, and its link to XLSA in humans." EMBO J **24**(18): 3166-3177.

Ator, M. A., S. K. David and P. R. Ortiz de Montellano (1987). "Structure and catalytic mechanism of horseradish peroxidase. Regiospecific meso alkylation of the prosthetic heme group by alkylhydrazines." J Biol Chem **262**(31): 14954-14960.

Aust, S., P. Obrist, W. Jaeger, M. Klimpfinger, G. Tucek, F. Wrba, E. Penner and T. Thalhammer (2004). "Subcellular localization of the ABCG2 transporter in

normal and malignant human gallbladder epithelium." Lab Invest **84**(8): 1024-1036.
Bachmanov, A. A., D. R. Reed, G. K. Beauchamp and M. G. Tordoff (2002). "Food intake, water intake, and drinking spout side preference of 28 mouse strains." Behav Genet **32**(6): 435-443.
Battioni, P., J. P. Mahy, M. Delaforge and D. Mansuy (1983). "Reaction of monosubstituted hydrazines and diazenes with rat-liver cytochrome P450. Formation of ferrous-diazene and ferric sigma-alkyl complexes." Eur J Biochem **134**(2): 241-248.
Beaune, P., P. Kremers, F. Letawe-Goujon and J. E. Gielen (1985). "Monoclonal antibodies against human liver cytochrome P-450." Biochem Pharmacol **34**(19): 3547-3552.
Bendova, P., E. Mackova, P. Haskova, A. Vavrova, E. Jirkovsky, M. Sterba, O. Popelova, D. S. Kalinowski, P. Kovarikova, K. Vavrova, D. R. Richardson and T. Simunek (2010). "Comparison of clinically used and experimental iron chelators for protection against oxidative stress-induced cellular injury." Chem Res Toxicol **23**(6): 1105-1114.
Bhadauria, S., R. Mishra, R. Kanchan, C. Tripathi, A. Srivastava, A. Tiwari and S. Sharma (2010). "Isoniazid-induced apoptosis in HepG2 cells: generation of oxidative stress and Bcl-2 down-regulation." Toxicol Mech Methods **20**(5): 242-251.
Bilgi, N., K. Bell, A. N. Ananthakrishnan and E. Atallah (2010). "Imatinib and Panax ginseng: a potential interaction resulting in liver toxicity." Ann Pharmacother **44**(5): 926-928.
Bing, C., C. Xiaomeia and L. Jinhenga (2011). "Gene dose effect of NAT2 variants on the pharmacokinetics of isoniazid and acetylisoniazid in healthy Chinese subjects." Drug Metabol Drug Interact **26**(3): 113-118.
Binkley, F., G. M. Christensen and W. N. Jensen (1952). "Pyridoxine and the transfer of sulfur." J Biol Chem **194**(1): 109-113.
Bishop, D. F., A. S. Henderson and K. H. Astrin (1990). "Human delta-aminolevulinate synthase: assignment of the housekeeping gene to 3p21 and the erythroid-specific gene to the X chromosome." Genomics **7**(2): 207-214.
Bjornsson, T. D., J. T. Callaghan, H. J. Einolf, V. Fischer, L. Gan, S. Grimm, J. Kao, S. P. King, G. Miwa, L. Ni, G. Kumar, J. McLeod, R. S. Obach, S. Roberts, A. Roe, A. Shah, F. Snikeris, J. T. Sullivan, D. Tweedie, J. M. Vega, J. Walsh, S. A. Wrighton, R. Pharmaceutical, G. Manufacturers of America Drug Metabolism/Clinical Pharmacology Technical Working, F. D. A. C. f. D. Evaluation and Research (2003). "The conduct of in vitro and in vivo drug-drug interaction studies: a Pharmaceutical Research and Manufacturers of America (PhRMA) perspective." Drug Metab Dispos **31**(7): 815-832.
Black, M., J. R. Mitchell, H. J. Zimmerman, K. G. Ishak and G. R. Epler (1975). "Isoniazid-associated hepatitis in 114 patients." Gastroenterology **69**(2): 289-302.
Blair, I. A., R. Mansilla Tinoco, M. J. Brodie, R. A. Clare, C. T. Dollery, J. A. Timbrell and I. A. Beever (1985). "Plasma hydrazine concentrations in man after isoniazid and hydralazine administration." Hum Toxicol **4**(2): 195-202.

Bloomer, J. R. (1997). "Hepatic protoporphyrin metabolism in patients with advanced protoporphyric liver disease." Yale J Biol Med **70**(4): 323-330.

Blumberg, H. M., W. J. Burman, R. E. Chaisson, C. L. Daley, S. C. Etkind, L. N. Friedman, P. Fujiwara, M. Grzemska, P. C. Hopewell, M. D. Iseman, R. M. Jasmer, V. Koppaka, R. I. Menzies, R. J. O'Brien, R. R. Reves, L. B. Reichman, P. M. Simone, J. R. Starke, A. A. Vernon, C. f. D. C. American Thoracic Society, Prevention and S. the Infectious Diseases (2003). "American Thoracic Society/Centers for Disease Control and Prevention/Infectious Diseases Society of America: treatment of tuberculosis." Am J Respir Crit Care Med **167**(4): 603-662.

Boelsterli, U. A. and K. K. Lee (2014). "Mechanisms of isoniazid-induced idiosyncratic liver injury: emerging role of mitochondrial stress." J Gastroenterol Hepatol **29**(4): 678-687.

Breen, R. A., R. F. Miller, T. Gorsuch, C. J. Smith, A. Schwenk, W. Holmes, J. Ballinger, L. Swaden, M. A. Johnson, I. Cropley and M. C. Lipman (2006). "Adverse events and treatment interruption in tuberculosis patients with and without HIV co-infection." Thorax **61**(9): 791-794.

Brewer, C. T. and T. Chen (2016). "PXR variants: the impact on drug metabolism and therapeutic responses." Acta Pharm Sin B **6**(5): 441-449.

Brewer, C. T. and T. Chen (2017). "Hepatotoxicity of Herbal Supplements Mediated by Modulation of Cytochrome P450." Int J Mol Sci **18**(11).

Buss, J. L., J. Neuzil and P. Ponka (2002). "The role of oxidative stress in the toxicity of pyridoxal isonicotinoyl hydrazone (PIH) analogues." Biochem Soc Trans **30**(4): 755-757.

Byrne, S. T., S. M. Denkin and Y. Zhang (2007). "Aspirin antagonism in isoniazid treatment of tuberculosis in mice." Antimicrob Agents Chemother **51**(2): 794-795.

Cai, Y., J. Yi, C. Zhou and X. Shen (2012). "Pharmacogenetic study of drug-metabolising enzyme polymorphisms on the risk of anti-tuberculosis drug-induced liver injury: a meta-analysis." PLoS One **7**(10): e47769.

Campbell, E. A., N. Korzheva, A. Mustaev, K. Murakami, S. Nair, A. Goldfarb and S. A. Darst (2001). "Structural mechanism for rifampicin inhibition of bacterial rna polymerase." Cell **104**(6): 901-912.

Cao, J., Y. Mi, C. Shi, Y. Bian, C. Huang, Z. Ye, L. Liu and L. Miao (2018). "First-line anti-tuberculosis drugs induce hepatotoxicity: A novel mechanism based on a urinary metabolomics platform." Biochem Biophys Res Commun **497**(2): 485-491.

Carlson, H. B., E. M. Anthony, W. F. Russell, Jr. and G. Middlebrook (1956). "Prophylaxis of isoniazid neuropathy with pyridoxine." N Engl J Med **255**(3): 119-122.

Centers for Disease, C. and Prevention (2001). "Update: Fatal and severe liver injuries associated with rifampin and pyrazinamide for latent tuberculosis infection, and revisions in American Thoracic Society/CDC recommendations--United States, 2001." MMWR Morb Mortal Wkly Rep **50**(34): 733-735.

Chamorro, J. G., J. P. Castagnino, R. M. Musella, M. Nogueras, F. M. Aranda, A. Frias, M. Visca, O. Aidar, S. Peres and G. F. de Larranaga (2013). "Sex, ethnicity, and

slow acetylator profile are the major causes of hepatotoxicity induced by antituberculosis drugs." J Gastroenterol Hepatol **28**(2): 323-328.

Chan, G. N., R. Patel, C. L. Cummins and R. Bendayan (2013). "Induction of P-glycoprotein by antiretroviral drugs in human brain microvessel endothelial cells." Antimicrob Agents Chemother **57**(9): 4481-4488.

Chang, K. C., C. C. Leung, W. W. Yew, T. Y. Lau and C. M. Tam (2008). "Hepatotoxicity of pyrazinamide: cohort and case-control analyses." Am J Respir Crit Care Med **177**(12): 1391-1396.

Charan, J. and N. D. Kantharia (2013). "How to calculate sample size in animal studies?" J Pharmacol Pharmacother **4**(4): 303-306.

Chatterjee, S., N. Lyle, A. Mandal and S. Kundu (2010). "GSTT1 and GSTM1 gene deletions are not associated with hepatotoxicity caused by antitubercular drugs." J Clin Pharm Ther **35**(4): 465-470.

Chaudhry, A. S., T. J. Urban, J. K. Lamba, A. K. Birnbaum, R. P. Remmel, M. Subramanian, S. Strom, J. H. You, D. Kasperaviciute, C. B. Catarino, R. A. Radtke, S. M. Sisodiya, D. B. Goldstein and E. G. Schuetz (2010). "CYP2C9*1B promoter polymorphisms, in linkage with CYP2C19*2, affect phenytoin autoinduction of clearance and maintenance dose." J Pharmacol Exp Ther **332**(2): 599-611.

Chen, T. (2008). "Nuclear receptor drug discovery." Curr Opin Chem Biol **12**(4): 418-426.

Chen, W., H. A. Dailey and B. H. Paw (2010). "Ferrochelatase forms an oligomeric complex with mitoferrin-1 and Abcb10 for erythroid heme biosynthesis." Blood **116**(4): 628-630.

Chen, X., J. Xu, C. Zhang, T. Yu, H. Wang, M. Zhao, Z. H. Duan, Y. Zhang, J. M. Xu and D. X. Xu (2011). "The protective effects of ursodeoxycholic acid on isoniazid plus rifampicin induced liver injury in mice." Eur J Pharmacol **659**(1): 53-60.

Chen, Y., S. S. Ferguson, M. Negishi and J. A. Goldstein (2004). "Induction of human CYP2C9 by rifampicin, hyperforin, and phenobarbital is mediated by the pregnane X receptor." J Pharmacol Exp Ther **308**(2): 495-501.

Cheng, J., K. W. Krausz, F. Li, X. Ma and F. J. Gonzalez (2013). "CYP2E1-dependent elevation of serum cholesterol, triglycerides, and hepatic bile acids by isoniazid." Toxicol Appl Pharmacol **266**(2): 245-253.

Cheng, J., X. Ma, K. W. Krausz, J. R. Idle and F. J. Gonzalez (2009). "Rifampicin-activated human pregnane X receptor and CYP3A4 induction enhance acetaminophen-induced toxicity." Drug Metab Dispos **37**(8): 1611-1621.

Chiu, N. T., E. S. Tomlinson Guns, H. Adomat, W. Jia and S. Deb (2014). "Identification of human cytochrome P450 enzymes involved in the hepatic and intestinal biotransformation of 20(S)-protopanaxadiol." Biopharm Drug Dispos **35**(2): 104-118.

Cilliers, K., D. Labadarios, H. S. Schaaf, M. Willemse, J. S. Maritz, C. J. Werely, G. Hussey and P. R. Donald (2010). "Pyridoxal-5-phosphate plasma concentrations in children receiving tuberculosis chemotherapy including isoniazid." Acta Paediatr **99**(5): 705-710.

Clare, K. E., M. H. Miller and J. F. Dillon (2017). "Genetic Factors Influencing Drug-Induced Liver Injury: Do They Have a Role in Prevention and Diagnosis?" Curr Hepatol Rep **16**(3): 258-264.

Collaborators, G. B. D. M. (2017). "Global, regional, and national under-5 mortality, adult mortality, age-specific mortality, and life expectancy, 1970-2016: a systematic analysis for the Global Burden of Disease Study 2016." Lancet **390**(10100): 1084-1150.

Crooks, D. R., M. C. Ghosh, R. G. Haller, W. H. Tong and T. A. Rouault (2010). "Posttranslational stability of the heme biosynthetic enzyme ferrochelatase is dependent on iron availability and intact iron-sulfur cluster assembly machinery." Blood **115**(4): 860-869.

Crouse, B. R., V. M. Sellers, M. G. Finnegan, H. A. Dailey and M. K. Johnson (1996). "Site-directed mutagenesis and spectroscopic characterization of human ferrochelatase: identification of residues coordinating the [2Fe-2S] cluster." Biochemistry **35**(50): 16222-16229.

Dailey, H. A., M. G. Finnegan and M. K. Johnson (1994). "Human ferrochelatase is an iron-sulfur protein." Biochemistry **33**(2): 403-407.

Davies, R., A. Schuurman, C. R. Barker, B. Clothier, T. Chernova, F. M. Higginson, D. J. Judah, D. Dinsdale, R. E. Edwards, P. Greaves, T. W. Gant and A. G. Smith (2005). "Hepatic gene expression in protoporphyic Fech mice is associated with cholestatic injury but not a marked depletion of the heme regulatory pool." Am J Pathol **166**(4): 1041-1053.

Day, A. L., B. M. Parsons and H. A. Dailey (1998). "Cloning and characterization of Gallus and Xenopus ferrochelatases: presence of the [2Fe-2S] cluster in nonmammalian ferrochelatase." Arch Biochem Biophys **359**(2): 160-169.

de Steenwinkel, J. E., R. E. Aarnoutse, G. J. de Knegt, M. T. ten Kate, M. Teulen, H. A. Verbrugh, M. J. Boeree, D. van Soolingen and I. A. Bakker-Woudenberg (2013). "Optimization of the rifampin dosage to improve the therapeutic efficacy in tuberculosis treatment using a murine model." Am J Respir Crit Care Med **187**(10): 1127-1134.

Deeken, J. F., R. W. Robey, S. Shukla, K. Steadman, A. R. Chakraborty, B. Poonkuzhali, E. G. Schuetz, S. Holbeck, S. V. Ambudkar and S. E. Bates (2009). "Identification of compounds that correlate with ABCG2 transporter function in the National Cancer Institute Anticancer Drug Screen." Mol Pharmacol **76**(5): 946-956.

Deeks, S. G., T. Wrin, T. Liegler, R. Hoh, M. Hayden, J. D. Barbour, N. S. Hellmann, C. J. Petropoulos, J. M. McCune, M. K. Hellerstein and R. M. Grant (2001). "Virologic and immunologic consequences of discontinuing combination antiretroviral-drug therapy in HIV-infected patients with detectable viremia." N Engl J Med **344**(7): 472-480.

Defranceschi, A. and V. Zamboni (1954). "Identification of two metabolites of isoniazid (isonicotinoylglycine and 1-isonicotinoyl-2-acetylhydrazine) by paper chromatography in rat urine." Biochim Biophys Acta **13**(2): 304-305.

Delaney, J. and J. A. Timbrell (1995). "Role of cytochrome P450 in hydrazine toxicity in isolated hepatocytes in vitro." Xenobiotica **25**(12): 1399-1410.

Demiroglu, H. and S. Dundar (1997). "Vitamin B6 responsive sideroblastic anaemia in a patient with tuberculosis." Br J Clin Pract **51**(1): 51-52.

den Braver, M. W., S. P. den Braver-Sewradj, N. P. Vermeulen and J. N. Commandeur (2016). "Characterization of cytochrome P450 isoforms involved in sequential two-step bioactivation of diclofenac to reactive p-benzoquinone imines." Toxicol Lett **253**: 46-54.

Desta, Z., N. V. Soukhova and D. A. Flockhart (2001). "Inhibition of cytochrome P450 (CYP450) isoforms by isoniazid: potent inhibition of CYP2C19 and CYP3A." Antimicrob Agents Chemother **45**(2): 382-392.

Desuzinges-Mandon, E., O. Arnaud, L. Martinez, F. Huche, A. Di Pietro and P. Falson (2010). "ABCG2 transports and transfers heme to albumin through its large extracellular loop." J Biol Chem **285**(43): 33123-33133.

Disease, G. B. D., I. Injury and C. Prevalence (2016). "Global, regional, and national incidence, prevalence, and years lived with disability for 310 diseases and injuries, 1990-2015: a systematic analysis for the Global Burden of Disease Study 2015." Lancet **388**(10053): 1545-1602.

Ellard, G. A. and P. T. Gammon (1976). "Pharmacokinetics of isoniazid metabolism in man." J Pharmacokinet Biopharm **4**(2): 83-113.

Elmorsy, E., S. M. Attalla, E. Fikry, A. Kocon, R. Turner, D. Christie, A. Warren, L. L. Nwidu and W. G. Carter (2016). "Adverse effects of anti-tuberculosis drugs on HepG2 cell bioenergetics." Hum Exp Toxicol.

Elmorsy, E., S. M. Attalla, E. Fikry, A. Kocon, R. Turner, D. Christie, A. Warren, L. L. Nwidu and W. G. Carter (2017). "Adverse effects of anti-tuberculosis drugs on HepG2 cell bioenergetics." Hum Exp Toxicol **36**(6): 616-625.

Elzi, L., C. Marzolini, H. Furrer, B. Ledergerber, M. Cavassini, B. Hirschel, P. Vernazza, E. Bernasconi, R. Weber, M. Battegay and H. I. V. C. S. Swiss (2010). "Treatment modification in human immunodeficiency virus-infected individuals starting combination antiretroviral therapy between 2005 and 2008." Arch Intern Med **170**(1): 57-65.

Evans, D. A., K. A. Manley and K. V. Mc (1960). "Genetic control of isoniazid metabolism in man." Br Med J **2**(5197): 485-491.

Feng, S. and X. He (2013). "Mechanism-based inhibition of CYP450: an indicator of drug-induced hepatotoxicity." Curr Drug Metab **14**(9): 921-945.

Ferreira, G. C. and J. Gong (1995). "5-Aminolevulinate synthase and the first step of heme biosynthesis." J Bioenerg Biomembr **27**(2): 151-159.

Fisher, K., R. Vuppalanchi and R. Saxena (2015). "Drug-Induced Liver Injury." Arch Pathol Lab Med **139**(7): 876-887.

Furukawa, T., H. Kohno, R. Tokunaga and S. Taketani (1995). "Nitric oxide-mediated inactivation of mammalian ferrochelatase in vivo and in vitro: possible involvement of the iron-sulphur cluster of the enzyme." Biochem J **310 (Pt 2)**: 533-538.

Ganey, P. E., J. P. Luyendyk, J. F. Maddox and R. A. Roth (2004). "Adverse hepatic drug reactions: inflammatory episodes as consequence and contributor." Chem Biol Interact **150**(1): 35-51.

Ganey, P. E., J. P. Luyendyk, S. W. Newport, T. M. Eagle, J. F. Maddox, N. Mackman and R. A. Roth (2007). "Role of the coagulation system in acetaminophen-induced hepatotoxicity in mice." Hepatology **46**(4): 1177-1186.

Gardner-Stephen, D., J. M. Heydel, A. Goyal, Y. Lu, W. Xie, T. Lindblom, P. Mackenzie and A. Radominska-Pandya (2004). "Human PXR variants and their differential effects on the regulation of human UDP-glucuronosyltransferase gene expression." Drug Metab Dispos **32**(3): 340-347.

Gaude, G. S., A. Chaudhury and J. Hattiholi (2015). "Drug-induced hepatitis and the risk factors for liver injury in pulmonary tuberculosis patients." J Family Med Prim Care **4**(2): 238-243.

Ghannam, M., S. Mansour, A. Nabulsi and Q. Abdoh (2017). "Anticonvulsant hypersensitivity syndrome after phenytoin administration in an adolescent patient: a case report and review of literature." Clin Mol Allergy **15**: 14.

Gogtay, N. J., S. R. Kapileshwar, S. U. Shah, S. R. Bendkhale, S. Ramakrishna, K. Sridharan, B. K. Thelma, U. M. Thatte and N. A. Kshirsagar (2016). "Evaluation of cytochrome P4502E1 polymorphisms in healthy adult Western Indians and patients with antituberculous drug-induced hepatotoxicity." Indian J Pharmacol **48**(1): 42-46.

Gong, H., S. V. Singh, S. P. Singh, Y. Mu, J. H. Lee, S. P. Saini, D. Toma, S. Ren, V. E. Kagan, B. W. Day, P. Zimniak and W. Xie (2006). "Orphan nuclear receptor pregnane X receptor sensitizes oxidative stress responses in transgenic mice and cancerous cells." Mol Endocrinol **20**(2): 279-290.

Gonzalez-Juarrero, M., L. K. Woolhiser, E. Brooks, M. A. DeGroote and A. J. Lenaerts (2012). "Mouse model for efficacy testing of antituberculosis agents via intrapulmonary delivery." Antimicrob Agents Chemother **56**(7): 3957-3959.

Gonzalez, F. J. (1988). "The molecular biology of cytochrome P450s." Pharmacol Rev **40**(4): 243-288.

Goodfellow, B. J., J. S. Dias, G. C. Ferreira, P. Henklein, V. Wray and A. L. Macedo (2001). "The solution structure and heme binding of the presequence of murine 5-aminolevulinate synthase." FEBS Lett **505**(2): 325-331.

Goodwin, B., E. Hodgson and C. Liddle (1999). "The orphan human pregnane X receptor mediates the transcriptional activation of CYP3A4 by rifampicin through a distal enhancer module." Mol Pharmacol **56**(6): 1329-1339.

Gotoh, S., T. Nakamura, T. Kataoka and S. Taketani (2011). "Egr-1 regulates the transcriptional repression of mouse delta-aminolevulinic acid synthase 1 by heme." Gene **472**(1-2): 28-36.

Gourishankar, A., F. Navarro, A. N. Debroy and K. C. Smith (2014). "Isoniazid hepatotoxicity with clinical and histopathology correlate." Ann Clin Lab Sci **44**(1): 87-90.

Granick, S. and R. D. Levere (1965). "The intracellular localization of heme by a fluorescence technique." J Cell Biol **26**(1): 167-176.

Guillouzo, A. and C. Guguen-Guillouzo (2008). "Evolving concepts in liver tissue modeling and implications for in vitro toxicology." Expert Opin Drug Metab Toxicol **4**(10): 1279-1294.

Guillouzo, A., F. Morel, O. Fardel and B. Meunier (1993). "Use of human hepatocyte cultures for drug metabolism studies." Toxicology **82**(1-3): 209-219.

Guo, G. L., J. S. Moffit, C. J. Nicol, J. M. Ward, L. A. Aleksunes, A. L. Slitt, S. A. Kliewer, J. E. Manautou and F. J. Gonzalez (2004). "Enhanced acetaminophen toxicity by activation of the pregnane X receptor." Toxicol Sci **82**(2): 374-380.

Guo, Y. X., X. F. Xu, Q. Z. Zhang, C. Li, Y. Deng, P. Jiang, L. Y. He and W. X. Peng (2015). "The inhibition of hepatic bile acids transporters Ntcp and Bsep is involved in the pathogenesis of isoniazid/rifampicin-induced hepatotoxicity." Toxicol Mech Methods **25**(5): 382-387.

Gupta, S., S. Tyagi, D. V. Almeida, M. C. Maiga, N. C. Ammerman and W. R. Bishai (2013). "Acceleration of tuberculosis treatment by adjunctive therapy with verapamil as an efflux inhibitor." Am J Respir Crit Care Med **188**(5): 600-607.

Gupta, V. H., M. Singh, D. N. Amarapurkar, P. Sasi, J. M. Joshi, R. Baijal, R. P. H, A. D. Amarapurkar, K. Joshi and P. P. Wangikar (2013). "Association of GST null genotypes with anti-tuberculosis drug induced hepatotoxicity in Western Indian population." Ann Hepatol **12**(6): 959-965.

Hayes, J. D. and D. J. Pulford (1995). "The glutathione S-transferase supergene family: regulation of GST and the contribution of the isoenzymes to cancer chemoprotection and drug resistance." Crit Rev Biochem Mol Biol **30**(6): 445-600.

He, K., R. E. Talaat, W. F. Pool, M. D. Reily, J. E. Reed, A. J. Bridges and T. F. Woolf (2004). "Metabolic activation of troglitazone: identification of a reactive metabolite and mechanisms involved." Drug Metab Dispos **32**(6): 639-646.

He, L., Y. Guo, Y. Deng, C. Li, C. Zuo and W. Peng (2017). "Involvement of protoporphyrin IX accumulation in the pathogenesis of isoniazid/rifampicin-induced liver injury: the prevention of curcumin." Xenobiotica **47**(2): 154-163.

Hope, D. B. (1964). "Cystathionine Accumulation in the Brains of Pyridoxine-Deficient Rats." J Neurochem **11**: 327-332.

Horne, D. J., C. Spitters and M. Narita (2011). "Experience with rifabutin replacing rifampin in the treatment of tuberculosis." Int J Tuberc Lung Dis **15**(11): 1485-1489, i.

Hu, Y., A. Liu, F. Ortega-Muro, L. Alameda-Martin, D. Mitchison and A. Coates (2015). "High-dose rifampicin kills persisters, shortens treatment duration, and reduces relapse rate in vitro and in vivo." Front Microbiol **6**: 641.

Huang, Y. S., H. D. Chern, W. J. Su, J. C. Wu, S. C. Chang, C. H. Chiang, F. Y. Chang and S. D. Lee (2003). "Cytochrome P450 2E1 genotype and the susceptibility to antituberculosis drug-induced hepatitis." Hepatology **37**(4): 924-930.

Huang, Y. S., W. J. Su, Y. H. Huang, C. Y. Chen, F. Y. Chang, H. C. Lin and S. D. Lee (2007). "Genetic polymorphisms of manganese superoxide dismutase, NAD(P)H:quinone oxidoreductase, glutathione S-transferase M1 and T1, and the susceptibility to drug-induced liver injury." J Hepatol **47**(1): 128-134.

Hughes, H. B. (1953). "On the metabolic fate of isoniazid." J Pharmacol Exp Ther **109**(4): 444-452.

Huwyler, J., M. B. Wright, H. Gutmann and J. Drewe (2006). "Induction of cytochrome P450 3A4 and P-glycoprotein by the isoxazolyl-penicillin antibiotic flucloxacillin." Curr Drug Metab **7**(2): 119-126.

Hwang, J. H., Y. H. Kim, J. R. Noh, G. T. Gang, K. S. Kim, H. K. Chung, S. Tadi, Y. H. Yim, M. Shong and C. H. Lee (2015). "The protective role of NAD(P)H:quinone

oxidoreductase 1 on acetaminophen-induced liver injury is associated with prevention of adenosine triphosphate depletion and improvement of mitochondrial dysfunction." Arch Toxicol **89**(11): 2159-2166.

Isenberg, S. L., M. D. Carter, B. S. Crow, L. A. Graham, D. Johnson, N. Beninato, K. Steele, J. D. Thomas and R. C. Johnson (2016). "Quantification of Hydrazine in Human Urine by HPLC-MS-MS." J Anal Toxicol **40**(4): 248-254.

Jang, Y. M., D. W. Kim, T. C. Kang, M. H. Won, N. I. Baek, B. J. Moon, S. Y. Choi and O. S. Kwon (2003). "Human pyridoxal phosphatase. Molecular cloning, functional expression, and tissue distribution." J Biol Chem **278**(50): 50040-50046.

Jenner, A. M. and J. A. Timbrell (1994). "Effect of acute and repeated exposure to low doses of hydrazine on hepatic microsomal enzymes and biochemical parameters in vivo." Arch Toxicol **68**(4): 240-245.

Johnson, W. J. (1954). "Biological acetylation of isoniazid." Nature **174**(4433): 744-745.

Jones, M. S. and O. T. Jones (1969). "The structural organization of haem synthesis in rat liver mitochondria." Biochem J **113**(3): 507-514.

Ju, Y., T. Mizutani, Y. Imamichi, T. Yazawa, T. Matsumura, S. Kawabe, M. Kanno, A. Umezawa, K. Kangawa and K. Miyamoto (2012). "Nuclear receptor 5A (NR5A) family regulates 5-aminolevulinic acid synthase 1 (ALAS1) gene expression in steroidogenic cells." Endocrinology **153**(11): 5522-5534.

Kaneo, Y., H. Kubo, T. Tabata, K. Matsuyama, A. Noda and S. Iguchi (1981). "Tissue distribution of isoniazid and its metabolites in rats." J Pharmacobiodyn **4**(8): 590-595.

Kester, N. M. (1971). "Isoniazid hepatotoxicity--fact of fantasy." JAMA **217**(5): 699.

Khan, S. R., A. G. Morgan, K. Michail, N. Srivastava, R. M. Whittal, N. Aljuhani and A. G. Siraki (2016). "Metabolism of isoniazid by neutrophil myeloperoxidase leads to isoniazid-NAD(+) adduct formation: A comparison of the reactivity of isoniazid with its known human metabolites." Biochem Pharmacol **106**: 46-55.

Kim, Y. M., H. A. Bergonia, C. Muller, B. R. Pitt, W. D. Watkins and J. R. Lancaster, Jr. (1995). "Loss and degradation of enzyme-bound heme induced by cellular nitric oxide synthesis." J Biol Chem **270**(11): 5710-5713.

Kishida, T., T. Onozato, T. Kanazawa, S. Tanaka and J. Kuroda (2012). "Increase in covalent binding of 5-hydroxydiclofenac to hepatic tissues in rats co-treated with lipopolysaccharide and diclofenac: involvement in the onset of diclofenac-induced idiosyncratic hepatotoxicity." J Toxicol Sci **37**(6): 1143-1156.

Kliewer, S. A., J. T. Moore, L. Wade, J. L. Staudinger, M. A. Watson, S. A. Jones, D. D. McKee, B. B. Oliver, T. M. Willson, R. H. Zetterstrom, T. Perlmann and J. M. Lehmann (1998). "An orphan nuclear receptor activated by pregnanes defines a novel steroid signaling pathway." Cell **92**(1): 73-82.

Kluth, D., A. Banning, I. Paur, R. Blomhoff and R. Brigelius-Flohe (2007). "Modulation of pregnane X receptor- and electrophile responsive element-mediated gene expression by dietary polyphenolic compounds." Free Radic Biol Med **42**(3): 315-325.

Kolluri, S., T. J. Sadlon, B. K. May and H. L. Bonkovsky (2005). "Haem repression of the housekeeping 5-aminolaevulinic acid synthase gene in the hepatoma cell line LMH." Biochem J **392**(Pt 1): 173-180.

Koningsberger, J. C., L. H. Rademakers, J. van Hattum, H. B. de la Faille, L. J. Wiegman, E. Italiaander, G. P. van Berge Henegouwen and J. J. Marx (1995). "Exogenous protoporphyrin inhibits Hep G2 cell proliferation, increases the intracellular hydrogen peroxide concentration and causes ultrastructural alterations." J Hepatol **22**(1): 57-65.

Krishnamurthy, P. and J. D. Schuetz (2011). "The role of ABCG2 and ABCB6 in porphyrin metabolism and cell survival." Curr Pharm Biotechnol **12**(4): 647-655.

Kubota, Y., K. Nomura, Y. Katoh, R. Yamashita, K. Kaneko and K. Furuyama (2016). "Novel Mechanisms for Heme-dependent Degradation of ALAS1 Protein as a Component of Negative Feedback Regulation of Heme Biosynthesis." J Biol Chem **291**(39): 20516-20529.

Kumar, B. S., B. C. Chung, O. S. Kwon and B. H. Jung (2012). "Discovery of common urinary biomarkers for hepatotoxicity induced by carbon tetrachloride, acetaminophen and methotrexate by mass spectrometry-based metabolomics." J Appl Toxicol **32**(7): 505-520.

Kumar, S., M. Jin, A. Ande, N. Sinha, P. S. Silverstein and A. Kumar (2012). "Alcohol consumption effect on antiretroviral therapy and HIV-1 pathogenesis: role of cytochrome P450 isozymes." Expert Opin Drug Metab Toxicol **8**(11): 1363-1375.

Laafi, J., C. Homedan, C. Jacques, N. Gueguen, C. Schmitt, H. Puy, P. Reynier, M. Carmen Martinez and Y. Malthiery (2014). "Pro-oxidant effect of ALA is implicated in mitochondrial dysfunction of HepG2 cells." Biochimie **106**: 157-166.

Lakehal, F., P. M. Dansette, L. Becquemont, E. Lasnier, R. Delelo, P. Balladur, R. Poupon, P. H. Beaune and C. Housset (2001). "Indirect cytotoxicity of flucloxacillin toward human biliary epithelium via metabolite formation in hepatocytes." Chem Res Toxicol **14**(6): 694-701.

Lamba, V., K. Yasuda, J. K. Lamba, M. Assem, J. Davila, S. Strom and E. G. Schuetz (2004). "PXR (NR1I2): splice variants in human tissues, including brain, and identification of neurosteroids and nicotine as PXR activators." Toxicol Appl Pharmacol **199**(3): 251-265.

Lauterburg, B. H., C. V. Smith, E. L. Todd and J. R. Mitchell (1985). "Oxidation of hydrazine metabolites formed from isoniazid." Clin Pharmacol Ther **38**(5): 566-571.

Lauterburg, B. H., C. V. Smith, E. L. Todd and J. R. Mitchell (1985). "Pharmacokinetics of the toxic hydrazino metabolites formed from isoniazid in humans." J Pharmacol Exp Ther **235**(3): 566-570.

Lauterburg, B. H., E. L. Todd, C. V. Smith and J. R. Mitchell (1985). "Cimetidine inhibits the formation of the reactive, toxic metabolite of isoniazid in rats but not in man." Hepatology **5**(4): 607-609.

Lee, G. H., B. Bhandary, E. M. Lee, J. K. Park, K. S. Jeong, I. K. Kim, H. R. Kim and H. J. Chae (2011). "The roles of ER stress and P450 2E1 in CCl(4)-induced steatosis." Int J Biochem Cell Biol **43**(10): 1469-1482.

Lehmann, J. M., D. D. McKee, M. A. Watson, T. M. Willson, J. T. Moore and S. A. Kliewer (1998). "The human orphan nuclear receptor PXR is activated by compounds that regulate CYP3A4 gene expression and cause drug interactions." J Clin Invest **102**(5): 1016-1023.

Leiro-Fernandez, V., D. Valverde, R. Vazquez-Gallardo, L. Constenla and A. Fernandez-Villar (2010). "Genetic variations of NAT2 and CYP2E1 and isoniazid hepatotoxicity in a diverse population." Pharmacogenomics **11**(9): 1205-1206; author reply 1207-1208.

Li, C., J. Long, X. Hu and Y. Zhou (2013). "GSTM1 and GSTT1 genetic polymorphisms and risk of anti-tuberculosis drug-induced hepatotoxicity: an updated meta-analysis." Eur J Clin Microbiol Infect Dis **32**(7): 859-868.

Li, F., J. Lu, J. Cheng, L. Wang, T. Matsubara, I. L. Csanaky, C. D. Klaassen, F. J. Gonzalez and X. Ma (2013). "Human PXR modulates hepatotoxicity associated with rifampicin and isoniazid co-therapy." Nat Med **19**(4): 418-420.

Li, F., Y. Miao, L. Zhang, S. A. Neuenswander, J. T. Douglas and X. Ma (2011). "Metabolomic analysis reveals novel isoniazid metabolites and hydrazones in human urine." Drug Metab Pharmacokinet **26**(6): 569-576.

Li, F., P. Wang, K. Liu, M. G. Tarrago, J. Lu, E. N. Chini and X. Ma (2016). "A High Dose of Isoniazid Disturbs Endobiotic Homeostasis in Mouse Liver." Drug Metab Dispos **44**(11): 1742-1751.

Lian, Y., J. Zhao, Y. M. Wang, J. Zhao and S. Q. Peng (2017). "Metallothionein protects against isoniazid-induced liver injury through the inhibition of CYP2E1-dependent oxidative and nitrosative impairment in mice." Food Chem Toxicol **102**: 32-38.

Lin, W., Y. M. Wang, S. C. Chai, L. Lv, J. Zheng, J. Wu, Q. Zhang, Y. D. Wang, P. R. Griffin and T. Chen (2017). "SPA70 is a potent antagonist of human pregnane X receptor." Nat Commun **8**(1): 741.

Lin, Y. H., H. M. Chang, F. P. Chang, C. R. Shen, C. L. Liu, W. Y. Mao, C. C. Lin, H. S. Lee and C. N. Shen (2013). "Protoporphyrin IX accumulation disrupts mitochondrial dynamics and function in ABCG2-deficient hepatocytes." FEBS Lett **587**(19): 3202-3209.

Liu, K., J. Yan, M. Sachar, X. Zhang, M. Guan, W. Xie and X. Ma (2015). "A metabolomic perspective of griseofulvin-induced liver injury in mice." Biochem Pharmacol.

Liu, K., J. Yan, M. Sachar, X. Zhang, M. Guan, W. Xie and X. Ma (2015). "A metabolomic perspective of griseofulvin-induced liver injury in mice." Biochem Pharmacol **98**(3): 493-501.

Loeffen, J., J. Smeitink, R. Triepels, R. Smeets, M. Schuelke, R. Sengers, F. Trijbels, B. Hamel, R. Mullaart and L. van den Heuvel (1998). "The first nuclear-encoded complex I mutation in a patient with Leigh syndrome." Am J Hum Genet **63**(6): 1598-1608.

Long, Q., H. Smith, T. Zhang, S. Tang and P. Garner (2011). "Patient medical costs for tuberculosis treatment and impact on adherence in China: a systematic review." BMC Public Health **11**: 393.

Lucena, M. I., R. J. Andrade, C. Martinez, E. Ulzurrun, E. Garcia-Martin, Y. Borraz, M. C. Fernandez, M. Romero-Gomez, A. Castiella, R. Planas, J. Costa, S. Anzola, J. A. Agundez and D. Spanish Group for the Study of Drug-Induced Liver (2008). "Glutathione S-transferase m1 and t1 null genotypes increase susceptibility to idiosyncratic drug-induced liver injury." Hepatology **48**(2): 588-596.

Lundgren, H., K. Martinsson, K. Cederbrant, J. Jirholt, D. Mucs, K. Madeyski-Bengtson, S. Havarinasab and P. Hultman (2017). "HLA-DR7 and HLA-DQ2: Transgenic mouse strains tested as a model system for ximelagatran hepatotoxicity." PLoS One **12**(9): e0184744.

Luo, G., M. Cunningham, S. Kim, T. Burn, J. Lin, M. Sinz, G. Hamilton, C. Rizzo, S. Jolley, D. Gilbert, A. Downey, D. Mudra, R. Graham, K. Carroll, J. Xie, A. Madan, A. Parkinson, D. Christ, B. Selling, E. LeCluyse and L. S. Gan (2002). "CYP3A4 induction by drugs: correlation between a pregnane X receptor reporter gene assay and CYP3A4 expression in human hepatocytes." Drug Metab Dispos **30**(7): 795-804.

Lyoumi, S., M. Abitbol, D. Rainteau, Z. Karim, F. Bernex, V. Oustric, S. Millot, P. Letteron, N. Heming, L. Guillmot, X. Montagutelli, G. Berdeaux, L. Gouya, R. Poupon, J. C. Deybach, C. Beaumont and H. Puy (2011). "Protoporphyrin retention in hepatocytes and Kupffer cells prevents sclerosing cholangitis in erythropoietic protoporphyria mouse model." Gastroenterology **141**(4): 1509-1519, 1519 e1501-1503.

Ma, X., Y. Shah, C. Cheung, G. L. Guo, L. Feigenbaum, K. W. Krausz, J. R. Idle and F. J. Gonzalez (2007). "The PREgnane X receptor gene-humanized mouse: a model for investigating drug-drug interactions mediated by cytochromes P450 3A." Drug Metab Dispos **35**(2): 194-200.

Machuca, A. and A. M. Milagres (2003). "Use of CAS-agar plate modified to study the effect of different variables on the siderophore production by Aspergillus." Lett Appl Microbiol **36**(3): 177-181.

Mahashur, A. A. (1992). "Isoniazid induced peripheral neuropathy." J Assoc Physicians India **40**(10): 651-652.

Maiga, M., B. A. Ahidjo, M. C. Maiga, L. Cheung, S. Pelly, S. Lun, F. Bougoudogo and W. R. Bishai (2015). "Efficacy of Adjunctive Tofacitinib Therapy in Mouse Models of Tuberculosis." EBioMedicine **2**(8): 868-873.

McKennis, H., Jr., A. S. Yard and E. V. Pahnelas (1956). "The production of fatty livers in rabbits by isoniazid and other hydrazine derivatives." Am Rev Tuberc **73**(6): 956-959.

McMaster, P. D. (1922). "Do Species Lacking a Gall Bladder Possess Its Functional Equivalent?" J Exp Med **35**(2): 127-140.

Medlock, A. E., M. T. Shiferaw, J. R. Marcero, A. A. Vashisht, J. A. Wohlschlegel, J. D. Phillips and H. A. Dailey (2015). "Identification of the Mitochondrial Heme Metabolism Complex." PLoS One **10**(8): e0135896.

Meier, Y., C. Pauli-Magnus, U. M. Zanger, K. Klein, E. Schaeffeler, A. K. Nussler, N. Nussler, M. Eichelbaum, P. J. Meier and B. Stieger (2006). "Interindividual variability of canalicular ATP-binding-cassette (ABC)-transporter expression in human liver." Hepatology **44**(1): 62-74.

Meng, X., J. L. Maggs, T. Usui, P. Whitaker, N. S. French, D. J. Naisbitt and B. K. Park (2015). "Auto-oxidation of Isoniazid Leads to Isonicotinic-Lysine Adducts on Human Serum Albumin." Chem Res Toxicol **28**(1): 51-58.

Metushi, I. G., P. Cai, L. Vega, D. M. Grant and J. Uetrecht (2014). "Paradoxical attenuation of autoimmune hepatitis by oral isoniazid in wild-type and N-acetyltransferase-deficient mice." Drug Metab Dispos **42**(6): 963-973.

Metushi, I. G., T. Nakagawa and J. Uetrecht (2012). "Direct oxidation and covalent binding of isoniazid to rodent liver and human hepatic microsomes: humans are more like mice than rats." Chem Res Toxicol **25**(11): 2567-2576.

Miguet, J. P., P. Mavier, C. J. Soussy and D. Dhumeaux (1977). "Induction of hepatic microsomal enzymes after brief administration of rifampicin in man." Gastroenterology **72**(5 Pt 1): 924-926.

Mitchell, J. R., U. P. Thorgeirsson, M. Black, J. A. Timbrell, W. R. Snodgrass, W. Z. Potter, H. R. Jollow and H. R. Keiser (1975). "Increased incidence of isoniazid hepatitis in rapid acetylators: possible relation to hydranize metabolites." Clin Pharmacol Ther **18**(1): 70-79.

Mitchell, J. R., H. J. Zimmerman, K. G. Ishak, U. P. Thorgeirsson, J. A. Timbrell, W. R. Snodgrass and S. D. Nelson (1976). "Isoniazid liver injury: clinical spectrum, pathology, and probable pathogenesis." Ann Intern Med **84**(2): 181-192.

Monteiro, T. P., K. B. El-Jaick, A. L. Jeovanio-Silva, P. E. Brasil, M. J. Costa, V. C. Rolla and L. de Castro (2012). "The roles of GSTM1 and GSTT1 null genotypes and other predictors in anti-tuberculosis drug-induced liver injury." J Clin Pharm Ther **37**(6): 712-718.

Morfouace, M., S. Cheepala, S. Jackson, Y. Fukuda, Y. T. Patel, S. Fatima, D. Kawauchi, A. A. Shelat, C. F. Stewart, B. P. Sorrentino, J. D. Schuetz and M. F. Roussel (2015). "ABCG2 Transporter Expression Impacts Group 3 Medulloblastoma Response to Chemotherapy." Cancer Res **75**(18): 3879-3889.

Murray, C. J., K. F. Ortblad, C. Guinovart, S. S. Lim, T. M. Wolock, D. A. Roberts, E. A. Dansereau, N. Graetz, R. M. Barber, J. C. Brown, H. Wang, H. C. Duber, M. Naghavi, D. Dicker, L. Dandona, J. A. Salomon, K. R. Heuton, K. Foreman, D. E. Phillips, T. D. Fleming, A. D. Flaxman, B. K. Phillips, E. K. Johnson, M. S. Coggeshall, F. Abd-Allah, S. F. Abera, J. P. Abraham, I. Abubakar, L. J. Abu-Raddad, N. M. Abu-Rmeileh, T. Achoki, A. O. Adeyemo, A. K. Adou, J. C. Adsuar, E. E. Agardh, D. Akena, M. J. Al Kahbouri, D. Alasfoor, M. I. Albittar, G. Alcala-Cerra, M. A. Alegretti, Z. A. Alemu, R. Alfonso-Cristancho, S. Alhabib, R. Ali, F. Alla, P. J. Allen, U. Alsharif, E. Alvarez, N. Alvis-Guzman, A. A. Amankwaa, A. T. Amare, H. Amini, W. Ammar, B. O. Anderson, C. A. Antonio, P. Anwari, J. Arnlov, V. S. Arsenijevic, A. Artaman, R. J. Asghar, R. Assadi, L. S. Atkins, A. Badawi, K. Balakrishnan, A. Banerjee, S. Basu, J. Beardsley, T. Bekele, M. L. Bell, E. Bernabe, T. J. Beyene, N. Bhala, A. Bhalla, Z. A. Bhutta, A. B. Abdulhak, A. Binagwaho, J. D. Blore, B. B. Basara, D. Bose, M. Brainin, N. Breitborde, C. A. Castaneda-Orjuela, F. Catala-Lopez, V. K. Chadha, J. C. Chang, P. P. Chiang, T. W. Chuang, M. Colomar, L. T. Cooper, C. Cooper, K. J. Courville, B. C. Cowie, M. H. Criqui, R. Dandona, A. Dayama, D. De Leo, L. Degenhardt, B. Del Pozo-Cruz, K. Deribe, D. C. Des Jarlais, M. Dessalegn, S. D. Dharmaratne, U. Dilmen, E. L. Ding, T. R. Driscoll, A. M. Durrani, R. G. Ellenbogen, S. P. Ermakov, A. Esteghamati, E. J. Faraon, F. Farzadfar, S. M. Fereshtehnejad, D. O. Fijabi, M. H. Forouzanfar, U. Fra Paleo, L. Gaffikin, A. Gamkrelidze, F. G. Gankpe, J. M. Geleijnse, B. D. Gessner, K. B. Gibney, I. A. Ginawi, E. L. Glaser, P. Gona, A. Goto, H. N. Gouda, H. C. Gugnani, R. Gupta, R. Gupta, N. Hafezi-Nejad, R. R. Hamadeh, M. Hammami, G. J. Hankey, H. L. Harb, J. M. Haro, R. Havmoeller, S. I. Hay, M. T. Hedayati, I.

B. Pi, H. W. Hoek, J. C. Hornberger, H. D. Hosgood, P. J. Hotez, D. G. Hoy, J. J. Huang, K. M. Iburg, B. T. Idrisov, K. Innos, K. H. Jacobsen, P. Jeemon, P. N. Jensen, V. Jha, G. Jiang, J. B. Jonas, K. Juel, H. Kan, I. Kankindi, N. E. Karam, A. Karch, C. K. Karema, A. Kaul, N. Kawakami, D. S. Kazi, A. H. Kemp, A. P. Kengne, A. Keren, M. Kereselidze, Y. S. Khader, S. E. Khalifa, E. A. Khan, Y. H. Khang, I. Khonelidze, Y. Kinfu, J. M. Kinge, L. Knibbs, Y. Kokubo, S. Kosen, B. K. Defo, V. S. Kulkarni, C. Kulkarni, K. Kumar, R. B. Kumar, G. A. Kumar, G. F. Kwan, T. Lai, A. L. Balaji, H. Lam, Q. Lan, V. C. Lansingh, H. J. Larson, A. Larsson, J. T. Lee, J. Leigh, M. Leinsalu, R. Leung, Y. Li, Y. Li, G. M. De Lima, H. H. Lin, S. E. Lipshultz, S. Liu, Y. Liu, B. K. Lloyd, P. A. Lotufo, V. M. Machado, J. H. Maclachlan, C. Magis-Rodriguez, M. Majdan, C. C. Mapoma, W. Marcenes, M. B. Marzan, J. R. Masci, M. T. Mashal, A. J. Mason-Jones, B. M. Mayosi, T. T. Mazorodze, A. C. McKay, P. A. Meaney, M. M. Mehndiratta, F. Mejia-Rodriguez, Y. A. Melaku, Z. A. Memish, W. Mendoza, T. R. Miller, E. J. Mills, K. A. Mohammad, A. H. Mokdad, G. L. Mola, L. Monasta, M. Montico, A. R. Moore, R. Mori, W. N. Moturi, M. Mukaigawara, K. S. Murthy, A. Naheed, K. S. Naidoo, L. Naldi, V. Nangia, K. M. Narayan, D. Nash, C. Nejjari, R. G. Nelson, S. P. Neupane, C. R. Newton, M. Ng, M. I. Nisar, S. Nolte, O. F. Norheim, V. Nowaseb, L. Nyakarahuka, I. H. Oh, T. Ohkubo, B. O. Olusanya, S. B. Omer, J. N. Opio, O. E. Orisakwe, J. D. Pandian, C. Papachristou, A. J. Caicedo, S. B. Patten, V. K. Paul, B. I. Pavlin, N. Pearce, D. M. Pereira, A. Pervaiz, K. Pesudovs, M. Petzold, F. Pourmalek, D. Qato, A. D. Quezada, D. A. Quistberg, A. Rafay, K. Rahimi, V. Rahimi-Movaghar, S. Ur Rahman, M. Raju, S. M. Rana, H. Razavi, R. Q. Reilly, G. Remuzzi, J. H. Richardus, L. Ronfani, N. Roy, N. Sabin, M. Y. Saeedi, M. A. Sahraian, G. M. Samonte, M. Sawhney, I. J. Schneider, D. C. Schwebel, S. Seedat, S. G. Sepanlou, E. E. Servan-Mori, S. Sheikhbahaei, K. Shibuya, H. H. Shin, I. Shiue, R. Shivakoti, I. D. Sigfusdottir, D. H. Silberberg, A. P. Silva, E. P. Simard, J. A. Singh, V. Skirbekk, K. Sliwa, S. Soneji, S. S. Soshnikov, C. T. Sreeramareddy, V. K. Stathopoulou, K. Stroumpoulis, S. Swaminathan, B. L. Sykes, K. M. Tabb, R. T. Talongwa, E. Y. Tenkorang, A. S. Terkawi, A. J. Thomson, A. L. Thorne-Lyman, J. A. Towbin, J. Traebert, B. X. Tran, Z. T. Dimbuene, M. Tsilimbaris, U. S. Uchendu, K. N. Ukwaja, S. B. Uzun, A. J. Vallely, T. J. Vasankari, N. Venketasubramanian, F. S. Violante, V. V. Vlassov, S. E. Vollset, S. Waller, M. T. Wallin, L. Wang, X. Wang, Y. Wang, S. Weichenthal, E. Weiderpass, R. G. Weintraub, R. Westerman, R. A. White, J. D. Wilkinson, T. N. Williams, S. M. Woldeyohannes, J. Q. Wong, G. Xu, Y. C. Yang, Y. Yano, G. K. Yentur, P. Yip, N. Yonemoto, S. J. Yoon, M. Younis, C. Yu, K. Y. Jin, M. El Sayed Zaki, Y. Zhao, Y. Zheng, M. Zhou, J. Zhu, X. N. Zou, A. D. Lopez and T. Vos (2014). "Global, regional, and national incidence and mortality for HIV, tuberculosis, and malaria during 1990-2013: a systematic analysis for the Global Burden of Disease Study 2013." Lancet **384**(9947): 1005-1070.

Muruganandan, S. and C. J. Sinal (2008). "Mice as clinically relevant models for the study of cytochrome P450-dependent metabolism." Clin Pharmacol Ther **83**(6): 818-828.

Muture, B. N., M. N. Keraka, P. K. Kimuu, E. W. Kabiru, V. O. Ombeka and F. Oguya (2011). "Factors associated with default from treatment among tuberculosis patients in Nairobi province, Kenya: a case control study." BMC Public Health **11**: 696.

Navarro, V. J. and J. R. Senior (2006). "Drug-related hepatotoxicity." N Engl J Med **354**(7): 731-739.

Nelson, S. D., J. R. Mitchell, J. A. Timbrell, W. R. Snodgrass and G. B. Corcoran, 3rd (1976). "Isoniazid and iproniazid: activation of metabolites to toxic intermediates in man and rat." Science **193**(4256): 901-903.

Nicod, L., C. Viollon, A. Regnier, A. Jacqueson and L. Richert (1997). "Rifampicin and isoniazid increase acetaminophen and isoniazid cytotoxicity in human HepG2 hepatoma cells." Hum Exp Toxicol **16**(1): 28-34.

Ogino, T., H. Kobuchi, K. Munetomo, H. Fujita, M. Yamamoto, T. Utsumi, K. Inoue, T. Shuin, J. Sasaki, M. Inoue and K. Utsumi (2011). "Serum-dependent export of protoporphyrin IX by ATP-binding cassette transporter G2 in T24 cells." Mol Cell Biochem **358**(1-2): 297-307.

Ohno, M., I. Yamaguchi, I. Yamamoto, T. Fukuda, S. Yokota, R. Maekura, M. Ito, Y. Yamamoto, T. Ogura, K. Maeda, K. Komuta, T. Igarashi and J. Azuma (2000). "Slow N-acetyltransferase 2 genotype affects the incidence of isoniazid and rifampicin-induced hepatotoxicity." Int J Tuberc Lung Dis **4**(3): 256-261.

Okano, S., L. Zhou, T. Kusaka, K. Shibata, K. Shimizu, X. Gao, Y. Kikuchi, Y. Togashi, T. Hosoya, S. Takahashi, O. Nakajima and M. Yamamoto (2010). "Indispensable function for embryogenesis, expression and regulation of the nonspecific form of the 5-aminolevulinate synthase gene in mouse." Genes Cells **15**(1): 77-89.

Oladimeji, P. O., W. Lin, C. T. Brewer and T. Chen (2017). "Glucose-dependent regulation of pregnane X receptor is modulated by AMP-activated protein kinase." Sci Rep **7**: 46751.

Pagala, V. R., A. A. High, X. Wang, H. Tan, K. Kodali, A. Mishra, K. Kavdia, Y. Xu, Z. Wu and J. Peng (2015). "Quantitative protein analysis by mass spectrometry." Methods Mol Biol **1278**: 281-305.

Pal, D., D. Kwatra, M. Minocha, D. K. Paturi, B. Budda and A. K. Mitra (2011). "Efflux transporters- and cytochrome P-450-mediated interactions between drugs of abuse and antiretrovirals." Life Sci **88**(21-22): 959-971.

Payton, M., A. Mushtaq, T. W. Yu, L. J. Wu, J. Sinclair and E. Sim (2001). "Eubacterial arylamine N-acetyltransferases - identification and comparison of 18 members of the protein family with conserved active site cysteine, histidine and aspartate residues." Microbiology **147**(Pt 5): 1137-1147.

Peretti, E., G. Karlaganis and B. H. Lauterburg (1987). "Acetylation of acetylhydrazine, the toxic metabolite of isoniazid, in humans. Inhibition by concomitant administration of isoniazid." J Pharmacol Exp Ther **243**(2): 686-689.

Peretti, E., G. Karlaganis and B. H. Lauterburg (1987). "Increased urinary excretion of toxic hydrazino metabolites of isoniazid by slow acetylators. Effect of a slow-release preparation of isoniazid." Eur J Clin Pharmacol **33**(3): 283-286.

Perez-Barriocanal, F., J. G. Redondo-Torres, G. R. Villanueva, E. Arteche, M. M. Berenson and J. J. Marin (1989). "Protoporphyrin IX-induced impairment of biliary lipid secretion in the rat." Clin Sci (Lond) **77**(5): 473-478.

Peyer, A. K., D. Jung, M. Beer, C. Gnerre, A. Keogh, D. Stroka, M. Zavolan and U. A. Meyer (2007). "Regulation of human liver delta-aminolevulinic acid synthase by bile acids." Hepatology **46**(6): 1960-1970.

Podvinec, M., C. Handschin, R. Looser and U. A. Meyer (2004). "Identification of the xenosensors regulating human 5-aminolevulinate synthase." Proc Natl Acad Sci U S A **101**(24): 9127-9132.

Preziosi, P. (2007). "Isoniazid: metabolic aspects and toxicological correlates." Curr Drug Metab **8**(8): 839-851.

Preziosi, P. and G. Porcellati (1953). "[Studies on the metabolism of isonicotinic hydrazide; preliminary report]." Boll Soc Ital Biol Sper **29**(3): 271-272.

Raucy, J. L. (2003). "Regulation of CYP3A4 expression in human hepatocytes by pharmaceuticals and natural products." Drug Metab Dispos **31**(5): 533-539.

Reagan-Shaw, S., M. Nihal and N. Ahmad (2008). "Dose translation from animal to human studies revisited." FASEB J **22**(3): 659-661.

Richards, V. E., B. Chau, M. R. White and C. A. McQueen (2004). "Hepatic gene expression and lipid homeostasis in C57BL/6 mice exposed to hydrazine or acetylhydrazine." Toxicol Sci **82**(1): 318-332.

Robles-Diaz, M., M. Garcia-Cortes, I. Medina-Caliz, A. Gonzalez-Jimenez, R. Gonzalez-Grande, J. M. Navarro, A. Castiella, E. M. Zapata, M. Romero-Gomez, S. Blanco, G. Soriano, R. Hidalgo, M. Ortega-Torres, E. Clavijo, P. M. Bermudez-Ruiz, M. I. Lucena, R. J. Andrade, D. R. Spanish and C. Faster Evidence-based Translation (2015). "The value of serum aspartate aminotransferase and gamma-glutamyl transpetidase as biomarkers in hepatotoxicity." Liver Int **35**(11): 2474-2482.

Rouault, T. A. and R. D. Klausner (1996). "Iron-sulfur clusters as biosensors of oxidants and iron." Trends Biochem Sci **21**(5): 174-177.

Roy, B., A. Chowdhury, S. Kundu, A. Santra, B. Dey, M. Chakraborty and P. P. Majumder (2001). "Increased risk of antituberculosis drug-induced hepatotoxicity in individuals with glutathione S-transferase M1 'null' mutation." J Gastroenterol Hepatol **16**(9): 1033-1037.

Rozwarski, D. A., G. A. Grant, D. H. Barton, W. R. Jacobs, Jr. and J. C. Sacchettini (1998). "Modification of the NADH of the isoniazid target (InhA) from Mycobacterium tuberculosis." Science **279**(5347): 98-102.

Sachar, M., F. Li, K. Liu, P. Wang, J. Lu and X. Ma (2016). "Chronic Treatment with Isoniazid Causes Protoporphyrin IX Accumulation in Mouse Liver." Chem Res Toxicol **29**(8): 1293-1297.

Sarich, T. C., S. P. Adams, G. Petricca and J. M. Wright (1999). "Inhibition of isoniazid-induced hepatotoxicity in rabbits by pretreatment with an amidase inhibitor." J Pharmacol Exp Ther **289**(2): 695-702.

Sarma, G. R., C. Immanuel, S. Kailasam, A. S. Narayana and P. Venkatesan (1986). "Rifampin-induced release of hydrazine from isoniazid. A possible cause of hepatitis during treatment of tuberculosis with regimens containing isoniazid and rifampin." Am Rev Respir Dis **133**(6): 1072-1075.

Sasaki, E., K. Matsuo, A. Iida, K. Tsuneyama, T. Fukami, M. Nakajima and T. Yokoi (2013). "A novel mouse model for phenytoin-induced liver injury: involvement of immune-related factors and P450-mediated metabolism." Toxicol Sci **136**(1): 250-263.

Schwab, C. E. and H. Tuschl (2003). "In vitro studies on the toxicity of isoniazid in different cell lines." Hum Exp Toxicol **22**(11): 607-615.

Schwyn, B. and J. B. Neilands (1987). "Universal chemical assay for the detection and determination of siderophores." Anal Biochem **160**(1): 47-56.

Schyschka, L., J. J. Sanchez, Z. Wang, B. Burkhardt, U. Muller-Vieira, K. Zeilinger, A. Bachmann, S. Nadalin, G. Damm and A. K. Nussler (2013). "Hepatic 3D cultures but not 2D cultures preserve specific transporter activity for acetaminophen-induced hepatotoxicity." Arch Toxicol **87**(8): 1581-1593.

Sellers, V. M., M. K. Johnson and H. A. Dailey (1996). "Function of the [2FE-2S] cluster in mammalian ferrochelatase: a possible role as a nitric oxide sensor." Biochemistry **35**(8): 2699-2704.

Sellers, V. M., K. F. Wang, M. K. Johnson and H. A. Dailey (1998). "Evidence that the fourth ligand to the [2Fe-2S] cluster in animal ferrochelatase is a cysteine. Characterization of the enzyme from Drosophila melanogaster." J Biol Chem **273**(35): 22311-22316.

Sendo, T., A. Noda, H. Noda, K. Y. Hsu and Y. Yamamoto (1984). "Metabolic hydrolysis of isoniazid by subcellular fractions of rat liver." J UOEH **6**(3): 249-255.

Sevigny, S. J. d. J., S. L. White, M. L. Halsey and F. A. Johnston (1966). "Effect of isoniazid on the loss of pyridoxal phosphate from, and its distribution in, the body of the rat." J Nutr **88**(1): 45-50.

Sharifzadeh, M., M. Rasoulinejad, F. Valipour, M. Nouraie and S. Vaziri (2005). "Evaluation of patient-related factors associated with causality, preventability, predictability and severity of hepatotoxicity during antituberculosis [correction of antituberclosis] treatment." Pharmacol Res **51**(4): 353-358.

Shehu, A. I., G. Li, W. Xie and X. Ma (2016). "The pregnane X receptor in tuberculosis therapeutics." Expert Opin Drug Metab Toxicol **12**(1): 21-30.

Shen, C., Q. Meng, G. Zhang and W. Hu (2008). "Rifampicin exacerbates isoniazid-induced toxicity in human but not in rat hepatocytes in tissue-like cultures." Br J Pharmacol **153**(4): 784-791.

Shih, T. Y., C. Y. Pai, P. Yang, W. L. Chang, N. C. Wang and O. Y. Hu (2013). "A novel mechanism underlies the hepatotoxicity of pyrazinamide." Antimicrob Agents Chemother **57**(4): 1685-1690.

Simunek, T., I. Klimtova, J. Kaplanova, M. Sterba, Y. Mazurova, M. Adamcova, R. Hrdina, V. Gersl and P. Ponka (2005). "Study of daunorubicin cardiotoxicity prevention with pyridoxal isonicotinoyl hydrazone in rabbits." Pharmacol Res **51**(3): 223-231.

Sinclair, J. C., J. Sandy, R. Delgoda, E. Sim and M. E. Noble (2000). "Structure of arylamine N-acetyltransferase reveals a catalytic triad." Nat Struct Biol **7**(7): 560-564.

Singh, M., P. Sasi, G. Rai, V. H. Gupta, D. Amarapurkar and P. P. Wangikar (2011). "Studies on toxicity of antitubercular drugs namely isoniazid, rifampicin, and pyrazinamide in an in vitro model of HepG2 cell line." Medicinal Chemistry Research **20**(9): 1611-1615.

Singla, N., D. Gupta, N. Birbian and J. Singh (2014). "Association of NAT2, GST and CYP2E1 polymorphisms and anti-tuberculosis drug-induced hepatotoxicity." Tuberculosis (Edinb) **94**(3): 293-298.

Srivastava, G., I. A. Borthwick, J. D. Brooker, J. C. Wallace, B. K. May and W. H. Elliott (1983). "Hemin inhibits transfer of pre-delta-aminolevulinate synthase into chick embryo liver mitochondria." Biochem Biophys Res Commun **117**(1): 344-349.

Stewart, C. F., M. Leggas, J. D. Schuetz, J. C. Panetta, P. J. Cheshire, J. Peterson, N. Daw, J. J. Jenkins, 3rd, R. Gilbertson, G. S. Germain, F. C. Harwood and P. J. Houghton (2004). "Gefitinib enhances the antitumor activity and oral bioavailability of irinotecan in mice." Cancer Res **64**(20): 7491-7499.

Stigliani, J. L., P. Arnaud, T. Delaine, V. Bernardes-Genisson, B. Meunier and J. Bernadou (2008). "Binding of the tautomeric forms of isoniazid-NAD adducts to the active site of the Mycobacterium tuberculosis enoyl-ACP reductase (InhA): a theoretical approach." J Mol Graph Model **27**(4): 536-545.

Su, X., Y. Chen, X. Wang, Y. Wang, P. Wang, L. Li and Q. Liu (2014). "PpIX induces mitochondria-related apoptosis in murine leukemia L1210 cells." Drug Chem Toxicol **37**(3): 348-356.

Suarez, J., K. Ranguelova, A. A. Jarzecki, J. Manzerova, V. Krymov, X. Zhao, S. Yu, L. Metlitsky, G. J. Gerfen and R. S. Magliozzo (2009). "An oxyferrous heme/protein-based radical intermediate is catalytically competent in the catalase reaction of Mycobacterium tuberculosis catalase-peroxidase (KatG)." J Biol Chem **284**(11): 7017-7029.

Sulkowski, M. S., D. L. Thomas, R. E. Chaisson and R. D. Moore (2000). "Hepatotoxicity associated with antiretroviral therapy in adults infected with human immunodeficiency virus and the role of hepatitis C or B virus infection." JAMA **283**(1): 74-80.

Suzuki, N., M. Irie, K. Iwata, H. Nakane, M. Yoshikane, Y. Koyama, Y. Uehara, Y. Takeyama, Y. Kitamura, T. Sohda, H. Watanabe, Y. Ikehara and S. Sakisaka (2006). "Altered expression of alkaline phosphatase (ALP) in the liver of primary biliary cirrhosis (PBC) patients." Hepatol Res **35**(1): 37-44.

Taketani, S., Y. Adachi and Y. Nakahashi (2000). "Regulation of the expression of human ferrochelatase by intracellular iron levels." Eur J Biochem **267**(15): 4685-4692.

Tang, N., R. Deng, Y. Wang, M. Lin, H. Li, Y. Qiu, M. Hong and G. Zhou (2013). "GSTM1 and GSTT1 null polymorphisms and susceptibility to anti-tuberculosis drug-induced liver injury: a meta-analysis." Int J Tuberc Lung Dis **17**(1): 17-25.

Teixeira, R. L., R. G. Morato, P. H. Cabello, L. M. Muniz, S. Moreira Ada, A. L. Kritski, F. C. Mello, P. N. Suffys, A. B. Miranda and A. R. Santos (2011). "Genetic polymorphisms of NAT2, CYP2E1 and GST enzymes and the occurrence of antituberculosis drug-induced hepatitis in Brazilian TB patients." Mem Inst Oswaldo Cruz **106**(6): 716-724.

Teschke, R., D. Larrey, D. Melchart and G. Danan (2016). "Traditional Chinese Medicine (TCM) and Herbal Hepatotoxicity: RUCAM and the Role of Novel Diagnostic Biomarkers Such as MicroRNAs." Medicines (Basel) **3**(3).

Timbrell, J. A., J. R. Mitchell, W. R. Snodgrass and S. D. Nelson (1980). "Isoniazid hepatoxicity: the relationship between covalent binding and metabolism in vivo." J Pharmacol Exp Ther **213**(2): 364-369.

To, K. K., D. C. Poon, Y. Wei, F. Wang, G. Lin and L. W. Fu (2015). "Vatalanib sensitizes ABCB1 and ABCG2-overexpressing multidrug resistant colon cancer cells to chemotherapy under hypoxia." Biochem Pharmacol **97**(1): 27-37.

Tostmann, A., M. J. Boeree, R. E. Aarnoutse, W. C. de Lange, A. J. van der Ven and R. Dekhuijzen (2008). "Antituberculosis drug-induced hepatotoxicity: concise up-to-date review." J Gastroenterol Hepatol **23**(2): 192-202.

Tostmann, A., M. J. Boeree, W. H. Peters, H. M. Roelofs, R. E. Aarnoutse, A. J. van der Ven and P. N. Dekhuijzen (2008). "Isoniazid and its toxic metabolite hydrazine induce in vitro pyrazinamide toxicity." Int J Antimicrob Agents **31**(6): 577-580.

Tujios, S. and R. J. Fontana (2011). "Mechanisms of drug-induced liver injury: from bedside to bench." Nat Rev Gastroenterol Hepatol **8**(4): 202-211.

Turpeinen, M., A. Tolonen, C. Chesne, A. Guillouzo, J. Uusitalo and O. Pelkonen (2009). "Functional expression, inhibition and induction of CYP enzymes in HepaRG cells." Toxicol In Vitro **23**(4): 748-753.

Ungo, J. R., D. Jones, D. Ashkin, E. S. Hollender, D. Bernstein, A. P. Albanese and A. E. Pitchenik (1998). "Antituberculosis drug-induced hepatotoxicity. The role of hepatitis C virus and the human immunodeficiency virus." Am J Respir Crit Care Med **157**(6 Pt 1): 1871-1876.

Upton, A., N. Johnson, J. Sandy and E. Sim (2001). "Arylamine N-acetyltransferases - of mice, men and microorganisms." Trends Pharmacol Sci **22**(3): 140-146.

van Hest, R., H. Baars, S. Kik, P. van Gerven, M. C. Trompenaars, N. Kalisvaart, S. Keizer, M. Borgdorff, M. Mensen and F. Cobelens (2004). "Hepatotoxicity of rifampin-pyrazinamide and isoniazid preventive therapy and tuberculosis treatment." Clin Infect Dis **39**(4): 488-496.

Vuilleumier, N., M. F. Rossier, A. Chiappe, F. Degoumois, P. Dayer, B. Mermillod, L. Nicod, J. Desmeules and D. Hochstrasser (2006). "CYP2E1 genotype and isoniazid-induced hepatotoxicity in patients treated for latent tuberculosis." Eur J Clin Pharmacol **62**(6): 423-429.

Walker, K., G. Ginsberg, D. Hattis, D. O. Johns, K. Z. Guyton and B. Sonawane (2009). "Genetic polymorphism in N-Acetyltransferase (NAT): Population distribution of NAT1 and NAT2 activity." J Toxicol Environ Health B Crit Rev **12**(5-6): 440-472.

Wang, P., K. Pradhan, X. B. Zhong and X. Ma (2016). "Isoniazid metabolism and hepatotoxicity." Acta Pharm Sin B **6**(5): 384-392.

Wang, X., Y. Li, Z. Wu, H. Wang, H. Tan and J. Peng (2014). "JUMP: a tag-based database search tool for peptide identification with high sensitivity and accuracy." Mol Cell Proteomics **13**(12): 3663-3673.

Wang, Y. G., H. S. Liu, X. X. Zhang, Y. Xiao, B. B. Lu, Z. C. Ma, Q. D. Liang, X. L. Tang, C. R. Xiao, H. L. Tan, B. L. Zhang and Y. Gao (2013). "[Screening of pregnane X receptor activation from ginsenosides]." Yao Xue Xue Bao **48**(1): 144-148.

Wang, Y. M., S. C. Chai, C. T. Brewer and T. Chen (2014). "Pregnane X receptor and drug-induced liver injury." Expert Opin Drug Metab Toxicol **10**(11): 1521-1532.

Wang, Y. M., S. S. Ong, S. C. Chai and T. Chen (2012). "Role of CAR and PXR in xenobiotic sensing and metabolism." Expert Opin Drug Metab Toxicol **8**(7): 803-817.

Watkins, R. E., P. R. Davis-Searles, M. H. Lambert and M. R. Redinbo (2003). "Coactivator binding promotes the specific interaction between ligand and the pregnane X receptor." J Mol Biol **331**(4): 815-828.

Watkins, R. E., J. M. Maglich, L. B. Moore, G. B. Wisely, S. M. Noble, P. R. Davis-Searles, M. H. Lambert, S. A. Kliewer and M. R. Redinbo (2003). "2.1 A crystal structure of human PXR in complex with the St. John's wort compound hyperforin." Biochemistry **42**(6): 1430-1438.

Weiss, T. S., S. Pahernik, I. Scheruebl, K. W. Jauch and W. E. Thasler (2003). "Cellular damage to human hepatocytes through repeated application of 5-aminolevulinic acid." J Hepatol **38**(4): 476-482.

Wen, X., J. S. Wang, P. J. Neuvonen and J. T. Backman (2002). "Isoniazid is a mechanism-based inhibitor of cytochrome P450 1A2, 2A6, 2C19 and 3A4 isoforms in human liver microsomes." Eur J Clin Pharmacol **57**(11): 799-804.

Windmill, K. F., A. Gaedigk, P. M. Hall, H. Samaratunga, D. M. Grant and M. E. McManus (2000). "Localization of N-acetyltransferases NAT1 and NAT2 in human tissues." Toxicol Sci **54**(1): 19-29.

Wit, F. W., D. H. Blanckenberg, K. Brinkman, J. M. Prins, M. E. van der Ende, M. M. Schneider, J. W. Mulder, F. de Wolf, J. M. Lange and A. S. Group (2005). "Safety of long-term interruption of successful antiretroviral therapy: the ATHENA cohort study." AIDS **19**(3): 345-348.

Wojciechowski, G. and P. R. de Montellano (2007). "Radical energies and the regiochemistry of addition to heme groups. Methylperoxy and nitrite radical additions to the heme of horseradish peroxidase." J Am Chem Soc **129**(6): 1663-1672.

Wolf, K. K., S. G. Wood, J. A. Hunt, B. W. Walton-Strong, K. Yasuda, L. Lan, S. X. Duan, Q. Hao, S. A. Wrighton, E. H. Jeffery, R. M. Evans, J. G. Szakacs, L. L. von Moltke, D. J. Greenblatt, M. H. Court, E. G. Schuetz, P. R. Sinclair and J. F. Sinclair (2005). "Role of the nuclear receptor pregnane X receptor in acetaminophen hepatotoxicity." Drug Metab Dispos **33**(12): 1827-1836.

Woolbright, B. L. and H. Jaeschke (2012). "Novel insight into mechanisms of cholestatic liver injury." World J Gastroenterol **18**(36): 4985-4993.

Xiang, Y., L. Ma, W. Wu, W. Liu, Y. Li, X. Zhu, Q. Wang, J. Ma, M. Cao, Q. Wang, X. Yao, L. Yang, A. Wubuli, C. Merle, P. Milligan, Y. Mao, J. Gu and X. Xin (2014). "The incidence of liver injury in Uyghur patients treated for TB in Xinjiang Uyghur autonomous region, China, and its association with hepatic enzyme polymorphisms nat2, cyp2e1, gstm1 and gstt1." PLoS One **9**(1): e85905.

Xie, W., J. L. Barwick, M. Downes, B. Blumberg, C. M. Simon, M. C. Nelson, B. A. Neuschwander-Tetri, E. M. Brunt, P. S. Guzelian and R. M. Evans (2000). "Humanized xenobiotic response in mice expressing nuclear receptor SXR." Nature **406**(6794): 435-439.

Xie, Y., M. R. McGill, K. Dorko, S. C. Kumer, T. M. Schmitt, J. Forster and H. Jaeschke (2014). "Mechanisms of acetaminophen-induced cell death in primary human hepatocytes." Toxicol Appl Pharmacol **279**(3): 266-274.

Yamada, S., M. Tang, K. Richardson, J. Halaschek-Wiener, M. Chan, V. J. Cook, J. M. Fitzgerald, R. K. Elwood, A. Brooks-Wilson and F. Marra (2009). "Genetic variations of NAT2 and CYP2E1 and isoniazid hepatotoxicity in a diverse population." Pharmacogenomics **10**(9): 1433-1445.

Yamamoto, T., T. Suou and C. Hirayama (1986). "Elevated serum aminotransferase induced by isoniazid in relation to isoniazid acetylator phenotype." Hepatology **6**(2): 295-298.

Yee, D., C. Valiquette, M. Pelletier, I. Parisien, I. Rocher and D. Menzies (2003). "Incidence of serious side effects from first-line antituberculosis drugs among patients treated for active tuberculosis." Am J Respir Crit Care Med **167**(11): 1472-1477.

Yew, W. W. and C. C. Leung (2006). "Antituberculosis drugs and hepatotoxicity." Respirology **11**(6): 699-707.

Yimer, G., M. Gry, W. Amogne, E. Makonnen, A. Habtewold, Z. Petros, G. Aderaye, I. Schuppe-Koistinen, L. Lindquist and E. Aklillu (2014). "Evaluation of patterns of liver toxicity in patients on antiretroviral and anti-tuberculosis drugs: a prospective four arm observational study in ethiopian patients." PLoS One **9**(4): e94271.

Yoshino, K., H. Munakata, O. Kuge, A. Ito and T. Ogishima (2007). "Haeme-regulated degradation of delta-aminolevulinate synthase 1 in rat liver mitochondria." J Biochem **142**(4): 453-458.

Yu, H., Q. Wang, Y. Sun, M. Shen, H. Li and Y. Duan (2015). "A new PAMPA model proposed on the basis of a synthetic phospholipid membrane." PLoS One **10**(2): e0116502.

Zabost, A., S. Brzezinska, M. Kozinska, M. Blachnio, J. Jagodzinski, Z. Zwolska and E. Augustynowicz-Kopec (2013). "Correlation of N-acetyltransferase 2 genotype with isoniazid acetylation in Polish tuberculosis patients." Biomed Res Int **2013**: 853602.

Zamboni, V. and A. Defranceschi (1954). "Identification of isonicotinoylhydrazones of pyruvic and alpha-ketoglutaric acid in rat urine after treatment with isonicotinic acid hydrazide (isoniazid)." Biochim Biophys Acta **14**(3): 430-432.

Zhang, J., P. Kuehl, E. D. Green, J. W. Touchman, P. B. Watkins, A. Daly, S. D. Hall, P. Maurel, M. Relling, C. Brimer, K. Yasuda, S. A. Wrighton, M. Hancock, R. B. Kim, S. Strom, K. Thummel, C. G. Russell, J. R. Hudson, Jr., E. G. Schuetz and M. S. Boguski (2001). "The human pregnane X receptor: genomic structure and identification and functional characterization of natural allelic variants." Pharmacogenetics **11**(7): 555-572.

Zhang, Y., W. Shi, W. Zhang and D. Mitchison (2013). "Mechanisms of Pyrazinamide Action and Resistance." Microbiol Spectr **2**(4): 1-12.

Zheng, J., Y. Shan, R. W. Lambrecht, S. E. Donohue and H. L. Bonkovsky (2008). "Differential regulation of human ALAS1 mRNA and protein levels by heme and cobalt protoporphyrin." Mol Cell Biochem **319**(1-2): 153-161.

Zhou, S., J. J. Morris, Y. Barnes, L. Lan, J. D. Schuetz and B. P. Sorrentino (2002). "Bcrp1 gene expression is required for normal numbers of side population stem cells in mice, and confers relative protection to mitoxantrone in hematopoietic cells in vivo." Proc Natl Acad Sci U S A **99**(19): 12339-12344.

Zollner, G., M. Wagner and M. Trauner (2010). "Nuclear receptors as drug targets in cholestasis and drug-induced hepatotoxicity." Pharmacol Ther **126**(3): 228-243.

VITA

Christopher Trent Brewer was born in Nashville, TN in 1988. He received his Bachelor of Science degree from Middle Tennessee State University with and graduated *cum laude* with distinction from the University Honors College. He majored in Biochemistry and Psychology and minored in Mental Health Services. He matriculated in the University of Tennessee Health Science Center College of Medicine in 2011. He joined the Ph.D. program in Biomedical Sciences in 2013 in the lab of Dr. Taosheng Chen.

Trent has presented at multiple local and national meetings and served previously as the Honor Council President for the University Honors College. After completion of his Ph.D. he will return to medical school to complete his graduate education.